AD-A082 527 SYRACUSE UNIV NY F/G 9/5

NONLINEAR SYSTEM ANALYSIS IN BIPOLAR INTEGRATED CIRCUITS.(U)

JAN 80 T FANG, J J WHALEN F30602-79-C-0011

UNCLASSIFIED RADC -TR-79-324 NL

1 OF 3

AD A

AD A082527

[illegible] SYSTEM ANALYSIS IN BIPOLAR INTEGRATED CIRCUITS

[illegible] University

[illegible]

APPROVED FOR PUBLIC RELEASE; DISTRIBUTION UNLIMITED

DTIC
ELECTE
APR 1 1980
S D
A

[illegible] AIR DEVELOPMENT CENTER
Air Force Systems Command
Griffiss Air Force Base, New York 13441

80 3 26 063

UNCLASSIFIED

SECURITY CLASSIFICATION OF THIS PAGE (When Data Entered)

19

REPORT DOCUMENTATION PAGE

READ INSTRUCTIONS BEFORE COMPLETING FORM

18

1. REPORT NUMBER: RADC TR-79-324

2. GOVT ACCESSION NO.

3. RECIPIENT'S CATALOG NUMBER

6

4. TITLE (and Subtitle): NONLINEAR SYSTEM ANALYSIS IN BIPOLAR INTEGRATED CIRCUITS.

5. TYPE OF REPORT & PERIOD COVERED: Phase Report. Sep 77 — Oct 79.

6. PERFORMING ORG. REPORT NUMBER: N/A

10

7. AUTHOR(s): Ta-Fang Fang, James J. Whalen

15

8. CONTRACT OR GRANT NUMBER(s): F30602-79-C-0011

9. PERFORMING ORGANIZATION NAME AND ADDRESS: Syracuse University, Syracuse NY 13210

16

10. PROGRAM ELEMENT, PROJECT, TASK AREA & WORK UNIT NUMBERS: 62702F, 2338[redacted]

17 03

11. CONTROLLING OFFICE NAME AND ADDRESS: Rome Air Development Center (RBCT), Griffiss AFB NY 13441

11

12. REPORT DATE: Jan[redacted]80

13. NUMBER OF PAGES: 267

14. MONITORING AGENCY NAME & ADDRESS (if different from Controlling Office): Same

12 267

15. SECURITY CLASS. (of this report): UNCLASSIFIED

15a. DECLASSIFICATION DOWNGRADING SCHEDULE: N/A

16. DISTRIBUTION STATEMENT (of this Report): Approved for public release; distribution unlimited.

17. DISTRIBUTION STATEMENT (of the abstract entered in Block 20, if different from Report): Same

18. SUPPLEMENTARY NOTES

RADC Project Engineer: Carmen A. Paludi, Jr. (RBCT)

This effort was conducted by the State University of New York at Buffalo. This effort was initiated under the Rome Air Development Center Post-Doctoral Program under Contract F30602-75-C-0122 and was completed under (Cont'd)

19. KEY WORDS (Continue on reverse side if necessary and identify by block number)

Integrated Circuit (IC)
Operational Amplifier
Cascode Amplifier
Radio Frequency Interference (RFI)
Electromagnetic Interference (EMI)
Electromagnetic Compatibility (EMC)
Nonlinear Effects
Nonlinear Circuit Analysis
Nonlinear Modeling
Nonlinear Measurements
Demodulation Effects
IC Modeling

20. ABSTRACT (Continue on reverse side if necessary and identify by block number)

Since analog bipolar integrated circuits (IC's) have become important components in modern communication systems, the study of the Radio Frequency Interference (RFI) effects in bipolar IC amplifiers is an important subject for electromagnetic compatibility (EMC) engineering. The investigation has focused on using the nonlinear circuit analysis program (NCAP) to predict RF demodulation effects in broadband bipolar IC amplifiers. The audio frequency (AF) voltage at the IC amplifier output terminal caused by an amplitude modulated (AM) RF signal at the IC amplifier input terminal was calculated and compared to measured values. Two

Cont'd

DD FORM 1 JAN 73 1473

UNCLASSIFIED

SECURITY CLASSIFICATION OF THIS PAGE (When Data Entered)

339600

Item 18 (Cont'd)

Syracuse University contract F30602-79-C-0011 under sponsorship of the Rome Air Development Center Compatibility Techniques Section for Rome Air Development Center.

Item 20 (Cont'd)

broadband IC amplifiers were investigated: (1) a cascode circuit using a CA3026 dual differential pair; (2) a unity gain voltage follower circuit using a μA741 operational amplifier (op amp).

Before using NCAP for RFI analysis, the model parameters for each bipolar junction transistor (BJT) in the integrated circuit were determined. Probe measurement techniques, manufacturer's data, and other researcher's data were used to obtain the required NCAP BJT model parameter values. An important contribution included in this effort is a complete set of NCAP BJT model parameters for most of the transistor types used in linear IC's.

The RF demodulation effects measured and calculated were characterized in terms of the second-order transfer function $H_2(f_1,-f_2)$ where $f_1 = f_{RF}$ and $f_2 = f_{RF} - f_{AF}$. The frequency f_{RF} is the RF carrier frequency, and the frequency f_{AF} is the AF modulation frequency. (The AF voltage V_M at the amplifier output terminals caused by a 50% AM modulated RF signal at the IC amplifier input terminal can be expressed as $V_M = (1/2\sqrt{2})\,|H_2(f_1,-f_2)|\,A^2$ where A is the RF carrier amplitude.) The experimental and calculated values for $H_2(f_1,-f_2)$ were determined for the RF frequency range 50 kHz to 50 MHz with an AM modulation frequency of 400 Hz or 1 kHz. For the CA3026 cascode amplifier the experimental and calculated values for H_2 agree within 4 to 12 dB over the RF frequency range 50 kHz to 10 MHz.

Above 10 MHz both the experimental and calculated values for $H_2(f_1,-f_2)$ decreased rapidly with increasing frequency. For the 741 unity gain voltage follower circuit the experimental and calculated values for $H_2(f_1,-f_2)$ also agree quite well over the RF frequency range 50 kHz to 50 MHz. The experimental and calculated values for $H_2(f_1,-f_2)$ for the 741 unity gain voltage follower circuit were approximately 40 dB less than those of the CA3026 cascode amplifier. This was a result of feedback in the op amp voltage follower circuit. A large increase in RFI effects was observed in the 741 op amp circuit when a 200 μF capacitor was connected to the 741 op amp inverting input. This increase was correctly predicted by NCAP. These comparisons demonstrate that the computer program NCAP can be used quite successfully to predict how AM modulated RF signals are demodulated in broadband IC amplifiers.

ACKNOWLEDGEMENTS

Many have contributed to the investigation of RFI effects in bipolar integrated circuits and to the report on the investigation. We are especially grateful to Professor Donald Weiner (Syracuse University) for his careful reading of a preliminary manuscript. Many of his comments, criticisms, and all of his suggestions which have helped the authors significantly, have been incorporated into the final manuscript. The additional manuscript proof-reading by Gordon Chen (SUNYAB) and Carmen Paludi (RADC) have also helped to reduce the errors in this report; their efforts are appreciated. Also appreciated is the assistance provided by Jon Valente (RADC) to us in using the computer program NCAP.

Finally, thanks to Mrs. Joan Bennett for her expert typing of this report and Ms. Barbara Evans for her excellent artwork. Their patience in making numerous changes is especially appreciated.

Accession For

TABLE OF CONTENTS

		PAGE
LIST OF TABLES		ix
LIST OF ILLUSTRATIONS		x
CHAPTER ONE:	INTRODUCTION	1
CHAPTER TWO:	TRANSISTOR MODELS AND PARAMETERS	6
	2.1 DC Characteristics and Large Signal Models	7
	2.1.1 The Basic Ebers-Moll Model	7
	2.1.2 Early Effect	11
	2.1.3 Diffusion Capacitances and Junction Capacitances	11
	2.1.4 Bias Dependence of Current Gain	15
	2.1.5 Impact Ionization	16
	2.1.6 High Current Effects	17
	2.1.7 Temperature Effects	17
	2.2 Linear Dynamic Characteristics and Small Signal Models	18
	2.2.1 Linear T-Model at Low Frequencies	19
	2.2.2 Linear T-Model at High Frequencies	25
	2.2.3 Linear Hybrid-Pi Equivalent Circuit	27
	2.3 Quasi-Linear Incremental Models	30
	2.3.1 Nonlinear Resistor	33
	2.3.2 Nonlinear Capacitor	34
	2.3.3 Nonlinear Inductor	35
	2.3.4 Nonlinear Dependent Current Source	36
	2.3.5 The Nonlinear Current Generator $K(v_2)$ and the Emitter-Base Nonlinear Resistive Coefficients	38

PAGE

2.3.6 The Nonlinear Current Generator $\gamma_c(v_3-v_2)$ and the Collector-Base Nonlinear Capacitance Coefficients 39

2.3.7 The Nonlinear Current Generator $g(v_2,v_3-v_1)$ and the Dependent Current Source Nonlinear Coefficients 40

CHAPTER THREE: MEASUREMENT OF BJT MODEL PARAMETERS 47

3.1 Large Signal Parameter Measurements 48

3.1.1 I_{ES}, Emitter Base Junction Saturation Current and Ref, Emitter Base Junction Diode Nonideality Factor 48

3.1.2 I_{CS}, Collector Base Junction Saturation Current and Rcf, Collector Base Junction Diode Nonideality Factor 51

3.1.3 I_S, Transistor Saturation Current 53

3.1.4 α_N, β_N, Forward Current Gains 55

3.1.5 a, h_{FEmax}, I_{Cmax}, h_{FE} Nonlinearity 55

3.1.6 α_I, β_I, Reverse Current Gains 58

3.1.7 R_{SC}, R_{SE}, Collector and Emitter Bulk Resistances 59

3.1.8 R_B, Base Bulk Resistance 62

3.1.9 V_{CBO}, η, Avalanche Nonlinearity and r_c, Collector Resistance 64

3.1.10 V_A, the Early Voltage 67

3.1.11 C_{jeo}, Φ_E, m_e, Emitter Junction Capacitance Parameters 68

3.1.12 C_{jco}, Φ_C, m_c, k, Collector Junction Capacitance Parameters 71

PAGE

3.2 Small Signal Parameter Measurements 76

3.2.1 r_b, Base Spreading Resistance 76

3.2.2 C_{je}, C_2', NCAP Emitter-Base Capacitance Parameters 81

3.2.3 τ_F, Forward Transit Time Constant 90

3.3 Large Signal Transient Measurements 90

3.4 Parasitic Elements 92

3.5 Summary of Parameter Values 94

CHAPTER FOUR: INTEGRATED CIRCUIT MODEL PARAMETERS 100

4.1 The CA3026 Dual Differential Pair 101

4.1.1 Direct Measurement of DC Operating Points 103

4.1.2 NCAP BJT Model Parameters 105

4.1.2.1 The Use of Manufacturer's Data 105

4.1.2.2 The Use of Measured Data 109

4.2 The μA741 Operational Amplifier 117

4.2.1 SPICE2 BJT Model Parameters 122

4.2.2 NCAP BJT Model Parameters 123

4.2.2.1 The Use of Measured Data 123

4.2.2.2 The Use of Wooley's Data 125

CHAPTER FIVE: NONLINEAR SYSTEM ANALYSIS 134

5.1 Volterra Series Description of a Nonlinear System 136

5.2 The NCAP Determination of the Nonlinear Transfer Function 143

CHAPTER SIX: COMPUTATION OF NONLINEAR TRANSFER FUNCTIONS 147

6.1 A Broadband JFET Amplifier Stage 147

6.2 Tuned RF Amplifier BJT Stage 160

6.2.1 Construction of the Linear Nodal Admittance Matrix Y and the Linear Current Excitation Source Vector J 163

6.2.2 Calculation of the Second-Order Current Source J_{d2} 166

6.2.3 Calculation of the Second-Order Transfer Functions 171

CHAPTER SEVEN: THE MEASUREMENT AND PREDICTION OF THE SECOND-ORDER TRANSFER FUNCTIONS IN INTEGRATED CIRCUITS 174

7.1 Linear Model of the CA3026 Cascode Amplifier 175

7.2 Linear Model of the μA741 Unity Gain Buffer Amplifier 180

7.3 The Measurement of Second-Order Transfer Functions 187

7.4 Comparison of Experimental and Calculated Values for the Second Order Transfer Functions 198

CHAPTER EIGHT: DISCUSSION AND CONCLUSION 216

APPENDIX I: STANDARD IEEE NOTATION 222

APPENDIX II: PROBE PREPARATION 224

APPENDIX III: μA741 BJT'S DC AND JUNCTION CAPACITANCE CHARACTERISTICS 226

APPENDIX IV: FORTRAN PROGRAM FOR CALCULATING FIRST AND SECOND-ORDER TRANSFER FUNCTIONS FOR THE TUNED RF AMPLIFIER SHOWN IN FIGURE 6-2 234

REFERENCES 245

LIST OF ILLUSTRATIONS

FIGURE		PAGE
2-1	(a) Physical Structure for the NPN Transistor	9
	(b) Basic Ebers-Moll Model for the NPN Transistor	9
2-2	Ebers-Moll Model in π-Version	12
2-3	Diagram Illustrating How the Early Voltage V_A of a BJT is Determined	12
2-4	Large Signal Transistor Model in π-Version	13
2-5	Small-Signal Voltages and Currents for an Intrinsic Transistor. For the Intrinsic Transistor the Parasitic Resistances R_B, R_{SE}, and R_{SC} Are Zero	20
2-6	Conventional Circuit Model Illustrating y-Parameters	22
2-7	Small Signal Equivalent Circuit in Turns of Admittances	22
2-8	Low to Medium Frequency Equivalent Circuits for BJT's (a) Large Early Effect Model (b) Small Early Effect Model	26
2-9	High Frequency Equivalent Circuit for Parasitic Elements Included	28
2-10	Linear Incremental Hybrid-Pi Model	28
2-11	Nonlinear Incremental π-Model. Note that the Nonlinear Behavior of Capacitors is not Explicitly Expressed in this Model.	32
2-12	Nonlinear Incremental T-Model. Note that the Emitter is Assumed to be the Datum Node.	32
2-13	Nonlinear Dependent Current Sources	36
3-1	Transistor Base-Emitter Characteristic Test Configuration (a) for Low Currents and (b) for High Currents	49
3-2	I_E Versus V_{BE} Plot for a 2N5179 Device	50
3-3	Transistor Base-Collector Characteristic Test Configuration	53
3-4	I_C Versus V_{BC} Plot for a 2N5179 Device	53

FIGURE		PAGE
3-5	Transistor I_C Versus V_{BE} Characteristic Test Configuration	54
3-6	I_C Versus V_{BE} Plot for a 2N5179 Device	54
3-7	(a) DC Test Circuit for Measuring α_N and β_N at Low Current Levels	56
	(b) Pulse Test Circuit for Measuring α_N and β_N at High Current Levels	56
3-8	$\beta_N(h_{FE})$ Versus I_C Plot for a 2N5179 Device	57
3-9	DC Test Circuit for Measuring α_I and β_I at Low Current Levels	60
3-10	β_I Versus I_E Plot for a 2N5179 Device	60
3-11	Circuit for the Measurement of Emitter and Collector Series Resistances	61
3-12	The Evaluation of R_{SE} and R_{SC} for a 2N5179 Transistor	61
3-13	Bulk Resistance (R_{SE} and R_{SC}) Determination with Two I_C-V_{CE} Curves	62
3-14	I_C Versus V_{CB} Plot for a 2N5179 Device	65
3-15	I_C Versus V_{CE} Plot for a 2N5179 Device Used to Determine Early Voltage V_A	69
3-16	Terminal Connections for Junction Capacitance Measurement (a) C_{je} Measurement and (b) C_{jc} Measurement	74
3-17	Typical Values of Emitter Junction Capacitance C_{meas}-C_x Vs $\Phi_E + \lvert V_{BE}\rvert$ for a 2N918 BJT	74
3-18	Circuit for Measuring h_{ie} and h_{fe}. Note that the Quantities V_s, I_b, etc., Are the Complex Amplitudes of Sinusoidal Quantities. See Appendix I on Notation.	79
3-19	Hybrid-Pi Model for a Junction Transistor	79
3-20	Small Signal Equivalent Circuit for Measuring Common-Emitter Short-Circuit Input Admittance $y_{ie} = I_b/V_{be}$. Note that the Quantities I_b, V_{be}, etc., are the Complex Amplitudes of Sinusoidal Quantities. See Appendix I on Notation.	79

FIGURE		PAGE
3-21	Small Signal Equivalent Circuit for Calculating the Common-Emitter Short-Circuit Input Impedance $h_{ie} = V_{be}/I_b$. Note that the Quantities I_b, V_{be}, etc., are the Complex Amplitudes of Sinusoidal Quantities. See Appendix I on Notation.	82
3-22	Input Impedance Locus Plot. The Intercepts of the Semicircle with the Real Axis Yield the Value of $r_b(R_B)$	82
3-23	Typical $Re(h_{ie})$ Versus $Im(h_{ie})$ Locus Plot for a 2N5109 BJT. These Circles were Obtained by Somewhat Judicious Choice of Three Points. Choice of a Different Set of Three Points will Yield Slightly Different Circles.	83
3-24	Conventional Asymptotic Plot of $\|h_{fe}\|$ Versus f	87
3-25	Plot of C_π Vs I_E Used to Determine NCAP Parameters C_{je} and C_2'	89
3-26	$1/2\pi f_T$ Versus $1/I_C$ Plot for a 2N5179 Device	91
3-27	Test Configuration and Waveforms for the Measurement and the Evaluation of the Reverse Transient Time τ_R	93
4-1	Schematic of RCA CA3026 Integrated Circuit	102
4-2	Schematic of CA3026 Cascode Amplifier	102
4-3	Typical Characteristics for Each Transistor in CA3026. (After Ref. (28)).	106
4-4	A Linear Plot of Emitter Capacitance Versus Emitter Current in Device CA3026	107
4-5	Representative Plot of I_E vs V_{BE} for an Individual BJT in Device CA3026	111
4-6	Representative Plot of h_{FE} vs I_C for an Individual BJT in Device CA3026	113
4-7	Representative Output Characteristics of an Individual BJT in Device CA3026	115
4-8	A Log-Log Plot of Collector-Base Junction Depletion Capacitance Versus Junction Voltage in Device CA3026	116

FIGURE		PAGE
4-9	Schematic of μA741 Operational Amplifier	118
4-10	Plan Views of the 741 Transistors. All Dimensions Are in Mils. (a) Small NPN (b) Large NPN (c) Lateral PNP (d) Large Substrate PNP (e) Dual-Collector Lateral PNP (f) Dual Emitter Substrate PNP. (After Wooley et al.[29])	120
4-11	SPICE2 Coding Diagram of μA741 Operational Amplifier Unity Gain Buffer. This Diagram Is Used to Determine (1) DC Operating Points of Each Individual BJT in the IC, and (2) the Linear Response of the Unity Gain Buffer.	121
4-12	Normalized Plot of h_{FE} vs Collector Current. Curve a for Small NPN, Large NPN, and Substrate PNP; Curve b for Lateral PNP	127
5-1	A Nonlinear System without Memory	135
6-1	The Circuit Diagrams of a Broadband JFET Amplifier (a) and Its AC Equivalent Circuit (b). Notations A, B, D, and E Represent the Nonlinear Transfer Functions at Nodes 1, 2, 3, and 4, respectively. Notations G, D, S', and S Represent Gate, Drain, Internal Source, and Source Terminals, Respectively.	148
6-2	A 2N5109 RF Amplifier NCAP Coding Circuit Diagram	161
6-3	A 2N5109 RF Amplifier Fortran NCAP Simulation Circuit Diagram, where Only the Linear Portion of the Amplifier is Shown.	162
6-4	Composite Branch Containing an Admittance Connected from Node i to Node j	164
6-5	Composite Branch Containing a Voltage-Controlled Current Source Along with the Controlling Branch	164
7-1	Experimental Systems for Measuring the First-Order Transfer Function $H_1(f)$ of the CA3026 Cascode Amplifier. Note that $H_1(f)$ = VOUT/VIN	176
7-2	Measured and Predicted Values for the First-Order Transfer Function VOUT/VIN of the Cascode Amplifier	177
7-3	Measured and Predicted Values for the First-Order Transfer Function VOUT/VIN of the Cascode Amplifier	178
7-4	A Linear Incremental Equivalent Circuit Model for the CA3026 Cascode Amplifier. Note That the Hybrid-Pi Model is Used for the BJT's	179

FIGURE		PAGE
7-5	Experimental System for Measuring the First-Order Transfer Function $H_1(f)$ of the μA741 Unity Gain Buffer. Note that $H_1(f)$ = VOUT/VIN	132
7-6	(a) Measured and Predicted Values for the First-Order Transfer Function VOUT/VIN of the Unity Gain Buffer.	133
	(b) Measured and Predicted Values for the First-Order Transfer Function VOUT/VIN of the Unity Gain Buffer (Note Change of the Scale.)	134
7-7	Measured and Predicted Values for the First-Order Transfer Function VOUT/VIN of the Unity Gain Buffer	185
7-8	Experimental System for Measuring Second-Order Transfer Functions $H_2(f_1,-f_2)$	188
7-9	CA3026 Cascode Amplifier Measured AF Voltage V_M at Wave Analyzer Input Versus Input Power Level	190
7-10	μA741 Op Amp Voltage Follower Measured AF Voltage V_M at the Wave Analyzer Input Vs Input Power Level Pgen	191
7-11	Schematic of the Thevenin Equivalent Circuit Measuring H_2	195
7-12	Calculated and Measured Responses for the Second-Order Transfer Function of the CA3026 Cascode Amplifier	199
7-13	Calculated and Measured Second-Order Transfer Functions for the μA741 Unity Gain Buffer. Inverting Input is Not Shunted with Capacitances. (C = 0.)	200
7-14	Cascode Amplifier Circuit Diagram Used to Determine NCAP Input Data	201
7-15	The NCAP Coding Circuit Diagram for the μA741 Unity Gain Buffer	203
7-16	Calculated and Measured Second-Order Transfer Functions of the μA741 Unity Gain Buffer. Inverting Input is Shunted with a 0.2 μF Capacitor	207
7-17	Calculated and Measured Second-Order Transfer Functions of the μA741 Unity Gain Buffer. Inverting Input is Shunted with a 200 μF Capacitor	208

FIGURE		PAGE
8-1	Schematic Cross Section of a Transistor with an Equivalent Circuit of Parasitic Elements (a), and the Suggested Nonlinear T-Model (b)	221
II-1	Sharp Tungsten Tip Preparation Diagram	225
III-1	Typical I_E vs V_{BE} Characteristics of BJT's in the μA741 Operational Amplifier	226
III-2	Typical Input Characteristics of BJT's in the μA741 Operational Amplifier	227
III-3	Typical DC Current Gain h_{FE} vs Collector Current I_C for BJT's in μA741 Operational Amplifier	228
III-4	Typical I-V Characteristics of the Small NPN Transistors (Data Obtained from Q5 Measurements)	230
III-5	Typical I-V Characteristics of the Large NPN Transistor (Data Obtained from Q14 Measurements)	230
III-6	Typical I-V Characteristics of the Lateral PNP Transistor (Data Obtained from Q3 Measurements)	231
III-7	Typical I-V Characteristics of the Large Substrate PNP Transistor (Data Obtained from Q20 Measurements)	231
III-8	Typical I-V Characteristics of the Dual-Collector Lateral PNP Transistor (Data Obtained from Q13 Measurements)	232
III-9	Typical I-V Characteristics of the Dual-Emitter Substrate PNP Transistor (Data Obtained from Q24 Measurements)	232
III-10	Typical Junction Capacitance vs Junction Voltage Plot of the BJT's in the μA741 Op Amp	233

LIST OF TABLES

TABLE		PAGE
2-1	NCAP INPUT PARAMETERS FOR 2N5109 BJT	45
2-2	NONLINEAR COEFFICIENTS FOR 2N5109 BJT	46
3-1	FORTRAN PROGRAM FOR DETERMINING JUNCTION CAPACITANCE PARAMETER VALUES	72
3-2	TYPICAL RESULTS OBTAINED USING THE FORTRAN PROGRAM IN TABLE 3-1	95
3-3	NCAP BIPOLAR JUNCTION TRANSISTOR MODEL PARAMETERS	96
3-4	SCEPTRE BIPOLAR JUNCTION TRANSISTOR MODEL PARAMETERS	97
3-5	SPICE2 BIPOLAR JUNCTION TRANSISTOR MODEL PARAMETERS	98
4-1	NCAP INPUT PARAMETERS FOR RCA CA3026 INTEGRATED CIRCUIT	104
4-2	SPICE2 μA741 BJT'S INPUT PARAMETERS	128
4-3	NCAP μA741 BJT'S INPUT PARAMETERS	130
4-4	741 OPERATIONAL AMPLIFIER SPICE2 CODING LIST	132
6-1	JFET NCAP MODEL PARAMETERS	157
6-2	CALCULATED VALUES FOR THE JFET NONLINEAR TRANSFER FUNCTIONS	159
6-3	CALCULATED RESULTS FOR THE FIRST AND SECOND-ORDER TRANSFER FUNCTIONs FOR THE 2N5109 TUNED RF AMPLIFIER AT THE OUTPUT NODE (20)	173
7-1	LINEAR INCREMENTAL HYBRID-PI PARAMETERS FOR BJT'S IN THE RCA CA3026 INTEGRATED CIRCUIT	181
7-2	SECOND-ORDER TRANSFER FUNCTION MEASUREMENT OF CA3026 CASCODE AMPLIFIER WITH Pgen = -35 dBm AND f_{AF} = 1 kHz	196
7-3	SECOND-ORDER TRANSFER FUNCTION MEASUREMENT OF μA741 UNITY GAIN BUFFER WITH Pgen = -10 dBm AND f_{AF} = 400 Hz	199
7-4	CASCODE AMPLIFIER NCAP PROGRAM CODING	209
7-5	UNITY GAIN VOLTAGE FOLLOWER NCAP PROGRAM CODING	211

EVALUATION

This investigation represents a significant and invaluable contribution to the Air Force Intrasystem Analysis Program (IAP) as pertaining to the Nonlinear Circuit Analysis Program (NCAP). By utilizing analysis, prediction and measurement techniques developed under the IAP, a new technique was developed which characterizes radio frequency (RF) demodulation effects in bipolar linear integrated circuits (IC's) which are designed to operate at audio frequency (AF). The results of this effort, which was performed in support of the RADC FY 77-79 Electromagnetic Compatibility (EMC) Technical Planning Objective (TPO) goal associated with the development of EMC prediction and analysis techniques, is twofold. It provides users of the IAP (particularly NCAP) with an application roadmap for performing nonlinear analysis on small scale bipolar linear integrated circuits. Secondly, a data base for linear IC input parameters required by NCAP has been established and will continue to expand with additional application. Because of the rigorous verification between measured and simulated data, input parameter measurements, and inclusion of parasitic effects, good agreement between measured results and NCAP predicted results is obtained. This agreement represents a sufficient degree of confidence in applying the technique developed in this effort of using NCAP to analyze and predict the nonlinear behavior, and the EMC profile of bipolar IC's.

Carmen A. Paludi, Jr.

CARMEN A. PALUDI, JR.
Project Engineer

CHAPTER ONE

INTRODUCTION

In recent years wideband monolithic analog integrated circuit amplifiers have become important building blocks in communication systems. These amplifiers, although designed to be linear, are not completely linear because of the inherent nonlinearity of the devices in the circuits. Therefore, in communication systems, where integrated circuits are used, nonlinear effects can cause some significant problems.

In the small signal amplifier circuit, a nonlinearity may generate a small amount of higher-order harmonic signals when excited by a single signal source or beat-frequency signals called Intermodulation Products (IMP's) when excited by two or more signal sources. (The unwanted signals will be referred to as distortion.) If the signal source excitations are sufficiently small, then the higher-order frequency components generated will be negligible when compared with the fundamental component. However, there are cases where the higher order frequency components are not negligible. An example is long-distance communication circuits, such as frequency-division wideband coaxial analog systems or cable TV systems, in which a repeater amplifier must be inserted every few miles to maintain signal strength. It has been observed that the undesirable higher order frequency components have a tendency to become additive along the line and can not always be neglected.[53] Also when electronic circuits are operated in a multi-signal Radio Frequency Interference (RFI) environment, the

strengths of stray signal sources are not necessarily small and severe RFI effects can result from a circuit nonlinearity. Perhaps the best known example is that a heart pacemaker can be affected by a microwave oven.[54] Therefore, the study of nonlinear distortion* to predict nonlinear effects such as gain compression, desensitization, cross-modulation, intermodulation and demodulation[56] due to RFI is important to electronic circuit design engineers as well as systems engineers who must meet stringent RFI performance specifications on electronic equipment. The predication of nonlinear effects using computer-aided design (CAD)[55] techniques can be especially useful to such circuit designers. This is the subject of this dissertation.

Although other nonlinear devices such as the junction field effect transistor (JFET) and metal-oxide-semiconductor field effect transistor (MOSFET) are used in integrated circuits, the bipolar junction transistor (BJT) remains the most widely used nonlinear device in integrated circuits. Unfortunately, when compared with the other devices, the BJT due to its inherent emitter-base junction nonlinearity[8,18] generates more distortions and is more susceptible to nonlinear effects when operated in multiple-signal RFI environments. Based upon different mathematical approaches which include the Volterra series,[31] the perturbation method,[33,34,35,37] and the Picard

* The term distortion will be used to describe a wide variety of nonlinear effects in electronic circuits such as the production of harmonic frequency terms and intermodulation products (IMP's).

iteration method,[57] the engineering literature includes many models that can be used to study the nonlinearities of the BJT. One such model is the integral charge control model (ICM),[11,15,16,36] and another is the nonlinear T-model.[33] In this dissertation the use of Nonlinear Circuit Analysis Program (NCAP) which incorporates the nonlinear T-model for the BJT and uses the Volterra series approach for the distortion analysis is described.[39,58,59] The program NCAP has been developed through the joint efforts of government, industry and university in order to provide the EMC community with a useable procedure for analysing electronic equipment operated in a multi-signal RFI environment.

The Volterra series representation for nonlinear components in electronic circuits has proved to be a useful analysis tool in the calculation of distortion. Since transistor distortion is frequency dependent, a memory-less power series expression is inadequate. However, the Volterra series is a generalization of the power series. When analyzing distortions in electronic circuits, it offers the distinct advantage of being able to characterize a frequency dependent system, which includes nonlinear components with memory.[33]

Appropriate nonlinear models for BJT analysis have to be chosen in order to predict accurately the actual transistor operation. However, there is tradeoff between the accuracy of device simulation and the complexity of the model. In NCAP, the nonlinear T-model, being a second-level transistor model, has been demonstrated to be an appropriate model for the calculation of distortion. In addition,

the 16 model parameters in the T-model can be easily extracted from measurements;[39] thus the nonlinear T-model can be used with relative ease.

As indicated by the literature, very little has been reported upon on RFI effects in BJT integrated circuits. The object of this dissertation is to study the RFI effects in BJT integrated circuit amplifiers by using NCAP.[37,60] Both NCAP and the Simulation Program with Integrated Circuit Emphasis (SPICE2) are used to demonstrate integrated circuit analysis.[3,4] The user-oriented programs NCAP and SPICE2 use frequency domain analysis to predict linear and nonlinear effects in electronic circuits. Although these two programs are both capable of distortion analysis, the program NCAP by using the Volterra series approach to calculate nonlinear transfer functions for a given system gives more accurate results for the nonlinear effect. The program SPICE2 is used mainly to find the dc operating points for the transistors in the integrated circuits and to predict the linear performance of the circuits. Two typical BJT integrated circuits are selected for the RFI study. One integrated circuit amplifier uses a CA3026 dual differential pair in a broadband cascode amplifier. The differential pair is selected because it is the basic building block in bipolar linear integrated circuits. The other integrated circuit amplifier uses a 741 operational amplifier in a unity gain voltage follower circuit. The 741 op amp is selected because it is the most widely used bipolar linear integrated circuit. To verify the NCAP RFI analyses the NCAP calculated results are compared to experimental results.

This dissertation is organized in the following manner. In Chapter Two transistor models are discussed. In Chapter Three measurement techniques for determining BJT model parameters are presented. The techniques described in Chapter Three are used to determine the parameter values for the BJT's in the CA3026 differential pair and 741 operational amplifier. The procedures and results are described in Chapter Four. In Chapter Five the fundamental procedures used for nonlinear system analysis are presented. Two examples of the basic nonlinear system analysis procedures are given in Chapter Six. One example involves a single stage junction field effect transistor (JFET) in a broadband amplifier circuit. The other example involves a bipolar junction transistor (BJT) in a tuned RF amplifier circuit. In Chapter Seven measured and predicted results for RFI effects in integrated circuits are compared. Briefly the computer program NCAP is used to calculate second-order transfer functions for the CA3026 differential pair in a broadband amplifier configuration and for the 741 op amp in the unity gain voltage follower configuration. The second-order transfer function calculated is directly related to the low frequency signal that appears at the IC output terminals when an amplitude modulated RF signal is incident upon the IC input terminals. A summary and conclusion is given in Chapter Eight.

CHAPTER TWO

TRANSISTOR MODELS AND PARAMETERS

The bipolar junction transistor (BJT) in integrated circuit (IC) form is easy to fabricate and occupies less space than a resistor or capacitor. Thus, the BJT in an IC costs less than a resistor or a capacitor in an IC. This development has brought a new era in electronic circuits. Now transistors rather than conventional components (resistors, capacitors, and inductors) are used predominantly. As a result the BJT has become one of the most widely used active devices in integrated circuits.[1,2]

The purpose of this chapter is to review several transistor models used in linear and nonlinear analysis of the BJT in integrated circuits. The most important model used in this dissertation is the NCAP nonlinear T-model. The NCAP nonlinear T-model is essentially a small signal incremental model. The nonlinear T-model parameters depend upon the transistor dc operating point. Therefore, an EMC engineer who wishes to use the program NCAP to analyze an electronic circuit containing BJT's must first perform a dc analysis. For an electronic circuit containing several active devices such as linear IC's, the use of an electronic circuit analysis program such as SPICE2 or SCEPTRE to perform the dc analysis is recommended. For this reason, the BJT models used in SPICE2 and SCEPTRE will be discussed. Furthermore, information on the BJT model parameters used in SPICE2 and SCEPTRE can be used to determine many (but not all) of the NCAP model parameters.[3,4,5]

The NCAP nonlinear T-model is an incremental model suitable for analyzing mild nonlinear effects in electronic circuits; for that reason, a review of linear incremental models for small signal analysis is presented. In particular how the NCAP nonlinear T-model corresponds to the widely used hybrid-pi model will be shown. Then the transition to the nonlinear T-model which is a nonlinear incremental (or ac) model is presented.

2.1 DC Characteristics and Large Signal Models

In this section the large signal models used in the electronic circuit analysis programs SPICE2 and SCEPTRE are described. These computer programs can be used to determine the dc operating point of all diodes and transistors in a linear bipolar integrated circuit. The operating point information is one of the inputs required by the computer program NCAP which is used to calculate RFI effects in linear bipolar IC's.

2.1.1 The Basic Ebers-Moll Model[6]

Under usual operating condition, the dc current-voltage characteristic of BJT's can be described by the basic Ebers-Moll model. Using the standard IEEE notation for the BJT terminal currents and voltages given in Appendix *I*, these dc current-voltage relationships are

$$I_E = -I_{ES}\,(\exp(qV'_{BE}/kT)-1) + \alpha_I I_{CS}(\exp(qV'_{BC}/kT)-1) \qquad (2\text{-}1)$$

$$I_C = -I_{CS}\,(\exp(qV'_{BC}/kT)-1) + \alpha_N I_{ES}(\exp(qV'_{BE}/kT)-1) \qquad (2\text{-}2)$$

where the Ebers-Moll model parameters are defined as follows*:

* Additional Ebers-Moll model parameters used in the computer program SCEPTRE are the ideality factors Ref and Rcf for the emitter-base and collector base junctions. These factors appear in the denominater of the exponents in Eqs. (2-1) and (2-2).

I_{ES}: emitter-base saturation current

I_{CS}: collector-base saturation current

α_N: large-signal forward-injection common-base short-circuit current gain

α_I: large-signal reverse-injection common-base short-circuit current gain

R_{SE}: emitter ohmic resistance

R_{SC}: collector ohmic resistance

R_B: base ohmic resistance

q: magnitude electronic charge

k: Boltzmann's constant

T: absolute temperature

β_N: large-signal forward-injection common-emitter short-circuit current gain

β_I: large-signal reverse-injection common-emitter short-circuit current gain

I_S: saturation current

where the junction voltages V_{BE}' and V_{BC}' are related to the terminal voltages by the expressions

$$V_{BE}' = V_{BE} + I_E R_{SE} - I_B R_B \tag{2-3}$$

$$V_{BC}' = V_{BC} + I_C R_{SC} - I_B R_B \tag{2-4}$$

The Ebers-Moll model for a NPN transistor is illustrated in Figure 2-1.

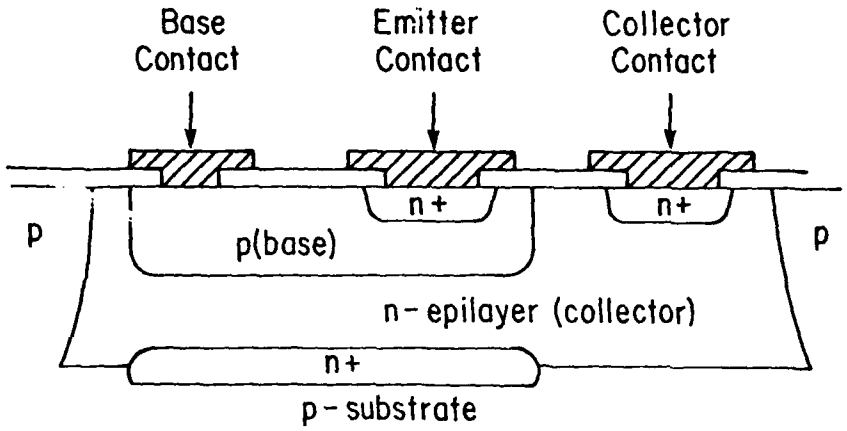

(a)

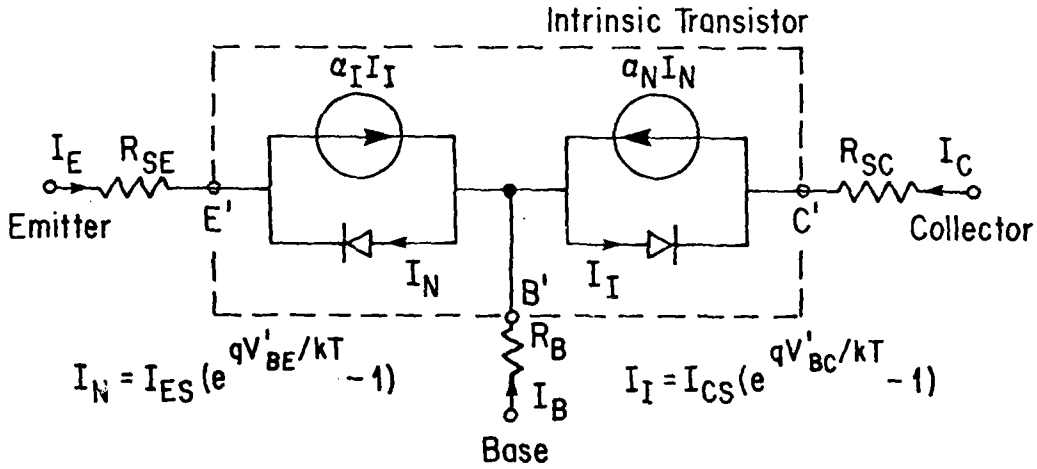

(b)

FIGURE 2-1 (a) Physical Structure for the NPN Transistor

(b) Basic Ebers-Moll Model for the NPN Transistor

In the forward active region, where emitter-base junction is forward biased and the collector-base junction is reverse biased, the Ebers-Moll model equations can be approximated as

$$I_E = - I_{ES} \exp(qV_{BE}'/kT) \tag{2-5}$$

$$I_C = \alpha_N I_{ES} \exp(qV_{BE}'/kT) \tag{2-6}$$

Since the dc base current is given by $I_B = -I_C - I_E$, the base current I_B can be written as

$$I_B = (1-\alpha_N)\ I_{ES} \exp(qV_{BE}'/kT) \tag{2-7}$$

We define the saturation current I_S and parameters β_N and β_I by:

$$I_S = I_{ES}\ \alpha_N = I_{CS}\ \alpha_I \tag{2-8}$$

$$\beta_N = \alpha_N/(1-\alpha_N) \tag{2-9}$$

$$\beta_I = \alpha_I/(1-\alpha_I) \tag{2-10}$$

Equations (2-1) and (2-2) can be written as

$$I_E=I_S\{[\exp(qV_{BC}'/kT)-1]-[\exp(qV_{BE}'/kT)-1]\}-(1/\beta_N)I_S[\exp(qV_{BE}'/kT)-1] \tag{2-11}$$

$$I_C=I_S\{[\exp(qV_{BE}'/kT)-1]-[\exp(qV_{BC}'/kT)-1]\}-(1/\beta_I)I_S[\exp(qV_{BC}'/kT)-1] \tag{2-12}$$

Based upon Eqs. (2-11) and (2-12) the basic Ebers-Moll model shown in Figure 2-1(b) can be recast into the π-model illustrated in Figure 2-2.

2.1.2 Early Effect[7]

The basic Ebers-Moll model should be modified to include the Early effect. J. M. Early described the dependence of α_N (α_I) upon collector-base voltage. This dependence is related to the dependence of base width upon collector voltage. This base-width modulation effect can cause a non-zero output conductance g_o in the BJT, i.e.

$$g_o = \partial I_C/\partial V_{CE}\Big|_{I_B} = I_B(\partial\alpha_N/\partial V_{CE}\Big|_{I_B})/(1-\alpha_N)^2 \neq 0 \qquad (2\text{-}13)$$

To account for the base-width modulation effect, the Early voltage is introduced. The Early voltage V_A is determined as shown in Figure 2-3. The Ebers-Moll π-model equation for I defined in Figure 2-2 is thus modified and becomes

$$I = -I_S\{[\exp(qV_{BC}'/kT)-1]-[\exp(qV_{BE}'/kT)-1]\}[1-V_{BC}'/V_A] \qquad (2\text{-}14)$$

2.1.3 Diffusion Capacitances and Junction Capacitances[8]

The large signal models in SPICE2 and SCEPTRE also account for the stored charges in the BJT. In modeling the stored charges in transistors, diffusion and junction capacitances both have to be considered. A suitable model is shown in Figure 2-4 with the capacitances defined as

C_{je}: emitter-base junction capacitance

C_b: emitter-base diffusion capacitance

C_{jc}: collector-base junction capacitance

C_d: collector-base diffusion capacitance

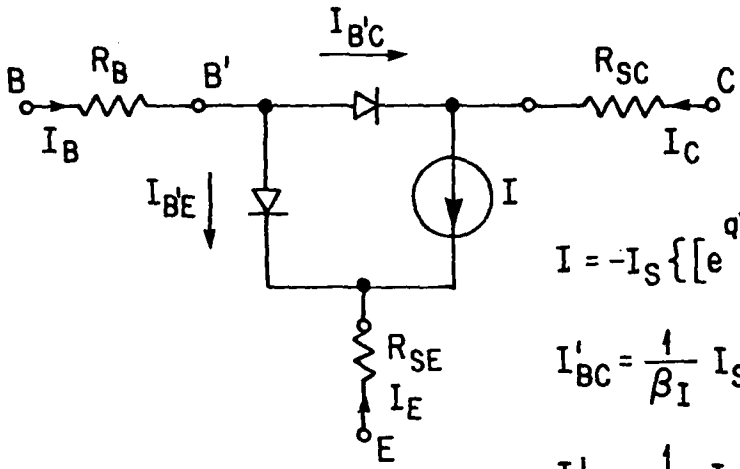

$$I = -I_S\left\{\left[e^{qV'_{BC}/kT} - 1\right] - \left[e^{qV'_{BE}/kT} - 1\right]\right\}$$

$$I'_{BC} = \frac{1}{\beta_I} I_S\left[e^{qV'_{BC}/kT} - 1\right]$$

$$I'_{BE} = \frac{1}{\beta_N} I_S\left[e^{qV'_{BE}/kT} - 1\right]$$

FIGURE 2-2 Ebers-Moll Model in π-Version

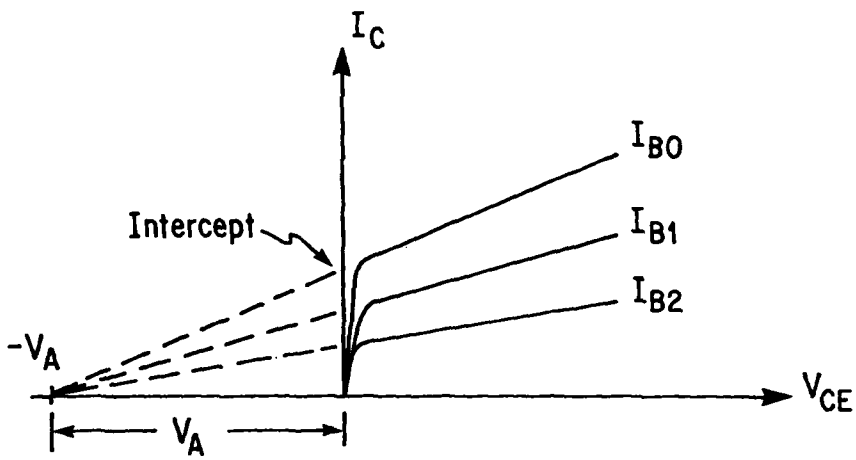

FIGURE 2-3 Diagram Illustrating How the Early Voltage V_A of a BJT is Determined

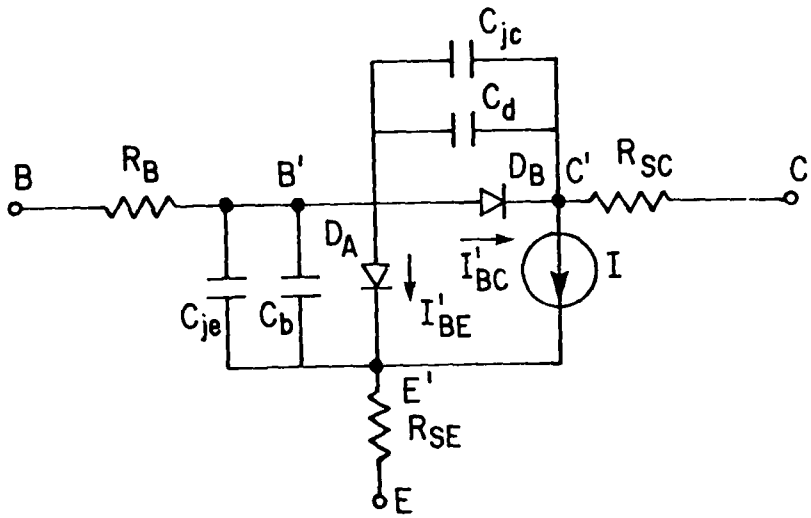

FIGURE 2-4 Large Signal Transistor Model in π-Version

The nonlinear charge stored in the base-emitter region is denoted by Q_{BE} and in the base-collector region is denoted by Q_{BC}. These are given by

$$Q_{BE} = \tau_F I_S[\exp(qV_{BE}'/kT)-1] + C_{jeo}\int_o^{V_{BE}'} (1-(V/\Phi_E))^{-m_e} dV \quad (2\text{-}15)$$

$$Q_{BC} = \tau_R I_S[\exp(qV_{BC}'/kT)-1] + C_{jco}\int_o^{V_{BC}'} (1-(V/\Phi_C))^{-m_c} dV \quad (2\text{-}16)$$

When the individual terms in the charge expressions are differentiated with respect to the appropriate junction voltage, we obtain the following expressions for the capacitances:

$$C_{je} = C_{jeo}\ (1-(V_{BE}'/\Phi_E))^{-m_e} \quad (2\text{-}17)$$

$$C_{jc} = C_{jco}\ (1-(V_{BC}'/\Phi_C))^{-m_c} \quad (2\text{-}18)$$

$$C_b = \tau_F(qI_S/kT)\exp(qV_{BE}'/kT) \approx \tau_F q|I_C|/kT \quad (2\text{-}19)$$

$$C_d = \tau_R(qI_S/kT)\exp(qV_{BC}'/kT) \approx \tau_R q|I_E|/kT \quad (2\text{-}20)$$

where the symbols introduced have the following definitions:

C_{jeo}: emitter-base junction capacitance at zero bias

C_{jco}: collector-base junction capacitance at zero bias

m_e: emitter-base capacitance exponent

m_c: collector-base capacitance exponent

Φ_E: emitter-base built-in potential

Φ_C: collector-base built-in potential

τ_F: forward transit time

τ_R: reverse transit time

In Eq. (2-19) the relationship $C_b \approx \tau_F\, q|I_C|/kT$ is valid when the BJT is operated in the normal region, and in Eq. (2-20) the relationship $C_d \approx \tau_R q|I_E|/kT$ is valid when the BJT is operated in the inverse region.

2.1.4 Bias Dependance of Current Gain[9,10]

The computer program NCAP accounts for the variation in the dc common-emitter short-circuit current gain parameter β_N (h_{FE} in NCAP).

The dc common-emitter short-circuit current gain parameter β_N varies with the value of the dc collector current I_C. At low collector current levels generation-recombination processes in the collector-base depletion region causes a decrease in β_N values. At high collector currents high-level injection effects in the neutral-base region cause a decrease in β_N. At high collector current levels there may also be an increase in the width of the neutral-base region. (This effect is called base push-out.) In the computer program NCAP the dependance of the parameter β_N (called h_{FE} in NCAP) is accounted for by the empirical relationship:

$$\beta_N = h_{FE} = h_{FEmax}/(1+a \log^2(I_C/I_{Cmax})) \qquad (2\text{-}21)$$

where h_{FEmax} is the maximum beta value and I_{Cmax} is the collector current level at which $\beta_N = h_{FEmax}$.

2.1.5 Impact Ionization[11,12]

The computer program NCAP also accounts for avalanche effects in the collector-base junction. The collector current for uniform avalanche multiplication in the collector base depletion region is given by

$$I_C = - \alpha_N M I_E \tag{2-22}$$

where M the multiplication factor is given empirically by

$$M = 1/(1-(V_{CB}/V_{CBO})^{\eta}) \tag{2-23}$$

The parameter V_{CBO} is the open-emitter common-base breakdown voltage and the exponent η is a constant of the order of 2 to 4 for silicon. At low collector-base voltages M is close to unity, and it increases as the voltage increases.

Under the open-base common-emitter condition, collector-emitter voltages will reach a breakdown voltage V_{CEO} at which the current I_C(or I_E) is limited only by the external resistance in the circuit.

The emitter-base breakdown voltage V_{CEO} is given by

$$V_{CEO} = V_{CBO}\ (1-\alpha_N)^{1/\eta} \tag{2-24}$$

For high gain transistors, the breakdown voltage of V_{CEO} is usually much less than V_{CBO}. The parameters V_{CBO} and η are used in NCAP but not in SPICE2 or SCEPTRE. These parameters can also be determined from the BJT common-emitter characteristics using Eq. (2-24).

2.1.6 High Current Effects[13,14]

At high current levels the basic Ebers-Moll current-voltage equations have to be modified to account for additional effects. One effect is called the base push-out effect. The base push-out effect is associated with the excessive amount of forward diffusion charges stored in the base region. These charges cause a shift in the location of the collector-base depletion layer region. Another effect at high current levels is the conductivity modulation effect. The high level of the injected minority carriers in the base region causes an increase in the base material conductivity, and an increase in the recombination rate in the base region. The base push-out effect and the conductivity modulation effect both contribute to the decrease in the parameter β_N (h_{FE}) at high current levels. In NCAP the decrease in the parameter β_N (h_{FE}) is accounted for by using Eq. (2-21). In the basic Ebers-Moll model used in SPICE2 and SCEPTRE, these effects are not accounted for at all. However, in SPICE2 a more complete BJT model called the Integral Charge Control Model (ICM) is available, and this model does account for high level injection by introducing additional model parameters.[15,16]

2.1.7 Temperature Effects[1]

The actual BJT junction temperature is a significant parameter. In some computer programs such as SPICE2, the BJT operating temperature T can be specified. In other computer programs such as NCAP, the junction operating temperature can not be specified directly. Fortunately, a

subterfuge can be used to account for the junction temperature T in the expression $(qV'_{BE}/(Ref)kT)$. The parameter Ref called the diode non-ideality factor can be modified to account for a junction temperature different from 300 K. For example if the actual values are T = 390 K and Ref = 1.0, the values T = 300 K and Ref = 1.3 can be used. The main point is that the product (Ref)·(kT) has the same value. This subterfuge does not account for the temperature variations in the parameters h_{FEmax} and I_{Cmax} which account for the variations in β_N (h_{FE}) with I_C. The BJT junction tempeature T can be estimated from data provided by the manufacturer for a small signal transistor such as a 2N918. The junction temperature T is estimated to increase 1 ^{o}C per milliwatt dissipated power. For a higher power transistor such as a 2N5109, the junction temperature increase is estimated to be 0.2 ^{o}C per milliwatt dissipated power.

2.2 Linear Dynamic Characteristics and Small Signal Models

As stated previously the NCAP nonlinear T-model is an incremental (ac) model suitable for analyzing mild nonlinear effects in integrated circuits. Before discussing the NCAP nonlinear T-model it seems desirable to review the linear incremental models frequently used for small signal analysis. In this way it is possible to show how the NCAP nonlinear T-model corresponds to the linear T-model and the widely used hybrid-pi model.

If the BJT is considered as a two port network, different representations such as y-parameters, z-parameters, h-parameters, and s-parameters, etc., can be used to predict the linear dynamic behavior

of the BJT. The adequacy of the modelling and the ease of determining the model parameters often determine how frequently these models are used by engineers.

Among the different representations, the y-parameter representation can be converted quite easily into a T-model small signal equivalent circuit. Since the T-model is used in the computer program NCAP in the analysis of BJT's, the derivations for both the low and high frequency T-models are briefly reviewed in this section. Also presented is the hybrid-pi model used in the computer analysis program SPICE2.

2.2.1 Linear T-Model at Low Frequencies

The linear T-model will be developed first for the intrinsic transistor. *Intrinsic transistor large signal models can be obtained* from the large signal models shown in Figures 2-1(b), 2-2 and 2-4 by setting the parasitic resistances R_B, R_{SE}, and R_{SC} equal to zero. Then the external transistor terminals E, B, and C and the internal model nodes E', B', and C' are identical as shown in Figure 2-5.

Using the notation given in Appendix I, the y-parameter representation for an intrinsic transistor in the common-base configuration is given as

$$i_e = y_{ib}v_{eb} + y_{rb}v_{cb} \tag{2-25}$$

$$i_c = y_{fb}v_{eb} + y_{ob}v_{cb} \tag{2-26}$$

where i_e, v_{eb} and i_c, v_{cb} are intrinsic small signal currents and voltages for the internal emitter-base and collector-base junctions

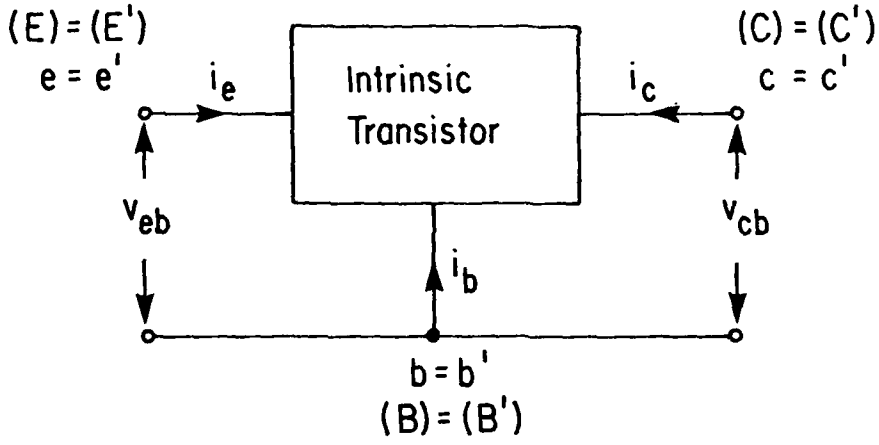

FIGURE 2-5 Small-Signal Voltages and Currents for an Intrinsic Transistor. For the Intrinsic Transistor the Parasitic Resistances R_B, R_{SE}, and R_{SC} Are Zero

respectively. (See Figure 2-5.) The symbol ' is used to denote intrinsic voltages. In the intrinsic transistor model the ohmic resistances R_{SE}, R_B, and R_{SC} illustrated in Figure 2-1 are omitted. The conventional circuit model used to illustrate the y-parameter is given in Figure 2-6. Using Thevenin's theorem, the small signal equivalent circuit shown in Figure 2-7 is obtained from Figure 2-6. Using Figures 2-6 or 2-7, the standard definition for the y-parameters can be given. Using standard IEEE notation for the total instantaneous variables, the equations defining y-parameters can be written as

$$y_{ib} = \partial i_E / \partial v'_{EB} \Big|_{v'_{CB} = V'_{CB}} \tag{2-27}$$

$$y_{rb} = \partial i_E / \partial v'_{CB} \Big|_{v'_{EB} = V'_{EB}} \tag{2-28}$$

$$y_{fb} = \partial i_C / \partial v'_{EB} \Big|_{v'_{CB} = V'_{CB}} \tag{2-29}$$

$$y_{ob} = \partial i_C / \partial v'_{CB} \Big|_{v'_{EB} = V'_{EB}} \tag{2-30}$$

The total instantaneous emitter current i_E and collector current i_C are given by

$$i_E = I_E + \frac{d}{dt}(Q_{BE}) \tag{2-31}$$

$$i_C = I_C + \frac{d}{dt}(Q_{BC}) \tag{2-32}$$

If the Early effect is not considered, we can find the y-parameters using Eqs. (2-1), (2-2), (2-15), and (2-16). When the BJT is operated in the normal region at low frequencies, the results are

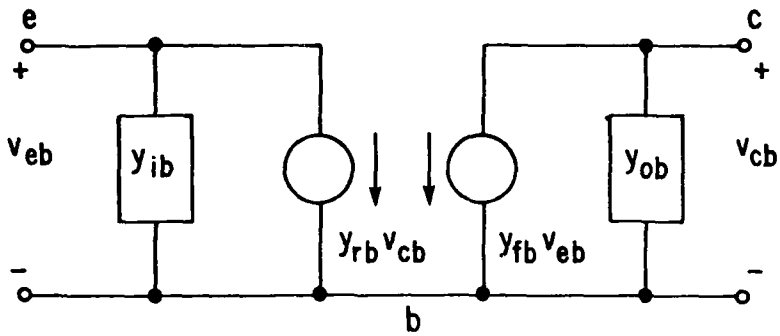

FIGURE 2-6 Conventional Circuit Model Illustrating y-Parameters

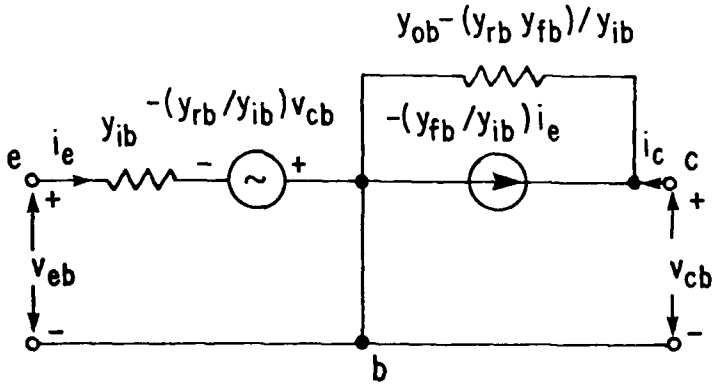

FIGURE 2-7 Small Signal Equivalent Circuit in Turns of Admittances

$$y_{ib} = q \mid I_E \mid /(kT) \qquad (2\text{-}33)$$

$$y_{rb} = \alpha_I I_{CS} \exp(qV'_{BC}/kT)\, q/(kT) \simeq 0 \qquad (2\text{-}34)$$

$$y_{fb} = \alpha_N q \mid I_E \mid /(kT) \qquad (2\text{-}35)$$

$$y_{ob} = I_{CS} \exp(qV'_{BC}/kT) q/(kT) \qquad (2\text{-}36)$$

$$\simeq 0$$

where Eqs. (2-33) - (2-36) are obtained without considering the capacitive effects.

If the Early effect (the base-width modulation effect) is considered, the magnitudes of admittances y_{rb} and y_{ob} have to be modified. However, the magnitudes of y_{ib} and Y_{fb} remain the same because they are not affected by the Early effect. The corrections for the Early effect can be obtained using the circuit shown in Figure 2-2 to obtain expressions for the dc collector current I_C and emitter current I_E. Using Eq. (2-14) for the current I illustrated in Figure 2-2, the approximate expressions for the dc collector current I_C and emitter current I_E at normal operating conditions for the BJT are

$$I_C = -I_S(\exp(qV'_{EB}/kT)(1-V_{BC}/V_A) \qquad (2\text{-}37)$$

$$I_E = -I_S(\exp(qV'_{EB}/kT))(1-V'_{BC}/V_A)(1+1/\beta_N) \qquad (2\text{-}38)$$

Next using the definitions for y_{rb} and y_{ob} given by Eqs. (2-28) and (2-30), the following results are obtained:

$$y_{ib} = 1/r_e \tag{2-39}$$

$$y_{rb} \simeq I_C/V_A \tag{2-40}$$

$$y_{fb} = \alpha_N/r_e \tag{2-41}$$

$$y_{ob} \simeq I_C/V_A \tag{2-42}$$

where the resistance parameter r_e is defined by

$$r_e = kT/q|I_E| \tag{2-43}$$

It is noted that the Early effect adds a nonzero real part to y_{rb} and y_{ob}.

The next step in developing the linear T-model equivalent circuit is to use Eqs. (2-39), (2-40), (2-41), and (2-42) to obtain expressions for the circuit elements shown in Figure 2-7. The resulting expressions are

$$y_{ib} = 1/r_e \tag{2-44}$$

$$(-y_{rb}/y_{ib})\ v_{cb} \simeq -\ (I_C/V_A)r_e\ v_{cb} \tag{2-45}$$

$$y_{ob}-y_{rb}y_{fb}/y_{ib} \simeq 1/r_c \tag{2-46}$$

$$(-y_{fb}/y_{ib})\ i_e = \alpha_N i_e \tag{2-47}$$

where the resistance parameter r_c is defined by

$$r_c = (V_A/I_C)/(1-\alpha_N) \tag{2-48}$$

and the voltage parameter v_a is defined by

$$v_a = -(I_C/V_A)\ r_e \tag{2-49}$$

The next step in developing the linear T-model is to insert the capacitors C_b, C_d, C_{je}, and C_{jc} to account for the energy storage elements in the transistor. The resulting linear T-model is shown in Figure 2-8(a). The collector capacitor C_d is neglected because C_d is small compared to the capacitance C_{jc} in the collector-base junction when the transistor is operated in the normal region. Equations (2-45) (2-46) and (2-47) are valid only at frequencies where y_{ib} and y_{ob} are real. Equation (2-44) is valid up to frequencies where the transistor short-circuit current gain approaches unity, however, Equation (2-46) appears valid at frequencies only up to near 10 MHz. In order to obtain the linear T-model used in NCAP, shown in Figure 2-8(b) it is necessary to ignore the voltage source v_a in the emitter-base branch. This is valid only when the Early voltage V_A is sufficiently large.

2.2.2 Linear T-Model at High Frequencies

At high frequencies, neither the parasitic resistances nor capacitances can be ignored. The high frequency equivalent circuit including parasitic elements developed by Abraham is shown in Figure 2-9. In Figure 2-9, the capacitances C_1, C_2, and C_3 represent direct parasitic capacitances between the various transistor terminals, and the resistances r_b', r_c', and r_e' represent bulk parasitic resistances in series with the intrinsic transistor terminals. These parasitic elements can also be added to the basic linear T-model shown in Figure 2-8. Thus, these parasitic elements can be easily incorporated into NCAP as external elements. The significant difference between the basic

T-model shown in Figure 2-8 and Abraham's model shown in Figure 2-9 is that the base diffusion capacitance C_b in Figure 2-8 is replaced by a series R-C combination. In this way Abraham's model accounts for the transit time effect in the neutral base region. For additional information on this model the reader is referred to Abraham's original paper.[17]

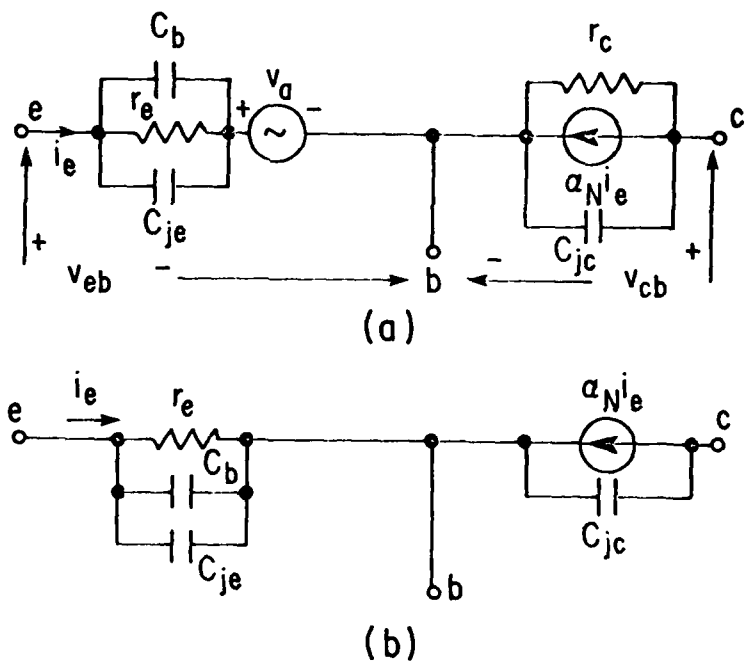

FIGURE 2-8 Low to Medium Frequency Equivalent Circuits for BJT's (a) Large Early Effect Model (b) Small Early Effect Model

2.2.3 Linear Hybrid-Pi Equivalent Circuit

The linear hybrid-pi equivalent circuit is used in the computer program SPICE2 to calculate the linear small signal performance of BJT circuits. The linear incremental hybrid-pi model shown in Figure 2-10 can be developed from the large signal π-model shown in Figure 2-4. In Figure 2-10 the resistors r_μ and r_π are the dynamic resistances of the diodes D_A and D_B shown in Figure 2-4. The transconductance parameter g_m is essentially the derivative $\partial I/\partial V_{BE}$ where I is given by Eq. (2-14). The resistance parameter r_o arises from the base-width modulation effect, and the value of r_o is approximately equal to r_μ/β_N. Detailed derivations of the hybrid-pi model can be found in Ref. (18).

The hybrid-pi model can be shown to be equivalent to the linear T-model for the usual case where the resistance r_μ is large. To establish this equivalence the internal collector current i_c at low frequencies can be written as:

$$i_c = g_m v_{be}$$

$$= g_m i_b r_\pi \qquad (2\text{-}50)$$

Next substituting $i_c = \beta_N i_b$ into Eq. (2-50), we have

$$g_m = \beta_N / r_\pi \qquad (2\text{-}51)$$

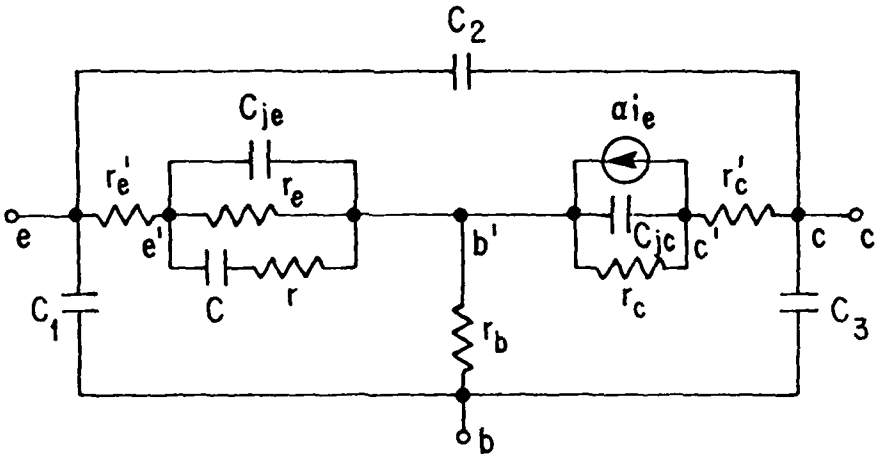

FIGURE 2-9 High Frequency Equivalent Circuit for Parasitic Elements Included

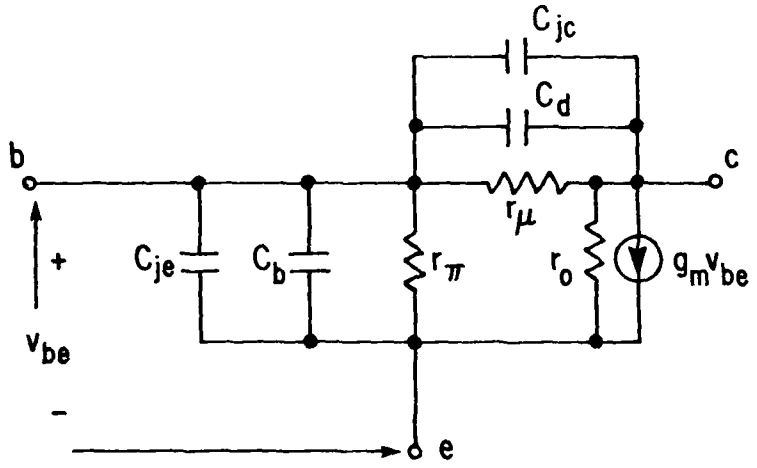

FIGURE 2-10 Linear Incremental Hybrid-Pi Model

Next the emitter current i_e can be written as

$$i_e = i_c + i_b$$

$$= g_m v_{be} + v_{be}/r_\pi$$

$$= (1 + \beta_N)\ v_{be}/r_\pi \qquad (2\text{-}52)$$

Defining the resistance r_π by the equation

$$r_\pi = r_e(1 + \beta_N) \qquad (2\text{-}53)$$

$$i_e = v_{be}/r_e \qquad (2\text{-}54)$$

and using Eqs. (2-51) and (2-54), we obtain

$$i_c = g_m v_{be}$$

$$= \beta_N v_{be}/r_\pi$$

$$= \beta_N v_{be}/(r_e(1 + \beta_N))$$

$$= \alpha_N v_{be}/r_e \qquad (2\text{-}55)$$

where $$\alpha_N = \beta_N/(1 + \beta_N) \qquad (2\text{-}56)$$

Equations (2-54) and (2-55) demonstrate the equivalence between the hybrid-pi model and the T-model. The parameters g_m and r_π in the hybrid-pi model transform to the parameters α_N and r_e in the linear T-model. The capacitive elements are identically the same in each model.

2.3 Quasi-Linear Incremental Models

When the amplitudes of the signal variations are sufficiently small, the linear incremental models just presented are valid. When the amplitudes of the signal variations are very large, the large signal Ebers-Moll model should be used. Of interest to us is the intermediate case where the amplitudes of the signal variations are not large compared to the dc values of the transistor currents and voltages but are large enough to cause weak nonlinear effects. This case is often called the quasi-linear case. Recall that the derivation for the linear model was based upon the expressions for the y-parameters given by the Eqs. (2-27) to (2-30). The y-parameters expressions included only the first-order derivatives of the total terminal currents with respect to the total terminal voltages. To account for weak nonlinear effects the higher-order derivatives (such as second-order and third-order) will be considered. (Although in this dissertation only the second and the third-order derivatives will be considered, the computer program NCAP includes derivatives of order greater than the third-order.)

Before presenting detailed mathematical expressions, it is instructive to show the circuit configuration of the nonlinear-incremental models for the BJT. First let us consider a nonlinear-incremental π-model which is based upon the large signal π-model shown in Figure 2-4. In Figure 2-4 the π-model currents I'_{BE}, I'_{BC} and I can be expressed in terms of a Taylor series. The number of terms included in the Taylor series depends upon the order of the distortion analysis

to be performed. Shown in Figure 2-11 is a nonlinear incremental π-model with three current generators. Each current generator corresponds to the appropriate Taylor series expansion for the current generators I'_{BC}, I'_{BE} and I. (The dc components are omitted.) Although several investigators have used this model, it is not the model used in NCAP.[19,20,21] The NCAP nonlinear incremental T-model is shown in Figure 2-12.

As presented in Figure 2-12, the nonlinear T-model differs from the linear incremental T-model shown in Figure 2-8 in the following aspects:

1. The base-emitter resistor r_e has been replaced by the nonlinear incremental current generator $K(v_2)$ for the base-emitter junction exponential nonlinearity. (The node voltages V_1, V_2 and V_3 are illustrated in Figure 2-12.)
2. The collector capacitances C_{jc} and C_d have been replaced by the nonlinear incremental current generator $\gamma_c(v_3-v_2)$.
3. The linear dependent current source $\alpha_N v_2/r_e$ has been replaced by the nonlinear incremental dependent current generator $g(v_2,v_3-v_1)$ which includes both the h_{FE} nonlinearity and the avalanche nonlinearity.
4. The emitter capacitances C_{je} and C_b have been represented by the nonlinear incremental current generator $\gamma_e(v_2)$.
5. Parasitic elements shown in Figure 2-9 such as the bulk resistances r_e' and r_c' and the parasitic capacitance C_2 between emitter and collector terminals are not included in the model. They may be added as external components by the NCAP user.

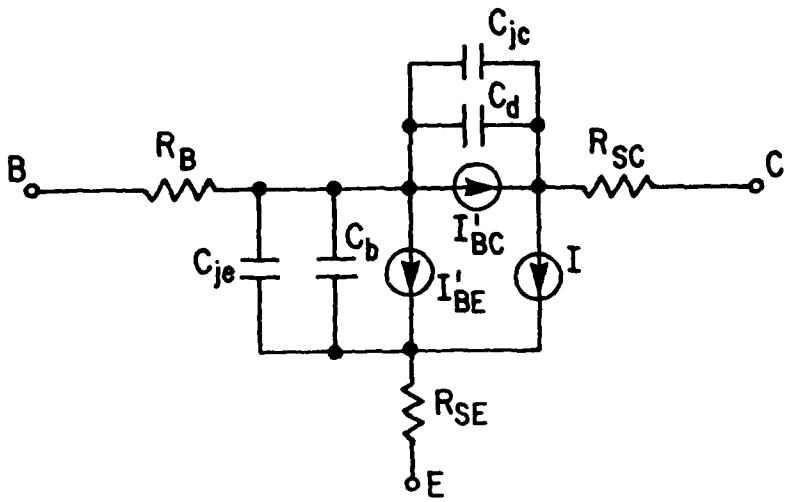

FIGURE 2-11. Nonlinear Incremental π-Model. Note that the Nonlinear Behavior of Capacitors Is not Explicitly Expressed in this Model.

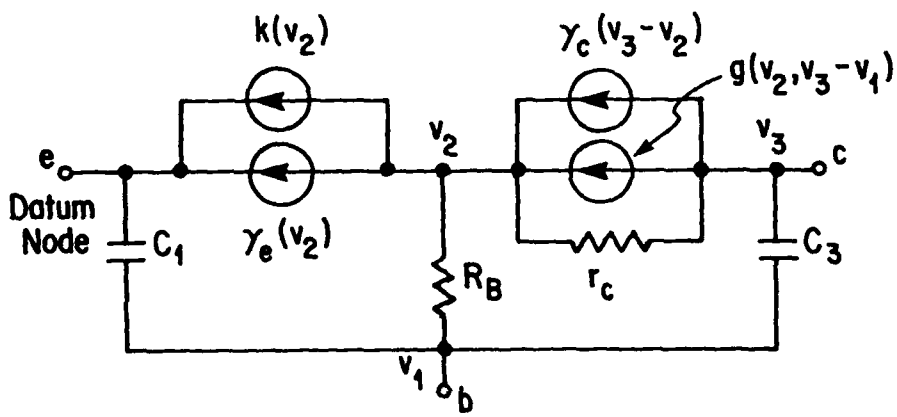

FIGURE 2-12. Nonlinear Incremental T-Model. Note that the Emitter Is Assumed to Be the Datum Node.

In the remainder of this section we shall derive expressions for three of the four nonlinear current generators in the NCAP nonlinear incremental T-model. Specifically expressions for the current generators $K(v_2)$, $\gamma_c(v_3 - v_2)$ and $g(v_2, v_3 - v_1)$ will be presented up to the third order. An expression for the current generator $\gamma_e(v_2)$ is derived in Section 3.2.2. However, the computer program NCAP does account for all four current generators. The nonlinear current generators in the NCAP nonlinear T-model exhibit three of the four basic nonlinear components available in NCAP. The four basic nonlinear components available in NCAP are the nonlinear resistor, the nonlinear capacitor, the nonlinear inductor and the nonlinear voltage-dependent current source. We shall begin with a discussion of the basic nonlinear components. Then we shall consider the NCAP nonlinear T-model current generators.

2.3.1 Nonlinear Resistor

A nonlinear resistor can be characterized by a current-voltage relationship $i_R(v_R)$. We can expand the nonlinear characteristic current i_R about its dc operating point (I_R, V_R) as follows:

$$\begin{aligned} i_R = I_R &+ (\partial i_R/\partial v_R\big|_{v_R = V_R})(v_R - V_R) \\ &+ (1/2)(\partial^2 i_R/\partial v_R^2\big|_{v_R = V_R})(v_R - V_R)^2 \\ &+ (1/6)(\partial^3 i_R/\partial v_R^3\big|_{v_R = V_R})(v_R - V_R)^3 \\ &+ \text{higher-order terms} \end{aligned} \tag{2-57}$$

Let us express the incremental resistor current i_r by $i_r = i_R - I_R$ and the incremental voltage v_r by $v_r = v_R - V_R$. From Eq. (2-57) we obtain

$$i_r = K_1 v_r + K_2 v_r^2 + K_3 v_r^3 + \text{higher-order terms} \qquad (2\text{-}58)$$

where

$$K_1 = \partial i_R / \partial v_R \big|_{v_R = V_R} \qquad (2\text{-}59)$$

$$K_2 = (1/2)(\partial^2 i_R / \partial v_R^2 \big|_{v_R = V_R}) \qquad (2\text{-}60)$$

$$K_3 = (1/6)(\partial^3 i_R / \partial v_R^3 \big|_{v_R = V_R}) \qquad (2\text{-}61)$$

2.3.2 Nonlinear Capacitor

A nonlinear capacitor can be characterized by a charge-voltage relationship $q_C(v_C)$, where q_C is the charge stored in the capacitor, and v_C is the voltage across the capacitor. The Taylor series expansion for the charge about its dc operating point is

$$\begin{aligned} q_C = Q_C &+ (\partial q_C / \partial v_C \big|_{v_C = V_C})(v_C - V_C) \\ &+ (1/2)(\partial^2 q_C / \partial v_C^2 \big|_{v_C = V_C})(v_C - V_C)^2 \\ &+ (1/6)(\partial^3 q_C / \partial v_C^3 \big|_{v_C = V_C})(v_C - V_C)^3 \\ &+ \text{higher-order terms} \end{aligned} \qquad (2\text{-}62)$$

Let the incremental charge $q_c = q_C - Q_C$ and the incremental voltage $v_c = v_C - V_C$. Then the charge q_c is given by

$$q_c = C_1 v_c + C_2 v_c^2 + C_3 v_c^3 + \text{higher-order terms} \qquad (2\text{-}63)$$

and the incremental capacitor current dq_c/dt is given by

$$i_c = C_1(dv_c/dt) + C_2(dv_c^2/dt) + C_3(dv_c^3/dt)$$

$$+ \text{ higher-order terms} \tag{2-64}$$

where

$$C_1 = \partial q_C/\partial v_C\big|_{v_C = V_C} \tag{2-65}$$

$$C_2 = (1/2)(\partial^2 q_C/\partial v_C^2\big|_{v_C = V_C}) = (1/2)(\partial C_1/\partial V_C) \tag{2-66}$$

$$C_3 = (1/6)(\partial^3 q_C/\partial v_C^3\big|_{v_C = V_C}) = (1/6)(\partial^2 C_1/\partial V_C^2) \tag{2-67}$$

2.3.3 Nonlinear Inductor

A nonlinear inductor can be characterized by a current-flux relationship $i_L(\phi_L)$ where i_L is the current through the inductor and ϕ_L is the stored inductor flux. The Taylor series expansion of $i_L(\phi_L)$ about its dc operating point is

$$i_L = I_L + (\partial i_L/\partial \phi_L\big|_{\phi_L=\Phi_L})(\phi_L - \Phi_L)$$

$$+ (1/2)(\partial^2 i_L/\partial \phi_L^2\big|_{\phi_L = \Phi_L})(\phi_L - \Phi_L)^2$$

$$+ (1/6)(\partial^3 i_L/\partial \phi_L^3\big|_{\phi_L = \Phi_L})\ (\phi_L - \Phi_L)^3$$

$$+ \text{ higher-order terms} \tag{2-68}$$

Let the incremental flux $\phi_\ell = \phi_L - \Phi_L$ and the incremental inductor current $i_\ell = i_L - I_L$. Then Eq. (2-68) becomes

$$i_\ell = \gamma_1\phi_\ell + \gamma_2\phi_\ell^2 + \gamma_3\phi_\ell^3 + \text{ higher-order terms} \tag{2-69}$$

where

$$\gamma_1 = \partial i_L/\partial\phi_L\Big|_{\phi_L = \Phi_L} \tag{2-70}$$

$$\gamma_2 = (1/2)(\partial^2 i_L/\partial\phi_L^{\,2}\Big|_{\phi_L = \Phi_L}) \tag{2-71}$$

$$\gamma_3 = (1/6)(\partial^3 i_L/\partial\phi_L^{\,3}\Big|_{\phi_L = \Phi_L}) \tag{2-72}$$

2.3.4 Nonlinear Dependent Current Source

A nonlinear dependent current source is illustrated in Figure 2-13:

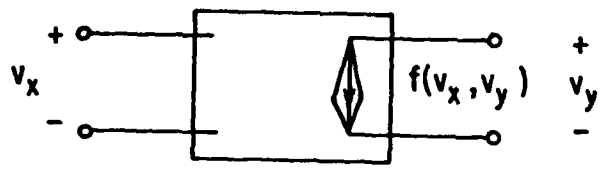

FIGURE 2-13. Nonlinear Dependent Current Source

The nonlinear dependent current source $f(v_X, v_Y)$ is dependent upon voltages v_X and v_Y. If we expand the current source $f(v_X, v_Y)$ about its dc operating point (V_X, V_Y), we obtain

$$f = f_{dc} + (\partial f/\partial v_X\big|_{(v_X,v_Y) = (V_X,V_Y)})(v_X - V_X)$$

$$+ (\partial f/\partial v_Y\big|_{(v_X,v_Y) = (V_x,V_Y)})(v_Y - V_Y)$$

$$+ (1/2)(\partial^2 f/\partial v_X{}^2\big|_{(v_X,v_Y) = (V_X,V_y)})(v_X - V_X)^2$$

$$+ (1/2)(\partial^2 f/\partial v_Y{}^2\big|_{(v_X,v_Y) = (V_X,V_Y)})(v_Y - V_Y)^2$$

$$+ (\partial^2 f/\partial v_X \partial v_Y\big|_{(v_x,v_Y) = (V_X,V_Y)})(v_X - V_X)(v_Y - V_Y)$$

$$+ \text{higher-order terms} \tag{2-73}$$

The incremental voltages v_x and v_y are given by $v_x = v_X - V_X$ and $v_y = v_Y - V_Y$, and the incremental current i_y is given by $i_y = f - f_{dc}$. Then Eq. (2-73) becomes

$$i_y = G(v_x, v_y)$$

$$= g_{10}v_x + g_{01}v_y + g_{20}v_x{}^2 + g_{02}v_y{}^2 + g_{11}v_x v_y$$

$$+ \text{higher-order terms}$$

$$= \sum_{m,n} g_{mn} v_x{}^m v_y{}^n \qquad m,n = 0,1,2,\ldots \qquad g_{oo} = 0 \tag{2-74}$$

where

$$g_{10} = (\partial f/\partial v_X\big|_{(v_X,v_Y) = (V_X,V_Y)}) \tag{2-75}$$

$$g_{01} = (\partial f/\partial v_Y\big|_{(v_X,v_Y) = (V_X,V_Y)}) \tag{2-76}$$

$$g_{20} = (1/2)(\partial^2 f/\partial v_X{}^2\big|_{(v_X,v_Y) = (V_X,V_Y)}) \tag{2-77}$$

$$g_{02} = (1/2)(\partial^2 f/\partial v_Y{}^2\big|_{(v_X,v_Y) = (V_X,V_Y)}) \tag{2-78}$$

$$g_{11} = (\partial^2 f/\partial v_X \partial v_Y\big|_{(v_X,v_Y) = (V_X,V_Y)}) \tag{2-79}$$

$$g_{30} = (1/6)(\partial^3 f/\partial v_X{}^3\big|_{(v_X,v_Y) = (V_X,V_Y)}) \tag{2-80}$$

$$g_{21} = (1/6)(\partial^3 f/\partial v_X{}^2 \partial v_Y\big|_{(v_X,v_Y) = (V_X,V_Y)}) \tag{2-81}$$

$$g_{12} = (1/6)(\partial^3 f/\partial v_X \partial v_Y{}^2\big|_{(v_X,v_Y) = (V_X,V_Y)}) \tag{2-82}$$

$$g_{03} = (1/6)(\partial^3 f/\partial v_Y{}^3\big|_{(v_X,v_Y) = (V_X,V_Y)}) \tag{2-83}$$

2.3.5 The Nonlinear Current Generator $K(v_2)$ and the Emitter-Base Nonlinear Resistive Coefficients

If the transistor is operated in the normal region, the total instantaneous emitter current i_E expressed by Eq. (2-5) can be approximated at low frequencies as

$$i_E = -I_{ES}\exp(qv_{BE}/RefkT) \tag{2-84}$$

where the ideality factor Ref used in NCAP and SCEPTRE has been included. Using a Taylor's series expansion about the operating point (I_E, V_{BE}), Equation (2-84) can be expanded as

$$i_E = I_E + \sum_{n=1}^{\infty}(1/n!)(v_{BE} - V_{BE})^n(\partial^n i_E/\partial v_{BE}{}^n\big|_{(v_{BE} = V_{BE})}) \tag{2-85}$$

We define the nonlinear current generator $K(v_2)$ using the relationships

$$K(v_2) = i_E - I_E \tag{2-86}$$

$$v_2 = v_{BE} - V_{BE} \tag{2-87}$$

where we continue to assume the emitter is the datum node.

Fron Eqs. (2-57) and (2-58), we obtain

$$K(v_2) = \sum_{n=1}^{\infty}(1/n!)v_2{}^n(\partial^n i_E/\partial v_{BE}{}^n\big|_{(v_{BE} = V_{BE})}) \tag{2-88}$$

The nonlinear coefficients K_1, K_2, and K_3 (Eqs. (2-59)-(2-61)) are given by

$$K_1 = \partial i_E/\partial v_{BE}\Big|(v_{BE} = V_{BE})$$

$$= (q/RefkT)I_E \tag{2-89}$$

$$K_2 = (1/2)(\partial^2 i_E/\partial v_{BE}{}^2)\Big|(v_{BE} = V_{BE})$$

$$= (1/2)(q/RefkT)^2 I_E \tag{2-90}$$

$$K_3 = (1/6)(\partial^3 i_E/\partial v_{BE}{}^3)\Big|(v_{BE} = V_{BE})$$

$$= (1/6)(q/RefkT)^3 I_E \tag{2-91}$$

2.3.6 The Nonlinear Current Generator $\gamma_c(v_3 - v_2)$ and the Collector-Base Nonlinear Capacitance Coefficients

When the BJT is operated in the normal region and when the magnitude of the collector-base voltage is large, the collector base capacitance term given by the sum of Eqs. (2-18) and (2-20) can be approximated as

$$C_{BC} \cong k\left|V_{CB}\right|^{-m_c} \tag{2-92}$$

where k is the scale factor, m_c the capacitance exponent, and V_{CB} the reverse bias voltage of the base-collector junction. Note that the assumption $|V_{CB}|>>|\Phi_C|$ is being made.

Referring to Eq. (2-64), the capacitance nonlinearity can be represented by a current source

$$\gamma_c(v_3 - v_2) = C_1(d(v_3 - v_2)/dt) + C_2(d(v_3 - v_2)^2/dt)$$

$$+ C_3(d(v_3 - v_2)^3/dt) + \text{higher-order terms} \quad (2\text{-}93)$$

with the nonlinear coefficients defined by Eqs. (2-65) - (2-67). Note that the coefficient C_1 in Eq. (2-65) is identical to the capacitance C_{BC} given by Eq. (2-92). The collector-base nonlinear capacitance coefficients are given by

$$C_1 = k\left|V_{CB}\right|^{-m_c} \quad (2\text{-}94)$$

$$C_2 = -(1/2)km_c\left|V_{CB}\right|^{-m_c - 1} \quad (2\text{-}95)$$

$$C_3 = (1/6)km_c(m_c + 1)\left|V_{CB}\right|^{-m_c - 2} \quad (2\text{-}96)$$

2.3.7 The Nonlinear Current Generator $g(v_2, v_3 - v_1)$ and the Dependent Current Source Nonlinear Coefficients

From Eqs. (2-9), and (2-22), the total instantaneous collector current i_C can be related to the total instantaneous emitter current i_E in the following manner:

$$i_C(1 + h_{FE})/h_{FE} = Mi_E \quad (2\text{-}97)$$

Again, applying a Taylor series expansion at the operating point (V_{CB}, I_C) to both sides of the above equation, we obtain

$$i_C(1 + h_{FE})/h_{FE}\Big|_{(V_{CB}, I_C)} + \sum_{n=1}^{\infty} (1/n!)(i_C - I_C)^n$$

$$\cdot(\partial^n(i_C(1 + h_{FE})/h_{FE})/\partial i_C^{\,n}\Big|_{(V_{CB}, I_C)})$$

$$= (M\Big|_{(V_{CB}, I_C)} + \sum_{n=1}^{\infty}(1/n!)(v_{CB} - V_{CB})^n(\partial^n M/\partial v_{CB}^{\,n}\Big|_{(V_{CB}, I_C)})$$

$$\cdot (I_E + i_e) \quad (2\text{-}98)$$

Equation (2-23) for M is repeated below

$$M = 1/(1 - (V_{CB}/V_{CBO})^n) \qquad (2\text{-}23)$$

If we assume the current I_C varies slowly enough that capacitive effects are negligible, and also if we neglect the resistance r_c in the collector, then the nonlinear dependent current generator $g(v_2, v_3-v_1)$ is defined by the relationship

$$g(v_2,v_3 - v_1) = i_C - I_C \qquad (2\text{-}99)$$

where

$$v_3 - v_1 = v_{CB} - V_{CB} \qquad (2\text{-}100)$$

Next we equate the first order incremental terms on both sides of Eq. (2-98) and by using Eqs. (2-99) to (2-101) obtain the result

$$\sum_{n=1}^{\infty}(1/n!)g(v_2,v_3 - v_1)^n(\partial^n(i_C(1+h_{FE})/h_{FE})/\partial i_C{}^n\big|_{(V_{CB},I_C)})$$

$$=\sum_{n=1}^{\infty}(1/n!)(v_3 - v_1)^n(\partial^n M/\partial v_{CB}{}^n\big|_{(V_{CB},I_C)})I_E + Mi_e \qquad (2\text{-}102)$$

where higher-order terms in the expression Mi_e have been ignored.*

Now we define the parameters z and a_n by expressions

$$z = \sum_{n=1}^{\infty}(1/n!)(v_3 - v_1)^n(\partial^n M/\partial v_{CB}{}^n\big|_{(V_{CB},I_C)})I_E + Mi_e \qquad (2\text{-}103)$$

and $$a_n = (1/n!)(\partial^n(i_C(1 + h_{FE})/h_{FE})/\partial i_C{}^n\big|_{(V_{CB},I_C)}) \qquad (2\text{-}104)$$

Equation (2-102) becomes

$$\sum_{n=1}^{\infty} a_n g(v_2,v_3 - v_1)^n = z \qquad (2\text{-}105)$$

* Here only the first order incremental terms are considered for simplicity. This simplification is only true when the transistor is operated at a region far away from that of avalanche. A complete treatment which includes all higher-order terms can be found in Ref. (40).

Assuming that the power series expression given in Eq. (2-104) can be inverted, a compositional inverse power series in z can be expressed as

$$g(v_2, v_3 - v_1) = \sum_{n=1}^{\infty} b_n z^n \tag{2-106}$$

with

$$b_1 = a_1^{-1} \tag{2-107}$$

$$b_2 = -a_2/(a_1^3) \tag{2-108}$$

$$b_3 = (2a_2^2 - a_1 a_3)/(a_1^5) \tag{2-109}$$

If we are interested in the nonlinearity only up to the third order, Eq. (2-103) can be expressed as

$$z = (x_1(v_3 - v_1) + x_2(v_3 - v_1)^2 + x_3(v_3 - v_1)^3) I_E + M(K_1 v_2 + K_2 v_2^2 + K_3 v_2^3) \tag{2-110}$$

where we use Eq. (2-85) to approximate* the nonlinear incremental current i_e:

$$i_e = K(v_2) = K_1 v_2 + K_2 v_2^2 + K_3 v_2^3 \tag{2-111}$$

The derivatives x_1, x_2, and x_3 are defined by

$$x_1 = \partial M/\partial v_{CB}\Big|_{(V_{CB}, I_C)} \tag{2-112}$$

$$x_2 = (1/2)(\partial^2 M/\partial v_{CB}^2\Big|_{(V_{CB}, I_C)}) \tag{2-113}$$

$$x_3 = (1/6)(\partial^3 M/\partial v_{CB}^3\Big|_{(V_{CB}, I_C)}) \tag{2-114}$$

* The approximation is that the $\gamma_e(v_2)$ contribution to i_e is ignored. However, in the computer program NCAP the $\gamma_e(v_2)$ contribution is fully accounted for.

From Eq. (2-110) we obtain for the terms z^2 and z^3 the expressions

$$z^2 = M^2K_1^2v_2^2 + 2K_1x_1MI_Ev_2(v_3 - v_1) + x_1^2I_E^2(v_3 - v_1)^2$$

$$+ 2x_1x_2I_E^2(v_3 - v_1)^3 + 2K_1K_2M^2v_2^3 + 2K_2Mx_1I_E(v_3 - v_1)$$

$$\cdot\ v_2^2 + 2x_2K_1MI_E(v_3 - v_1)^2v_2 + \text{higher-order terms} \quad (2\text{-}115)$$

and $$z^3 = M^3K_1^3v_2^3 + x_1^3I_E^3(v_3 - v_1)^3 + 3M^2K_1^2x_1I_Ev_2^2(v_3 - v_1)$$

$$+ 3MK_1x_1^2I_E^2v_2(v_3 - v_1) + \text{higher-order terms} \quad (2\text{-}116)$$

Substituting Eqs. (2-110), (2-115) and (2-116) into (2-106), we obtain the following expression for the nonlinear current generator $g(v_2, v_3 - v_1)$

$$g(v_2, v_3 - v_1) = v_2b_1MK_1 + (v_3 - v_1)b_1x_1I_E + v_2^2(b_1MK_2$$

$$+ b_2M^2K_1^2) + (v_3 - v_1)^2(b_1x_2I_E + b_2x_1^2I_E^2)$$

$$+ 2v_2(v_3 - v_1)b_2K_1x_1MI_E + v_2^3(b_1MK_3$$

$$+ 2b_2K_1K_2M^2 + b_3M^3K_1^3) + (v_3 - v_1)^3(b_1x_3I_E$$

$$+ 2b_2x_1x_2I_E^2 + b_3x_1^3I_E^3) + v_2^2(v_3 - v_1)$$

$$\cdot\ (2b_2K_2Mx_1I_E + 3b_3M^2K_1^2x_1I_E) + v_2(v_3 - v_1)^2$$

$$\cdot\ (2b_2x_2K_1MI_E + 3b_3MK_1x_1^2I_E^2)$$

$$+ \text{higher-order terms}$$

$$= g_{10}v_2 + g_{01}(v_3 - v_1) + g_{20}v_2^2 + g_{11}v_2(v_3 - v_1)$$

$$+ g_{02}(v_3 - v_1)^2 + g_{30}v_2^3 + g_{21}v_2^2(v_3 - v_1)$$

$$+ g_{12}v_2(v_3 - v_1)^2 + g_{03}(v_3 - v_1)^3$$

$$+ \text{higher-order terms} \quad (2\text{-}117)$$

Therefore, the coefficients g_{ij} are given by*

$$g_{10} = b_1 M K_1 \tag{2-118}$$

$$g_{01} = b_1 I_E x_1 \tag{2-119}$$

$$g_{20} = b_1 M K_2 + b_2 M^2 K_1^{\ 2} \tag{2-120}$$

$$g_{02} = b_1 I_E x_2 + b_2 x_1^{\ 2} I_E^{\ 2} \tag{2-121}$$

$$g_{11} = 2 b_2 K_1 M x_1 I_E \tag{2-122}$$

$$g_{30} = b_1 M K_3 + 2 b_2 K_1 K_2 M^2 + b_3 M^3 K_1^{\ 3} \tag{2-123}$$

$$g_{21} = 2 b_2 K_2 M x_1 I_E + 3 b_3 M^2 K_1^{\ 2} x_1 I_E \tag{2-124}$$

$$g_{12} = 2 b_2 K_1 M x_2 I_E + 3 b_3 M K_1 x_1^{\ 2} I_E^{\ 2} \tag{2-125}$$

$$g_{03} = b_1 x_3 I_E + 2 b_2 x_1 x_2 I_E^{\ 2} + b_3 x_1^{\ 3} I_E^{\ 3} \tag{2-126}$$

At a given operating point (V_{CB}, I_C), all the coefficients defined in Sections (2.3.5) to (2.3.7) can be calculated when the NCAP parameters for a BJT are known. The NCAP parameters for a 2N5109 BJT were measured using the techniques to be described in the next chapter. The 2N5109 BJT parameter values are listed in Table 2-1. Using the parameters listed in Table 2-1, the nonlinear coefficents for 2N5109 BJT were calculated. The results are given in Table 2-2.

* As mentioned previously these expressions for g_{ij} are valid only when the transistor is operated at a region far away from that of avalanche - the usual situation. For transistors operated near the avalanche region, the complete expressions given by Weiner and Spina should be used. See Ref. (40).

TABLE 2-1

NCAP INPUT PARAMETERS FOR 2N5109 BJT

Parameter Name	Description	Value
η	Avalanche exponent	6.0
V_{CB} (V)	Collector base bias voltage	5.0
V_{CBO} (V)	Avalanche voltage	40.0
Mu	Collector capacitance exponent	0.285
I_C (mA)	Collector bias current	50.0
I_{Cmax} (mA)	Collector current at maximum Dc current gain	18.0
a	h_{FE} nonlinearity coefficient	0.363
h_{FEmax}	Maximum d.c. current gain	84.6
k ($pF\text{-}V^{1/2}$)	Collector capacitor scale factor	0.42
Ref	Diode nonlinearity factor	1.0
C_{je} (pF)	Base-emitter junction space charge capacitance	10.0
C'_2 (pF/mA)	Derivative of base-emitter diffusion capacitance	3.6
r_b (Ω)	Base resistance	15
r_c ($k\Omega$)	Collector resistance	32.9
C_1 (pF)	Base-emitter capacitance	0.1
C_3 (pF)	Base-collector and overlap capacitance	0.56

TABLE 2-2

NONLINEAR COEFFICIENTS FOR 2N5109 BJT

Nonlinear Incremental Current Generator	Coefficient	Value
	K_1 (mho)	1.9724
$K(v_2)$	K_2 (mho/V)	38.419
	K_3 (mho/V^2)	498.87
	C_1 (F)	0.26549×10^{-12}
$\gamma_C(V_3-V_2)$	C_2 (F/V)	-0.75664×10^{-14}
	C_3 (F/V^2)	0.64819×10^{-15}
	g_{01} (mho)	0.22851×10^{-6}
	g_{10} (mho)	1.9446
	g_{02} (mho/V)	0.11426×10^{-6}
	g_{20} (mho/V)	37.754
$g(V_2,V_3-V_1)$	g_{11} (mho/V)	-0.28734×10^{-7}
	g_{03} (mho/V^2)	0.30475×10^{-7}
	g_{30} (mho/V^2)	487.88
	g_{12} (mho/V^2)	-0.14367×10^{-7}
	g_{21} (mho/V^2)	-0.2718×10^{-6}

CHAPTER THREE

MEASUREMENT OF BJT MODEL PARAMETERS

In the previous chapter large signal BJT models used in SPICE2 and SCEPTRE were discussed. These models can be used to determine the dc operating point information for the individual diodes and transistors in bipolar integrated circuits. The dc operating point information is required by the program NCAP used to predict RFI effects in bipolar IC's. Also discussed were linear incremental models for BJT's. These models included the linear π-model and the linear T-model used in NCAP. Also discussed was the nonlinear T-model used in NCAP. All these models contain parameters which must be specified. In this chapter, the experimental techniques used to measure the important model parameters will be presented. The data processing techniques used to extract the model parameters and certain parasitic elements from experimental results will also be presented.

This chapter is organized in the following manner. First dc and pulse techniques used to determine many of the large signal model parameters will be described. Then the small signal techniques used to determine many of the incremental model parameters will be presented. Finally for completeness transient techniques useful in determining other model parameters will be given. At the end of this chapter, a table is presented which contains values for the 2N5179 and 2N918 BJT parameters used in the computer programs SPICE2, SCEPTRE and NCAP.

3.1 Large Signal Parameter Measurements

3.1.1 I_{ES}, Emitter Base Junction Saturation Current and Ref, Emitter Base Junction Diode Nonideality Factor

The saturation current I_{ES} and parameter Ref are determined from active region measurements of the emitter base junction voltage as a function of emitter current. The test configuration used in obtaining the emitter-base characteristics is shown in Figure 3-1. Shown in Figure 3-1(a) is a dc measurement method useful when the emitter current I_E is less than 0.1 mA. For I_E values greater than 5 mA, the pulse method shown in Figure 3-1(b) is recommended. Below 5 mA the pulse method was difficult to carry out. Consequently the curve for currents between 0.1 mA and 5 mA is interpolated from the results of the two methods. The equipment illustrated in Figure 3-1 is standard laboratory equipment.

Typical data are plotted in Figure 3-2. For $-I_E < 0.1$ mA the dc data points are observed to lie on a straight line. For $-I_E > 0.1$ mA, increases in the junction temperatures cause the dc data points to deviate from the straight line drawn through the dc data points for $-I_E < 0.1$ mA. Now let us examine the pulse data at $-I_E > 1$ mA; the parasitic base spreading resistance R_B and parasitic emitter resistance R_{SE} have a significant effect. The voltage drop across these resistors cause the pulse data to lie to the right of the straight line drawn through the dc data obtained for $-I_E < 0.1$ mA.

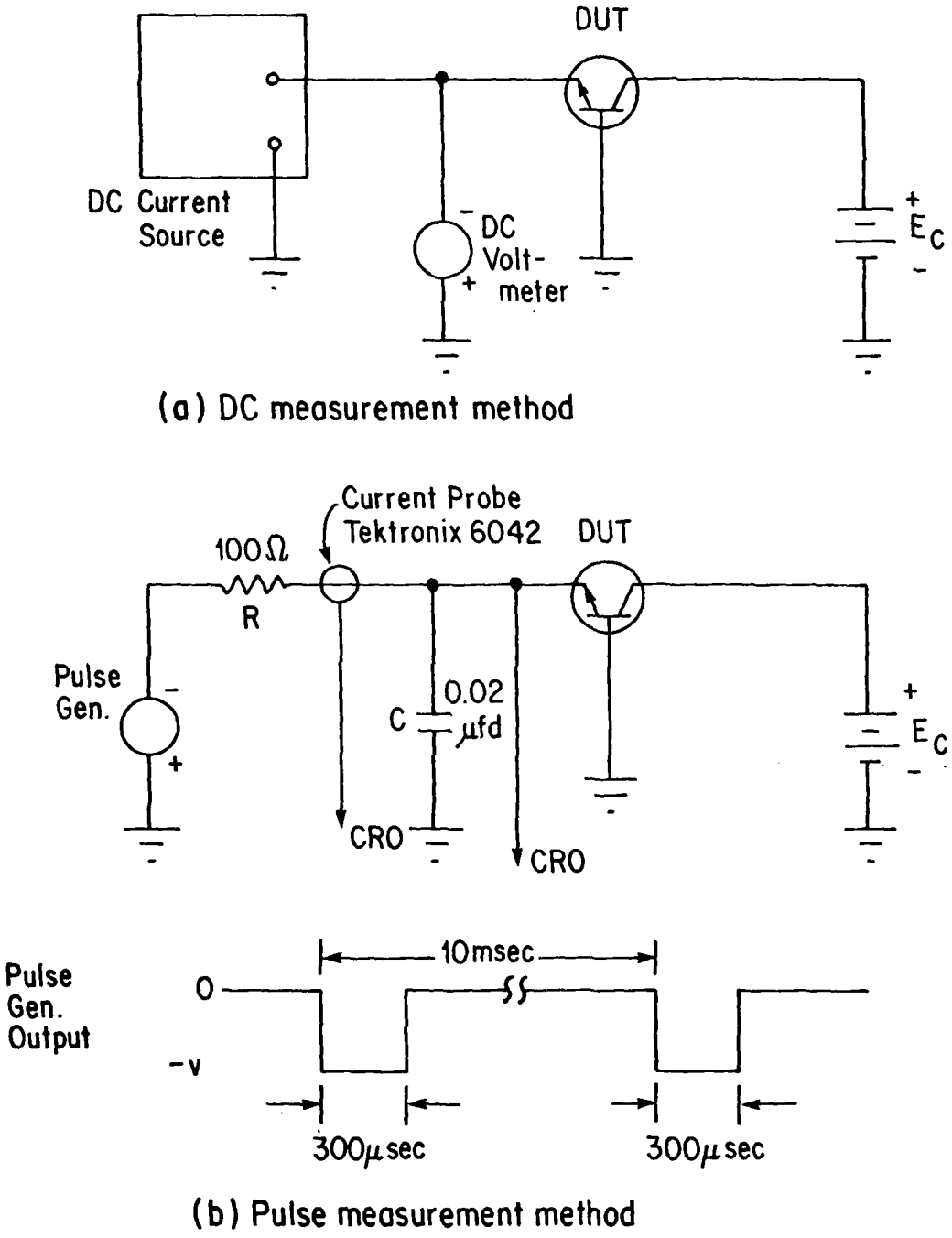

FIGURE 3-1 Transistor Base-Emitter Characteristic Test Configuration (a) for Low Currents and (b) for High Currents

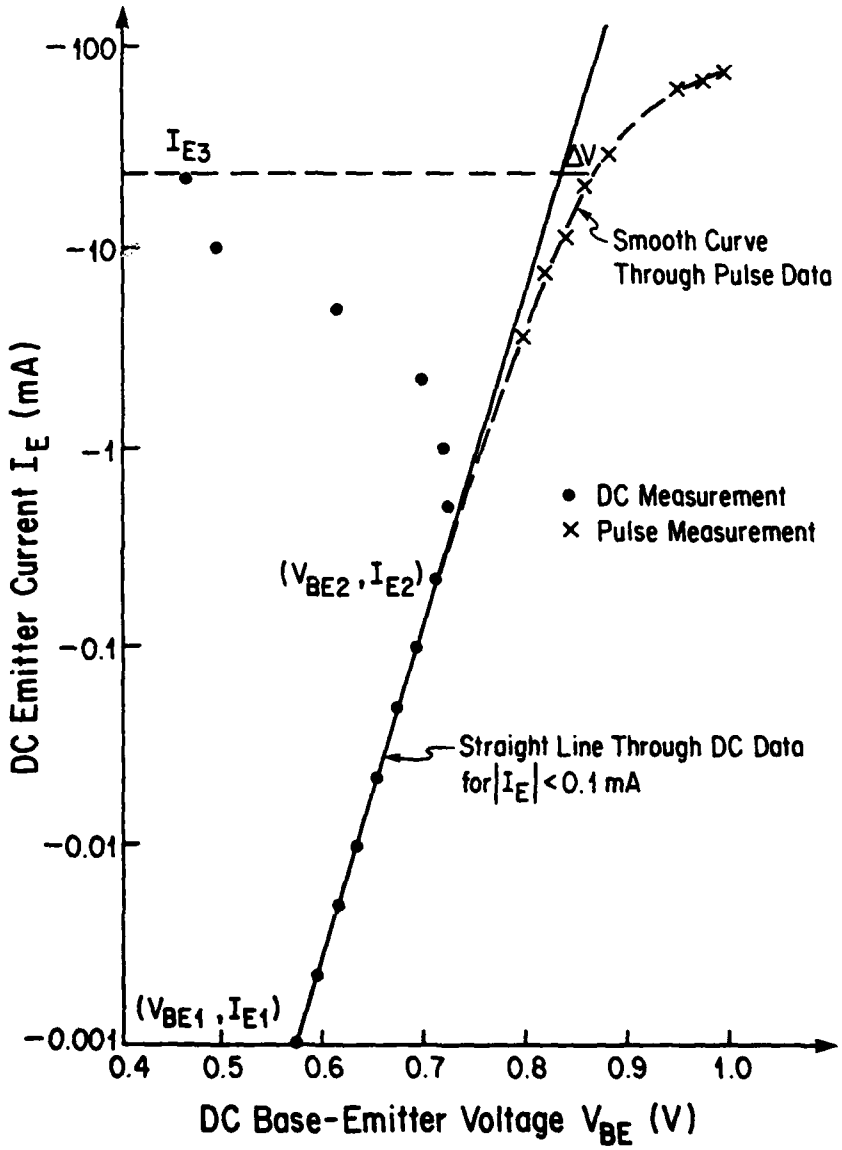

FIGURE 3-2 I_E Versus V_{BE} Plot for a 2N5179 Device

At I_E values low enough, the voltages drops across the parasitic resistances R_B and R_{SE} can be neglected. Then under normal operating conditions Eq. (2-5) relating the emitter current I_E to the base-emitter voltage V_{BE} can be written as

$$I_E = -I_{ES}\exp(qV_{BE}/RefkT) \qquad (3\text{-}1)$$

where the parameter Ref used in NCAP and SCEPTRE has been inserted.

The emitter base junction coefficient Ref is calculated by evaluating Eq. (3-1) at two points (i.e. (V_{BE1},I_{E1}) and (V_{BE2},I_{E2})) on the straight line portion of the log I_E vs V_{BE} plot shown in Figure 3-2. The equation used to calculate the parameter Ref is

$$Ref = (\ell n(I_{E1}/I_{E2})/(V_{BE1} - V_{BE2}))q/kT \qquad (3\text{-}2)$$

Solving Eq. (3-1) for the saturation current I_{ES}, we obtain

$$I_{ES} = -I_E/\exp(qV_{BE}/RefkT) \qquad (3\text{-}3)$$

The saturation current I_{ES} is determined by evaluating Eq. (3-3) at any point (V_{BE},I_E) on the straight line portion of log I_E versus V_{BE} plot shown in Figure 3-2.

3.1.2 I_{CS}, Collector Base Junction Saturation Current and Rcf, Collector Base Junction Diode Nonideality Factor

The saturation current I_{CS} and diode nonideality factor Rcf are determined in a manner similar to that used in the previous section except that the emitter and collector terminals are interchanged.

(The transistor is actually operated in the region known as inverse region.) Since only low current level measurements are needed, pulse measurements are not required. The dc measurement test configuration is shown in Figure 3-3. Typical data are shown in Figure 3-4.

As shown in Figure 3-4 a straight line is drawn through the dc data at low I_C values. Points on this straight line are used to determine values for parameters Rcf and I_{CS}. The procedures used are identical to those described in Section 3.1.1. The equations used are

$$Rcf = (\ln(I_{C1}/I_{C2})/(V_{BC1} - V_{BC2}))q/kT \qquad (3\text{-}4)$$

and

$$I_{CS} = I_{C1}/(\exp(qV_{BC1}/RcfkT) - 1) \qquad (3\text{-}5)$$

where the points (V_{BC1}, I_{C1}) and (V_{BC2}, I_{C2}) lie on the straight line shown in Figure 3-4.

3.1.3 I_S, Transistor Saturation Current

When the transistor is operated in its normal active region at low current levels so that the voltages across the parasitic resistance R_B and R_{SE} are negligible, the collector current expressed by Eq. (2-12) can be written as

$$I_C = I_S(\exp(qV_{BE}/RefkT) - 1) \qquad (3\text{-}6)$$

Again the emitter-base diode nonideality factor Ref has been introduced. The parameter I_S (Ref is assumed known) can be determined using the procedures described in Section 3.1.1. Values of the dc

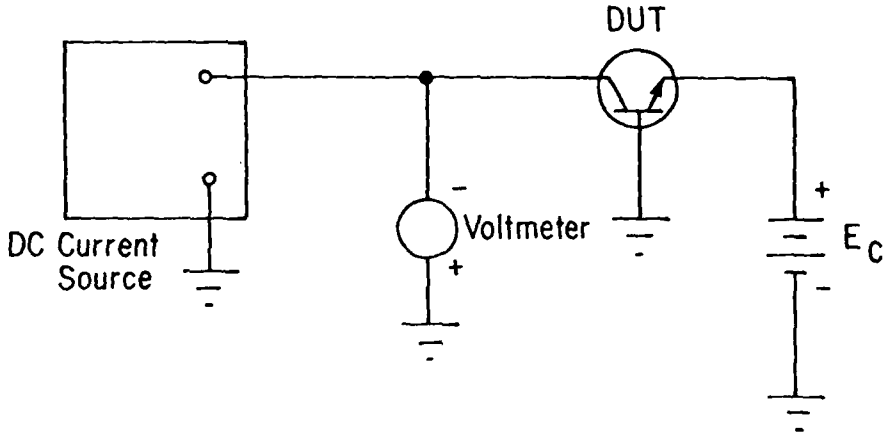

FIGURE 3-3 Transistor Base-Collector Characteristic Test Configuration

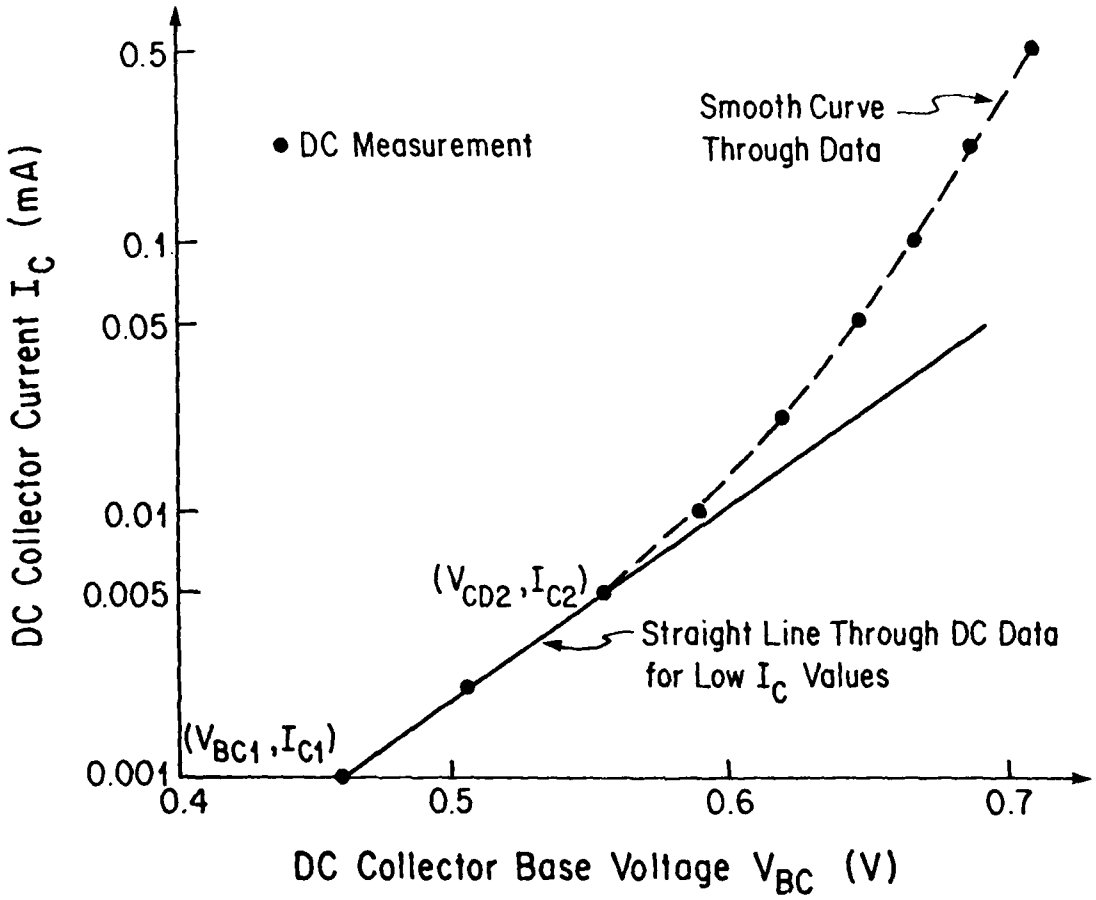

FIGURE 3-4 I_C Versus V_{BC} Plot for a 2N5179 Device

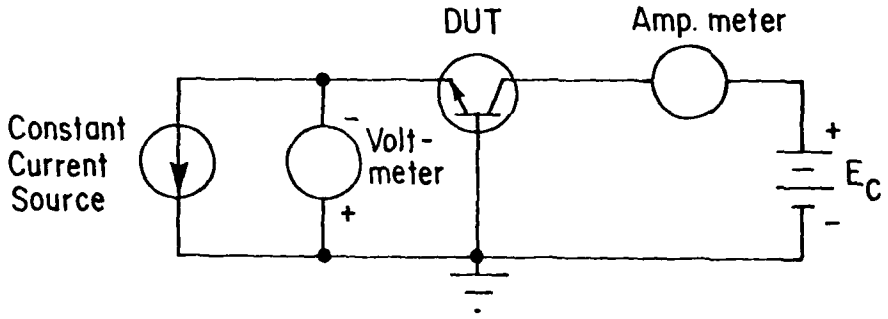

FIGURE 3-5 Transistor I_C Versus V_{BE} Characteristic Test Configuration

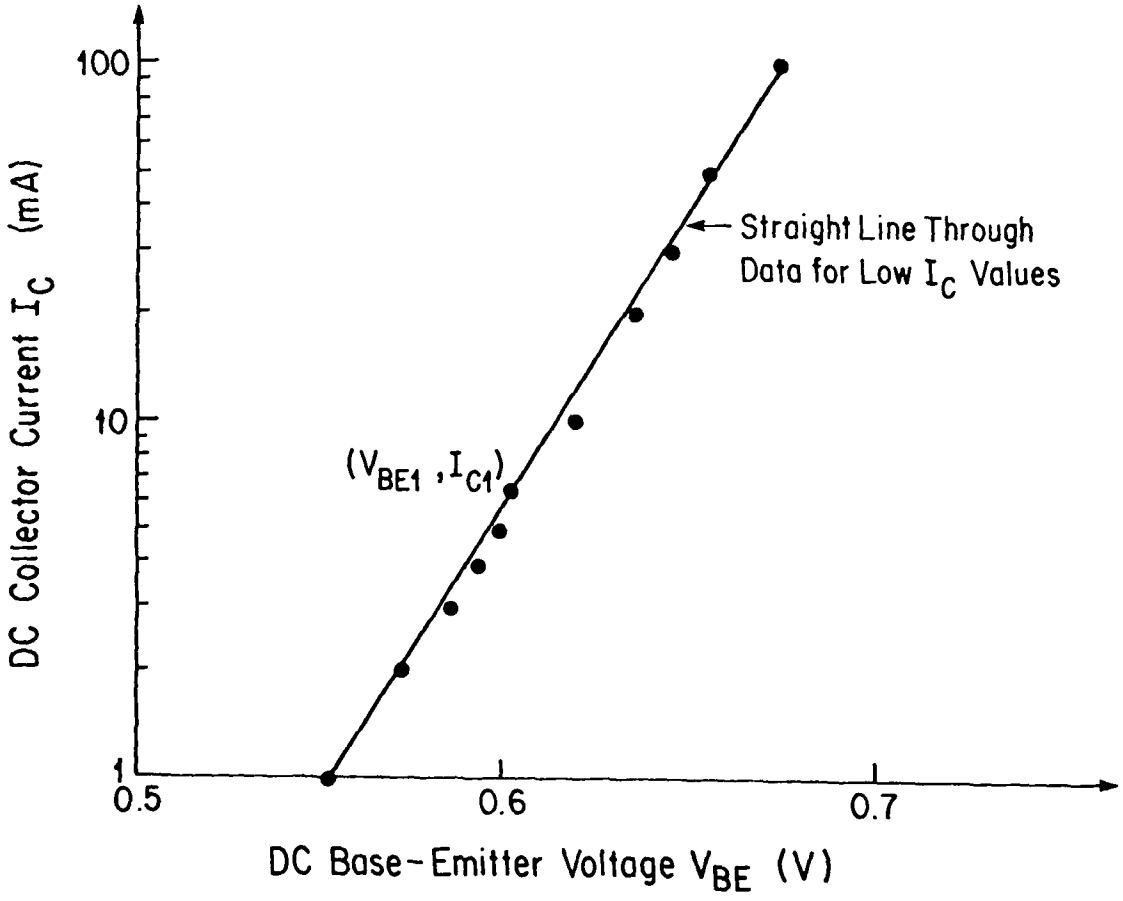

FIGURE 3-6 I_C Versus V_{BE} Plot for a 2N5179 Device

collector current I_C as a function of the dc base-emitter voltage V_{BE} are measured using the circuit shown in Figure 3-5. Typical data are shown in Figure 3-6.

Solve Eq. (3-6) for the saturation current I_S. Then evaluate the resulting equation at a point (V_{BE1}, I_{C1}) on the straight line shown on Figure 3-6 which is drawn through the data at low I_C values. The saturation current I_S is given by the expression

$$I_S = I_{C1}/(\exp(qV_{BE1}/RefkT) - 1) \qquad (3\text{-}7)$$

3.1.4 α_N, β_N, Forward Current Gains

The forward current gain parameters α_N and β_N are determined as a function of collector current in the normal operating region. The dc base current I_B and the dc collector current I_C are measured. The parameter α_N and β_N are calculated using the expressions;

$$\alpha_N = I_C/(I_B + I_C) \qquad (3\text{-}8)$$

$$\beta_N = I_C/I_B \qquad (3\text{-}9)$$

The dc test circuit shown in Figure 3-7(a) was used for measurements at low current levels ($I_C < 1$ mA). The pulse test circuit shown in Figure 3-7(b) was used for measurements at high current levels ($I_C > 1$ mA). Typical β_N data are given in Figure 3-8.

3.1.5 a, h_{FEmax}, I_{Cmax}, h_{FE} Nonlinearity

As shown in Figure 3-8, the forward current gain β_N (h_{FE}) varies as the collector current levels changes. The parameter h_{FEmax} and

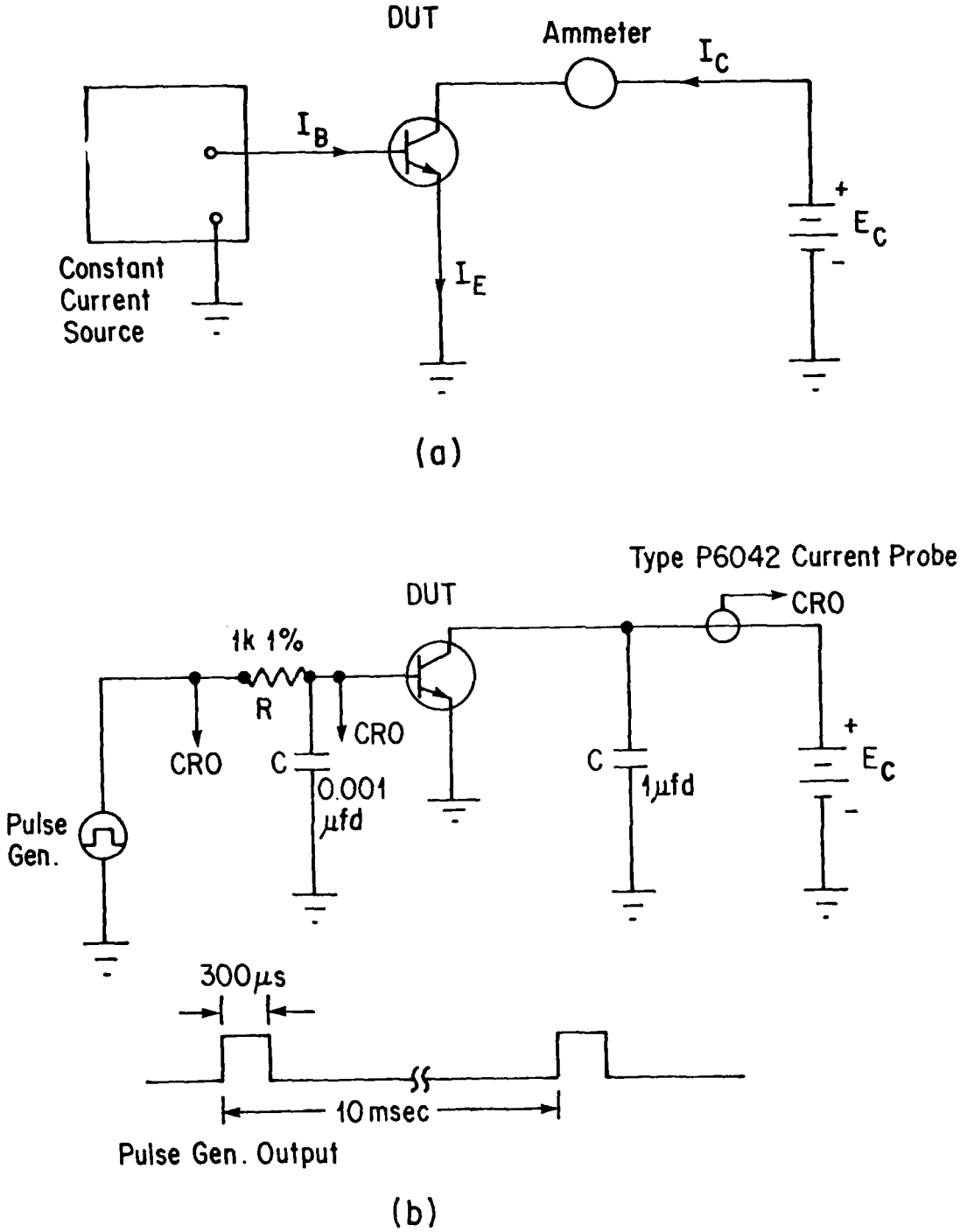

FIGURE 3-7 (a) DC Test Circuit for Measuring α_N and β_N at Low Current Levels

(b) Pulse Test Circuit for Measuring α_N and β_N at High Current Levels

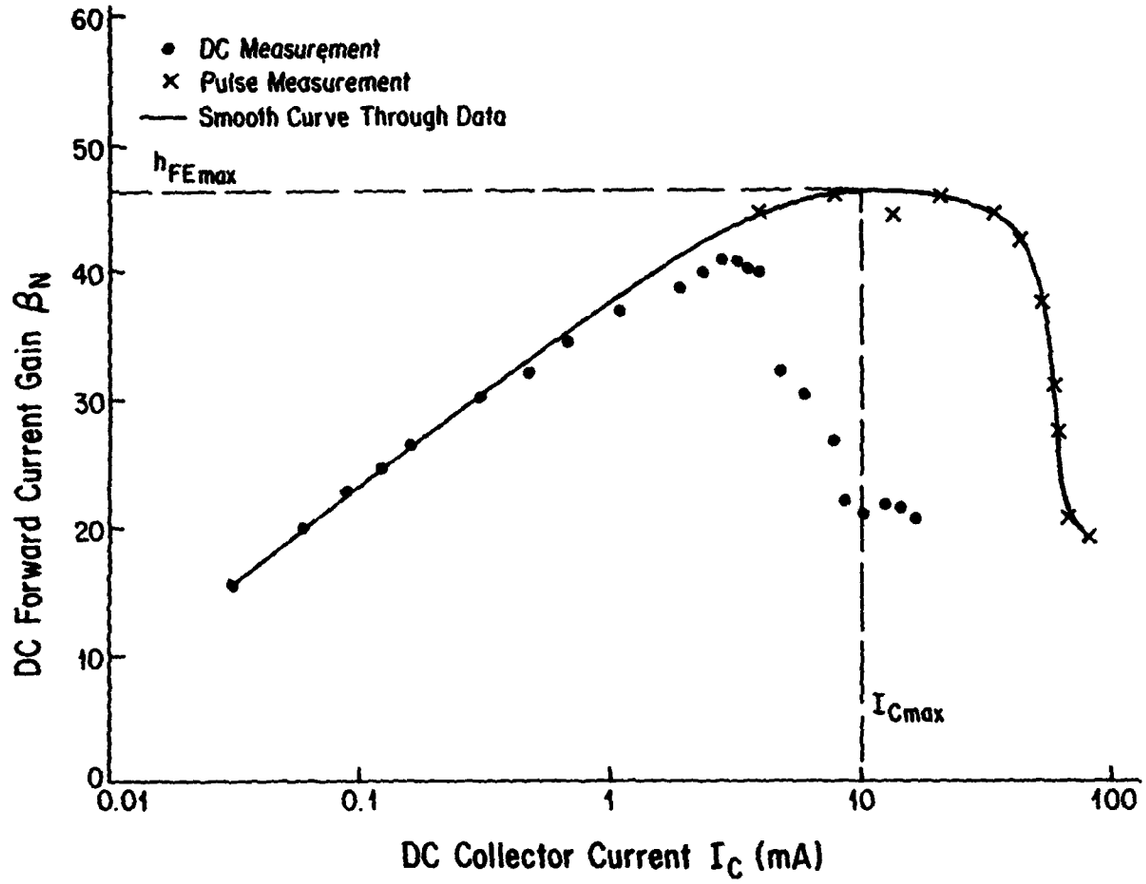

FIGURE 3-8 $\beta_N(h_{FE})$ Versus I_C Plot for a 2N5179 Device

I_{Cmax} are determined from the smooth curve drawn through the data shown in Figure 3-8. The maximum value for h_{FE} is the parameter h_{FEmax} and the collector current corresponding to h_{FEmax} is the parameter I_{Cmax}. The parameter a may be determined by using the parameter values I_{Cmax} and h_{FEmax} and the values of I_C and h_{FE} at the dc operating point using the expression

$$a = (h_{FEmax} - h_{FE})/(h_{FE} \log^2(I_C/I_{Cmax})) \tag{3-10}$$

An alternate method for determining a involves choosing two points (I_{C1}, h_{FE1}) and (I_{C2}, h_{FE2}) on the smooth curve drawn through the h_{FE} vs I_C data; the two points should be chosen so that $I_{C1} < I_C < I_{C2}$ where I_C is the dc operating current. The parameter a can be calculated using the expression

$$a = (h_{FE}(I_{C2}) - h_{FE}(I_{C1}))/(h_{FE}(I_{C1})\log^2(I_{C1}/I_{Cmax}) - h_{FE}(I_{C2})\log^2(I_{C2}/I_{Cmax})) \tag{3-11}$$

3.1.6 α_I, β_I, Reverse Current Gains

The reverse current gain parameters α_I and β_I used in SCEPTRE can be measured using techniques identical to those described in the previous section except that the emitter and collector terminals are interchanged. Since the current levels involved are low, a dc measurement technique is usually satisfactory. The dc emitter current I_E and dc base current I_B are measured. The test circuit is shown in Figure 3-9. The parameters α_I and β_I are calculated by using the expressions

$$\alpha_I = I_E/(I_B + I_E) \tag{3-12}$$

$$\beta_I = I_E/I_B \tag{3-13}$$

Shown in Figure 3-10 is a plot of β_I vs I_E for 2N5179 BJT.

3.1.7 R_{SC}, R_{SE}, Collector and Emitter Bulk Resistances[22,23]

The emitter bulk resistance R_{SE} can be determined by measuring the voltage across the transistor from collector to grounded emitter as a function of base current with the collector current constrained to be zero. The dc measurement circuit used is shown in Figure 3-11. A pulse measurement technique could also be used.

Using Ebers-Moll model Eqs. (2-1), (2-2), and (2-8) with $I_C = 0$, and assuming that the transistor is operated in the saturation region where both the emitter and collector junctions are forward biased we obtain the relationship

$$V_{CE} = -(kT/q)\ln\alpha_I + I_B R_{SE} \tag{3-14}$$

The plot (a) of V_{CE} vs I_B shown in Figure 3-12 is a straight line and its slope gives the value of R_{SE}.

If the transistor collector and emitter terminals are interchanged, a value for R_{SC} can be determined. In Eq. (3-14) the parameters α_N and R_{SC} are substituted for the parameters α_I and R_{SE}; the plot (b) of V_{CE} vs I_B is a straight line and its slope gives the value of R_{SC}. Results measured for a 2N5179 transistor are given in Figure 3-12.

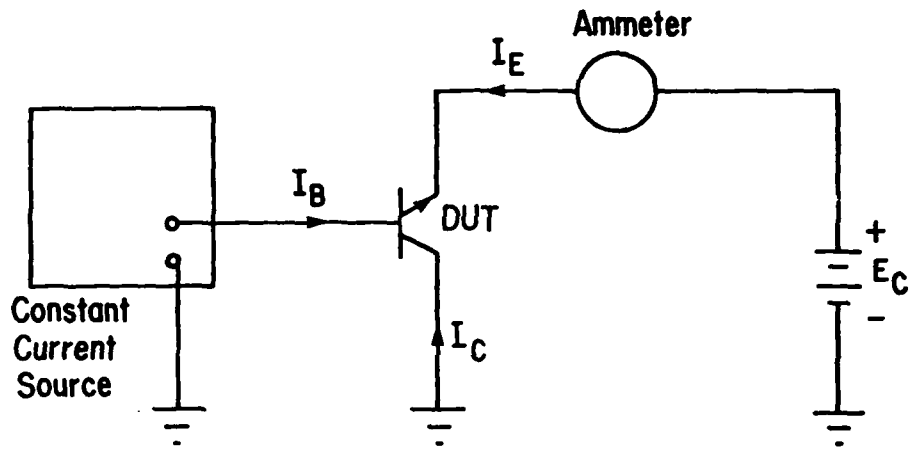

FIGURE 3-9. DC Test Circuit for Measuring α_I and β_I at Low Current Levels

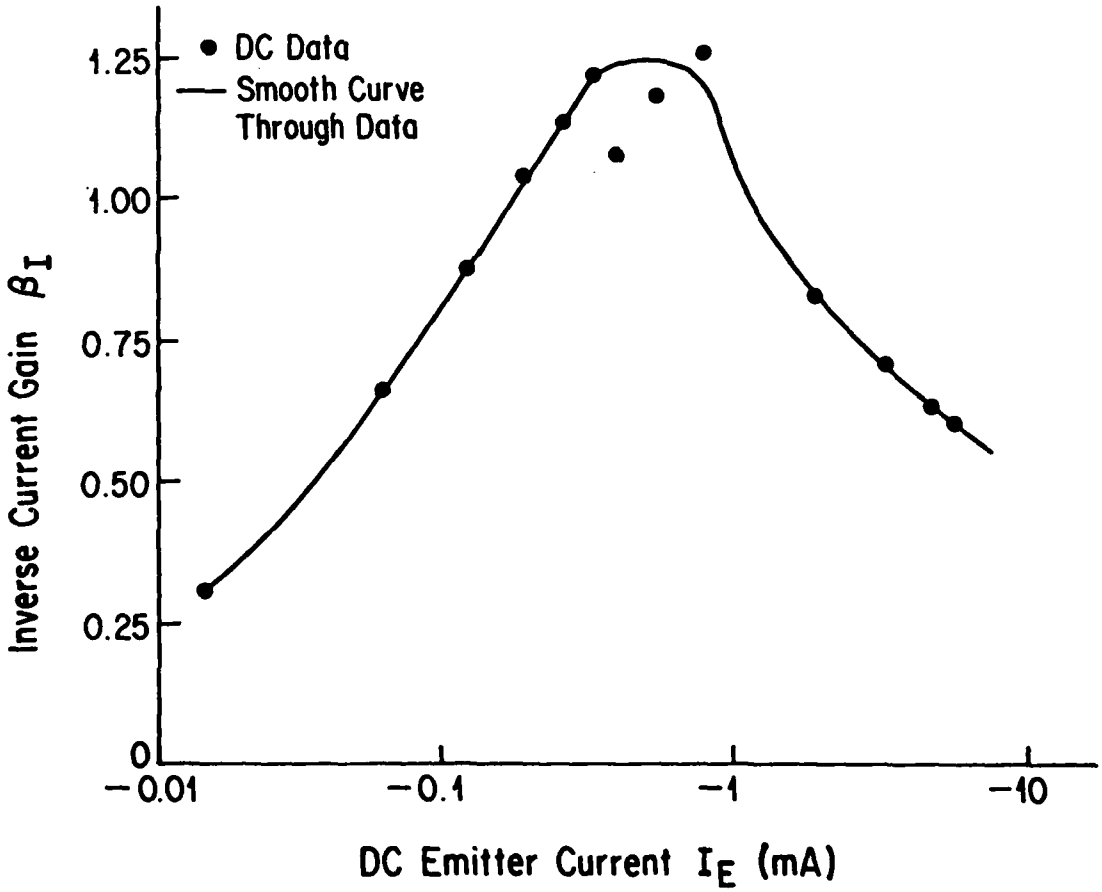

FIGURE 3-10. β_I Vs I_E Plot for a 2N5179 Device

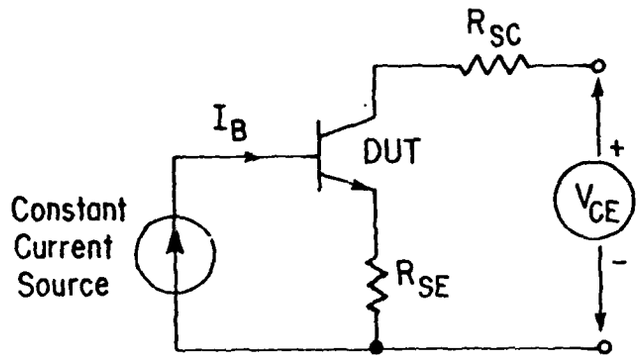

FIGURE 3-11 Circuit for the Measurement of Emitter and Collector Series Resistances

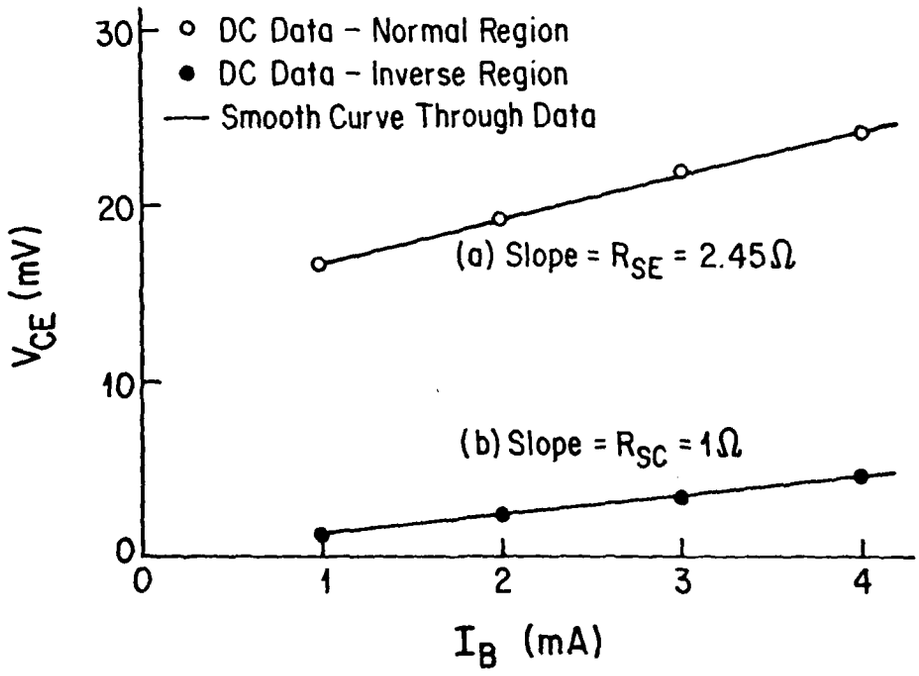

FIGURE 3-12 The Evaluation of R_{SE} and R_{SC} for a 2N5179 Transistor

The resistances R_{SC} and R_{SE} can also be rapidly determined by using a transistor curve tracer. Two measurements are made of the collector-emitter saturation voltage at low I_C values. The base current values used are widely separated (i.e. 0.1 mA and 10 mA). The experimental results are illustrated in Figure 3-13. The resistances R_{SE} and R_{SC} can be obtained using the information given on Figure 3-13.

3.1.8 R_B, Base Bulk Resistance

The base bulk resistance R_B can be determined from the dc and pulse data for I_E vs V_{BE} plot shown in Figure 3-2. As discussed previously in Section 2.1.1 the base-emitter terminal voltage V_{BE} is related to the intrinsic base-emitter voltage V'_{BE} by

$$V_{BE} = V'_{BE} + I_E R_{SE} + I_B R_B \qquad (3\text{-}15)$$

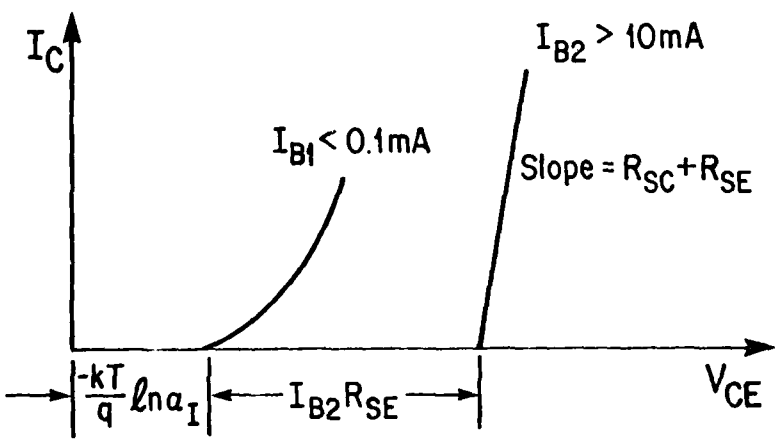

FIGURE 3-13. Bulk Resistance (R_{SE} and R_{SC}) Determination with Two I_C-V_{CE} Curves

Equation (3-1) relates the emitter current to the base-emitter voltage at low current levels, and this voltage is V'_{BE}. Substituting V'_{BE} for V_{BE} in Eq. (3-1) and solving for V'_{BE}, we obtain

$$V'_{BE} = (kT/q)Ref\ell n(-I_E/I_{ES}) \qquad (3\text{-}16)$$

Equation (3-16) is represented in Figure 3-2 by the straight line drawn through the dc data for low I_E values. Next this straight line is extended to high current values. At a high current level I_{E3} (I_{E3} > 10 mA) the voltage difference ΔV between the actual terminal voltage V_{BE} and internal base-emitter voltage V'_{BE} is illustrated in Figure 3-2. Solving Eq. (3-15) for $\Delta V = V_{BE} - V'_{BE}$, we obtain

$$\Delta V = I_E R_{SE} + I_B R_B \qquad (3\text{-}17)$$

Next we relate I_B to I_E using $I_B = I_E/(\beta_N + 1)$. The result is

$$\Delta V = I_E R_{SE} + (I_E/(\beta_N + 1))R_B \qquad (3\text{-}18)$$

The value for β_N (h_{FE}) is taken from Figure 3-8 assuming $I_C = -I_E$. Solving Eq. (3-18) for R_B, we obtain the result

$$R_B = (\Delta V - I_E R_{SE})/(I_E/(\beta_N + 1)) \qquad (3\text{-}19)$$

Using values for ΔV and I_{E3} shown in Figure 3-2, the β_N value taken from Figure 3-8 at $I_C = I_{E3}$, and the value for R_{SE} determined from previous section, Equation (3-19) can be solved for the base bulk resistance R_B.

Some comments are in order concerning the measurement techniques

described for R_B in this section and R_{SE} in the previous section. Inconsistancies have been observed. Occassionally the R_B value obtained using Eq. (3-19) is negative. Part of the difficulty may result from using low current levels to determine R_{SE} and high current levels to measure R_B. The R_{SE} value illustrated in the previous section was R_{SE} = 2.45 ohms. This value appears to be too large. Since values for R_{SE} are expected to be a fraction of an ohm, the term $I_E R_{SE}$ in Eq. (3-19) is often omitted.[5]

It is worthwhile to mention that the base bulk resistance R_B does depend upon the base current level. Furthermore for ac signals this resistance (denoted r_b in incremental models) also depends upon the frequency. Thus, the value for the base bulk resistance r_b used in incremental models should be measured at the actual dc operating point and at the frequency of interest. In a subsequent section a small signal technique used to determine the resistance r_b is described. Finally it should be pointed out that representing the base bulk resistance by a simple resistor is a gross over simplification. The base bulk resistance region is more properly represented by a distributed R-C model.[24]

3.1.9 V_{CBO}, η, Avalanche Nonlinearity and r_c Collector Resistance

The parameters η and V_{CBO} and resistance r_c can be obtained from the common base output characteristics as shown in Figure 3-14. These characteristics can be measured on a transistor curve tracer. Using Eqs. (2-22) and (2-23) and assuming $\alpha_N = 1$, the collector current

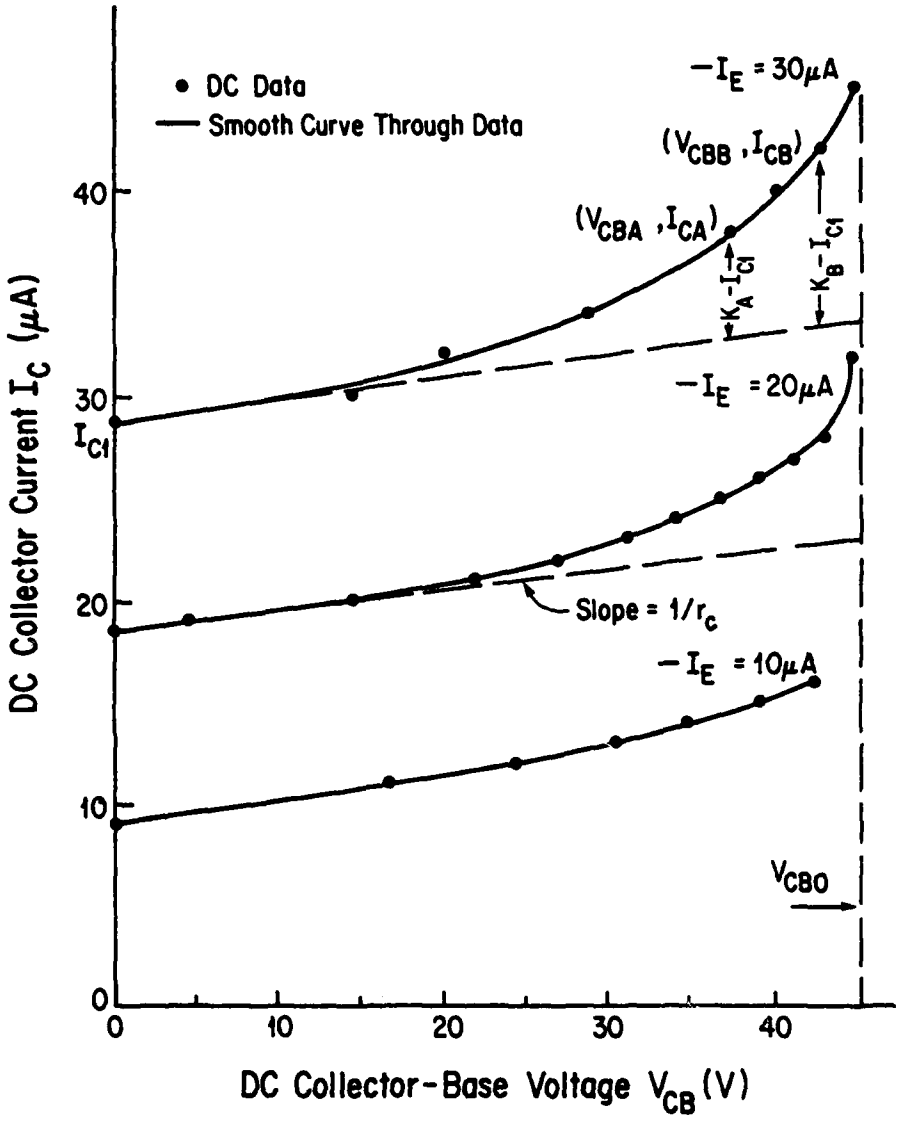

FIGURE 3-14 I_C Versus V_{CB} Plot for a 2N5179 Device

I_C corresponding to the emitter current I_E can be approximated by

$$I_C = -I_E/(1 - (V_{CB}/V_{CBO})^{\eta}) + V_{CB}/r_c \qquad (3\text{-}20)$$

where the additive term V_{CB}/r_c accounts for the slope of the linear portion of the curve when $V_{CB} \ll V_{CBO}$. The resistor r_c is related to the Early effect discussed in Section 2.1.2. The resistor r_c can be determined from the slope of the linear portions of the curves I_C vs V_{CB} as shown in Figure 3-14. The parameters η and V_{CBO} are obtained by selecting two data points with V_{CB} values near V_{CBO} such as (V_{CBA}, I_{CA}) and (V_{CBB}, I_{CB}). From Eq. (3-20), we have

$$I_{CA} = I_{C1}/(1 - (V_{CBA}/V_{CBO})^{\eta}) + V_{CBA}/r_c \qquad (3\text{-}21)$$

and

$$I_{CB} = I_{C1}/(1 - (V_{CBB}/V_{CBO})^{\eta}) + V_{CBB}/r_c \qquad (3\text{-}22)$$

where I_{C1} is the intercept of the linear portion of the I_C vs V_{CB} plot on the I_C axis. If we define the parameters K_A and K_B by the expressions

$$K_A = I_{CA} - V_{CBA}/r_c = I_{C1}/(1 - (V_{CBA}/V_{CBO})^{\eta}) \qquad (3\text{-}23)$$

$$K_B = I_{CB} - V_{CBB}/r_c = I_{C1}/(1 - (V_{CBB}/V_{CBO})^{\eta}) \qquad (3\text{-}24)$$

we have

$$(V_{CBA}/V_{CBO})^{\eta} = 1 - (I_{C1}/K_A) \qquad (3\text{-}25)$$

and

$$(V_{CBB}/V_{CBO})^{\eta} = 1 - (I_{C1}/K_B) \qquad (3\text{-}26)$$

Division of the two expressions yields the result

$$(V_{CBA}/V_{CBB})^{\eta} = (K_B/K_A)((K_A - I_{C1})/(K_B - I_{C1})) \qquad (3\text{-}27)$$

Taking the logarithm of both sides of the above equation, the following

expression for the avalanche exponent η is obtained

$$\eta = \log((K_B/K_A)(K_A - I_{C1})/(K_B - I_{C1}))/\log(V_{CBA}/V_{CBB}) \quad (3\text{-}28)$$

The value for V_{CBO} can be calculated using the expression

$$V_{CBO} = V_{CBA}/((K_A - I_{C1})/K_A)^{1/\eta} \quad (3\text{-}29)$$

or can be determined directly from the common-base characteristics shown in Figure 3-14. If measurements of the parameters η and V_{CBO} at high collector current levels are made, the characteristics of the collector currents will be observed to increase slowly with time because of junction heating effects. To avoid junction heating effects the dc curve tracer method could be replaced by a pulse technique method to measure the common base output characteristics.

3.1.10 V_A, The Early Voltage

The Early voltage V_A can be determined from the common emitter output characteristics obtained from a transistor curve tracer. Upon examining the I_C vs V_{CE} characteristics shown in Figure 2-3, a geometrical procedure for the Early voltage can be developed. The slope of the straight line portion of the I_C vs V_{CE} curve is usually called the output conductance g_o. Let the intercept of the straight line portion extended through the I_C axis be denoted as I_{C1}. Then the Early voltage can be determined using a relationship

$$V_A = I_{C1}/g_o \quad (3\text{-}30)$$

This geometrical procedure is illustrated on the I_C vs V_{CE} common emitter output characteristics shown in Figure 3-15. Typical value of V_A ranges from 20 to 100 V.

3.1.11 C_{jeo}, Φ_E, m_e, Emitter Junction Capacitance Parameters

The emitter junction capacitance parameters C_{jeo}, Φ_E, and m_e can be determined from measurements made on a 1 MHz capacitance bridge. Measurements of the junction capacitance C_{je} vs the junction voltage V_{BE} are made. The transistor terminal connections are given in Figure 3-16(a).

For an NPN BJT, Equation (2-17) gives the variation of the emitter junction capacitance with the base-emitter junction voltage.* Because device parasitic capacitances related to packaging exist, an extra constant capacitance C_x is present in the capacitance C_{meas} measured. Adding the capacitance C_x to the junction capacitance C_{je}, we obtain

$$C_{meas} = C_{jeo} \left(1-(V_{BE}/\Phi_E)\right)^{-m_e} + C_x \qquad (3\text{-}31)$$

The capacitance C_x can be determined in four ways: (1) by estimation (the range 0.4 to 0.7 pF is appropriate for TO-5 cans), (2) by measurement (for a discrete device a dummy can is used), (3) by computer parameter optimization, or (4) by a graphical technique.

* This expression is reasonably accurate for negative values of base-emitter voltage such that the ratio V'_{BE}/Φ_E is less than -0.5.

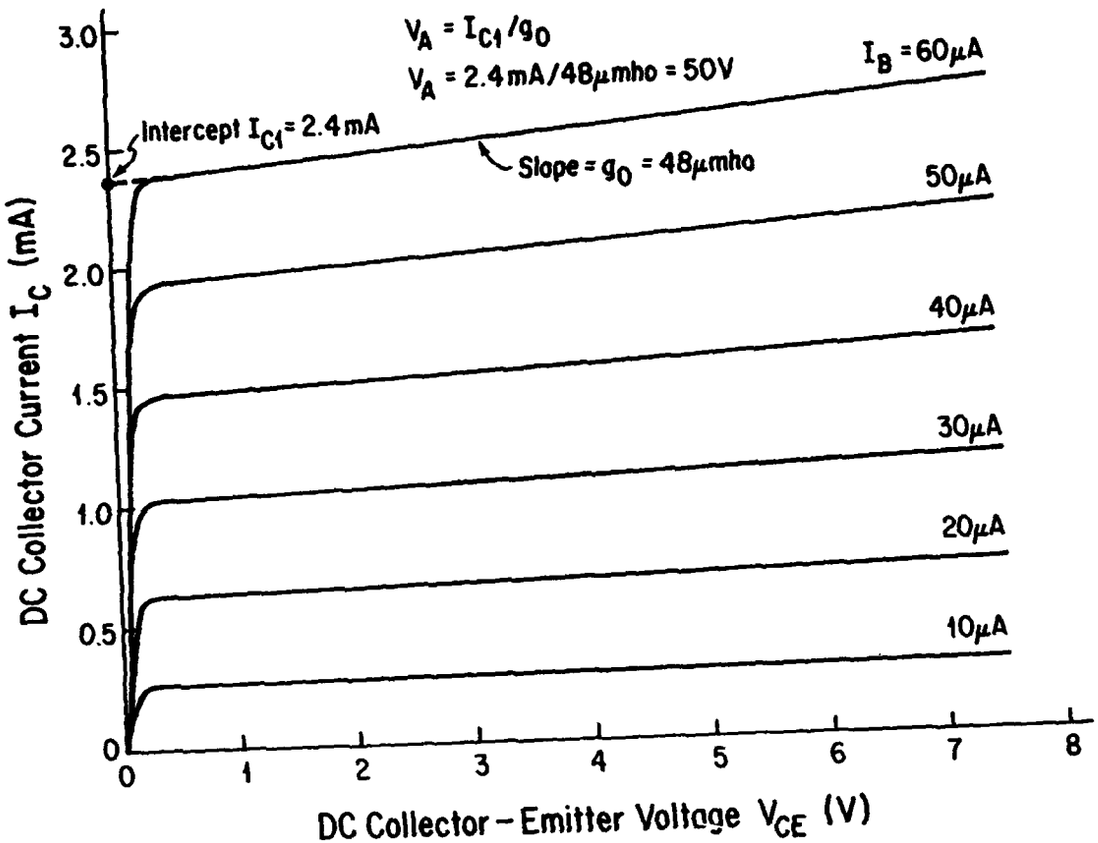

FIGURE 3-15 I_C Versus V_{CE} Plot for a 2N5179 Device Used to Determine Early Voltage V_A

For a discrete BJT the dummy can method is recommended. This method requires an identical device to be destroyed before C_x is measured. The emitter-base junction is destroyed in order to obtain an open circuit. This can usually be accomplished by putting a very large current through the emitter-base junction with the collector terminal not connected. For a damaged transistor with an emitter-base open circuit the capacitance measured is just C_x. The C_x value is assumed to be the same for all BJT's of one type. Next the C_{je} vs V_{BE} data for a good transistor is measured with the base-emitter junction reverse biased. Knowing the C_x value and using the Eq. (3-31), the parameter values for C_{jeo}, Φ_E and m_e can be obtained either by a graphical method or by a computer optimization technique. The graphical technique will be described later in this section. The computer optimization technique uses the Fortran program given in Table 3-1. This program is based upon a least-square-fit algorithm. Typical results obtained using the computer program optimization technique are given in Table 3-2 at the end of this chapter.* It should be pointed out that the computer program optimization technique does not yield a unique solution. The computer solution obtained does depend upon the initial values used.

A graphical method can also be used to determine the parameters C_{jeo}, Φ_E, m_e, and C_x. An initial value for C_x is assumed. For a BJT in a TO-5 can typical values for C_x lie in the range 0.4 -

* Table 3-2 is placed at the end of the chapter with Tables 3-3 through 3-5 so that all data are located at one place.

0.7 pF. An initial value for the parameter Φ_E is also assumed. For silicon BJT's typical values for Φ_E lie in the range 0.5 - 0.7 V. Next values of $(C_{meas} - C_x)$ are plotted vs $\Phi_E + V_{BE}$ on log-log paper. If a straight line having a reasonable slope (-0.5 to -0.167) is obtained, the values chosen for the parameters C_x and Φ_E are assumed to be correct. If the resulting plot is not a straight line, a second guess of C_x and Φ_E is made and another plot is made. If the curve is concave, the Φ_E value is decreased and the C_x is increased. If the curve is convex, the Φ_E value is increased and the C_x value is decreased. This process is iterated until a straight line is obtained. This graphical method is illustrated in Figure 3-17. The set of parameter values obtained using the graphical technique is not unique. For silicon BJT's solution sets with the parameter Φ_E near 0.7 V and m_e near 0.333 are recommended.

3.1.12 C_{jco}, Φ_C, m_c, k, Collector Junction Capacitance Parameters

The collector junction capacitance parameters C_{jco}, Φ_C, and m_c are determined in the same manner as the emitter junction capacitance parameters. Measurements of the junction capacitance C_{jc} vs the junction voltage V_{BC} are made. The transistor terminal connections are shown in Figure 3-16(b). For silicon BJT's typical values for the parameter Φ_C lie in the range 0.5 - 0.7 V and typical values for the parameter m_c lie in the range 0.5 to 0.167. There is also a device parasitic capacitance C_y related to packaging. For a silicon BJT in a TO-5 can typical values for C_y lie in the range 0.4 - 0.7 pF. The capacitance C_y can be measured

TABLE 3-1

JUNCTION CAPACITANCE VOLTAGE LEAST-SQUARE-FIT PROGRAM

```
      PROGRAM FANG(INPUT,OUTPUT,TAPE5=INPUT,TAPE6=OUTPUT)
      DIMENSION A(10,3),B(3,1),C(10,1),F(10,1),V(10,1),R(3,10),S(3,3),WO
     1RK1(3),WORK2(3),T(3,10),CF(10,1),DELTA(3,1),BOLD(3,1)
      DIMENSION CC(12),VV(12),LABEL(8,3),FAC(3),NCHAR(3)
100   FORMAT(3F5.2)
200   FORMAT(2F5.2)
300   FORMAT(1X,24HDIVERGENT IN THE PROCESS)
400   FORMAT(1X,5HCO = ,F5.2,6HPHI = ,F5.2,4HM = ,F5.2,12HITERATION = ,I
     12)
500   FORMAT(I5,7A10,A5)
600   FORMAT(3F10.0)
C
C READ IN INITIAL CO, PHI, AND M
C
      READ(5,100) (B(I,1),I=1,3)
C
C READ IN MEASURED C AND V
C
      READ(5,200)(C(I,1),V(I,1),I=1,10)
      DO 6 I=1,10
      V(I,1)=-V(I,1)
6     CONTINUE
C
C SET UP THE CAPACITANCE FORMULUS
C
      NN=1
25    DO 5 I=1,10
      F(I,1)=B(1,1)*(1.-V(I,1)/B(2,1))**(-B(3,1))
5     CONTINUE
C
C SET UP THE LEAST SQUARE MATRIX A
C
      DO 10 I=1,10
      A(I,1)=(1.-V(I,1)/B(2,1))**(-B(3,1))
      A(I,2)=-(B(1,1)/(B(2,1)*B(2,1)))*B(3,1)*V(I,1)*(1.-V(I,1)/B(2,1))*
     1*(-1.-B(3,1))
      A(I,3)=-B(1,1)*ALOG(1.-V(I,1)/B(2,1))*(1.-V(I,1)/B(2,1))**(-B(3,1)
     1)
10    CONTINUE
C
C CALCULATES THE INCREMENT OF B TO UPDATE THE PARAMETERS
C
      NP=1
      NR=10
      NC=3
      CALL GMTRA(A,R,NR,NC)
      CALL GMPRD(R,A,S,NC,NR,NC)
      CALL MINV(S,NC,D,WORK1,WORK2)
      CALL GMPRD(S,R,T,NC,NC,NR)
      DO 15 I=1,10
      CF(I,1)=C(I,1)-F(I,1)
15    CONTINUE
      CALL GMPRD(T,CF,DELTA,NC,NR,NP)
```

TABLE 3-1 (Continued)

```
C
C UPDATE THE PARAMETERS B
C
      DO 20 I=1,3
      BOLD(I,1)=B(I,1)
      B(I,1)=B(I,1)+DELTA(I,1)
      IF(B(I,1).LE.0.)B(I,1)=BOLD(I,1)
20    CONTINUE
C
C TEST THE CONVERGENCE
C
      NN=NN+1
      IF(NN.GT.20)GO TO 30
      T1=ABS(DELTA(1,1)/B(1,1))
      T2=ABS(DELTA(2,1)/B(2,1))
      T3=ABS(DELTA(3,1)/B(3,1))
      IF(T1.LT.0.1.AND.T2.LT.0.1.AND.T3.LT.0.1)GO TO 35
      GO TO 25
C
C PRINT OUT DIVERGENT MESSAGE
C
30    WRITE(6,300)
35    WRITE(6,400)(B(I,1),I=1,3),NN
      DO 40 I=1,10
      CC(I)=C(I,1)
      VV(I)=-V(I,1)+B(2,1)
40    CONTINUE
      CALL PLOTS
      N=10
      KODE=2
      READ(5,500)(NCHAR(I),(LABEL(J,I),J=1,8),I=1,3)
      READ(5,600)FAC
      CALL LGPLOT(VV,CC,N,KODE,LABEL,NCHAR,FAC)
      ISYMB=0
      KKODE=ISYMB+100
      N1=10
      DO 50 I=1,10
      CC(I)=B(1,1)*(1.-V(I,1)/B(2,1))**(-B(3,1))
50    CONTINUE
      CALL LGPLOT(VV,CC,-N1,KKODE)
      CALL FFPLOT
      STOP
      END
```

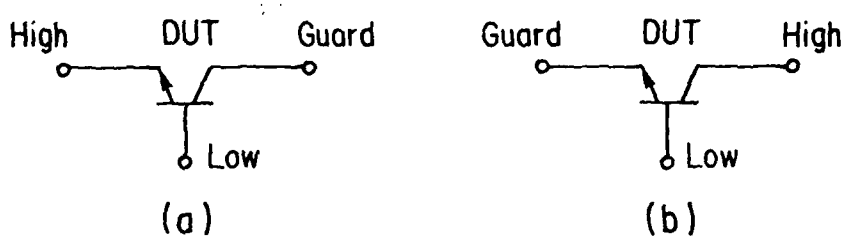

FIGURE 3-16 Terminal Connections for Junction Capacitance Measurement (a) C_{je} Measurement and (b) C_{jc} Measurement

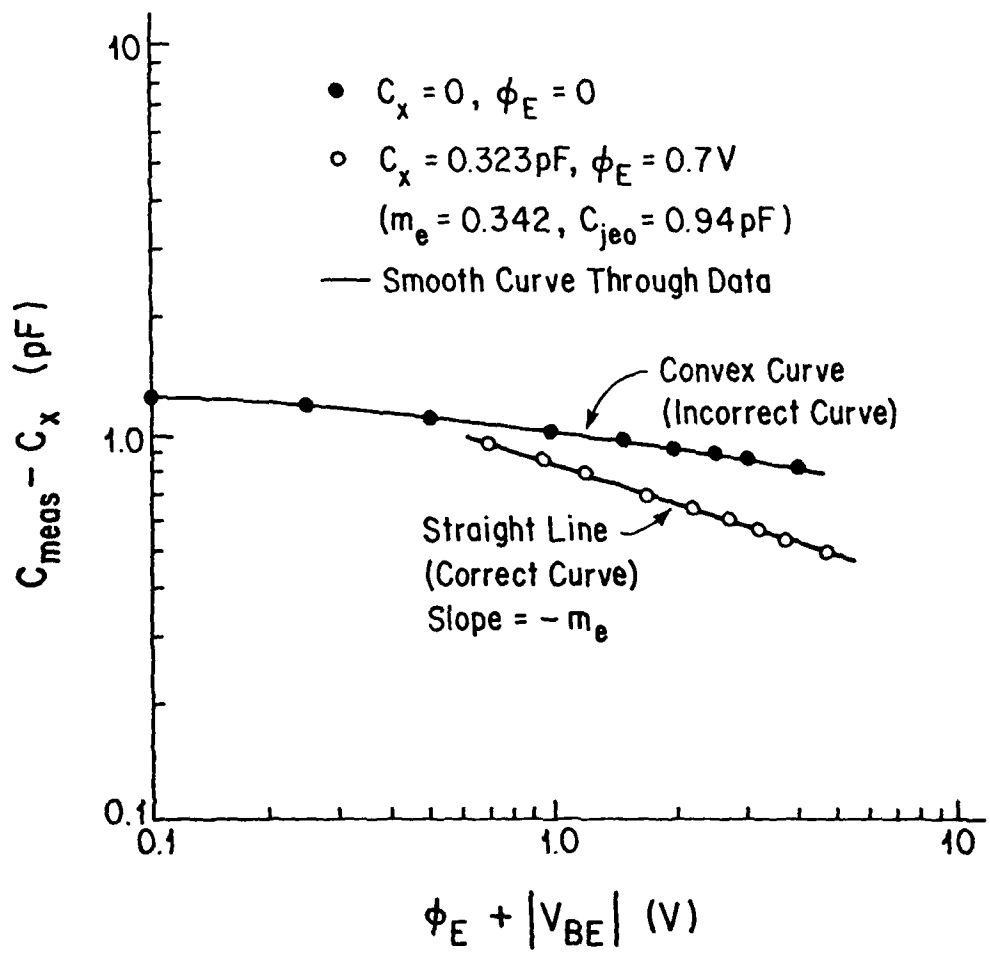

FIGURE 3-17 Typical Values of Emitter Junction Capacitance $C_{meas}-C_x$ Vs $\Phi_E + |V_{BE}|$ for a 2N918 BJT

using the dummy can procedure described in the previous section. The collector-base junction is destroyed intentionly at high collector current levels in order to obtain an open circuit in the collector-base junction. The capacitance measured for the damaged device with the terminal connections shown in Figure 3-16(b) is C_y. The measured values for the capacitance C_{meas} vs the collector-base voltage V_{CB} are processed in the manner described in the previous section to obtain values for the parameters C_{jco}, Φ_C, m_c, and C_y.

The computer program NCAP uses the following relationship for the collector-base junction capacitance C_{BC}

$$C_{BC} = k \, |V_{BC}|^{-\mu} \tag{2-92}$$

where the parameter k is called the collector-base capacitance scale factor and the parameter μ is called the collector-base capacitance exponent. By comparing Eq. (2-92) to Eq. (2-18), the following relationship can be obtained for the special case where

$$|V_{BC}/\Phi_C| >> 1 :$$

$$k = C_{jco} \, \Phi_c^{m_c} \tag{3-32}$$

$$\mu = m_c \tag{3-33}$$

An alternative procedure is to fit Eq. (2-92) directly to measured data using a computer simulation procedure or a graphical procedure similar to those described in the previous section. Of course the parasitic capacitance C_y should be taken into account.

3.2 Small Signal Parameter Measurements

The BJT model parameters used in SPICE2, SCEPTRE and NCAP are essentially large signal model parameters. Exceptions are the junction capacitance parameters discussed in Sections 3.1.11 and 3.1.12. Other exceptions are the NCAP emitter-base diffusion capacitance parameters C_{je} and C_2'. These parameters are measured using small signal techniques. It is also desirable to make a small signal measurement for the base spreading resistance r_b because this parameter depends on the operating frequency. In this section small signal measurements for these parameters are discussed.

3.2.1 r_b, Base Spreading Resistance

The incremental model base spreading resistance r_b can be measured in many ways. In this section both low frequency and high frequency methods will be discussed. (Note that the base parasitic resistance for large signal analysis was denoted by R_B.)

(a) Low Frequency AC Measurement

The base spreading resistance r_b can be determined from measurements of the small signal transistor h-parameters h_{ie} and h_{fe} at 1 kHz. The parameters h_{ie} and h_{fe} are defined respectively as the incremental input impedance and the incremental forward current gain of the BJT in the common emitter configuration with the output shorted. The appropriate equations are

$$h_{ie} = \partial v_{be}/\partial i_b \Big|_{v_{ce} = 0} \tag{3-34}$$

$$h_{fe} = \partial i_c/\partial i_b \Big|_{v_{ce} = 0} \tag{3-35}$$

The parameters h_{ie} and h_{fe} can be measured by using the test configurations shown in Figure 3-18.[25] (The branch containing the 50 Ω resistor and capacitor C_2 is considered to be a short-circuit at 1 kHz.)

Expressions for h-parameters will be given in terms of parameters of the hybrid-pi model shown in Figure 2-10. This model is shown in conventional form in Figure 3-19 where the capacitances C_μ and C_π are defined by[18]

$$C_\mu = C_{jc} + C_d \tag{3-36}$$

$$C_\pi = C_{je} + C_b \tag{3-37}$$

At 1 kHz these capacitors are essentially open circuits and the parameters h_{ie} and h_{fe} are given approximately by

$$h_{ie} = r_b + r_\pi \tag{3-38}$$

$$h_{fe} = g_m r_\pi \tag{3-39}$$

where the assumption that r_μ is large has been made.

Using Eq. (2-51) for g_m which is $g_m = q|I_C|/kT$ in the above equations, the following expression for r_b is obtained

$$r_b = h_{ie} - (kT/q|I_C|)h_{fe} \tag{3-40}$$

(b) High Frequency AC Measurement

Figure 3-20 shows a small signal equivalent circuit that can be used to calculate the common-emitter short-circuit input admittance y_{ie}. The following equation is obtained:

$$y_{ie} = i_b/v_{be}\Big|_{v_{bc} = 0} = \frac{g_b(g_\pi+g_\mu+j\omega(C_\pi+C_\mu))}{g_b+g_\pi+g_\mu+j\omega(C_\pi+C_\mu)} \tag{3-41}$$

where

$$g_b = 1/r_b,\ g_\mu=1/r_\mu,\ \text{and}\ g_\pi=1/r_\pi.$$

If the frequency is high so that the following inequalities are true

$$g_b << \omega(C_\pi + C_\mu) \tag{3-42}$$

$$g_\pi << \omega\ (C_\pi + C_\mu) \tag{3-43}$$

$$g_\mu << \omega\ (C_\pi + C_\mu) \tag{3-44}$$

then Eq. (3-41) yields the result

$$r_b = 1/\mathrm{Re}(y_{ie}) \tag{3-45}$$

By using an admittance bridge to measure y_{ie} at a single high frequency, a value for r_b can be obtained.

The method for determining the incremental base-spreading resistance r_b just described is very much an oversimplified method. Both the parasitic base resistance r_b and emitter resistance r_e' depend upon the current level and the frequency. This subject has

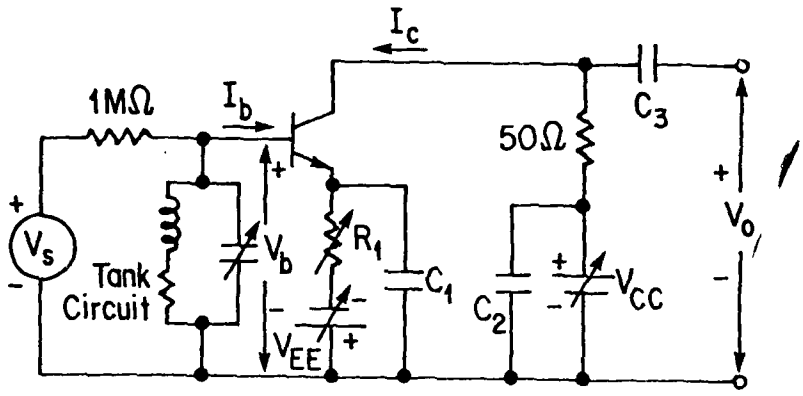

$$h_{ie} = 1M\Omega \ V_b/V_s$$

$$h_{fe} = (1M\Omega/50\Omega)\ V_o/V_s$$

FIGURE 3-18 Circuit for Measuring h_{ie} and h_{fe}. Note that the Quantities V_s, I_b, etc., Are the Complex Amplitudes of Sinusoidal Quantities. See Appendix I on Notation.

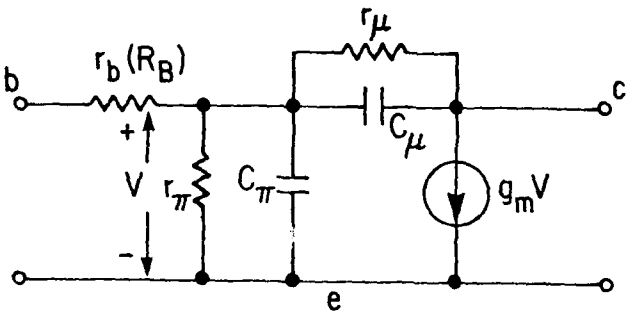

FIGURE 3-19 Hybrid-Pi Model for a Jun tion Transistor

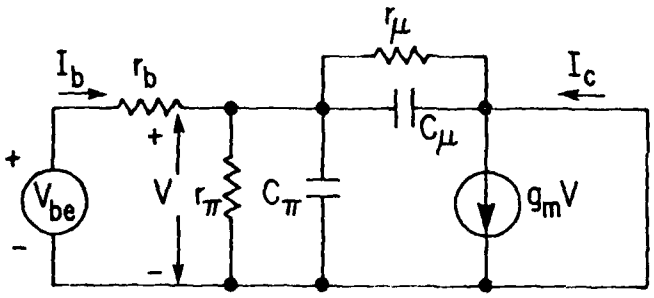

FIGURE 3-20 Small Signal Equivalent Circuit for Measuring Common-Emitter Short-Circuit Input Admittance $y_{ie} = I_b/V_{be}$. Note that the Quantities I_b, V_{be}, etc., are the Complex Amplitudes of Sinusoidal Quantities. See Appendix I on Notation.

AD-A082 527 SYRACUSE UNIV NY F/G 9/5

NONLINEAR SYSTEM ANALYSIS IN BIPOLAR INTEGRATED CIRCUITS.(U)

JAN 80 T FANG, J J WHALEN F30602-79-C-0011

UNCLASSIFIED RADC -TR-79-324 NL

2 OF 3

AD A
082527

been discussed by several investigators.[21,26] An excellent review paper on this subject is the one by Sansen and Meyer. Although it is not our intent to discuss this paper fully in this dissertation it is worthwhile to point out that the determination of the incremental parasitic resistances r_b and r_e' is complicated by several effects. These effects are caused by parasitic capacitances associated with package wires, bond wires, and the distributed resistive and capacitive aspects of the base region responsible for r_b. One of the methods reviewed in the paper by Sansen and Meyer is the circle diagram method. This method involves plotting the locus of the short-circuit input impedance h_{ie} ($h_{ie} = 1/y_{ie}$) in the complex plane as a function of frequency. Using the circuit shown in Figure 3-21, a first-order analysis indicates that the locus for h_{ie} is a semicircle that intercepts the real axis at low frequencies where

$$h_{ie} = r_\pi + r_b + (1+g_m r_\pi)\, r_e' \tag{3-46}$$

and at high frequencies where

$$h_{ie} = r_b + r_e' \tag{3-47}$$

This locus is shown in Figure 3-22. (The actual device experimental results may deviate from this locus at high frequencies because of the effects due to other parasitic elements not shown in Figure 3-21.)

Of particular interest to us is Eq. 3-47 which can be used to determine a value for $r_b + r_e'$. By plotting the experimental re-

sults for h_{ie} at high frequencies on the complex plane as shown in Figure 3-23 for a 2N5109 BJT, the high frequency real axis intercept can be determined by drawing a circle through the data. The value for $r_b + r_e'$ is observed to lie in the range 30 to 35 ohms. For alternate data processing techniques the reader is referred to the original paper of Sansen and Meyer.[26]

3.2.2 C_{je}, C_2', NCAP Emitter-Base Capacitance Parameters*

The NCAP emitter-base capacitance parameters C_{je} and C_2' can be determined from measurements of the parameter f_T versus the dc emitter current I_E. The parameter f_T is the frequency at which the magnitude of the common emitter incremental short-circuit current gain extrapolates to unity. In order to establish how the parameters C_{je} and C_2' are determined from measurements of f_T, the theoretical expression for the NCAP nonlinear current generator $\gamma_e(v_{be})$ shown in Figure 2-12 must be established. The necessary relationships will now be derived.

Rewriting Eq. (2-15) for the charge stored in the emitter-base region in terms of the total instantaneous charge q_{BE} and intrinsic emitter-base voltage v_{BE}', we have

$$q_{BE} = \tau_F I_s\{\exp(qv_{BE}'/kT)-1\} + C_{jeo}\int_0^{v_{BE}'} (1-V/_{\phi E})^{-m_e} dV \qquad (3\text{-}48)$$

* Note that the parameter C_{je} used in NCAP is not actually the emitter-base junction depletion layer capacitance. Instead it is a parameter determined by an extrapolation process as is discussed in this section.

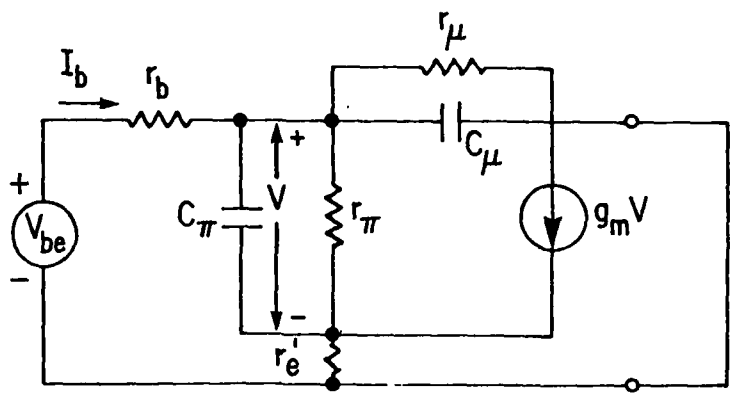

FIGURE 3-21 Small Signal Equivalent Circuit for Calculating the Common-Emitter Short-Circuit Input Impedance $h_{ie} = V_{be}/I_b$. Note that the Quantities I_b, V_{be}, etc., are the Complex Amplitudes of Sinusoidal Quantities. See Appendix I on Notation.

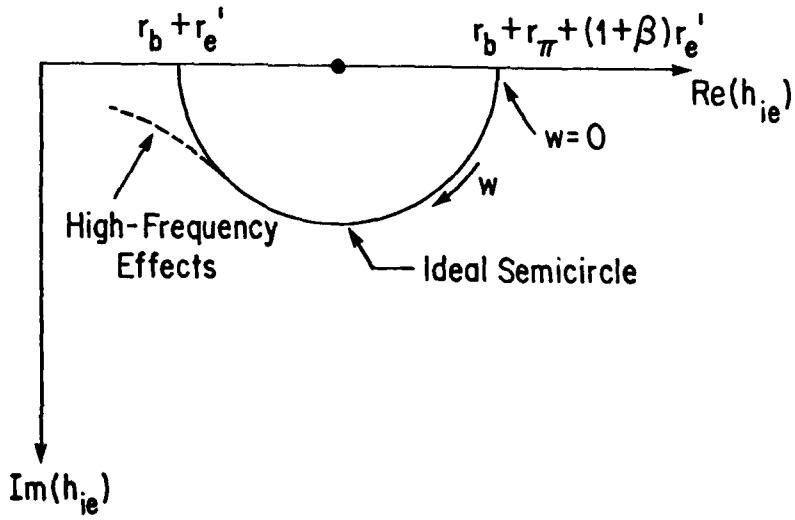

FIGURE 3-22 Input Impedance Locus Plot. The Intercepts of the Semicircle with the Real Axis Yield the Value of $r_b(R_B)$

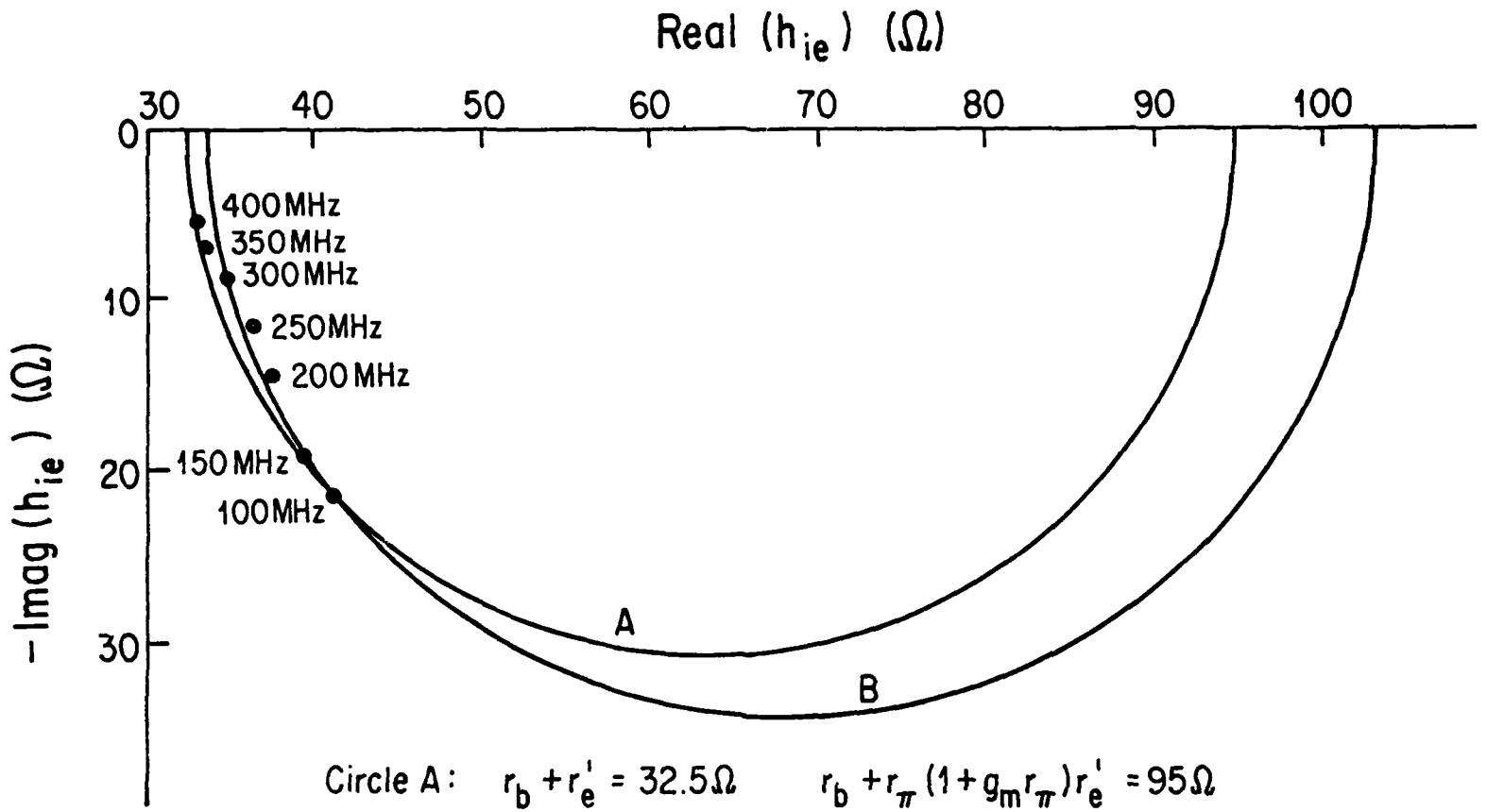

Circle A: $r_b + r_e' = 32.5\Omega$ $\quad r_b + r_\pi(1+g_m r_\pi)r_e' = 95\Omega$

Circle B: $r_b + r_e' = 33.5\Omega$ $\quad r_b + r_\pi(1+g_m r_\pi)r_e' = 103\Omega$

$V_{CE} = 15V$, $I_C = 50\,mA$

FIGURE 3-23 Typical Re(h_{ie}) Versus Im(h_{ie}) Locus Plot for a 2N5109 BJT. These Circles were Obtained by Somewhat Judicious Choice of Three Points. Choice of a Different Set of Three Points will Yield Slightly Different Circles.

Our goal is to relate the NCAP nonlinear current generator $\gamma_e(v'_{be})$ to the current dq_{BE}/dt evaluated in the vicinity of the BJT operating point (V'_{BE}, I_E). For a BJT operated in the normal region, the emitter-base junction is forward-biased. Expanding Eq. (3-48) about the operating point and differentiating the result with respect to time t, the following result is obtained

$$\gamma_e(v'_{be}) = \tau_F I_E \sum_{n=1}^{\infty} (1/n!)(q/kT)^n \frac{d}{dt}(v'_{be})^n$$

$$+ \sum_{n=1}^{\infty} \frac{1}{n!} \left\{ \frac{\partial^{n-1}[C_{jeo}(1-v'_{BE}/\phi_E)^{-m_e}]}{\partial v'^{\,n-1}_{BE}} \right\} \frac{d}{dt}(v'^{\,n}_{be}) \quad (3\text{-}49)$$

Note that the NCAP parameter list does not include the parameters C_{jeo}, ϕ_E or m_e used in SPICE2 and SCEPTRE. Instead the NCAP computer code is written for an approximate version of the above equation. The approximation is believed to be that the second sum is represented by a single linear term (n = 1) which is $C_{je}dv'_{be}/dt$. Thus the NCAP nonlinear current generator $\gamma_e(v'_{be})$ must be equivalent to

$$\gamma_e(v'_{be}) = \tau_F I_E \sum_{n=1}^{\infty} (1/n!)(q/kT)^n \frac{d}{dt}(v'_{be})^n$$

$$+ C_{je}\, dv'_{be}/dt \quad (3\text{-}50)$$

The parameter τ_F is not used in NCAP. Instead a parameter C'_2 is used. The parameter C'_2 is the derivative of the coefficient of the linear term in the above equation with respect to the dc emitter current I_E. The linear term in the above equation is the current $\gamma_e^{(1)}(v'_{be})$ where $\gamma_e^{(1)}(v'_{be})$ is given by

$$\gamma_e^{(1)}(v'_{be}) = (\tau_F I_E(q/kT) + C_{je})dv'_{be}/dt \quad (3\text{-}51)$$

The coefficient $(\tau_F I_E(q/kT) + C_{je})$ is identical to the parameter C_π in the hybrid-pi model. This can be seen by noting that the term $\tau_F I_E(q/kT)$ is approximately equal to the capacitor C_b defined by Eq. (2-19) because $|I_E| \cong |I_C|$ for a BJT operated in the normal region. The hybrid-pi model parameter C_π is given by $C_\pi = C_b + C_{je}$. Thus the hybrid-pi model parameter C_π can be expressed by

$$C_\pi = (\tau_F I_E(q/kT)) + C_{je} \tag{3-52}$$

The NCAP parameter C_2' is thus given by*

$$C_2' = dC_\pi/dI_E = \tau_F(q/kT) \tag{3-53}$$

By plotting the hybrid-pi parameter C_π versus the dc emitter current I_E, the NCAP parameters C_2' and C_{je} can be determined from the slope and intercept of the resulting curve.

Next we want to relate the cutoff frequency f_T to C_π. The relationship between f_T and C_π can be derived by beginning with the definition of the common emitter short-circuit current gain h-parameter h_{fe} at a frequency f. From Figure 3-20 the parameter h_{fe} can be calculated assuming that $r_\mu >> 1/\omega C_\mu$; the result is

$$h_{fe} = I_c/I_b \cong g_m r_\pi/(1+j\omega(C_\pi+C_\mu)r_\pi) \tag{3-54}$$

Equation (3-54) is plotted in Figure 3-24 in the conventional manner which is a plot of log $|h_{fe}|$ vs log f. The low frequency asymptote is $g_m r_\pi$ which is the h_{fe} value measured at 1 kHz. The corner frequency f_β is given by $f_\beta = 1/2\pi r_\pi(C_\pi + C_\mu)$. The

* The NCAP parameter C_2' can be determined directly from the large signal model parameter τ_F used in SPICE2 and SCEPTRE by using Eq. (3-53).

frequency at which $|h_{fe}| = 1$ is by definition the frequency f_T. Let the measurement frequency f_m have any value in the range $f_\beta < f_m < f_T$, then the important result[18]

$$f_T = f_m |h_{fe}(f_m)| \tag{3-55}$$

can be obtained by geometrical arguments based upon Figure 3-24. Thus by measuring $|h_{fe}(f)|$ at a frequency f_m in the range $f_\beta < f_m < f_T$, a value for f_T can be determined using Eq. (3-55). Measurements of the frequency f_T were made on a commercial bridge (Automatic Measurement, Inc. Model OH-100) specifically developed for this purpose at f_m = 100 MHz.

When the operating frequency becomes very large, the term 1 in the Eq. (3-54) can be neglected compared with the term $j\omega(C_\pi+C_\mu)r_\pi$. Therefore Eq. (3-54) can be written as

$$h_{fe} \simeq g_m/(j\omega(C_\pi+C_\mu)) \tag{3-56}$$

Using the definition of f_T that $|h_{fe}| = 1$ at $f = f_T$, we obtain

$$|h_{fe}(f=f_T)| = g_m/2\pi f_T(C_\pi + C_\mu) = 1 \tag{3-57}$$

Since $|I_E| \cong |I_C|$ in the normal region, we may express g_m by $g_m = q|I_E|/kT$ and substitute this result in Eq. (3-57) to obtain the desired result for the capacitiance C_π which is

$$C_\pi = (1/2\pi)(q/kT)|I_E|/f_T - C_\mu \tag{3-58}$$

By measuring values of the cutoff frequencies f_T* at different emitter current levels, we can use Eq. (3-58) to calculate values

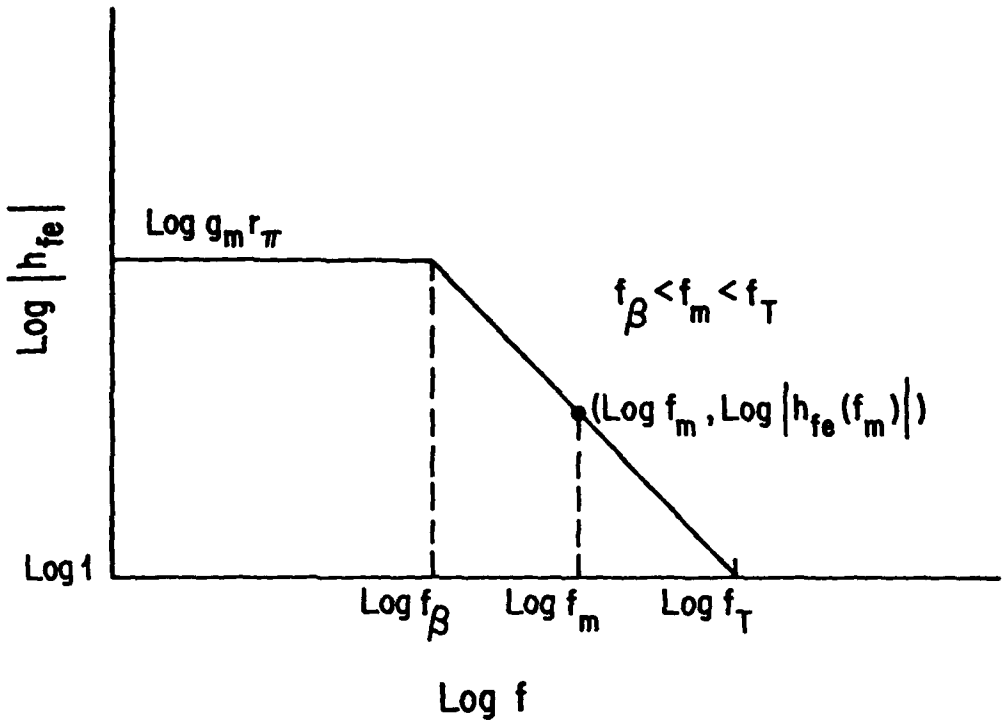

FIGURE 3-24. Conventional Asymptotic Plot of $|h_{fe}|$ vs f

for the capacitance C_π. Usually when the BJT is operated in normal region, the capacitance C_μ is negligible in comparison with the capacitance C_π. The C_π values are plotted as a function of emitter current level I_E. Typical measured data for C_π vs I_E for a 2N5179 BJT are plotted as shown in Figure 3-25. The intercept on the C_π axis yields a value for C_{je} = 4.5 pF. The slope yields a value for C_2' = 4.77 pF/mA.

*It should be noted that the parameter f_T is not a constant but depends upon the emitter current I_E. This is specially true at low values of emitter current I_E where the dominent contribution to the charge stored in the emitter-base region is the depletion layer charge given by Eq. (2-17). It should be further noted that the plot of C_π as defined by Eq. (3-58) does not have the value C_{jeo} at I_E=0. Instead the value of C_π as defined by Eq. (3-58) at I_E=0 is C_{je}, which is the parameter used in NCAP.

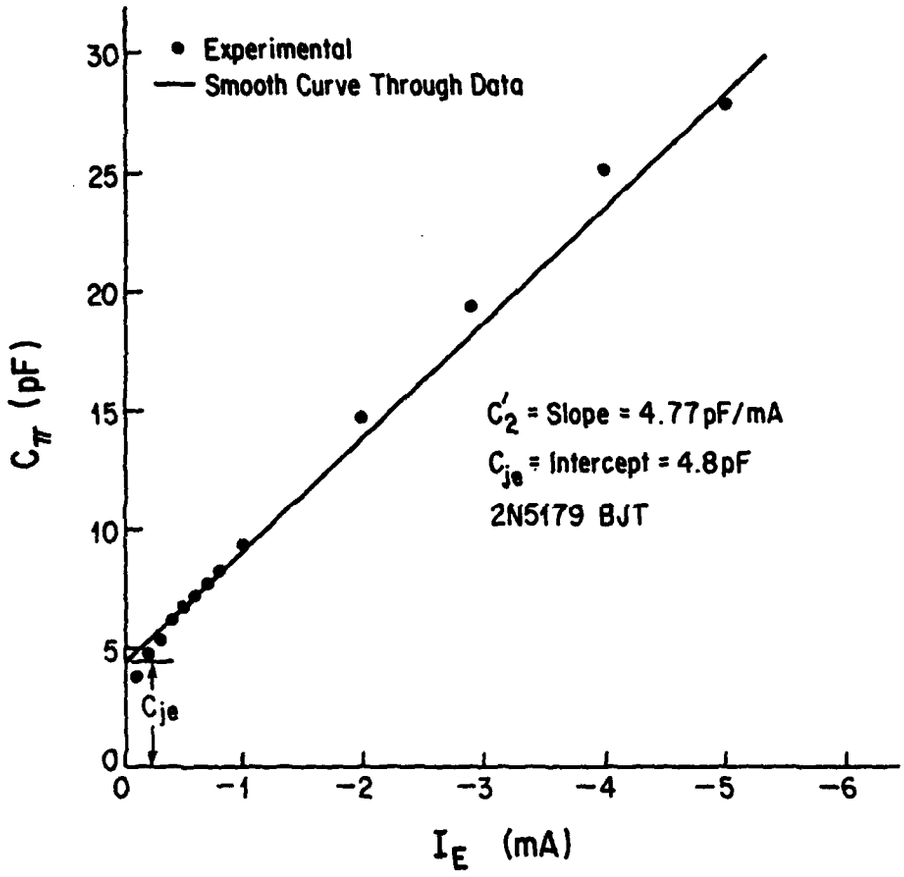

FIGURE 3-25 Plot of C_π Vs I_E Used to Determine NCAP Parameters C_{je} and C'_2

3.2.3 τ_F, Forward Transit Time Constant

The transit time τ_F is used in both the computer programs SPICE2 and SCEPTRE. A value for τ_F is needed in order to determine the capacitor C_π which appears in the linear equivalent circuit (the hybrid-pi model) used for ac analysis in both of these programs. It is also required for transient analysis.

Equating Eqs. (3-52) and (3-58) for C_π and using the approximation $|I_E| = |I_C|$, the following expression relating the cutoff frequency f_T and the forward transit time τ_F is obtained.

$$1/(2\pi f_T) = \tau_F + (C_{je}+C_\pi)kT/(q|I_C|) \qquad (3\text{-}59)$$

By plotting the factor $1/2\pi f_T$ vs the dc collector current I_C, a value for the forward transit time τ_F can be determined from the intercept as shown in Figure 3-26. This method works very well for high frequency transistors having values of $f_T > 300$ MHz and values for $\tau_F < 0.5$ nsec.

3.3 Large Signal Transient Measurements

The forward transit time τ_F and the reverse transit time τ_R used in the computer program SPICE2 and SCEPTRE can be measured in the time domain. The small signal method used to determine the τ_F value just described seems superior to transient measurement methods. This is specially true for τ_F values less than 0.5 nsec. However, the small signal method can not be used to determine a value for the reverse transit time τ_R because the short-circuit current gain is less than 1 for a BJT operated in reverse region.

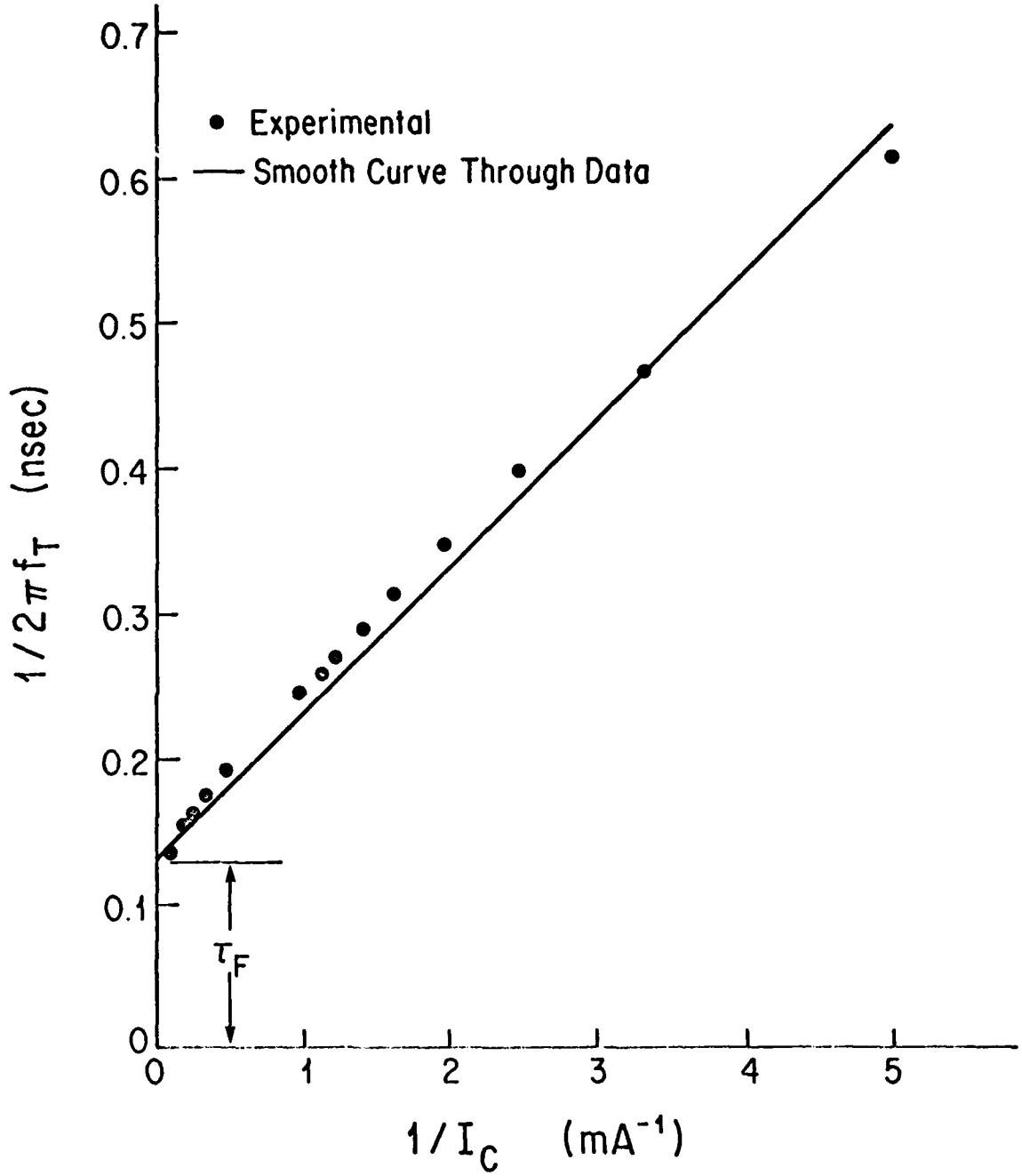

FIGURE 3-26 $1/2\pi f_T$ Versus $1/I_C$ Plot for a 2N5179 Device

Thus a time domain measurement method for the reverse transit time is used.[27]

The basic scheme used to measure the reverse transit time τ_R is illustrated in Figure 3-27. Three pulses with rise times short compared to the pulse duration are used. The pulse amplitudes V_1, V_2, and V_3 are adjusted so that the emitter-base voltage v_{EB} observed on an oscilloscope (CRO) is zero. The procedure used is to set V_2 at a low value and to adjust the amplitudes V_1 and V_3 until the v_{EB} transient response vanishes. The amplitude for $V_1 = V_1^o$, $V_2 = V_2^o$ and $V_3 = V_3^o$ are recorded.

Next the amplitude V_2 is increased, and the procedure is repeated. By plotting the time $(V_3^o / V_2^o)\ CR_2$ vs the current (V_2^o / R_2) as shown in Figure 3-27, a value for τ_R can be determined. For additional details the reader is referred to Ref 27. Finally it should be noted that since the BJT is operated in the normal region that the reverse transit time τ_R is not an important parameter. In this case a default value such as $\tau_R = 100$ nsec can be used.

3.4 Parasitic Elements

At frequency greater than 100 MHz many parasitic elements may affect BJT operation. These include the lead inductances associated with the bond wires attached to the emitter and base metallizations and the three BJT leads used to make external circuit connections. Also important are the capacitive parasitic elements. In the computer program NCAP the parasitic capacitors C_1 and C_3 are used to denote the

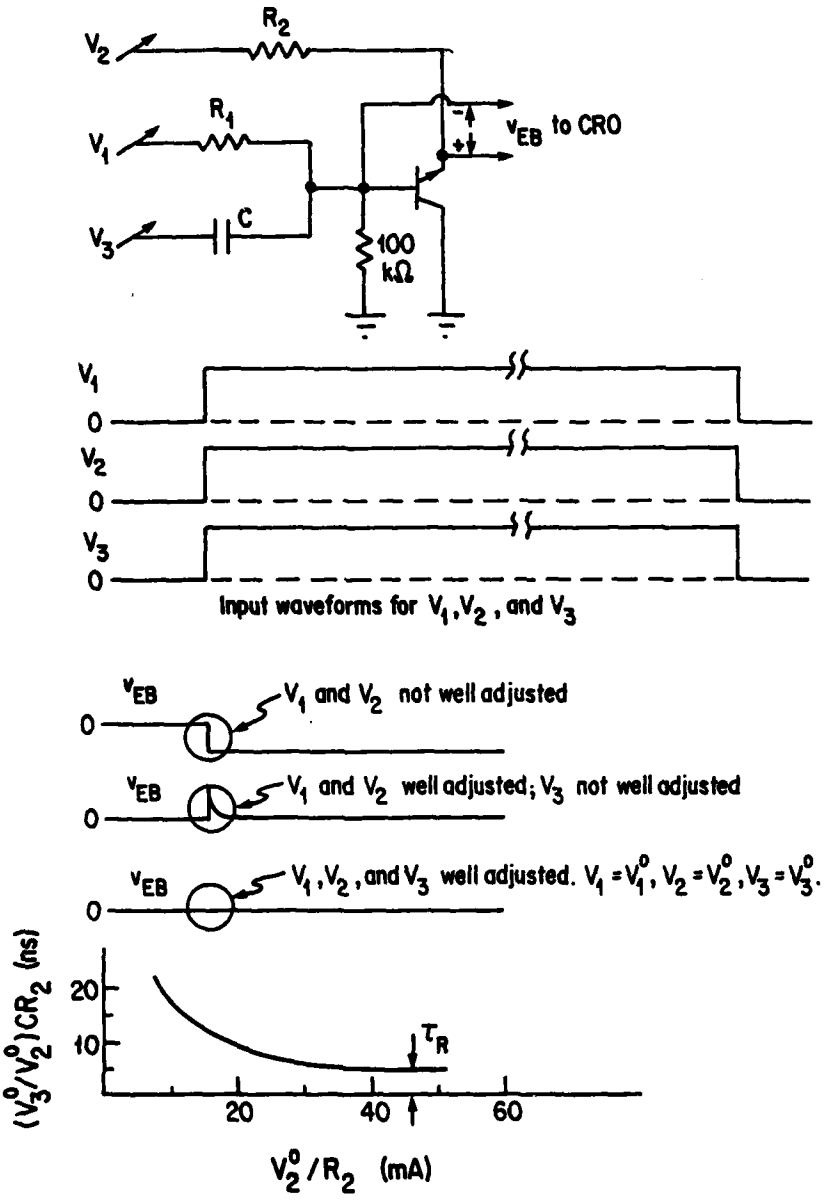

FIGURE 3-27 Test Configuration and Waveforms for the Measurement and the Evaluation of the Reverse Transient Time τ_R

capacitances between emitter and base leads and between collector and base leads respectively. Another parasitic capacitance between collector and emitter leads also exists. In an integrated circuit additional parasitic capacitances exists for the BJT. These include the junction capacitance of each PN junction used to provide isolation. One of these is denoted in SPICE2 as the substrate capacitance C_{CS}, which is the capacitance between the collector region and the substrate.

There is really no way to determine values for each individual parasitic component directly. The most widely used procedure is to include the parasitic elements in a small signal linear incremental model for a tansistor and to adjust parasitic element values to obtain the best fit between measured and calculated parameters such as y-parameters.[24] Although this procedure is tedious and time consuming and does not usually lead to a unique set of parasitic elements values, there is simply no other way.[24]

3.5 Summary of Parameter Values

In this section the parameter values measured for two discrete transistors are summarized. In Table 3-3 the NCAP parameter values are presented for two NPN BJT's: the 2N5179 and the 2N918. In Table 3-4 the SCEPTRE parameter values for these transistors are given. In Table 3-5 the SPICE2 parameter values are given for these transistors. Since there are actually two different large signal models available in SPICE2, parameter values for both models are given. The procedures

used to determine the Ebers-Moll model parameters have been described in this chapter. Additional methods not described in this chapter were used to obtain values for the SPICE Integral Charge Control Model (ICM) parameters. For completeness ICM model parameters are also included in Table 3-5.

TABLE 3-2

TYPICAL RESULTS OBTAINED USING THE COMPUTER PROGRAM OPTIMIZATION TECHNIQUE LISTED IN TABLE 3-1

Input Data

C_{meas} (pF)	V_{bias} (V)	C_x (pF)	$C_{meas}-C_x$ (pF)
3.6	0.002	1.24	2.36
3.46	0.119	1.24	2.22
3.38	0.219	1.24	2.14
3.31	0.319	1.24	2.07
3.21	0.509	1.24	1.97
3.04	1.01	1.24	1.8
2.86	1.97	1.24	1.62
2.74	3.01	1.24	1.5
2.60	5.0	1.24	1.36

Output Data

C_{jeo} (pF)	Φ_E (V)	m_e	No. of Iteration
2.36	0.36	0.2	4

TABLE 3-3

NCAP BIPOLAR JUNCTION TRANSISTOR MODEL PARAMETERS

PARAMETER	DESCRIPTION	2N5179	2N918
η	Avalanche Exponent	3.26	8.61
V_{CB}(V)	Collector Base Bias Voltage	5.0	5.0
V_{CBO}(V)	Avalanche Voltage	45	60
μ	Collector Capacitance Exponent	0.37	0.328
I_C(mA)	Collector Bias Current	1.0	1.0
I_{Cmax}(mA)	Collector Current at Maximum DC Current Gain	10	3
a	h_{FE} Nonlinearity Coefficient	0.122	0.879
h_{FEmax}	Maximum DC Current Gain	46	48
k(pF-$V^{1/2}$)	Collector Capacitor Scale Factor	0.588	0.85
Ref	Diode Nonideality Factor	1.006	1.027
C_{je}(pF)	Base-Emitter Junction Space Charge Capacitance	4.5	5.0
C_2'(pF/mA)	Derivative of Base-Emitter Diffusion Capacitance	4.77	5.68
r_b(Ω)	Base Resistance	50	39
r_c(MΩ)	Collector Resistance	1.254	0.473
C_1(pF)	Base-Emitter Capacitance	7.16	7.0
C_3(pF)	Base-Collector and Overlap Capacitance	0.48	1.27

TABLE 3-4

SCEPTRE BIPOLAR JUNCTION TRANSISTOR MODEL PARAMETERS

PARAMETER	DESCRIPTION	2N5179	2N918
$\theta_E(=q/(Ref)kT)$	Emitter-Base Junction Constant	38.23	37.45
$\theta_C(=q/(Rcf)kT)$	Collector-Base Junction Constant	16.65	-
$I_{ES}(A)$	Emitter-Base Saturation Current	2.4E-16	8.62E-16
$I_{CS}(A)$	Collector-Base Saturation Current	4.6E-10	-
α_N	Forward Current Gain	0.979	0.98
α_I	Inverse Current Gain	0.556	0.636
$n_E(=m_e)$	Emitter Junction Grading Constant	0.283	0.342
$n_C(=m_c)$	Collector Junction Grading Constant	0.37	0.328
$\phi_E(V)$	Emitter-Base Junction Contact Potential	0.7	0.7
$\phi_C(V)$	Collector-Base Junction Contact Potential	0.5	0.5
$COE(=C_{jeo}\phi_E^{m_e})(pF\text{-}V^{1/2})$	Emitter Transition Capacitance Constant	0.65	0.83
$COC(=C_{jco}\phi_C^{m_c})(pF\text{-}V^{1/2})$	Collector Transition Capacitance Constant	0.59	0.85
$T_E(=\tau_F)$(nsec)	Emitter Diffusion Capacitance Constant	0.13	0.15
$T_S(=\tau_R)$(nsec)	Collector Diffusion Capacitance Constant	50	115
RB $(=R_B=r_b)$ (Ω)	Base Bulk Resistance	50	39
RC $(=R_{SC}=r'_c)$ (Ω)	Collector Bulk Resistance	1	1.11
R1 (Ω)	Emitter-Base Junction Leakage Resistance	-	-
R2 $(=r_c)$ $(k\Omega)$	Collector-Base Junction Leakage Resistance	1250	475

TABLE 3-5

SPICE2 BIPOLAR JUNCTION TRANSISTOR MODEL PARAMETERS

PARAMETER	DESCRIPTION	2N5179	2N918	TYPICAL VALUE
BF($=\beta_N$)	Ideal Forward Current Gain	46	48	100
BR($=\beta_I$)	Ideal Reverse Current Gain	1.25	-	0.1
IS($=I_S$)(A)	Saturation Current	2.4E-16	8.6E-16	1.0E-16
RB($=R_B=r_b$)(Ω)	Base Ohmic Resistance	50	39	100
RC($=R_{SC}=r'_c$)(Ω)	Collector Ohmic Resistance	1	1.11	10
RE($=R_{SE}=r'_e$)(Ω)	Emitter Ohmic Resistance	2.45	1.75	1
VA($=V_A$)(V)	Forward Early Voltage	50	28	200
*VB(V)	Reverse Early Voltage	32.5	27.5	200
*IK(mA)	Forward High-Current Knee Current	7	10	10
*C2	Forward Low-Current Nonideal Base Current Coefficient	80.4	930	1000.0
*NE	Nonideal Low-Current Base-Emitter Emission Coefficient	1.393	1.644	2.0
*IKR (mA)	Reverse High-Current Knee Current	100†	100†	100
*C4	Reverse Low-Current Nonideal Base Current Coefficient	1.0†	1.0†	1.0
*NC	Nonideal Low-Current Base-Collector Emission Coefficient	2.0†	2.0†	2.0
TF($=\tau_F$)(nsec)	Forward Transit Time	0.13	0.15	0.1
TR($=\tau_R$)(nsec)	Reverse Transit Time	50	115	10
CCS($=C_{CS}$)(pF)	Collector-Substrate Capacitance	1.28	1.3	2.0
CJE($=C_{jeo}$)(pF)	Zero-Bias B-E Junction Capacitance	0.72	0.94	2.0
PE($=\Phi_E$)(V)	B-E Junction Potential	0.7	0.7	0.7
*ME($=m_e$)	B-E Junction Grading Coefficient	0.283	0.342	0.33

TABLE 3-5 (Continued)

PARAMETER	DESCRIPTION	2N5179	2N918	TYPICAL VALUE
CJC($=C_{jeo}$)(pF)	Zero-Bias B-C Junction Capacitance	0.76	1.065	1.0
PC($=\Phi_C$)(V)	B-C Junction Potential	0.5	0.5	0.5
*MC($=m_c$)	B-C Junction Grading Coefficient	0.37	0.328	0.33
EG (eV)	Energy Gap	1.11	1.11	1.11
**PT	Saturation Current Temperature Exponent	3.0†	3.0†	3.0
**KF	Flicker Noise Coefficient	6.6E-16†	6.6E-16†	6.6E-16
**AF	Flicker Noise Exponent	1†	1†	1
*FC	Forward-Bias Nonideal Junction Capacitance Coefficient	0.5†	0.5†	0.5

* Integral Charge Control Model Parameters

** Flicker Noise Model Parameters

† Typical Values are Used

CHAPTER FOUR

INTEGRATED CIRCUIT MODEL PARAMETERS

In this dissertation two integrated circuits have been investigated. One is a dual differential pair and the other is an operational amplifier. The RCA CA3026 dual differential pair was selected because the differential pair is the basic building block used in integrated circuit and because it is relatively simple to analyze. The Fairchild μA741 monolithic operational amplifier was selected because it is one of the most widely used linear integrated circuits.

In this chapter procedures used to determine the transistor model parameters for the BJT's in these two integrated circuits will be described. Parameter values were determined in three ways. One method involves the use of the manufacturer's data, when such data are available for individual BJT's in the IC.* The second method involves the use of probe techniques. The IC case is opened and the metallization areas of an individual BJT are contacted with small area metal probes. The third method involves using the model parameters reported by other investigators.

In the next section BJT model parameter for the RCA CA3026 dual differential pair will be discussed. Then the model parameters for the BJT's in the Fairchild μA741 operational amplifier will be discussed.

* Manufacturer's data for the individual transistors in the CA3026 dual differential pair were available. This is very unusual. Such data are normally not available.

4.1 The CA3026 Dual Differential Pair

Shown in Figure 4-1 is a schematic diagram of the RCA CA3026. There are two separate differential pair circuits in this IC. The transistors Q1, Q2, and Q3 form one unit and the transistors Q4, Q5, and Q6 form the other unit. All the six transistors are identical in structure. A cascode amplifier using a CA3026 dual differential pair was built. It is a two stage amplifier with a common-emitter first stage and a common-base second stage. Since the input impedance of the common-base stage is low, the amplifier has a wide bandwidth with a decent voltage gain.[18]

As shown in Figure 4-2, the cascode amplifier uses four of the BJT's in the CA3026. The transistor Q3 serves as the gain stage in a C-E configuration; the transistor Q2 serves as a buffer stage in a C-B configuration. The transistor Q1 which is often used for automatic gain control (AGC) has its collector connected to ac ground through a capacitor C5 so that no AGC action is provided by Q1 in the cascode amplifier circuit shown in Figure 4-2. The transistor Q4 is used as part of the dc bias circuitry as a current mirror diode. Resistors R1, R2, R3, and R4 are used for dc bias. The input signal for the amplifier is coupled into the base terminal of the Q3 through a coupling capacitor C1, and the output signal is coupled out at the node between the resistors R5 and R6. The output impedance of the amplifier was set near 51 ohms at midband frequencies by the resistor R5 so that 50 ohms input impedance measuring instruments could be connected directly to the amplifier.

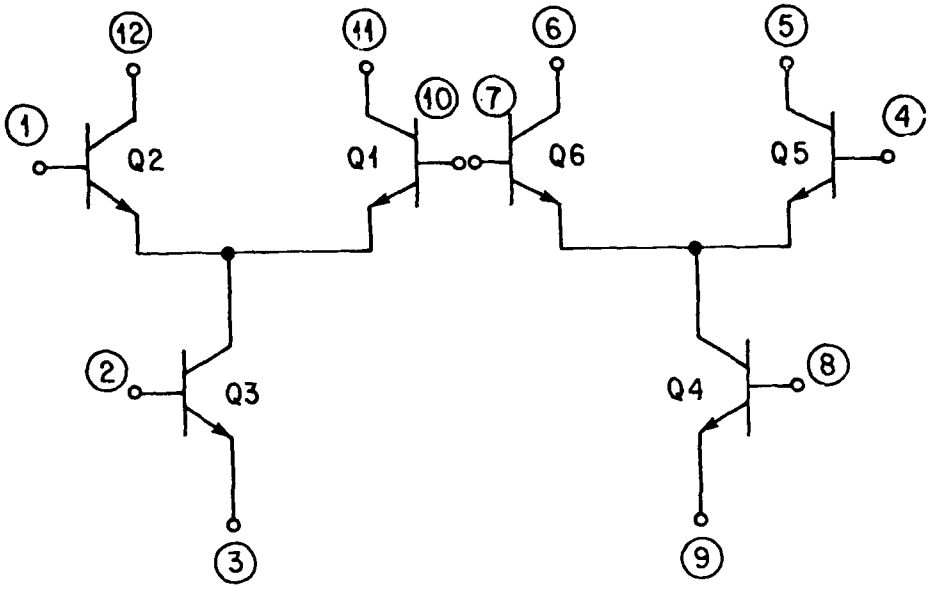

FIGURE 4-1 Schematic of RCA CA3026 Integrated Circuit

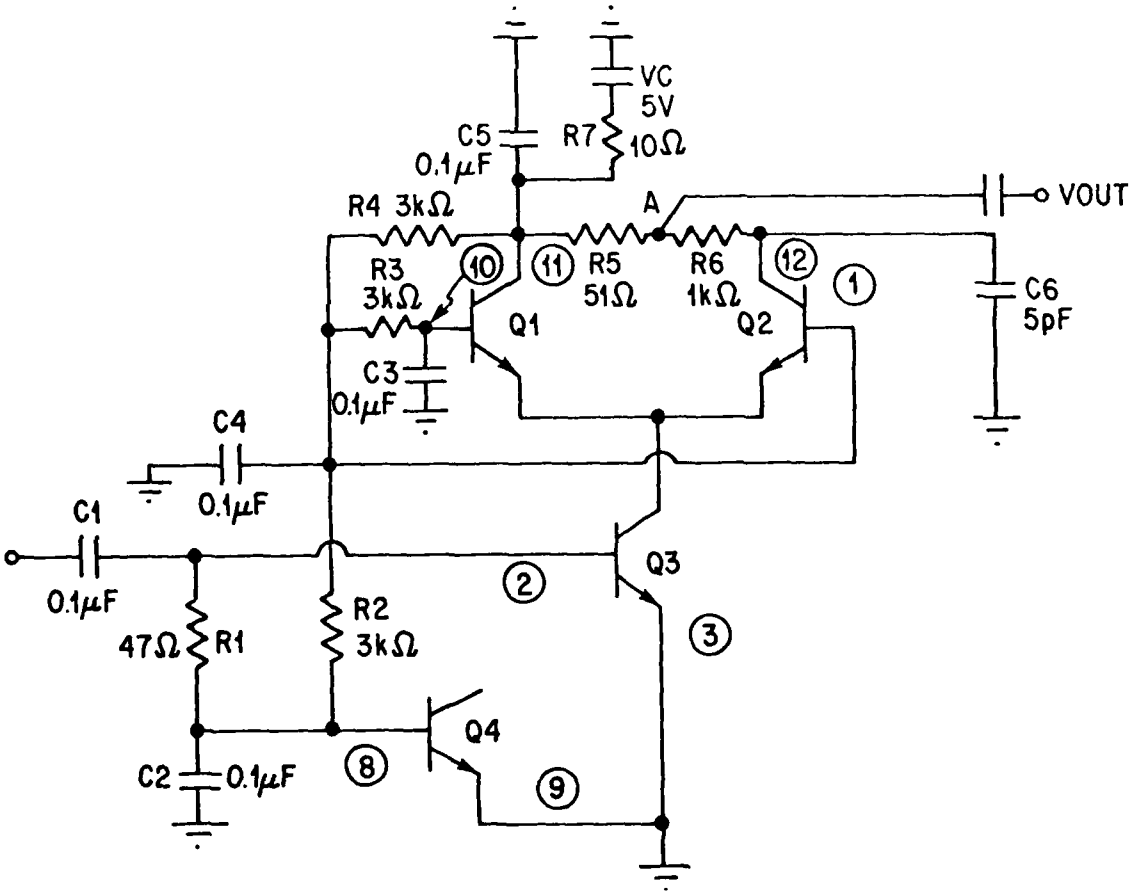

FIGURE 4-2 Schematic of CA3026 Cascode Amplifier

Since the computer program NCAP will be used to calculate the nonlinear performance of this amplifier, dc operating point information for all transistors is needed. This information will be determined first.

4.1.1 Direct Measurement of DC Operating Points

The resistors R1-R4 were selected to provide dc collector currents in the 1-5 mA range. By measuring the voltages across the resistors R4, R5, R6 and R7 shown in Figure 4-2, the dc collector currents I_{C1} and I_{C2} for transistor Q1 and Q2 can be determined. The emitter current I_{E3} for Q3 is approximately the sum of I_{C1} and I_{C2}. By measuring the voltage across the resistor R2, the emitter current I_{E4} for Q4 can be determined. Since the transistor Q4 is operated in a diode mode and is shunted by a large capacitor (C2 = 0.1 μF), the transistor Q4 does not affect the cascode amplifier ac operation. Thus the transistor model parameters for Q4 are not presented. The collector-base voltages V_{CB1} and V_{CB2} for the transistors Q1 and Q2 can be measured directly. The collector-base voltage V_{CB3} can be determined by measuring the voltage V_{82} between pin 8 and pin 2. The voltage V_{CB3} is given approximately by V_{82} -0.6 V where a base-emitter voltage value of 0.6 V is assumed for the transistor Q_1. A summary of the dc operating points for the BJT's in the CA3026 cascode amplifier is given in Table 4-1.

TABLE 4-1

NCAP INPUT PARAMETERS FOR RCA CA3026 INTEGRATED CIRCUIT

Parameter	Method	Q_1	Q_2	Q_3
η	Meas.[a]	4.67	4.67	4.67
V_{CB}(V)	Meas.	2.20	0.25	1.36
V_{CBO}(V)	Meas.	60.0	60.0	60.0
μ	Meas.	0.34	0.34	0.34
I_C(mA)	Meas.	1.25	1.83	3.12
I_{Cmax}(mA)	Meas.	2.00	2.00	2.00
a	Meas.	0.5	0.5	0.5
h_{FEmax}	Meas.	110.0	110.0	110.0
k(pF-$V^{\frac{1}{2}}$)	Meas.	1.99	1.99	1.99
Ref	Meas.	1.04	1.04	1.04
C_{je}(pF)	Manu.[b]	5.13	5.13	5.13
C_2'(pF/mA)	Manu.	9.86	9.86	9.86
r_b(ohm)	Manu.	512.0	554.0	483.0
r_c(kohm)	Meas.	40.0	50.0	50.0
C_1(pF)	-	0.1	0.1	0.1
C_3(pF)	-	0.1	0.1	0.1

[a] Meas: Determined from Measurements

[b] Manu: Determined from Typical Transistor Data Provided by Manufacturer.[28]

4.1.2 NCAP BJT Model Parameters

Also given in Table 4-1 are typical values for all the NCAP BJT model parameters for the CA3026. These typical parameter values were determined in two ways. When available the typical data for the individual transistors in the CA3026 provided by the manufacturer were used. Unfortunately not all the NCAP model parameters for the BJT's in the CA3026 can be determined from manufacturer's data. Probe techniques were used to determine the additional data required. The probe techniques are destructive techniques. By destructive techniques we mean that a CA3026 which has been probed to determine the BJT's model parameters used in NCAP can no longer be used in the cascode amplifier shown in Figure 4-2. Therefore, the NCAP model parameters for the CA3026 determined by probing are representative values determined from the 10 - 15 IC's probed. First we shall describe how some of the parameter values can be determined from manufacturer's data and then how the remaining parameter values can be determined by using probing techniques.

4.1.2.1 The Use of Manufacturer's Data[28]

Shown in Figure 4-3 are typical characteristics for an individual transistor in the CA3026 provided by the manufacturer. From these data, values for the NCAP parameters C_2', C_{je}, and r_b can be determined.

The high frequency parameters C_{je} and C_2' can be determined using the data given in the plot of the gain-bandwidth product f_T vs collector current I_C. The procedures described in Section 3.2.2 are used.

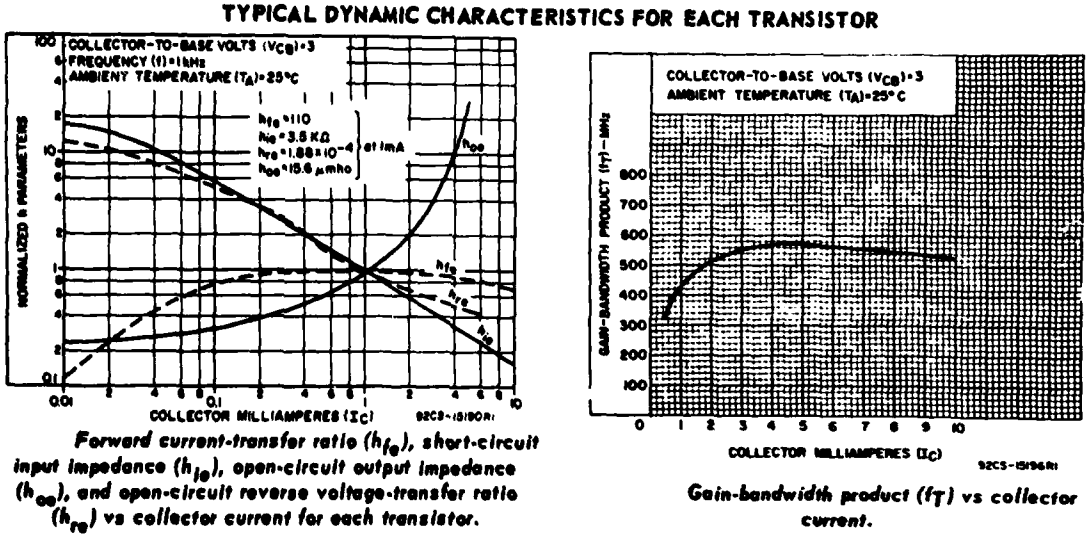

FIGURE 4-3 Typical Characteristics for Each Transistor in CA3026. (After Ref. (28)).

Equation (3-58) is modified by including the emitter base diode nonlinearity factor Ref and by neglecting C_μ. The result is

$$C_\pi = q|I_E|/(2\pi f_T \mathrm{Ref} kT) \qquad (4\text{-}1)$$

It is also assumed that the dc emitter current I_E and dc collector current I_C are equal. (A value for Ref = 1.044 was determined using probe techniques to be described later.) Convenient values of $I_E(I_C)$ are selected and the corresponding values of f_T are determined from Figure 4-3. Next the values of C_π are calculated by using Eq. (4-1) and plotted vs I_E as shown in Figure 4-4. The numerical values of parameters I_E, f_T, and C_π used are tabulated on the following page.

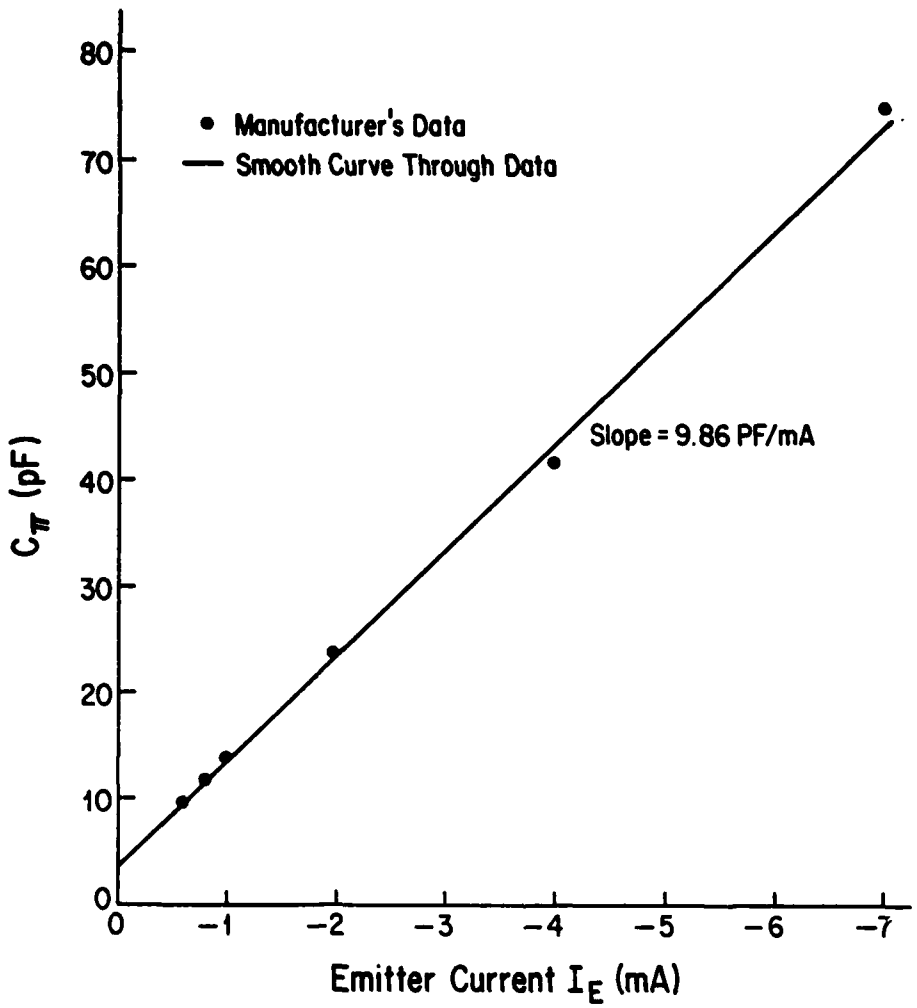

FIGURE 4-4 A Linear Plot of Emitter Capacitance Versus Emitter Current in Device CA3026

I_E (mA)	0.6	0.8	1.0	2.0	4.0	7.0	10.0
f_T (MHz)	370	400	430	510	570	569	530
C_π (pF)	9.62	11.9	13.8	23.3	41.6	74.2	111.9

From Figure 4-4, the slope (C_2') and the intercept (C_{je}) were found to be*

$$C_2' = 9.86 \text{ pF/mA}$$

$$C_{je} \approx 5.13 \text{ pF}$$

These values are given in Table 4-1.

Values for the base spreading resistance r_b can be determined using Eq. (3-40) and the data presented in Figure 4-3 for the short-circuit input impedance h_{ie} and the short-circuit current gain h_{fe}. Values for the dc operating point collector current I_C are taken from Table 4-1. The following table summarizes the numerical results:

	Q1	Q2	Q3
I_C(mA)	1.25	1.85	3.12
h_{fe}	110	110	110
h_{ie} (ohm)	2.8k	2.1k	1.4k
r_b (ohm)	512	554	483

* Upon examining Figure 4-4 the value C_{je} = 4 pF now appears more appropriate then the value C_{je} = 5.13 pF. However the value C_{je} = 5.13 pF is entered in Table 4-1 and was used in the NCAP analysis.

The values determined for r_b for each transistor are also listed in Table 4-1. It is appropriate to point out that the manufacturer's data given in Figure 4-3 were measured at 1 kHz. At frequencies greater than 10 MHz, the values for r_b may be less. As discussed in Section 3.2.1 the base region modelled by the resistor r_b is actually a distributed R-C transmission line.

It is also possible to determine a typical parameter value for the collector resistance r_c using the manufacturer's data for the open circuit reverse transfer parameter h_{re} shown in Figure 4-3. Furthermore if it is assumed that the large signal forward-injection common-emitter short-circuit current gain h_{FE} is equal to the small signal common-emitter short-circuit current gain h_{fe}, values for the NCAP parameters I_{Cmax}, h_{FEmax}, and a could be determined using the data shown in Figure 4-3. This was not the procedure used in this dissertation. These parameters were determined by using probing techniques as described next.

4.1.2.2 The Use of Measured Data

In this section the procedures used to determine the NCAP BJT parameters by direct measurements will be described. In an IC such as the CA3026 the BJT's are all interconnected. It is not possible to measure the characteristics of one BJT in the CA3026 by making measurements at the IC terminals. The best procedure seems to be one based upon probing techniques. The first step is to cut off the transistor header. This was done on a lathe. Next the glass passivation layer

is removed from the areas to be probed. This was done using a sharp probe with a tungsten tip under a microscope. (See Appendix II on probe preparation.) Considerable care, effort, and time are required. Next a single transistor on the IC is isolated from all other transistors on the IC. This was done by using a sharp probe with a tungsten tip to cut the metallizations connected to the transistor. Finally the emitter, base, and collector metallizations of the isolated transistor are contacted with sharp metal probes held in micromanipulators and viewed under a microscope with magnification 200X.

(1) Ref, Base-Emitter Diode Nonideality Factor

Using the procedures described in Section 3.1.1, the emitter base diode nonideality factor Ref can be determined. Values of the dc emitter current I_E are plotted vs dc emitter-base voltage V_{BE} for a representative BJT in the CA3026 as shown in Figure 4-5. Data measured for other BJT's in the CA3026 are similar. Using Eq. (3-2) and the points (V_{BE1} = 0.639 V, I_{E1} = 20 μA) and (V_{BE2} = 0.759 V, I_{E2} = 500 μA), we obtain Ref = 1.044. This representative value for Ref is listed in Table 4-1. Values determined for Ref for BJT's in other CA3026 IC's are the following: 0.998, 0.880, 1.057.

(2) h_{FEmax}, I_{Cmax}, h_{FE} Nonlinearity Parameters

Using the procedures described in Section 3.1.5, the maximum dc current gain h_{FEmax} and the collector current at maximum dc current gain I_{Cmax} can be determined. Values of the dc common-emitter forward-injection short-circuit current gain h_{FE} are plotted

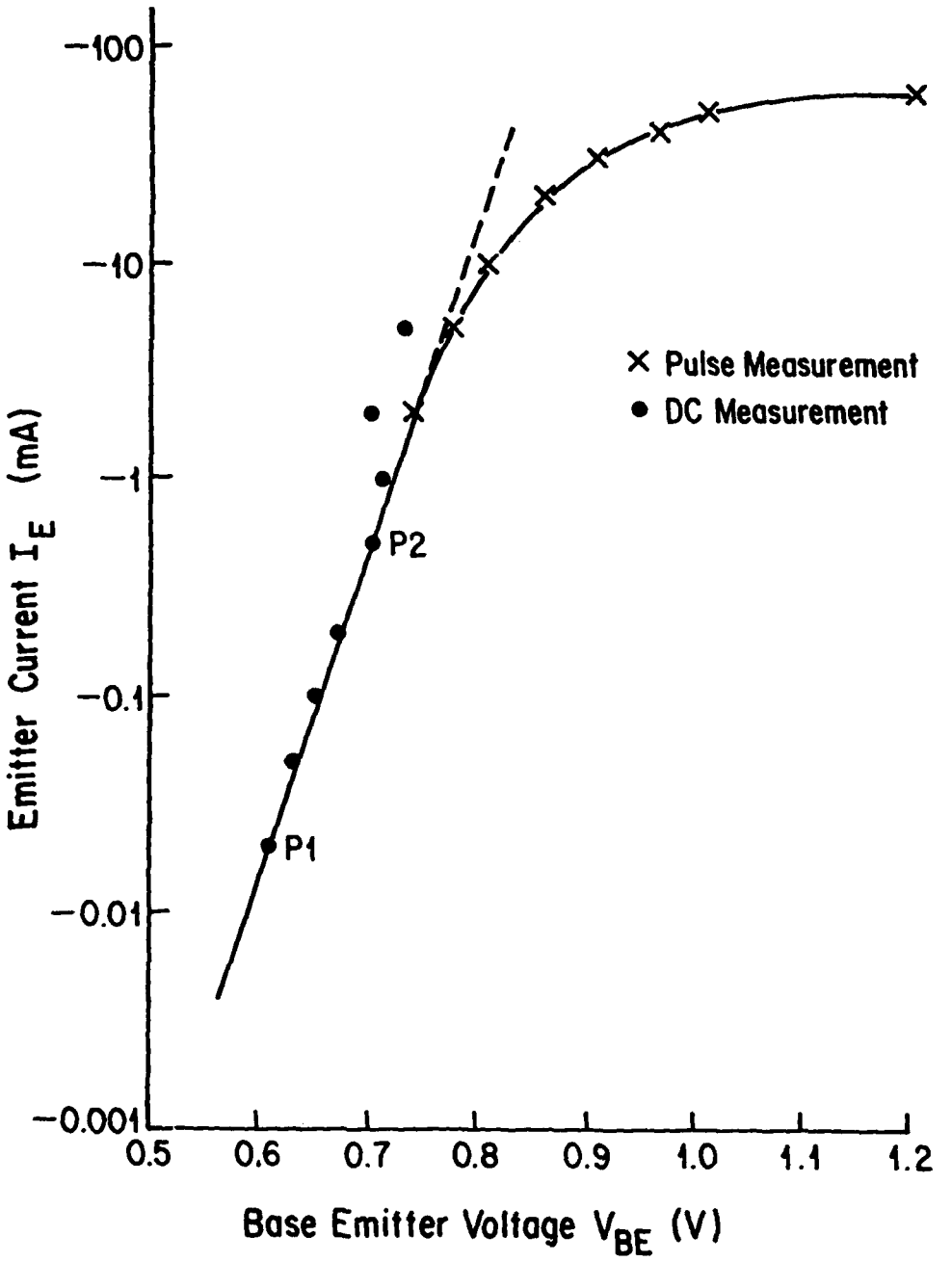

FIGURE 4-5. Representative Plot of I_E vs V_{BE} for an Individual BJT in Device CA3026

vs dc collector current I_C as shown in Figure 4-6 for a representative BJT in the CA3026. Values for h_{FEmax} = 110 and I_{Cmax} = 2 mA taken directly from this figure are listed in Table 4-1. Values for other BJT's in other CA3026 IC's are the following: h_{FEmax}, 113, 133; I_{Cmax}, 1 mA, 2 mA. The value for a is calculated using Eq. (3-10). The values for a depends upon the point (I_C, h_{FE}) used in Eq. (3-10). At several sample points (I_C, h_{FE}) a value for a is calculated. The following results were obtained.

I_C (mA)	h_{FE}	a
0.5	99	0.3065
5	99	0.701

An average value a = 0.5 was entered in Table 4-1 for all transistors. Values for other BJT's in other CA3026 IC's would be similar.

(3) V_{CBO}, η, Avalanche Nonlinearity Parameters and r_c Collector Resistance

Using the procedures described in Section 3.1.9, the collector-base breakdown voltage V_{CBO}, the avalanche nonlinearity parameter η, and the collector resistance r_c can be determined. Values for the collector base breakdown voltage V_{CBO} and the collector emitter breakdown voltage V_{CEO} were determined directly from transistor curve tracer displays. Typical measured values for several CA3026 BJT's were V_{CBO} = 60 V and V_{CEO} = 35 V. Using Eq. (2-24) and assuming value for α_N approximately equal to 0.9 at the vicinity of avalanche

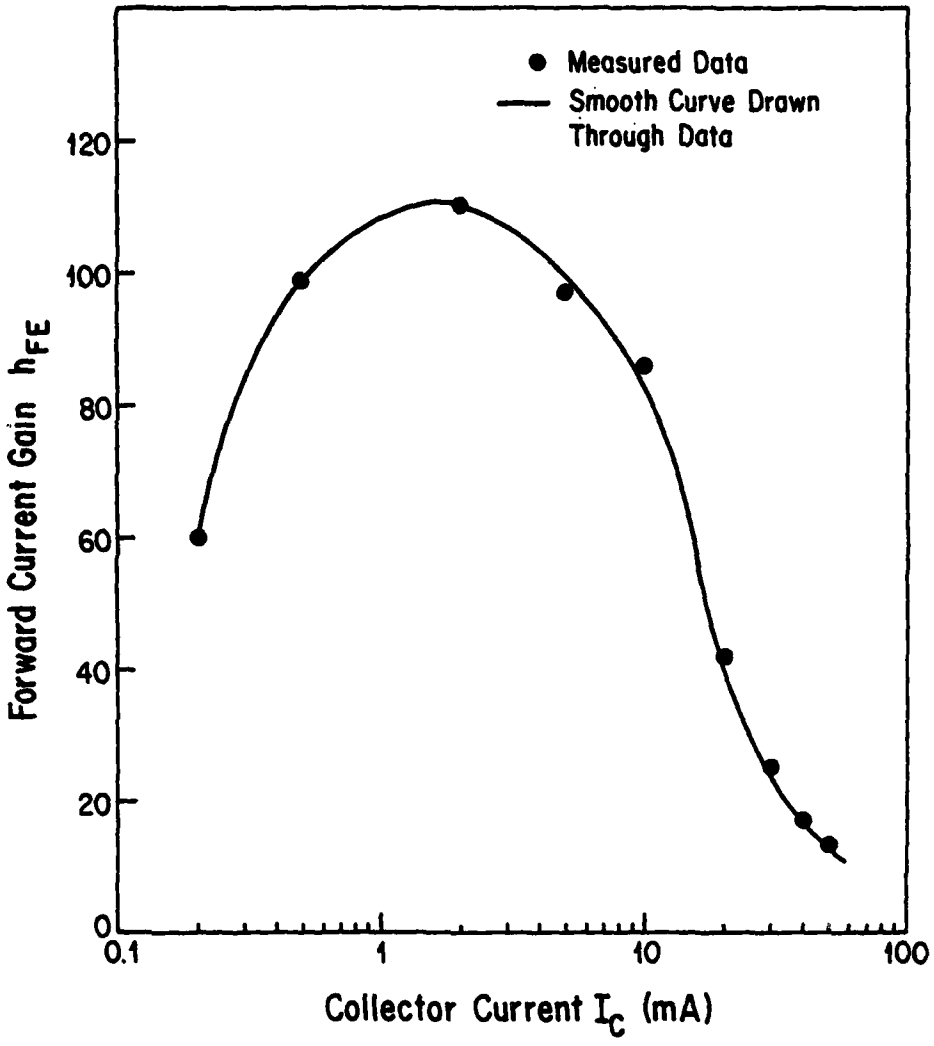

FIGURE 4-6 Representative Plot of h_{FE} vs I_C for an Individual BJT in Device CA3026

breakdown, a value for $\eta = 4.67$ was obtained. This value is given in Table 4-1. Values for other BJT's in the other CA3026 IC's are similar. Values for the collector resistance r_c were determined from the common-emitter I_C-V_{CE} characteristics such as those shown in Figure 4-7. The value for r_c was calculated using the relationship $1/r_c = (\Delta I_C/\Delta V_{CE})/h_{FE}$. This equation is essentially Eq. (2-48) with $1 - \alpha_N$ replaced by $1/h_{FE}$. The following results were obtained:

$$r_c(Q1)=50\ k\Omega; \qquad r_c(Q2) = 50\ k\Omega; \quad \text{and} \qquad r_c(Q3) = 40\ k\Omega.$$

These values are listed in Table 4-1. Again values for other BJT's in other CA3026 IC's would be similar.

(4) k, μ, Collector Base Capacitance Parameters

Using the procedures described in Section 3.1.12, the collector base capacitance scale factor k and the collector base capacitance exponent μ can be determined. Values for the collector base junction capacitance vs collector base junction voltage for a representative CA3026 BJT are plotted in the manner shown in Figure 4-8. A value for the collector-base junction potential $\Phi_C = 0.7$ V was assumed (see Section 3.1.12). A value for $\mu = -0.34$ is determined directly from the slope of the capacitance vs voltage plot. The capacitance C_{jeo} is determined at $V_{CB} = 0$ directly from this plot as shown in Figure 4-8. The value $C_{jeo} = 2.25$ pF was obtained; using Eq. (3-32) the value k = 1.993 pF was calculated. These values are given in Table 4-1. Values determined for other BJT's in other IC's are the following:

μ, 0.20, 0.25, 0.11; k, 1.92, 2.60, 2.20 pF-$V^{\frac{1}{2}}$.

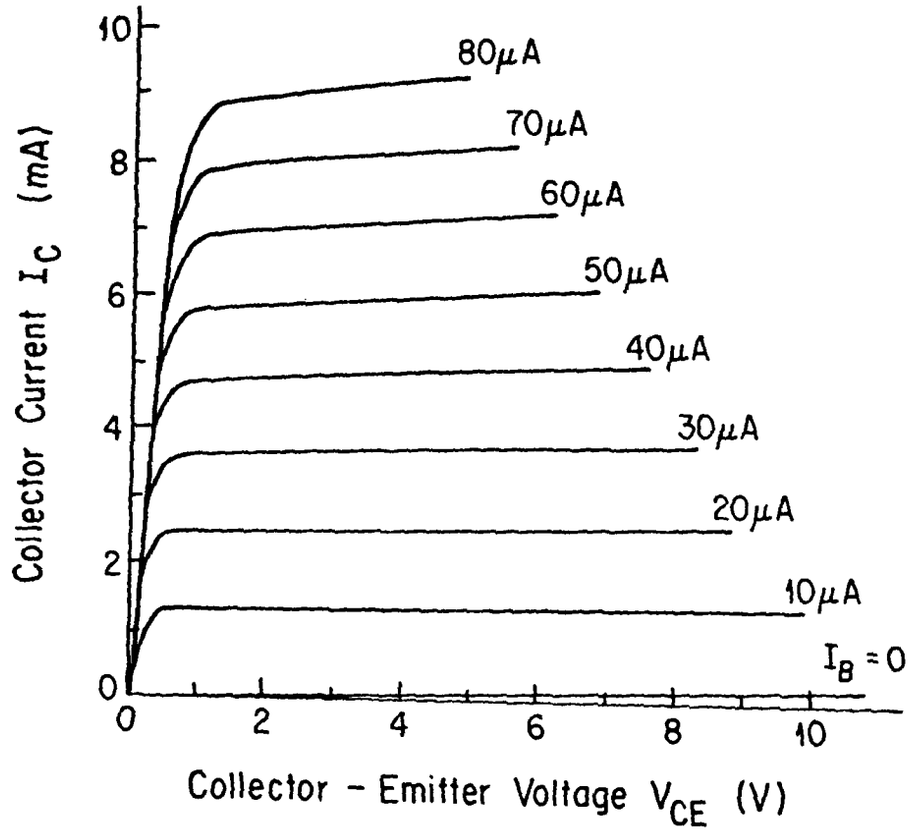

FIGURE 4-7 Representative Output Characteristics of an Individual BJT in Device CA3026

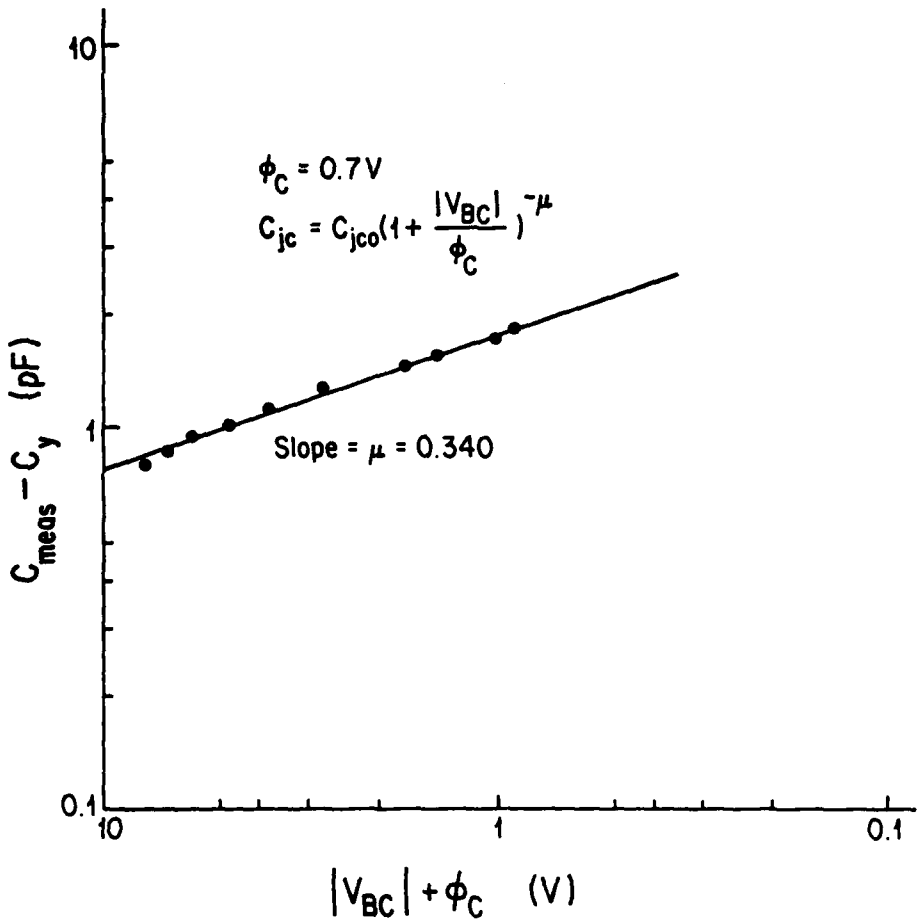

FIGURE 4-8 A Log-Log Plot of Collector-Base Junction Depletion Capacitance Versus Junction Voltage in Device CA3026

4.2 The μA741 Operational Amplifier

The schematic of a μA741 operational amplifier and the top view connection diagram for a TO-99 package are shown in Figure 4-9. There are 24 component BJT's in the circuit diagram. The transistors Q7, Q8, Q9, Q10, Q11, Q12, and Q13 constitute the bias circuitry of the operational amplifier. The input transistors Q1 and Q2 are emitter followers that maintain high input impedance and low input current. The two transistors drive the emitters of the common-base differential pair of PNP devices Q3 and Q4. The transistors Q5 and Q6 form an active load for Q3 and Q4 to provide high voltage gain in the input stage. The six transistors Q1, Q2, Q3, Q4, Q5, and Q6 of the input stage provide features such as a differential input with high common-mode rejection, level shifting, and differential to single-ended conversion.

The transistor Q16 is an emitter follower that buffers the loading effect of Q17 to the active load formed by Q5 and Q6. The transistor Q17 is a common-emitter amplifier that has an active load formed by Q13B (designated as Q26 in SPICE2 and NCAP simulations), and this stage gives a large voltage gain. The transistor Q24A (designated as Q24 in SPICE2 and NCAP simulations) is another emitter follower that reduces the loading effect of the output stage on the gain stage. The output stage is composed of transistors Q14 and Q20. These two transistors provide a class AB output. The transistors Q19 and Q21 serve as a level-shifting unit, whereas the transistors Q15, Q23, Q25, and Q24B are included for protection to prevent damage that might occur to Q14,

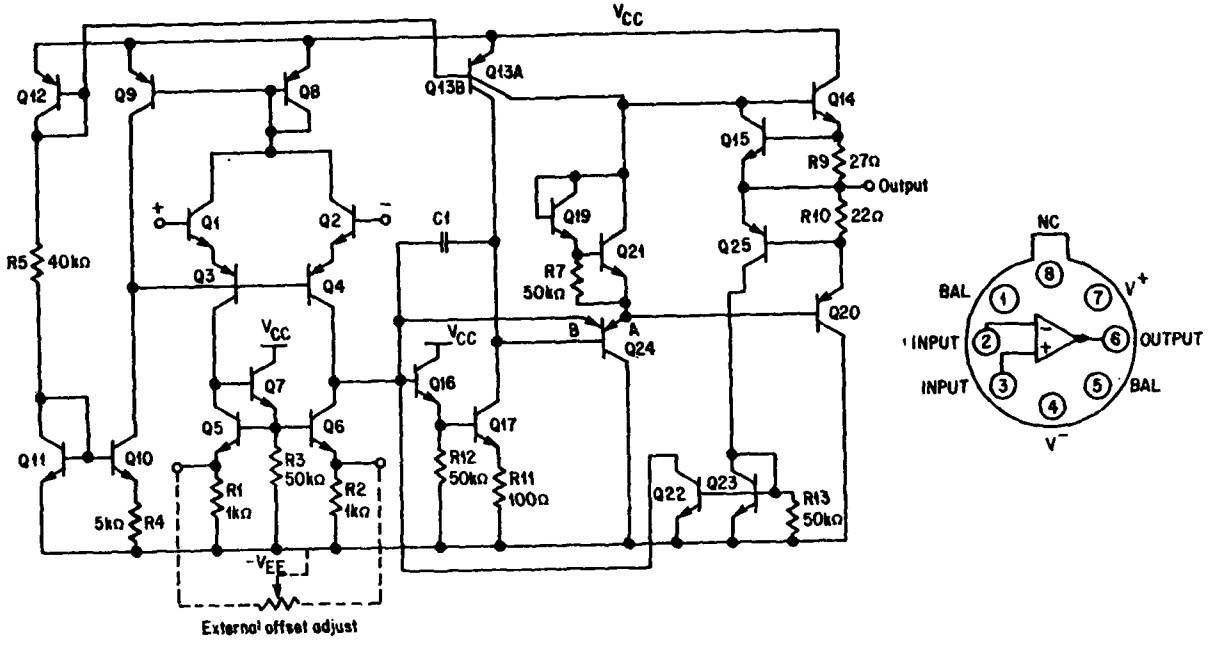

FIGURE 4-9 Schematic of μA741 Operational Amplifier

Q17, and Q20. Since the transistor Q24B is not active under normal operating conditions, the device Q24B (designated as diode D1 in SPICE2 and NCAP simulations) is modelled as a small capacitance.

The BJT's in the μA741 op amp can be catalogued into five categories as illustrated in Figure 4-10. These are the small NPN (Q1, Q2, Q5, Q6, Q7, Q10, Q11, Q15, Q16, Q17, Q19, Q21, Q22, Q23), the large NPN (Q14), the lateral PNP (Q3, Q4, Q8, Q9, Q12, Q25), the large substrate PNP (Q20), the dual-collector lateral PNP (Q13A, Q13B), and the dual-emitter substrate PNP (Q24A, Q24B).

Resistors R1, R2, R3, R4, R5, R7, R9, R10, R11, R12, and R13 are used in the μA741 as part of the bias and level-shifting circuitry. A 30 pF capacitor C1 is used in the μA741 op amp for internal frequency compensation. This compensation capacitor is connected around the Darlington pair Q16-Q17 and produces a pole with magnitude about 4.9 Hz. This action makes the unity gain frequency of the op amp to be 1.25 MHz, the phase margin 80° and the low-frequency gain 108 dB.

A unity gain buffer amplifier with a μA741 IC was selected for the investigation of RFI effects in 741 operational amplifiers (op amp). Shown in Figure 4-11 is the circuit diagram of the unity gain buffer amplifier. The resistor RO = 620 Ω is used as a feedback resistor connected from the output terminal of the μA741 (node 6) to the inverting input terminal (node 2). The resistor RG is the source impedance of the signal generator VG. For a Hewlett Packard model 650A signal generator, the value for RG is 600 Ω. Thus at midband frequencies, the magnitude of the voltage gain which is RO/RG of the

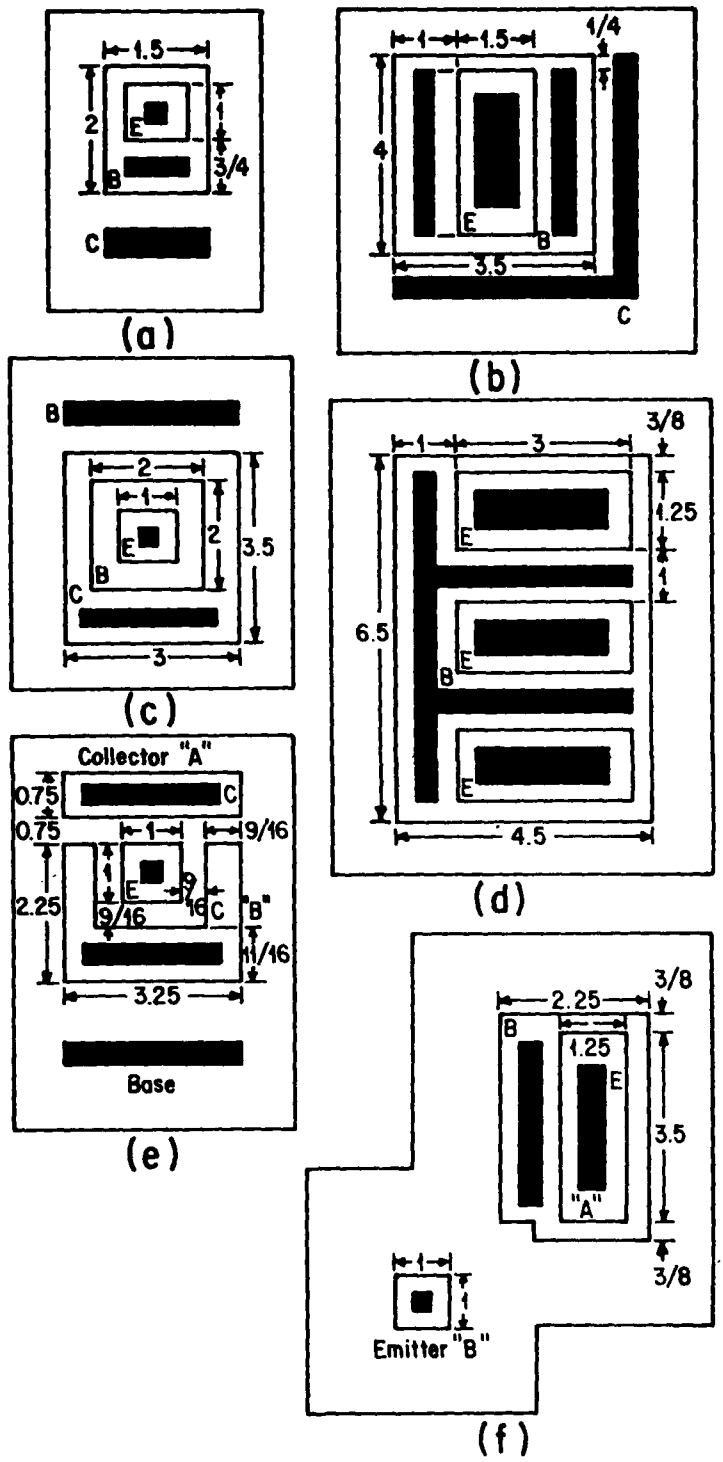

FIGURE 4-10 Plan Views of the 741 Transistors. All Dimensions Are in Mils. (a) Small NPN (b) Large NPN (c) Lateral PNP (d) Large Substrate PNP (e) Dual-Collector Lateral PNP (f) Dual Emitter Substrate PNP. (After Wooley et al.[29])

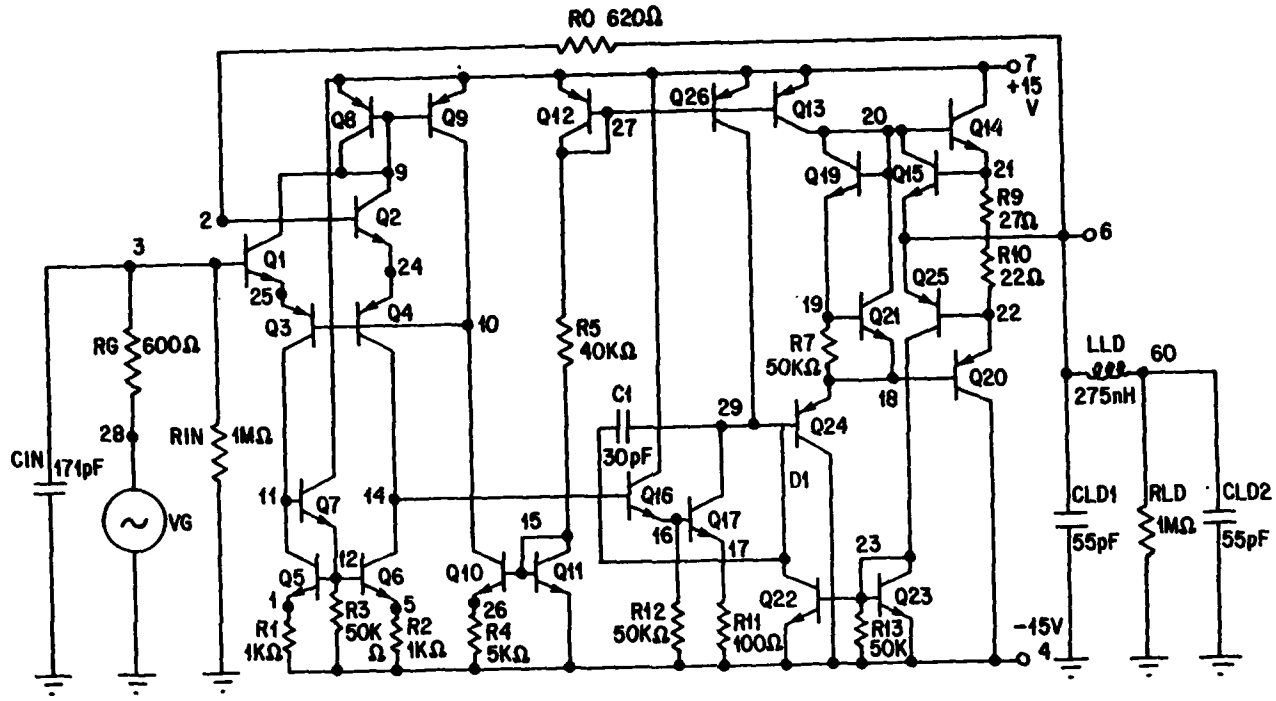

FIGURE 4-11 SPICE2 Coding Diagram of μA741 Operational Amplifier Unity Gain Buffer. This Diagram Is Used to Determine (1) DC Operating Points of Each Individual BJT in the IC, and (2) the Linear Response of the Unity Gain Buffer.

amplifier is about 1.03 (= 620/600).

Since the computer program NCAP will be used to calculate the nonlinear performance of this amplifier, dc operating point information for all transistors is needed. This information will be determined by a SPICE2 simulation. Since the computer program SPICE2 will be used to calculate the dc operating point information of the transistors in the op amp, the SPICE2 BJT model parameters values for all transistors are required. Values of the SPICE2 BJT model parameters will be determined first.

4.2.1 SPICE2 BJT Model Parameters

Given in Table 4-2 are two sets of representative values for most of the SPICE2 BJT model parameters for the μA741. One set of values were obtained from the results reported by Wooley, Wong, and Pederson.[29] The other set of values were determined using the probe measurement techniques discussed in Section 4.1.2.2. However, probe techniques were not used to determine the SPICE2 BJT parameters BR, TF, TR, CCS, and EG. Typical values suggested by SPICE2 users' manual (BR = 0.1, TF = 0.1 nsec, TR = 10 nsec, CCS = 2 pF, and EG = 1.11 eV) are used in this dissertation.

By using probing techniques dc characteristics and junction capacitance characteristics were obtained. Shown in Figures III-1 to III-10 given in Appendix III are representative dc and junction capacitance characteristics for the BJT's in the μA741 op amp.

Values for the BJT parameters shown in Table 4-2 were determined

from these figures by using the procedures described in Chapter Three. Using the procedures described in Sections 3.1.3, 3.1.4, 3.1.7, 3.1.10, 3.1.11, 3.1.12, and 3.2.1 the values for the saturation current IS, the forward current gain BF, the collector ohmic resistance RC, the Early voltage VA, the zero-bias emitter junction capacitance CJE, the zero-bias collector junction capacitance CJC, the built-in potentials PE and PC, and the base spreading resistance RB for the BJT's in the μA741 op amp can be determined. If Eq. (3-40) is used to determine values of RB, values of the h-parameter h_{ie} have to be known first. From the definition of $h_{ie} = \partial v_{be}/\partial i_b \big|_{v_{ce}=0}$, the values of h_{ie} can be readily obtained from the base current I_B vs base-emitter voltage V_{BE} plots given in Figure III-2 in Appendix III.

4.2.2 NCAP BJT Model Parameters

By using the computer program SPICE2 with the BJT's parameter values given in Table 4-2, the dc operating points for all the BJT's in the μA741 were calculated. The calculated dc operating points information (V_{CB}, I_C) of all the BJT's are listed in Table 4-3. The SPICE2 μA741 op amp computer program input data coding list is given in Table 4-4 while the coding circuit diagram is illustrated in Figure 4-11. In order to avoid redundancy, only the Wooley's SPICE2 BJT's data are presented in the Table 4-4.

4.2.2.1 The Use of Measured Data

Also shown in Table 4-3 are values for the other NCAP model parameters for the BJT's in the μA741. These parameter values except

those for C_{je} and C_2' were determined by using the procedures described in Section 4.1.2.1. By utilizing the information given in Appendix III, values for these parameters (except C_{je} and C_2') can be readily determined.

Values for the high-frequency parameters C_{je} and C_2' for the BJT's were calculated from C_π vs I_E data as described in Sections 3.2.2 and 4.1.2.1. The parameter C_2' is the slope of a straight line drawn through the C_π vs I_E data and the parameter C_{je} is the intercept of that line on the C_π axis. The value for C_{je} used is that given in Table 4-2 for CJE. This value is the zero-bias emitter-base junction depletion layer capacitance C_{jeo}. An approximation is involved here in that the C_{je} value used in NCAP is that for a forward-biased emitter-base junction at $I_E = 0$. The actual value of C_{je} should be larger than that of C_{jeo}. Next a value for C_π is calculated using Eq. (4-1). The values for the cutoff frequency f_T at the corresponding emitter current level I_E for the various types of BJT's given in Ref. (30) were used. These values are listed below. The value for C_2' is calculated using $C_2' = (C_\pi - C_{je})/(I_E - 0)$.

Device Type	f_T(MHz)	I_E(mA)	Comment
Small NPN	500	1	Q1, Q2
Small NPN	350	1	Q5, Q6, Q7, Q10, Q11, Q15, Q16, Q17, Q19, Q21, Q22, Q23
Large NPN	300	10	Q14
Lateral PNP	5	0.1	Q3, Q4, Q8, Q9, Q12, Q25
Large sub PNP	15	0.1	Q20
Dual-collector lateral PNP	5	0.1	Q13, Q26
Dual-emitter substrate PNP	15	0.1	Q24

As an illustration, sample calculations in determining the parameters C_2' for the BJT's Q1 and Q3 are tabulated below:

Device	Q1	Q3
Type	Small NPN	Lateral PNP
f_T(MHz)	500	5
I_E(mA)	1	0.1
Ref	1.091	1.336
C_π (pF)	11.22	91.64
C_{je}(pF)	1.23	0.88
C_2' (pF/mA)	9.09	908

4.2.2.2 The Use of Wooley's Data

The NCAP BJT model parameters obtained based upon Wooley's results are also presented in the Table 4-3. Beacuse Wooley's data do not provide enough information for the parameters η, μ, and Ref, typical values for these parameters are used as tabulated below:

Device/Parameter	η	μ	Ref
Small NPN	4	0.333	1
Lateral PNP	1.5	0.333	1
Large substrate PNP	1.5	0.333	1
Dual-emitter sub PNP	3.5	0.333	1
Large NPN	1.5	0.333	1
Dual-collector lateral PNP	1.5	0.333	1

The characteristics of the dc short-circuit current gain h_{FE} versus the dc collector current I_C are provided from Wooley's paper in a normalized plot as shown in Figure 4-12. Using the data in Figure 4-12 and the procedures described in Section 4.1.2.2 (2), the parameter values can be obtained. The results are listed in Table 4-3. The parameter values for C_2' were determined using Eq. (3-54); i.e. $C_2' = \tau_F(q/kT)$. Again the zero-bias emitter-base junction capacitance C_{jeo} value is assumed to be equal to the parameter C_{je} value. Values for C_2' and C_{je} are tabulated in Table 4-3. Also the collector capacitor scale factor k can be obtained using Eq. (3-32). A value for the built-in potential $\Phi_C = 0.7$ V is assumed for all the BJT's in the μA741.

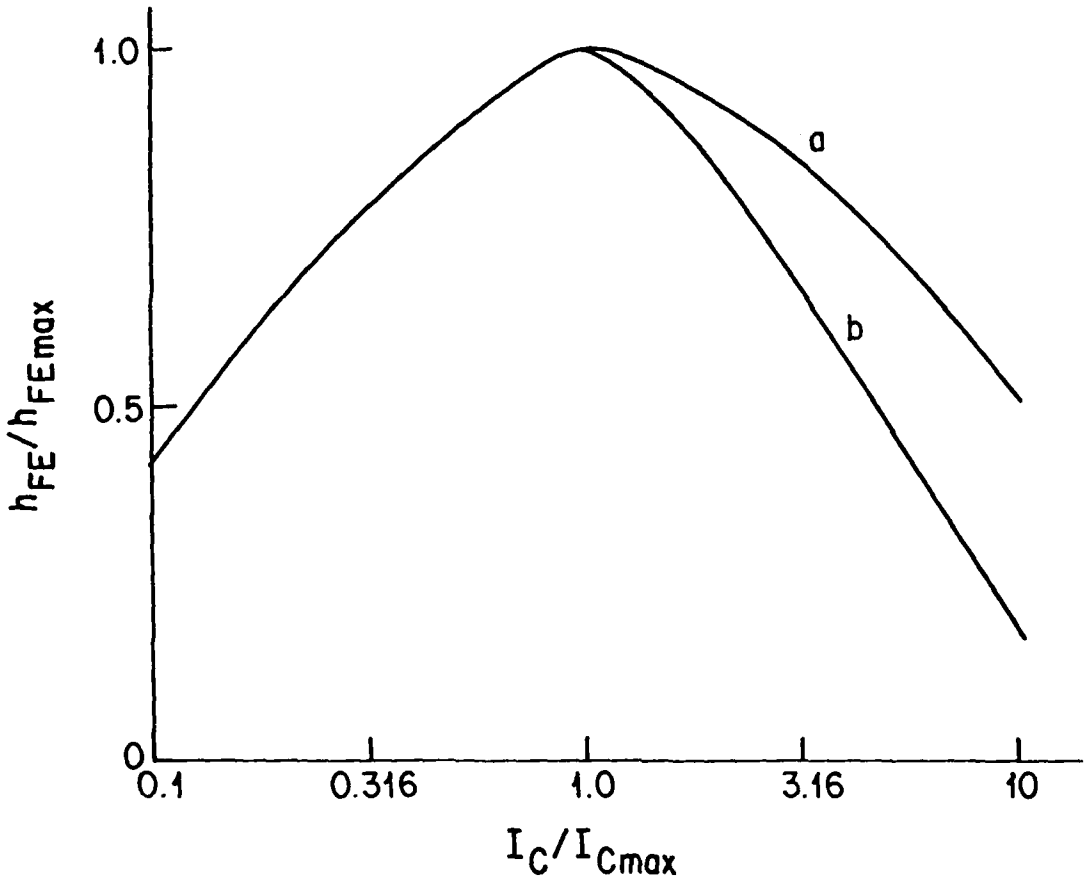

FIGURE 4-12 Normalized Plot of h_{FE} vs Collector Current. Curve a for Small NPN, Large NPN, and Substrate PNP; Curve b for Lateral PNP

TABLE 4-2

SPICE2 μA741 BJT'S INPUT PARAMETERS

Pa / De	BF	BR	IS (10^{-15} A)	RB (Ω)	RC (Ω)	RE (Ω)	VA (V)	TF (nsec)	TR (nsec)	CCS (pF)	CJE (pF)	PE (V)	CJC (pF)	PC (V)	EG (eV)	COM-MENT
Q1 *	210	2.5	1.26	670	300	0	180	1.15	405	3.2	0.65	0.7	0.36	0.5	1.11	Small NPN
Q1 #	400	(0.1)	46	830	190	0	20	(0.1)	(10)	(2)	1.23	0.7	1.37	0.7	(1.11)	
Q2 *	210	2.5	1.26	670	300	0	180	1.15	405	3.2	0.65	0.7	0.36	0.5	1.11	Small NPN
Q2 #	400	(0.1)	46	830	190	0	20	(0.1)	(10)	(2)	1.23	0.7	1.37	0.5	(1.11)	
Q3 *	75	3.8	3.15	500	150	0	55	27.4	2540	5.1	0.1	0.7	1.05	0.5	1.11	Lateral PNP
Q3 #	35	(0.1)	769	520	100	0	50	(0.1)	(10)	(2)	0.23	0.7	1.0	0.5	(1.11)	
Q4 *	75	3.8	3.15	500	150	0	55	27.4	2540	5.1	0.1	0.7	1.05	0.5	1.11	Lateral PNP
Q4 #	35	(0.1)	769	520	100	0	50	(0.1)	(10)	(2)	0.23	0.7	1.0	0.5	(1.11)	
Q5 *	210	2.5	1.26	670	300	0	180	1.15	405	3.2	0.65	0.7	0.36	0.5	1.11	Small NPN
Q5 #	300	(0.1)	9.97	1040	465	0	85	(0.1)	(10)	(2)	0.88	0.7	0.72	0.5	(1.11)	
Q6 *	210	2.5	1.26	670	300	0	180	1.15	405	3.2	0.65	0.7	0.36	0.5	1.11	Small NPN
Q6 #	300	(0.1)	9.97	1040	465	0	85	(0.1)	(10)	(2)	0.88	0.7	0.72	0.5	(1.11)	
Q7 *	210	2.5	1.26	670	300	0	180	1.15	405	3.2	0.65	0.7	0.36	0.5	1.11	Small NPN
Q7 #	300	(0.1)	9.97	1040	465	0	85	(0.1)	(10)	(2)	0.88	0.7	0.72	0.5	(1.11)	
Q8 *	75	3.8	3.15	500	150	0	55	27.4	2540	5.1	0.1	0.7	1.05	0.5	1.11	Lateral PNP
Q8 #	35	(0.1)	769	681	100	0	50	(0.1)	(10)	(2)	0.23	0.7	1.0	0.5	(1.11)	
Q9 *	75	3.8	3.15	500	150	0	55	27.4	2540	5.1	0.1	0.7	1.05	0.5	1.11	Lateral PNP
Q9 #	35	(0.1)	769	681	100	0	50	(0.1)	(10)	(2)	0.23	0.7	1.0	0.5	(1.11)	
Q10 *	210	2.5	1.26	670	300	0	180	1.15	405	3.2	0.65	0.7	0.36	0.5	1.11	Small NPN
Q10 #	300	(0.1)	9.97	1040	465	0	85	(0.1)	(10)	(2)	0.88	0.7	0.72	0.5	(1.11)	
Q11 *	210	2.5	1.26	670	300	0	180	1.15	405	3.2	0.65	0.7	0.36	0.5	1.11	Small NPN
Q11 #	300	(0.1)	9.97	1040	465	0	85	(0.1)	(10)	(2)	0.88	0.7	0.72	0.5	(1.11)	
Q12 *	75	3.8	3.15	500	150	0	55	27.4	2540	5.1	0.1	0.7	1.05	0.5	1.11	Lateral PNP
Q12 #	35	(0.1)	769	681	100	0	50	(0.1)	(10)	(2)	0.23	0.7	1.0	0.5	(1.11)	

TABLE 4-2 (continued)

Pa / De	BF	BR	IS (10^{-15}A)	RB (Ω)	RC (Ω)	RE (Ω)	VA (V)	TF. (nsec)	TR (nsec)	CCS (pF)	CJE (pF)	PE (V)	CJC (pF)	PC (V)	EG (eV)	COM-MENT
Q13 *	0.38	1.4	0.9	1000	80	0	84	27.4	55	4.8	0.1	0.7	0.3	0.5	1.11	Dual Coll.
Q13 #	0.6	(0.1)	192	681	625	0	77	(0.1)	(10)	(2)	0.36	0.7	0.58	0.5	(1.11)	L. PNP
Q14 *	400	6.1	0.395	185	15	0	270	0.76	243	7.8	2.8	0.7	1.55	0.5	1.11	Large
Q14 #	300	(0.1)	19.9	501	65	0	45	(0.1)	(10)	(2)	3.0	0.7	1.25	0.5	(1.11)	NPN
Q15 *	210	2.5	1.26	670	300	0	180	1.15	405	3.2	0.65	0.7	0.36	0.5	1.11	Small
Q15 #	300	(0.1)	9.97	1040	465	0	85	(0.1)	(10)	(2)	0.88	0.7	0.72	0.5	(1.11)	NPN
Q16 *	210	2.5	1.26	670	300	0	180	1.15	405	3.2	0.65	0.7	0.36	0.5	1.11	Small
Q16 #	300	(0.1)	9.97	1040	465	0	85	(0.1)	(10)	(2)	0.88	0.7	0.72	0.5	(1.11)	NPN
Q17 *	210	2.5	1.26	670	300	0	180	1.15	405	3.2	0.65	0.7	0.36	0.5	1.11	Small
Q17 #	300	(0.1)	9.97	1040	465	0	85	(0.1)	(10)	(2)	0.88	0.7	0.72	0.5	(1.11)	NPN
Q19 *	210	2.5	1.26	670	300	0	180	1.15	405	3.2	0.65	0.7	0.36	0.5	1.11	Small
Q19 #	300	(0.1)	9.97	1040	465	0	85	(0.1)	(10)	(2)	0.88	0.7	0.72	0.5	(1.11)	NPN
Q20 *	120	4.8	1 7.6	80	156	0	58	26.5	2430	-	4.05	0.7	2.8	0.5	1.11	Substrate
Q20 #	60	(0.1)	120	190	50	0	60	(0.1)	(10)	-	1.25	0.7	2.2	0.5	(1.11)	PNP
Q21 *	210	2.5	1.26	670	300	0	180	1.15	405	3.2	0.65	0.7	0.36	0.5	1.11	Small
Q21 #	300	(0.1)	9.97	1040	465	0	85	(0.1)	(10)	(2)	0.88	0.7	0.72	0.5	(1.11)	NPN
Q22 *	210	2.5	1.26	670	300	0	180	1.15	405	3.2	0.65	0.7	0.36	0.5	1.11	Small
Q22 #	300	(0.1)	9.97	1040	465	0	85	(0.1)	(10)	(2)	0.88	0.7	0.72	0.5	(1.11)	NPN
Q23 *	210	2.5	1.26	670	300	0	180	1.15	405	3.2	0.65	0.7	0.36	0.5	1.11	Small
Q23 #	300	(0.1)	9.97	1040	465	0	85	(0.1)	(10)	(2)	0.88	0.7	0.72	0.5	(1.11)	NPN
Q24 *	81	1.5	0.79	1100	170	0	80	26.5	9550	-	1.1	0.7	2.4	0.5	1.11	Dual Em.
Q24 #	80	(0.1)	15400	195	35	0	35	(0.1)	(10)	-	1.75	0.7	6.0	0.5	(1.11)	Sub. PNP
Q25 *	75	3.8	3.15	500	150	0	55	27.4	2540	5.1	0.1	0.7	1.05	0.5	1.11	Lateral
Q25 #	35	(0.1)	769	681	100	0	50	(0.1)	(10)	(2)	0.23	0.7	1.0	0.5	(1.11)	PNP
Q26 *	1.76	1.5	2.25	1600	120	0	84	27.4	220	4.8	0.1	0.7	0.9	0.5	1.11	Dual Coll.
Q26 #	0.6	(0.1)	577	681	625	0	77	(0.1)	(10)	(2)	0.36	0.7	1.74	0.5	(1.11)	L. PNP

* Data obtained from Wooley's result.

\# Data obtained from our probe data except for BR, TF, TR, CCS, and EG. Typical values ( ) are used for them.

TABLE 4-3

NCAP uA741 BJT's INPUT PARAMETERS

De \ Pa		η	V_{CB} (V)	V_{CBo} (V)	μ	I_C (μA)	I_{Cmax} (mA)	a	h_{FEmax}	k ($pF\text{-}V^{\frac{1}{2}}$)	Ref	C_{je} (pF)	C_2 (pF/m)	R_B (Ω)	R_C ($M\Omega$)	C1 (pF)	C2 (pF)
Q1	*	4	14.42	100	0.333	9.66	0.3	4.35	210	0.286	1.0	0.65	44.6	670	5.0	0.1	0.1
	#	4.34	14.57	20	0.165	7.85	0.5	12	400	1.23	1.091	1.23	9.09	830	5.33	0.1	0.1
Q2	*	4	14.42	100	0.333	9.66	0.3	4.35	210	0.286	1.0	0.65	44.6	670	5.0	0.1	0.1
	#	4.34	14.57	20	0.165	7.85	0.5	12	400	1.23	1.091	1.23	9.09	830	5.33	0.1	0.1
Q3	*	1.5	12.65	95	0.333	9.58	0.11	0.807	75	0.834	1.0	0.1	1060	500	0.5	0.1	0.1
	#	1.48	13.05	100	0.376	7.69	0.1	1.07	35	0.77	1.34	0.23	914	520	0.575	0.1	0.1
Q4	*	1.5	12.61	95	0.333	9.58	0.11	0.807	75	0.834	1.0	0.1	1060	500	0.5	0.1	0.1
	#	1.48	13.0	100	0.376	7.69	0.1	1.07	35	0.77	1.34	0.23	914	520	0.575	0.1	0.1
Q5	*	4	0.594	100	0.333	9.52	0.3	4.35	210	0.286	1.0	0.65	44.6	670	5.0	0.1	0.1
	#	3.79	0.53	100	0.254	7.66	0.5	1.21	300	0.61	1.04	0.88	15.07	1040	15.3	0.1	0.1
Q6	*	4	0.641	100	0.333	9.52	0.3	4.35	210	0.286	1.0	0.65	44.6	670	5.0	0.1	0.1
	#	3.79	0.585	100	0.254	7.66	0.5	1.21	300	0.61	1.04	0.88	15.07	1040	15.3	0.1	0.1
Q7	*	4	28.81	100	0.333	12.0	0.3	4.35	210	0.286	1.0	0.65	44.6	670	5.0	0.1	0.1
	#	3.79	28.93	100	0.254	10.8	0.5	0.84	300	0.61	1.04	0.8	15.07	1040	15.3	0.1	0.1
Q8	*	1.5	0.1	95	0.333	18.8	0.11	0.912	75	0.834	1.0	0.1	1060	500	0.5	0.1	0.1
	#	1.4	0.1	100	0.376	14.9	0.1	1.23	35	0.77	1.34	0.23	914	681	0.575	0.1	0.1
Q9	*	1.5	15.57	95	0.333	18.8	0.11	0.912	75	0.834	1.0	0.1	1060	500	0.5	0.1	0.1
	#	1.48	15.45	100	0.376	19.5	0.1	1.17	35	0.77	1.34	0.23	914	681	0.575	0.1	0.1
Q10	*	4	13.14	100	0.333	19.1	0.3	1.81	210	0.286	1.0	0.65	44.6	670	5.0	0.1	0.1
	#	3.79	13.46	100	0.254	19.8	0.5	0.62	300	0.61	1.04	0.88	15.07	1040	15.3	0.1	0.1
Q11	*	4	0.1	100	0.333	712	0.3	1.61	210	0.286	1.0	0.65	44.6	670	5.0	0.1	0.1
	#	3.79	0.1	100	0.254	718	0.5	0	300	0.61	1.04	0.88	15.07	1040	15.3	0.1	0.1
Q12	*	1.5	0.1	95	0.333	615	0.11	1.61	7.5	0.34	1.0	0.1	1060	500	0.5	0.1	0.1
	#	1.48	0.1	100	0.376	549	0.1	1.37	35	0.77	1.34	0.23	914	681	0.575	0.1	0.1

TABLE 4-3 (continued)

Pa / De		η	V_{CB} (V)	V_{CBO} (V)	μ	I_C (μA)	I_{Cmax} (mA)	a	h_{FEmax}	k ($pF\text{-}V^{\frac{1}{2}}$)	Ref	C_{je} (pF)	C_j (pF/m)	R_B (Ω)	R_C ($M\Omega$)	C1 (pF)	C2 (pF)
Q13	*	1.5	13.68	95	0.333	22	0.03	8.6	0.3	0.24	1.0	0.1	1060	1000	1.0	0.1	0.1
	#	1.72	13.89	130	0.32	45.3	0.2	0.48	0.6	0.38	1.22	0.36	1000	6 1	1.14	0.1	0.1
Q14	*	1.5	14.36	100	0.333	22.4	0.3	5.06	400	1.23	1.0	2.8	29.5	1 5	4.0	0.1	0.1
	#	1.42	14.42	100	0.327	110	2.0	1.26	300	1.0	1.05	3.0	19.1	500	3.96	0.1	0.1
Q15	*	4	0.64	100	0.333	4.37E-8	0.3	10	210	0.286	1.0	0.65	44.6	670	5.0	0.1	0.1
	#	3.79	0.573	100	0.254	2.43E-6	0.5	4.33	300	0.61	1.04	0.88	15.07	1040	15.3	0.1	0.1
Q16	*	4	28.76	100	0.333	13.1	0.3	3.54	210	0.286	1.0	0.65	44.6	670	5.0	0.1	0.1
	#	3.79	28.88	100	0.254	11.9	0.5	0.89	300	0.61	1.04	0.88	15.07	1040	15.3	0.1	0.1
Q17	*	4	13.19	100	0.333	61.0	0.3	0.82	210	0.286	1.0	0.65	44.6	670	5.0	0.1	0.1
	#	3.79	13.50	100	0.254	66.6	0.5	0.65	300	0.61	1.04	0.88	15.07	1040	15.3	0.1	0.1
Q19	*	4	0.1	100	0.333	11.8	0.3	4.35	210	0.286	1.0	0.65	44.6	670	5.0	0.1	0.1
	#	3.79	0.1	100	0.254	11.4	0.5	0.87	300	0.61	1.04	0.88	15.07	1040	15.3	0.1	0.1
Q21	*	4	0.594	100	0.333	10.1	0.3	4.35	210	0.286	1.0	0.65	44.6	670	5.0	0.1	0.1
	#	3.79	0.54	100	0.254	33.6	0.5	0.73	300	0.61	1.04	0.88	15.07	1040	15.3	0.1	0.1
Q20	*	2.5	14.46	90	0.333	22.3	0.11	2.44	117	2.22	1.0	4.05	1030	80	0.15	0.1	0.1
	#	2.67	14.47	90	0.565	109	0.3	1.03	60	1.5	1.13	1.25	360	190	0.147	0.1	0.1
Q22	*	4	1.24	100	0.333	8.45E-8	0.3	10	210	0.286	1.0	0.65	44.6	670	5.0	0.1	0.1
	#	3.79	1.12	100	0.254	4.76E-6	0.5	4.65	300	0.61	1.04	0.88	15.07	1040	15.3	0.1	0.1
Q23	*	4	0.1	100	0.333	6.1 E-21	0.3	10	210	0.286	1.0	0.65	44.6	670	5.0	0.1	0.1
	#	3.79	0.1	100	0.254	9.75E-11	0.5	1.85	300	0.61	1.04	0.88	15.07	1040	15.3	0.1	0.1
Q24	*	3.5	13.84	90	0.333	21.8	0.015	5.4	80	1.906	1.0	1.1	1030	1100	10.0	0.1	0.1
	#	3.69	14.09	50	0.252	46.2	0.2	7.4	80	5.08	1.45	1.75	280	195	13.1	0.1	0.1
Q25	*	1.5	15.0	95	0.333	2.31E-6	0.11	10	75	0.834	1.0	0.1	1060	500	0.5	0.1	0.1
	#	1.48	15.0	100	0.376	5.04E-3	0.1	1.66	35	0.77	1.34	0.23	1307	681	0.575	0.1	0.1
Q26	*	1.5	15.49	95	0.333	60.8	0.07	1.0	1.5	0.715	1.0	0.1	1060.	1600	1.0	0.1	0.1
	#	1.72	15.37	130	0.32	663	0.2	0.87	0.6	1.14	1.22	0.36	1000	681	1.14	0.1	0.1

* Data obtained from Wooley's results.

\# Data obtained from our probed data except for C1 and C2.

TABLE 4-4

741 OPERATIONAL AMPLIFIER SPICE2 CODING LIST

```
*741 OPERATIONAL AMPLIFIER UNIT GAIN BUFFER
*CIRCUIT DIAGRAM IS DESCRIBED AS FOLLOWS
*MODIFIED VERSION ON 8/6/78
*RESISTORS
*BUFFER FEEDBACK RESISTOR
RO 2 6 620
*SOURCE RESISTOR
RG 28 3 600
R1 1 4 1K
R2 4 5 1K
R3 4 12 50K
R4 4 26 5.0K
R5 15 27 40K
R7 19 18 50K
R9 6 21 27
R10 6 22 22
R11 4 17 100
R12 4 16 50K
R13 23 4 50K
RLD 60 0 1MEG
RIN 3 0 1MEG
*CAPACITOR
CLD1 6 0 55P
CLD2 60 0 55P
CIN 3 0 171PF
C1 14 29 30P
CD1 14 29 1P
LLD 6 60 275N
*DIODES
Q8 9 9 7 Q9
Q11 15 15 4 Q5
Q12 27 27 7 Q9
Q19 20 20 19 Q5
Q23 23 23 4 Q5
*JUNCTION TRANSISTORS
Q1 9 3 25 Q1
Q2 9 2 24 Q1
Q3 11 10 25 Q3
Q4 14 10 24 Q3
Q5 11 12 1 Q1
Q6 14 12 5 Q1
Q7 7 11 12 Q1
Q9 10 9 7 Q3
Q10 10 15 26 Q1
Q13 20 27 7 Q13
Q14 7 20 21 Q14
Q15 20 21 6 Q1
Q16 7 14 16 Q1
Q17 29 16 17 Q1
Q20 4 18 22 Q20
Q21 20 19 18 Q1
```

TABLE 4-4 (Continued)

```
Q22 14 23 4 Q1
Q24 4 29 18 Q24
Q25 23 22 6 Q3
Q26 29 27 7 Q26
*TRANSISTOR MODELS
.MODEL Q1 NPN(BF=210 BR=2.5 IS=1.26E-15 RB=670 RC=300 RE=0
+VA=180 TF=1.15N TR=405N CCS=3.2P CJE=0.65P PE=0.7 CJC=0.36P
+PC=0.5 EG=1.11)
.MODEL Q3 PNP(BF=75 BR=3.8 IS=3.15E-15 RB=500 RC=150 RE=0
+VA=55 TF=27.4N TR=2540N CCS=5.1P CJE=0.1P PE=0.7 CJC=1.05P
+PC=0.5 EG=1.11)
.MODEL Q13 PNP(BF=0.38 BR=1.4 IS=0.9E-15 RB=1000 RC=80 RE=0
+VA=84 TF=27.4N TR=55N CCS=4.8P CJE=0.1P PE=0.7 CJC=0.3P
+PC=0.5 EG=1.11)
.MODEL Q14 NPN(BF=400 BR=6.1 IS=0.395E-15 RB=180 RC=15 RE=0
+VA=270 TF=0.76N TR=243N CCS=7.8P CJE=2.8P PE=0.7 CJC=1.55P
+PC=0.5 EG=1.11)
.MODEL Q20 PNP(BF=120 BR=4.8 IS=17.6E-15 RB=80 RC=156 RE=0
+VA=58 TF=26.5N TR=2430N CCS=0 CJE=4.05P PE=0.7 CJC=2.8P
+PC=0.5 EG=1.11)
.MODEL Q24 PNP(BF=81 BR=1.5 IS=0.79E-15 RB=1100 RC=170 RE=0
+VA=80 TF=26.5N TR=9550N CCS=0 CJE=1.1P PE=0.7 CJC=2.4P
+PC=0.5 EG=1.11)
.MODEL Q26 PNP(BF=1.76 BR=1.5 IS=2.25E-15 RB=1600 RC=120
+RE=0 VA=84 TF=27.4N TR=220N CCS=4.8P CJE=0.1P PE=0.7
+CJC=0.9P PC=0.5 EG=1.11)
*DC POWER SUPPLY
VP 7 0 DC 15
VN 4 0 DC -15
*SIGNAL SOURCE
VG 28 0 AC 1.0
*OUTPUT
.PRINT AC VDB(60)
.CALPLT AC 1
.PRINT AC VDB(3)
.CALPLT AC 1
.PRINT AC VP(60)
.CALPLT AC 1
.PRINT AC VP(3)
.CALPLT AC 1
*FREQUENCY RANGE
.AC DEC 10 1 10MEG
.END
```

CHAPTER FIVE

NONLINEAR SYSTEM ANALYSIS

The RFI effects in an electronic communication system such as crossmodulation and intermodulation products can be generated by interactions between unwanted signals and desired signals. The interactions generating the RFI effects are the result of system nonlinearities. In this chapter, the use of Volterra series[31] expressions to characterize the nonlinearities of a communication system is discussed. Also discussed is the Nonlinear Circuit Analysis Program NCAP which can be used by electromagnetic compatibility (EMC) engineers to calculate RFI effects in electronic circuits. The actual use of NCAP for the computation of a nonlinear transfer function is demonstrated in the next chapter.

To illustrate the fundamental computational procedures, we shall begin with a simple case of a nonlinear system without memory. Referring to Figure 5-1, a memory-free nonlinearity can be effectively represented by a power series expansion:

$$y(t) = \sum_{n=1}^{\infty} a_n x^n(t) \qquad (5\text{-}1)$$

where y(t) is the output response, x(t) is the input excitation, and the coefficients a_n determine the nonlinear behavior of the system. For a linear system, the coefficients a_n for $n \geq 2$ are all equal to zero.

FIGURE 5-1 A Nonlinear System without Memory

Suppose that the input x(t) is composed of a desired signal $S_1(t)$ and an unwanted modulated signal $I_2(t)$

$$S_1(t) = S_1 \cos\omega_1 t \tag{5-2}$$

$$I_2(t) = I_2(1 + m(t))\cos\omega_2 t, \; m<1 \tag{5-3}$$

where ω_1 and ω_2 are angular frequencies. Then the output signal y(t) at frequency ω_1 will include the following terms:

$$y(t) = a_1 S_1 (1 + \frac{3a_3}{4a_1} S_1^2 + \frac{3}{2} \frac{a_3}{a_1} I_2^2 + \frac{3a_3}{a_1} m I_2^2)\cos \omega_1 t \tag{5-4}$$

where the terms with factors $(3a_3/4a_1)S_1^2$, $(3a_3/2a_1)I_2^2$, and $(3a_3 m/a_1)$ I_2^2 in the above expression are called the compression, the desensitization, and the crossmodulation respectively.

Should the input x(t) be composed of three unmodulated tones

$$x(t) = S_1\cos\omega_1 t + I_2\cos\omega_2 t + I_3\cos\omega_3 t \tag{5-5}$$

then the output response y(t) is given as:

$$y(t) = a_1 S_1 [1 + \frac{3a_3}{4a_1} S_1^{\,2} + \frac{3}{2}\frac{a_3}{a_1}(I_2^{\,2} + I_3^{\,2})]\cos\omega_1 t$$

$$+ a_2 I_2 I_3 [\cos(\omega_2+\omega_3)t + \cos(\omega_2-\omega_3)t]$$

$$+ \frac{3}{4} a_3 [I_2^{\,2} I_3 \cos(2\omega_2 \pm \omega_3)t + I_2 I_3^{\,2} \cos(2\omega_3 \pm \omega_2)t]$$

$$+ \ . \ . \ . \ \text{(other terms)} \qquad (5\text{-}6)$$

In the right-hand side of the above equation the terms at frequencies $\omega_2 \pm \omega_3$ are second-order intermodulation products (IMP's), while the third terms at frequencies $2\omega_2 \pm \omega_3$ and $2\omega_3 \pm \omega_2$ are third-order IMP's. If any of these frequency combinations fall in the system passband near ω_1, the IMP's can cause a serious RFI problem.

5.1 Volterra Series Description of a Nonlinear System

In a nonlinear system, distortion* can be generated by the nonlinear interaction of multiple-input signals. This distortion can be accurately analyzed using NACP which uses a frequency domain approach where the Volterra functional series expressions are employed.

The Volterra functional series was first applied to nonlinear circuit problems by Wiener[32] in 1942. Narayanan[33] used the same technique to analyze distortion in a transistor amplifier in 1967 and in cascade and feedback amplifiers at a later time[34,35]. In 1972, Poon used Volterra analysis to study the third-order distortions in BJT

* The term distortion is used to describe a wide variety of nonlinear effects including RFI effects.

stages using an integral charge control transistor model[36]. In the same year Kuo developed a computer program to calculate the distortion in amplifier circuits[37]. The Volterra analysis was also used by Meyer in an investigation of crossmodulation effects in amplifiers[38]

A Volterra functional G(x(t)) can be expanded into a series of homogeneous functionals F_n of various degrees n[31]

$$G(x(t)) = \sum_{n=0}^{\infty} F_n(x(t))$$

$$= K_0 + \int_a^b K_1(u)x(u)du + \int_a^b \int_a^b K_2(u_1,u_2)x(u_1)x(u_2)du_1du_2$$

$$+ \ldots \qquad (5\text{-}7)$$

where

$$F_n(x(t)) = \int_a^b \int_a^b \ldots \int_a^b K_n(u_1,u_2,\ldots,u_n)x(u_1)x(u_2)\ldots x\ (u_n)du_1..du_n$$

(5-8)

Applying the Volterra series expansion to a nonlinear system in the time domain with the input expressed as x(t) and the output as y(t), we have[39]

$$y(t) = \sum_{n=1}^{\infty} y_n(t)$$

$$y_1(t) = \int_{-\infty}^{\infty} h_1(\tau)x(t-\tau)d\tau$$

$$y_2(t) = \int_{-\infty}^{\infty}\int_{-\infty}^{\infty} h_2(\tau_1,\tau_2)x(t-\tau_1)x(t-\tau_2)d\tau_1d\tau_2 \qquad (5\text{-}9)$$

$$\ldots$$

$$y_n(t) = \int_{-\infty}^{\infty}\int_{-\infty}^{\infty}\ldots\int_{\infty}^{\infty} h_n(\tau_1,\ldots,\tau_n) \prod_{i=1}^{n} x(t-\tau_i)d\tau_i$$

The function $h_n(\tau_1,\tau_2,\ldots\tau_n)$ may be interpreted as the nth order nonlinear impulse response of the system. The nth order Fourier transformation of the nth order nonlinear impulse response of the system $h_n(\tau_1,\ldots,\tau_n)$ transforms a time domain signal into the frequency domain. We use the following relationships to make such transformations:

$$H_n(f_1,f_2,\ldots f_n)= \int_{-\infty}^{\infty}\cdots\int_{-\infty}^{\infty} h_n(\tau_1,\ldots,\tau_n)e^{-j2\pi(f_1\tau_1+\ldots+f_n\tau_n)} d\tau_1 d\tau_2\ldots d\tau_n \tag{5-10}$$

$$h_n(\tau_1,\ldots,\tau_n) = \int_{-\infty}^{\infty}\cdots\int_{-\infty}^{\infty} H_n(f_1,f_2,\ldots,f_n)e^{j2\pi(f_1\tau_1+\ldots+f_n\tau_n)} df_1 df_2\ldots df_n \tag{5-11}$$

Substituting Eq. (5-11) for h_n into Eq. (5-9) for the output response $y(t)$, we obtain

$$y(t) = \sum_n y_n(t)$$

$$y_n(t) = \int_{-\infty}^{\infty}\cdots\int_{-\infty}^{\infty}\left[\int_{-\infty}^{\infty}\cdots\int_{-\infty}^{\infty} df_1\ldots df_n H_n(f_1,\ldots,f_n)e^{j2\pi(f_1\tau_1+f_2\tau_2+\ldots+f_n\tau_n)}\right]$$

$$\cdot \prod_{i=1}^{n} x(t-\tau_i)\, d\tau_i \tag{5-12}$$

$$= \int_{-\infty}^{\infty}\cdots\int_{-\infty}^{\infty} df_1 df_2\ldots df_n H_n(f_1\ldots f_n)\left\{\int_{-\infty}^{\infty}\cdots\int_{-\infty}^{\infty}\prod_{i=1}^{n} d\tau_i \prod_{i=1}^{n} x(t-\tau_i)\right.$$

$$\left.\cdot \exp[j2\pi(f_1\tau_1+\ldots+f_n\tau_n)]\right\}$$

The multiple integral in the bracket in Eq. (5-12) can be further expressed as

$$\int_{-\infty}^{\infty}\cdots\int_{-\infty}^{\infty} d\tau_1\ldots d\tau_n x(t-\tau_1)x(t-\tau_2)\ldots x(t-\tau_n)e^{j2\pi(f_1\tau_1+\ldots+f_n\tau_n)}$$

$$= \int_{-\infty}^{\infty} d\tau_1 x(t-\tau_1)e^{j2\pi f_1\tau_1}\int_{-\infty}^{\infty} d\tau_2 x(t-\tau_2)e^{j2\pi f_2\tau_2}\ldots\int_{-\infty}^{\infty} d\tau_n x(t-\tau_n)e^{j2\pi f_n\tau_n} \tag{5-13}$$

Using the Fourier transformation expressions

$$F(x(t)) = \int_{-\infty}^{\infty} x(t)\exp(-j2\pi ft)dt = X(f) \tag{5-14}$$

and

$$\int_{-\infty}^{\infty} d\tau_1 x(t-\tau_1)\exp(j2\pi f_1\tau_1)$$

$$= \int_{-\infty}^{\infty} d\tau_1 x(t-\tau_1)\exp[-j2\pi f_1(t-\tau_1)]\exp(j2\pi f_1 t)$$

$$= \exp(j2\pi f_1 t)\int_{+\infty}^{-\infty} d(t-\tau_1)\exp[-j2\pi f_1(t-\tau_1)]$$

$$= \exp(j2\pi f_1 t)X(f_1) \tag{5-15}$$

We have

$$\int_{-\infty}^{\infty}\cdots\int_{-\infty}^{\infty} d\tau_1 d\tau_2\ldots d\tau_n x(t-\tau_1)x(t-\tau_2)\ldots x(t-\tau_n)$$

$$\cdot \exp[j2\pi(f_1\tau_1+\ldots+ f_n\tau_n)]$$

$$= \exp[j2\pi(f_1+f_2+\ldots+f_n)t]X(f_1)\ldots X(f_n) \tag{5-16}$$

or

$$y_n(t) = \int_{\infty}^{\infty}\cdots\int_{\infty}^{\infty} df_1\ldots df_n H_n(f_1,\ldots,f_n)$$

$$\cdot\ X(f_1)X(f_2)\ldots X(f_n)\exp[j2\pi(f_1+\ldots+f_n)t] \tag{5-17}$$

Note that $H(f_1, f_2,\ldots,f_n)$ is not the nth order transform of $y_n(t)$. However, $H_n\ (f_1,\ldots,f_n)\ X\ (f_1)\ \ldots\ X\ (f_n)$ is the nth order transform of $y_n\ (t_1, t_2, \ldots, t_n)$.* We mention here that the computer program NCAP calculates $H_n(f_1,f_2,\ldots,f_n)$ in the frequency domain.

Now let us consider the important special case where the input signal x(t) is a M/2-tone input where M is an even integer. The Fourier transformation of x(t) will be

$$X(f) = \frac{1}{2}\sum_{m=1}^{M} A_m\,\delta(f-f_m);\quad f_{\frac{M}{2}+i} = -f_i,\quad A_{\frac{M}{2}+i} = A_i^{*} \qquad (5\text{-}18)$$

where the coefficient A_m is the complex amplitude of the m-th tone at f_m. Then the first-order output response becomes

$$y_1(t) = \int_{-\infty}^{\infty} df\; H_1(f)\,\frac{1}{2}\sum_{m=1}^{M} A_m\delta(f-f_m)\exp(j2\pi ft)$$

$$= \frac{1}{2}\sum_{m=1}^{M} A_m\, H_1(f_m)\exp(j2\pi f_m t) \qquad (5\text{-}19)$$

and the second-order output response is given as

$$y_2(t) = \int_{-\infty}^{\infty}\int_{-\infty}^{\infty} df_1 df_2 H_2(f_1,f_2)\frac{1}{2}\sum_{m_1=1}^{M} A_{m_1}\delta(f_1-f_{m_1})\frac{1}{2}\sum_{m_2=1}^{M} A_{m_2}\delta(f_2-f_{m_2})$$

$$\cdot\ \exp[j2\pi(f_1+f_2)t]$$

$$= \frac{1}{4}\sum_{m_1=1}^{M}\sum_{m_2=1}^{M} A_{m_1}A_{m_2}H_2(f_{m_1},f_{m_2})\exp[j2\pi(f_{m_1}+f_{m_2})t] \qquad (5\text{-}20)$$

For a single-tone input M equals 2, and X(f) becomes

$$X(f) = \frac{1}{2}A_1\delta(f-f_1) + \frac{1}{2}A_2\delta(f-f_2) \qquad (5\text{-}21)$$

* $y_n(t_i,\ldots,t_n)$ equals $\int\cdots\int h_n(\tau_i,\tau_n)\prod_{i=1}^{n} x(t_i-\tau_i)\,dt_i$

Note that $y_n(t) = y_n(t_i,\ldots,t_n)$ where $t_1 = t_2 = \ldots = t_n = t$.

where $f_2 = -f_1$. The first-order response $y_1(t)$ and the second-order response $y_2(t)$ are given by

$$y_1(t) = \frac{1}{2} A_1 H_1(f_1)\exp(j2\pi f_1 t) + \frac{1}{2} A_2 H_1(f_2)\exp(j2\pi f_2 t)$$

$$y_2(t) = \frac{1}{4} A_1^2 H_2(f_1,f_1)\exp[j2\pi(2f_1)t] + \frac{1}{2} A_1 A_2 H_2(f_1,f_2)\exp[j2\pi(f_1+f_2)t]$$

$$+ \frac{1}{4} A_2^2 H_2(f_2,f_2)\exp[j2\pi(2f_2)t] \qquad (5\text{-}22)$$

For a double-tone input M equals 4, and X(f) becomes

$$X(f) = \frac{1}{2} A_1\delta(f-f_1) + \frac{1}{2} A_2\delta(f-f_2) + \frac{1}{2} A_3\delta(f-f_3) + \frac{1}{2} A_4\delta(f-f_4) \qquad (5\text{-}23)$$

where $f_3 = -f_1$, $f_4 = -f_2$, $A_3 = A_1^*$, and $A_4 = A_2^*$. The first-order response $y_1(t)$ and the second-order response $y_2(t)$ are given by

$$y_1(t) = \frac{1}{2} A_1 H_1(f_1)\exp(j2\pi f_1 t) + \frac{1}{2} A_2 H_1(f_2)\exp(j2\pi f_2 t)$$

$$+ \frac{1}{2} A_3 H_1(f_3)\exp(j2\pi f_3 t) + \frac{1}{2} A_4 H_1(f_4)\exp(j2\pi f_4 t)$$

$$y_2(t) = \frac{1}{4} A_1^2 H_2(f_1,f_1)\exp[j2\pi(2f_1)t] + \frac{1}{2} A_1 A_2 H_2(f_1,f_2)\exp[j2\pi(f_1+f_2)t]$$

$$+ \frac{1}{2} A_1 A_3 H_2(f_1,f_3)\exp[j2\pi(f_1+f_3)t] + \frac{1}{2} A_1 A_4 H_2(f_1,f_4)\exp[j2\pi(f_1+f_4)t]$$

$$+ \frac{1}{4} A_2^2 H_2(f_2,f_2)\exp[j2\pi(2f_2)t] + \frac{1}{2} A_2 A_3 H_2(f_2,f_3)\exp[j2\pi(f_2+f_3)t]$$

$$+ \frac{1}{2} A_2 A_4 H_2(f_2,f_4)\exp[j2\pi(f_2+f_4)t] + \frac{1}{4} A_3^2 H_2(f_3,f_3)\exp[j2\pi(2f_3)t]$$

$$+ \frac{1}{2} A_3 A_4 H_2(f_3,f_4)\exp[j2\pi(f_3+f_4)t] + \frac{1}{4} A_4^2 H_2(f_4,f_4)\exp[j2\pi(2f_4)t]$$

$$(5\text{-}24)$$

In general, the nth degree output response for a M/2-tone input (where M/2 must be an integer) can be given as

$$y_n(t) = \int_{-\infty}^{\infty} \cdots \int_{-\infty}^{\infty} df_1 df_2 \ldots df_n \; H_n(f_1,\ldots,f_n)X(f_1)\ldots X(f_n)$$

$$\cdot \exp[j2\pi(f_1+\ldots+f_n)t]$$

$$= \int_{-\infty}^{\infty} \cdots \int_{-\infty}^{\infty} df_1 df_2 \ldots df_n H_n(f_1,\ldots,f_n)[\frac{1}{2} \sum_{q_1=1}^{M} A_{q_1} \delta(f-f_{q_1})] \ldots$$

$$[\frac{1}{2} \sum_{q_n=1}^{M} A_{q_n} \delta(f-f_{q_n})] \exp\,[j2\pi(f_{q_1}+\ldots+f_{q_n})t]$$

$$= (\frac{1}{2})^n \sum \frac{n! A_1^{m_1} A_2^{m_2} \ldots A_M^{m_M}}{m_1! m_2! \ldots m_M!} H_n(\overbrace{f_1,\ldots,f_1}^{m_1},\overbrace{f_2,\ldots,f_2}^{m_2},\ldots,\overbrace{f_M,\ldots,f_M}^{m_M})$$

$$\cdot \exp(j2\pi f_\Sigma t) \qquad (5\text{-}25)$$

where m_i denotes the number of times the frequency f_i appears in a particular frequency mix f_Σ. Equation (5-25) is valid for $n > M$, and M is the number of discrete frequencies (M/2 is the number of positive frequency terms) in the input frequency spectrum with

$$f_\Sigma = m_1 f_1 + m_2 f_2 + \ldots + m_M f_M \qquad (5\text{-}26)$$

$$n = m_1 + m_2 + \ldots + m_M \qquad (5\text{-}27)$$

Note that in the above expressions the summations are made on all possible combinations of m_1, m_2,..., and m_M, where m_j denotes the number of times the frequency f_j is repeated in an nth order transfer function.

Equation (5-25) determines the terms of nth order transfer functions for an input signal with M frequency components. For additional information on this subject the reader is referred to Refs. 39 and 40.

5.2 The NCAP Determination of the Nonlinear Transfer Functions

Let the nonlinear system have a single input $V_G(t)$ which can be expressed as a sum of exponential functions

$$V_G(t) = \sum_{i=1}^{M} \exp(j2\pi f_i t) \qquad (5\text{-}28)$$

where $f_i = f_1, f_2, \ldots\ldots, f_M$. Note that M may be an odd or even integer. An output response $V_L(t)$ can be expressed as a sum of nonlinear responses which up to the 3rd order are

$$V_L(t) = \sum_{i=1}^{M} H_1(f_i)\exp(j2\pi f_i t) + \sum_{i=1}^{M}\sum_{j=1}^{M} H_2(f_i,f_j)\exp(j2\pi(f_i+f_j)t)$$

$$+ \sum_{i=1}^{M}\sum_{j=1}^{M}\sum_{k=1}^{M} H_3(f_i,f_j,f_k)\exp(j2\pi(f_i+f_j+f_k)t)+\ldots. \qquad (5\text{-}29)$$

If the output voltage $V_L(t)$ can be determined and put into the form of Eq. (5-29), the linear and the nonlinear transfer functions at the output node and at the specified frequencies can be identified by matching the coefficients of the exponential terms. Note that the coefficient of $\exp(j2\pi f_\Sigma)$ at the frequency f_Σ contains a number of terms. It is quite tedious to find a nonlinear transfer function in this manner. However, from Eqs. (5-25), (5-26) and (5-27), for an M/2 tone input which produces M complex exponentials the amplitude of an nth degree output response $y_n(t)$ at frequency f_Σ determines the nonlinear transfer function $H_n(\underline{f})$ where $\underline{f}$ is the particular frequency mix $(\overbrace{f_1,\ldots,f_1}^{m_1}, \overbrace{f_2,\ldots,f_2}^{m_2},\ldots,\overbrace{f_M,\ldots,f_M}^{m_M})$ Based upon this fact, the computer program NCAP calculates the nonlinear transfer function $H_n(\underline{f})$ for a given system by computing the amplitude of the nth degree output response $y_n(t)$ at the frequency f_Σ. The

computer program NCAP analyses the equations of the system by using a frequency domain small signal ac circuit analysis approach.

The procedures used by NCAP to find the transfer functions are outlined below:

(1) The nodal equations are constructed according to the network topology using the Kirchhoff Current Law (KCL).

The KCL states that the nodal admittance matrix Y, the nodal voltage vector V, and the equivalent nodal current source vector J are related to one another in frequency domain by

$$Y(s)V(s) = J(s) \tag{5-30}$$

or

$$Y(s)(V_\ell(s) + V_d(s)) = J_\ell(s) + J_d(s) \tag{5-31}$$

where $J_\ell(s)$ denotes the linear equivalent nodal current source vector and $J_d(s)$ the nonlinear equivalent nodal current source vector, while $V_\ell(s)$ is the linear node-to-datum voltage vector, $V_d(s)$ the nonlinear node-to-datum voltage vector. The parameter s denotes $j\omega$. Equations (5-30) and (5-31) are evaluated at appropriate discrete values of $s = j\omega = j2\pi f$ corresponding to the M values of the frequencies f_i in the input signal spectrum. For a single (M = 1) input excitation $V_G(t) = \exp(j2\pi f_i t)$, and the current column vector J_ℓ can be expressed in time domain as

$$J_\ell(t) = (1/Z_g)(\exp(j2\pi f_i t), 0,\ldots,0)^T \tag{5-32}$$

where Z_g is the source impedance operator. The vector J_ℓ can also be expressed in frequency domain as

$$J_\ell(s) = (1/Z_g)(1,\ 0, \ldots,\ 0)^T \qquad (5\text{-}33)$$

where T denotes the transpose of the row matrix and Z_g the source impedance of the voltage excitation V_G.

(2) The network first-order (linear) responses with the current source $J(f_i) = J_\ell(f_i)$ at all the frequencies f_i in the input signal spectrum are determined.

$$H_1(f_i) = [Y(f_i)]^{-1} J_\ell(f_i);\ i=1,\ 2, \ldots, M \qquad (5\text{-}34)$$

(3) The second-order nonlinear current source vector $J_d(f_i,f_j)$ is determined at the frequency $f_i + f_j$ using the values for the first-order node voltages at the two frequencies f_i and f_j for all i and j. The network second-order transfer function $H_2(f_i,f_j)$ is calculated using the expression

$$H_2(f_i,f_j) = \frac{1}{2}[Y(f_i + f_j)]^{-1}\ J_d(f_i,f_j);\ \text{for all } i,j \qquad (5\text{-}35)$$

The value for the second-order transfer function $H_2(f_i,f_j)$ depends upon the value of the network admittance matrix evaluated at the frequency $f_i + f_j$ and upon the second-order current vector $J_d(f_i,\ f_j)$.

(4) The third-order nonlinear current source vector $J_d(f_i,f_j,f_k)$ is determined at the frequency $f_i + f_j + f_k$. To determine values for $J_d(f_i,\ f_j,\ f_k)$, the values for the first-order transfer functions $H_1(f_i)$, $H_1(f_j)$, and $H_1(f_k)$ and for the second-order transier functions $H_2(f_j,f_k)$, $H_2(f_i,f_k)$, and $H_2(f_i,f_j)$ are used. Then the network third-order transfer function $H_3(f_i,f_j,f_k)$ is calculated using the expression

$$H_3(f_i,f_j,f_k) = \frac{1}{6}\ [Y(f_i+f_j+f_k)]^{-1}\ J_d(f_i,f_j,f_k);\ \text{for all } i,j,k \qquad (5\text{-}36)$$

The value for the third-order transfer function $H_3(f_i,f_j,f_k)$ depends upon the value of the network admittance matrix evaluated at the frequency $f_i + f_j + f_k$ and upon the third-order current source vector $J_d(f_i,f_j,f_k)$.

The fourth and higher-order transfer functions can be found by using a similar process. In practice the need to evaluate the nonlinear transfer function of fourth and high orders does not occur often. The computer program NCAP can calculate nonlinear transfer functions to the 6th order.

The procedures that NCAP uses to calculate nonlinear transfer functions of the nth order can be made much clearer by studying specific examples. In fact it may be that the NCAP computational procedures can be best understood by studying specific examples. For this reason two such examples will be given in the next chapter.

CHAPTER SIX

COMPUTATION OF NONLINEAR TRANSFER FUNCTIONS

In this chapter two examples are given to illustrate how the NCAP algorithm is implemented to calculated linear and nonlinear transfer functions. These examples will also demonstrate some computational techniques used for nonlinear circuit analysis. One example involves a simple junction-gate field effect transistor (JFET) in a broadband amplifier circuit*. The other example involves a bipolar junction transistor (BJT) in a tuned RF amplifier stage. First, second, and third order transfer functions will be calculated by using a direct process and by using the computer program NCAP. The two sets of values calculated will be compared.

6.1 A Broadband JFET Amplifier Stage

The circuit diagram for a broadband JFET amplifier stage is shown in Figure 6-1. Since the third-order transfer function is to be calculated, the input signal source $v_s(t)$ consists of three complex exponentials of unit amplitude and is given by

$$v_s(t) = \sum_{i=1}^{3} \exp(j2\pi f_i t)$$

First the matrix equations for the network will be developed. Then the nonlinear coefficients of the JFET will be given. Finally the calculated values for the nonlinear transfer functions (up to third-order) will be presented.

* This example is chosen to illustrate the direct process used to calculate nonlinear transfer functions. Although the dissertation is devoted to bipolar integrated circuits, the JFET is chosen because the JFET nonlinear analysis is relatively simple.

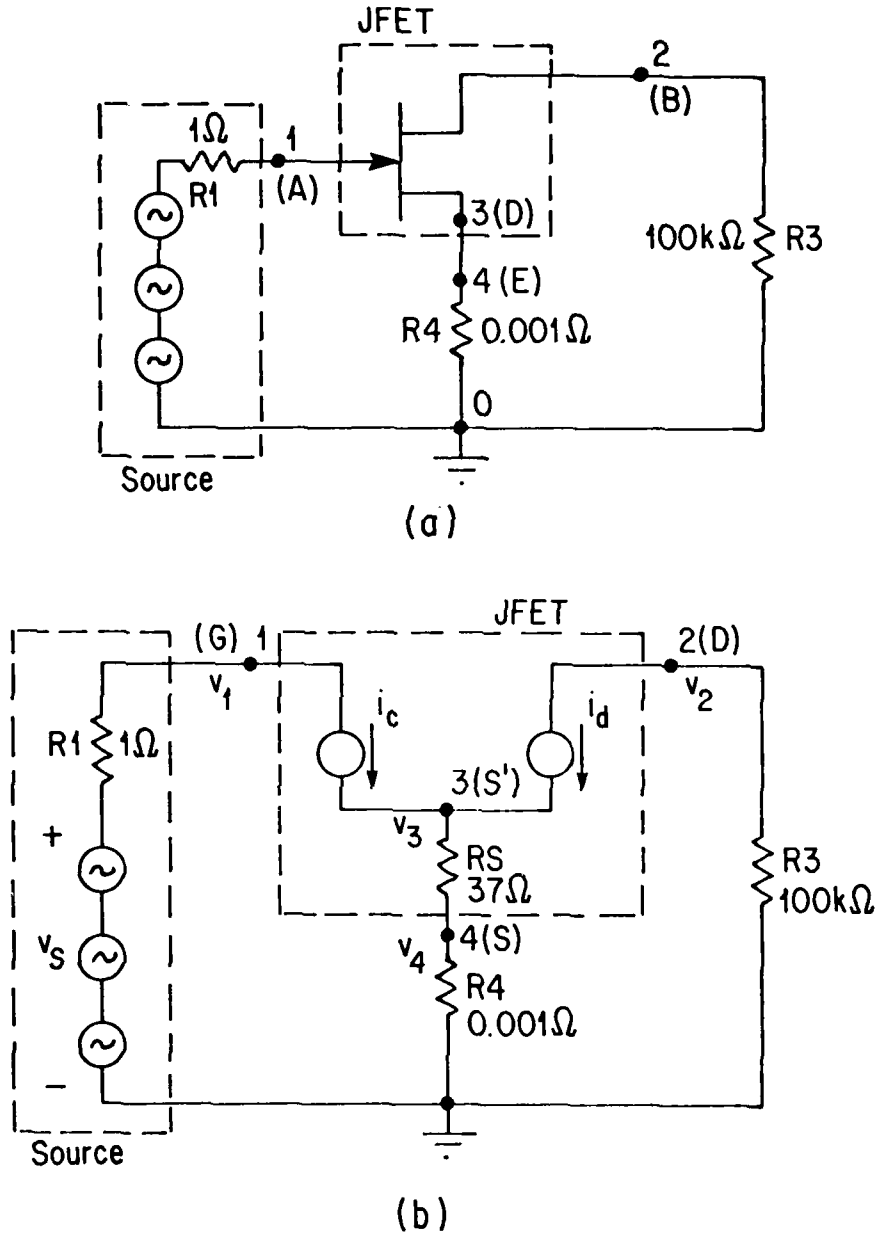

FIGURE 6-1 The Circuit Diagrams of a Broadband JFET Amplifier (a) and Its AC Equivalent Circuit (b). Notations A, B, D, and E Represent the Nonlinear Transfer Functions at Nodes 1, 2, 3, and 4, respectively. Notations G, D, S', and S Represent Gate, Drain, Internal Source, and Source Terminals, Respectively.

The incremental gate current i_c is the current generator that corresponds to a nonlinear capacitor which was discussed in Section 2.3.2. The incremental drain current i_d is a voltage controlled nonlinear dependent current source which was discussed in Section 2.3.4. The incremental gate current i_c and drain current i_d are given by[41]

$$i_c = C_1 \frac{d}{dt} v_{13} + C_2 \frac{d}{dt} v_{13}^2 + C_3 \frac{d}{dt} v_{13}^3 + \text{higher-order terms} \tag{6-1}$$

$$i_d = \alpha_1 v_{13} + \alpha_2 v_{13}^2 + \alpha_3 v_{13}^3 + \text{higher-order terms} \tag{6-2}$$

where $v_{13} = v_1 - v_3$.

Using the Kirchhoff current law and neglecting fourth and higher-order terms, we obtain

$$\frac{v_s - v_1}{R1} - C_1 \frac{d}{dt}(v_1 - v_3) - C_2 \frac{d}{dt}(v_1 - v_3)^2 - C_3 \frac{d}{dt}(v_1 - v_3)^3 = 0 \tag{6-3}$$

$$C_1 \frac{d}{dt}(v_1 - v_3) + C_2 \frac{d}{dt}(v_1 - v_3)^2 + C_3 \frac{d}{dt}(v_1 - v_3)^3 + \alpha_1 (v_1 - v_3)$$

$$+ \alpha_2 (v_1 - v_3)^2 + \alpha_3 (v_1 - v_3)^3 + (v_4 - v_3)/RS = 0 \tag{6-4}$$

$$\frac{v_3}{RS} + v_4 \left(-\frac{1}{RS} - \frac{1}{R4}\right) = 0 \tag{6-5}$$

$$-\alpha_1 (v_1 - v_3) - \alpha_2 (v_1 - v_3)^2 - \alpha_3 (v_1 - v_3)^3 - \frac{v_2}{R3} = 0 \tag{6-6}$$

Next Eqs. (6-3) to (6-6) can be recast in a matrix form as

$$\begin{pmatrix} -\frac{1}{R1} - C_1 \frac{d}{dt} & 0 & C_1 \frac{d}{dt} & 0 \\ C_1 \frac{d}{dt} + \alpha_1 & 0 & -C_1 \frac{d}{dt} - \alpha_1 - \frac{1}{RS} & \frac{1}{RS} \\ 0 & 0 & \frac{1}{RS} & -\frac{1}{RS} - \frac{1}{R4} \\ -\alpha_1 & -\frac{1}{R3} & \alpha_1 & 0 \end{pmatrix} \begin{pmatrix} v_1 \\ v_2 \\ v_3 \\ v_4 \end{pmatrix}$$

$$= -\frac{1}{R1}\begin{pmatrix} v_s \\ 0 \\ 0 \\ 0 \end{pmatrix} + \begin{pmatrix} C_2 \frac{d}{dt}(v_1-v_3)^2 + C_3 \frac{d}{dt}(v_1-v_3)^3 \\ -(\alpha_2 + C_2 \frac{d}{dt})(v_1-v_3)^2 - (\alpha_3 + C_3 \frac{d}{dt})(v_1-v_3)^3 \\ 0 \\ \alpha_2(v_1-v_3)^2 + \alpha_3(v_1-v_3)^3 \end{pmatrix} \tag{6-7}$$

To obtain the first-order transfer functions, we omit the quadratic and cubic terms in Eq. (6-7) and assume an excitation v_s of the form $v_s = V_s \exp(j2\pi f_i t)$ with $V_s = 1$.

Then the first-order transfer function can be calculated using

$$\begin{pmatrix} -\frac{1}{R1} - C_1 j\omega_i & 0 & C_1 j\omega_i & 0 \\ C_1 j\omega_i + \alpha_1 & 0 & -C_1 j\omega_i - \alpha_1 - \frac{1}{RS} & \frac{1}{RS} \\ 0 & 0 & \frac{1}{RS} & -\frac{1}{RS} - \frac{1}{R4} \\ -\alpha_1 & -\frac{1}{R3} & \alpha_1 & 0 \end{pmatrix} \begin{pmatrix} A_1(f_i) \\ B_1(f_i) \\ D_1(f_i) \\ E_1(f_i) \end{pmatrix} = \begin{pmatrix} -\frac{1}{R1} \\ 0 \\ 0 \\ 0 \end{pmatrix} \tag{6-8}$$

where the A_1, B_1, D_1, and E_1 denote the first-order node voltages (transfer functions) at nodes 1, 2, 3, and 4 respectively. The subscript 1 denotes first-order transfer functions.

In order to obtain the matrix equation for the second-order transfer functions we begin by expressing v_1, v_2, v_3, and v_4 in form of a summation of exponential functions. These equations are

$$v_1 = \sum_{i=1}^{3} [A_1(f_i)\exp(j2\pi f_i t)+A_2(f_i,f_i)\exp(j4\pi f_i t)$$

$$+A_3(f_i,f_i,f_i)\exp(j6\pi f_i t) + \sum_{\substack{j=1 \\ j\neq i}}^{3} [A_2(f_i,f_j)\exp(j2\pi(f_i+f_j)t)$$

$$+3A_3(f_i,f_i,f_j)\exp(j2\pi(2f_i+f_j)t)]]$$

$$+6A_3(f_1,f_2,f_3)\exp(j2\pi(f_1+f_2+f_3)t) \quad + \text{high-order terms}$$

$$\triangleq F\ (A) \tag{6-9}$$

$$v_2 \triangleq F\ (B) \tag{6-10}$$

$$v_3 \triangleq F\ (D) \tag{6-11}$$

$$v_4 \triangleq F\ (E) \tag{6-12}$$

where in Eqs. (6-9), (6-10), (6-11), and (6-12) the $A_2(f_i,f_j)$, $B_2(f_i,f_j)$, $D_2(f_i,f_j)$, and $E_2(f_i,f_j)$ denote the second-order voltage transfer functions at nodes 1, 2, 3, and 4 at frequency $f_i + f_j$ respectively. The $A_3(f_i,f_j,f_k)$, $B_3(f_i,f_j,f_k)$, $D_3(f_i,f_j,f_k)$, and $E_3(f_i,f_j,f_k)$ denote the third-order voltage transfer functions at nodes 1, 2, 3, and 4 at frequency $f_i + f_j + f_k$ respectively. The function F (A) for the voltage v_1 is defined by Eq. (6-9). The functions F (B), F (D), and F (E) for the voltages v_2, v_3, and v_4 are defined in a similar manner.

Equations (6-9) to (6-12) are substituted in Eq. (6-7). Then coefficients of identical terms on both sides of the resulting equation are equated. As an example the coefficients of $\exp(j2\pi(f_i+f_j)t)$ for $i \neq j$ will be given.

The coefficient of this term in the expression $C_2 \frac{d}{dt}(v_1-v_3)^2 + C_3 \frac{d}{dt}(v_1-v_3)^3$ is

$$C_2 j4\pi(f_i+f_j)[A_1(f_i)-D_1(f_i)][A_1(f_j)-D_1(f_j)]$$

The coefficient of this term in the expression $-(\alpha_2+C_2 \frac{d}{dt})(v_1-v_3)^2 -(\alpha_3+C_3 \frac{d}{dt})(v_1-v_3)^3$ is

$$-2[\alpha_2+C_2 j2\pi(f_i+f_j)][A_1(f_i)-D_1(f_i)][A_1(f_j)-D_1(f_j)]$$

The coefficient of this term in the expression $\alpha_2(v_1-v_3)^2+\alpha_3(v_1-v_3)^3$ is

$$2\alpha_2[A_1(f_i)-D_1(f_i)][A_1(f_j)-D_1(f_j)]$$

Using these results the matrix Eq. (6-7) at the second-order frequency $f_i + f_j$ can be written as

$$
2\begin{bmatrix} -1/R1-C_1 j2\pi(f_i+f_j) & 0 & C_1 j2\pi(f_i+f_j) & 0 \\ C_1 j2\pi(f_i+f_j)+\alpha_1 & 0 & -\alpha_1-\frac{1}{RS}-C_1 j2\pi(f_i+f_j) & \frac{1}{RS} \\ 0 & 0 & 1/RS & -\frac{1}{RS}-\frac{1}{R4} \\ -\alpha_1 & -1/R3 & \alpha_1 & 0 \end{bmatrix}
\begin{bmatrix} A_2(f_i,f_j) \\ B_2(f_i,f_j) \\ D_2(f_i,f_j) \\ E_2(f_i,f_j) \end{bmatrix}
$$

$$
= 2\begin{bmatrix} C_2 j2\pi(f_i+f_j)[A_1(f_i)-D_1(f_i)][A_1(f_j)-D_1(f_j)] \\ -[\alpha_2+j2\pi C_2(f_i+f_j)][A_1(f_i)-D_1(f_i)][A_1(f_j)-D_1(f_j)] \\ 0 \\ \alpha_2[A_1(f_i)-D_1(f_i)][A_1(f_j)-D_1(f_j)] \end{bmatrix} \qquad (6\text{-}13)
$$

Note that the time domain operator d/dt becomes the term $j2\pi(f_i + f_j)$ in the frequency domain. Therefore, the second-order nonlinear transfer functions $A_2(f_i,f_j)$, $B_2(f_i,f_j)$, $D_2(f_i,f_j)$, and $E_2(f_i,f_j)$ can be obtained by solving the matrix Eq. (6-13). Note that i and j take on the values 1, 2, 3 and that there are three distinct frequencies $f_1 + f_2$, $f_2 + f_3$, and $f_3 + f_1$ for which $f_i \neq f_j$.

The third-order matrix equation at the frequency $f_1 + f_2 + f_3$ is obtained by equating the coefficients of the exponential $\exp(j2\pi(f_1+f_2+f_3)t)$.

The coefficient in the expression for $C_2 \frac{d}{dt}(v_1-v_3)^2+C_3 \frac{d}{dt}(v_1-v_3)^3$ is

$$C_2 j8\pi(f_1+f_2+f_3)\{[A_1(f_1)-D_1(f_1)][A_2(f_2,f_3)-D_2(f_2,f_3)]+[A_1(f_2)-D_1(f_2)][A_2(f_1,f_3)$$

$$-D_2(f_1,f_3)]+[A_1(f_3)-D_1(f_3)][A_2(f_2,f_1)-D_2(f_2,f_1)]\}+C_3 j12\pi(f_1+f_2+f_3)$$

$$\cdot[A_1(f_1)-D_1(f_1)][A_1(f_2)-D_1(f_2)][A_1(f_3)-D_1(f_3)]$$

and that in the expression for $-(\alpha_2+C_2\frac{d}{dt})(v_1-v_3)^2-(\alpha_3+C_3\frac{d}{dt})(v_1-v_3)^3$ is

$$-4[\alpha_2+j2\pi C_2(f_1+f_2+f_3)]\{[A_1(f_1)-D_1(f_1)][A_2(f_2,f_3)-D_2(f_2,f_3)]+[A_1(f_2)-D_1(f_2)]$$

$$\cdot[A_2(f_1,f_3)-D_2(f_1,f_3)]+[A_1(f_3)-D_1(f_3)][A_2(f_2,f_1)-D_2(f_2,f_1)]\}$$

$$-6[\alpha_3+jC_3 2\pi(f_1+f_2+f_3)][A_1(f_1)-D_1(f_1)][A_1(f_2)-D_1(f_2)][A_1(f_3)-D_1(f_3)]$$

and that in the expression for $\alpha_2(v_1-v_3)^2+\alpha_3(v_1-v_3)^3$ is

$$4\alpha_2\{[A_1(f_1)-D_1(f_1)][A_2(f_2,f_3)-D_2(f_2,f_3)]+[A_1(f_2)-D_1(f_2)][A_2(f_1,f_3)-D_2(f_1,f_3)]$$

$$+[A_1(f_3)-D_1(f_3)][A_2(f_2,f_1)-D_2(f_2,f_1)]\}+6\alpha_3[A_1(f_1)-D_1(f_1)][A_1(f_2)-D_1(f_2)]$$

$$\cdot[A_1(f_3)-D_1(f_3)]$$

Using these results the matrix Eq. (6-7) at the third-order frequency $f_1 + f_2 + f_3$ can be written as

$$
6\begin{bmatrix}
-\frac{1}{R1}-C_1 j(\omega_1+\omega_2+\omega_3) & 0 & C_1 j(\omega_1+\omega_2+\omega_3) & 0 \\
C_1 j(\omega_1+\omega_2+\omega_3)+\alpha_1 & 0 & -(\alpha_1+\frac{1}{RS})-jC_1(\omega_1+\omega_2+\omega_3) & 1/RS \\
0 & 0 & 1/RS & -\frac{1}{RS}-\frac{1}{R4} \\
-\alpha_1 & -\frac{1}{R3} & \alpha_1 & 0
\end{bmatrix}
\begin{bmatrix}
A_3(f_1,f_2,f_3) \\
B_3(f_1,f_2,f_3) \\
D_3(f_1,f_2,f_3) \\
E_3(f_1,f_2,f_3)
\end{bmatrix}
$$

$$
=\begin{bmatrix}
C_2 j8\pi(f_1+f_2+f_3)\{[A_1(f_1)-D_1(f_1)][A_2(f_2,f_3)-D_2(f_2,f_3)]+[A_1(f_2)-D_1(f_2)][A_2(f_1,f_3) \\
-D_2(f_1,f_3)]+[A_1(f_3)-D_1(f_3)][A_2(f_2,f_1)-D_2(f_2,f_1)]\}+C_3 j12\pi(f_1+f_2+f_3) \\
\cdot[A_1(f_1)-D_1(f_1)][A_1(f_2)-D_1(f_2)][A_1(f_3)-D_1(f_3)] \\
\\
-4[\alpha_2+j2\pi C_2(f_1+f_2+f_3)]\{[A_1(f_1)-D_1(f_1)][A_2(f_2,f_3)-D_2(f_2,f_3)]+[A_1(f_2)-D_1(f_2)] \\
\cdot[A_2(f_1,f_3)-D_2(f_1,f_3)]+[A_1(f_3)-D_1(f_3)][A_2(f_2,f_1)-D_2(f_2,f_1)]\} \\
-6[\alpha_3+jC_3 2\pi(f_1+f_2+f_3)][A_1(f_1)-D_1(f_1)][A_1(f_2)-D_1(f_2)][A_1(f_3)-D_1(f_3)] \\
\\
0 \\
\\
4\alpha_2\{[A_1(f_1)-D_1(f_1)][A_2(f_2,f_3)-D_2(f_2,f_3)]+[A_1(f_2)-D_1(f_2)][A_2(f_1,f_3)-D_2(f_1,f_3)] \\
+[A_1(f_3)-D_1(f_3)][A_2(f_2,f_1)-D_2(f_2,f_1)]\}+6\alpha_3[A_1(f_1)-D_1(f_1)][A_1(f_2)-D_1(f_2)] \\
\cdot[A_1(f_3)-D_1(f_3)]
\end{bmatrix}
\qquad (6\text{-}14)
$$

The matrix Eq. (6-8) can be solved for the first-order transfer functions $A_1(f_i)$, $B_1(f_i)$, $D_1(f_i)$, and $E_1(f_i)$. The matrix Eq. (6-13) can be solved for the second-order transfer functions $A_2(f_i,f_j)$, $B_2(f_i,f_j)$, $D_2(f_i,f_j)$ and $E_2(f_i,f_j)$. The matrix Eq. (6-14) can be solved for the third-order transfer functions $A_3(f_i,f_j,f_k)$, $B_3(f_i,f_j,f_k)$, $D_3(f_i,f_j,f_k)$, and $E_3(f_i,f_j,f_k)$. This is best done numerically using a digital computer. In order to solve these equations numerically, values for the nonlinear coefficients C_1, C_2, C_3, α_1, α_2, and α_3 must be known.

Values for the JFET nonlinear coefficients α_1, α_2, and α_3 can be determined by using the equation that relates the JFET drain current I_D to the internal gate-source voltage V'_{GS}. Values for the JFET nonlinear coefficients C_1, C_2, and C_3 can be determined by using the equation that relates the JFET gate-source capacitance C to the internal gate-source voltage V'_{GS}. The JFET saturated drain current formula used in NCAP is given by[42]

$$I_D = 3I_{DMAX}\,\rho\{-\frac{\rho}{2} + \frac{1}{2}[\rho^2 + 4(\frac{1}{3} - \frac{V'_{GS} + \psi}{V_p + \psi} + \frac{2}{3}(\frac{V'_{GS} + \psi}{V_p + \psi})^{3/2})]^{1/2}\} \qquad (6\text{-}15)$$

The parameters used in Eq. (6-15) are described in Table 6-1. Typical values are also given.

TABLE 6-1

JFET NCAP MODEL PARAMETERS

Parameter	Value	Description
I_{DMAX}	0.013 A	Drain Current Parameter
ψ	-0.5 V	JFET Barrier Potential
V_p	-1.70 V	Pinch-off Voltage
V_{GS}	-1.50 V	External Gate-Source Voltage
RS	37 Ω	Source Resistance
ρ	1.722	Drain Current Parameter
K	2.20 pF-$V^{\frac{1}{2}}$	Gate-Source Capacitance Parameter
V_o	-0.5 V	Gate-Source Capacitor Built-in Voltage
m	0.5	Asymtotic Slope of $C(V'_{GS})$

The first step is to determine the JFET operating point. By an iterative method, the drain current for the circuit shown in Figure 6-1 was calculated to be 7.938×10^{-5}A, and the voltage V'_{GS} $(=V_{GS}-I_D R_s)$ was calculated to be -1.503 V. Knowing I_D and V'_{GS}, the nonlinear coefficeints α_1, α_2, and α_3 can be calculated from the following equations:

$$\alpha_1 = \frac{\partial I_D}{\partial V'_{GS}} \tag{6-16}$$

$$\alpha_2 = \frac{1}{2}\frac{\partial^2 I_D}{\partial V'^2_{GS}} \tag{6-17}$$

$$\alpha_3 = \frac{1}{6}\frac{\partial^3 I_D}{\partial V'^3_{GS}} \tag{6-18}$$

The following values were obtained

$$\alpha_1 = 8.115 \times 10^{-4} \text{ mho}$$

$$\alpha_2 = 2.103 \times 10^{-3} \text{ mho/V}$$

$$\alpha_3 = -1.460 \times 10^{-4} \text{ mho/V}^2$$

The nonlinear capacitance-voltage relationship used in NCAP for the gate-source capacitance C is given by

$$C = K|V_o + V'_{GS}|^{-m} \tag{6-19}$$

The parameters used in Eq. (6-19) are described in Table 6-1. Typical values are also given. The nonlinear coefficients C_1, C_2, and C_3 can be calculated using

$$C_1 = C(V'_{GS}) \tag{6-20}$$

$$C_2 = (1/2) \frac{\partial C}{\partial V'_{GS}} \tag{6-21}$$

$$C_3 = (1/6) \frac{\partial^2 C}{\partial V'^2_{GS}} \tag{6-22}$$

The following values were obtained.

$$C_1 = 1.555 \times 10^{-12} \text{ F}$$

$$C_2 = 1.940 \times 10^{-13} \text{ F/V}$$

$$C_3 = 4.844 \times 10^{-14} \text{ F/V}^2$$

Using these values for the coefficients α_1, α_2, α_3, C_1, C_2, and C_3, and the matrix Eqs. (6-8), (6-13), and (6-14), values for first-order, second-order, and third-order transfer functions were calculated. Standard subroutines in computer libraries such as IMSL[43] available at SUNYAB were used. The results are given in Table

6-2. Also given in Table 6-2 are the numerical results calculated using the computer program NCAP at Rome Air Development Center, Griffiss Air Force Base, New York. The two sets of results agree well for the dominant transfer functions. The differences observed for the very low valued terms are believed to be related to numerical inaccuracies in the matrix inversion routines used.

TABLE 6-2

CALCULATED VALUES FOR THE JFET NONLINEAR TRANSFER FUNCTIONS

Transfer Function	IMSL (SUNYAB)	NCAP(RADC)
A_1(1 kHz)	-j0.948E-8	1-j0.948E-15
B_1(1 kHz)	-78.79+j0.00002839	-78.78+j0.00227
D_1(1 kHz)	0.0292+j0.340E-6	0.0292+j0.280E-4
E_1(1 kHz)	0.788E-6+j0.920E-11	0.788E-6+j0.757E-9
A_2(1 kHz,0.9 kHz)	-0.901E-15-j0.862E-9	-0.219E-18+j0.350E-15
B_2(1 kHz,0.9 kHz)	-0.192E3+j0.719E-4	-0.192E3+j0.209E-1
D_2(1 kHz,0.9 kHZ)	0.712E-1+j0.528E-8	0.712E-1+j0.124E-3
E_2(1 kHz,0.9 kHz)	0.192E-5+j0.143E-12	0.192E-5+j0.336E-8
A_3(1 kHz,0.9 kHz,1.1 kHz)	0.182E-14-j0.776E-9	0.188E-18-j0.151E-15
B_3(1 kHz,0.9 kHz,1.1 kHz)	0.412E2-j0.224E-4	0.152E2+j0.509E-1
D_3(1 kHz,0.9 kHz,1.1 kHz)	-0.152E-1+j0.370E-7	-0.564E-2+j0.353E-4
E_3(1 kHz,0.9 kHz,1.1 kHz)	-0.412E-6+j0.100E-11	-0.152E-6-j0.954E-9

6.2 Tuned RF Amplifier BJT Stage

In this section a second-order transfer function for a tuned RF amplifier BJT stage will be calculated. Results obtained using a direct calculation procedure and the computer program NCAP will be presented and compared. The direct calculation procedure involves the use of computational techniques for computer-aided circuit analysis programs. This is necessary because the network equations used to calculate the second-order transfer functions are complicated.

Shown in Figure 6-2 is the circuit for a tuned RF amplifier stage using a 2N5109 NPN bipolar junction transistor (BJT). Results for this circuit including the linear equivalent circuit have been reported upon previously.[44] It is instructive to show the computational procedures used by NCAP to calculate first and second-order transfer functions. The bookkeeping involved in calculating third-order transfer functions is so complicated that it was not attempted. The calculation of the third-order transfer functions for the circuit shown in Figure 6-2 is a task best left to the computer program NCAP. Since this example will illustrate both first and second-order transfer function calculations, the BJT stage is excited by two independent voltage sources of unit amplitude at frequencies f_1 and f_2 as shown in Figure 6-2. The voltage sources are transformed to current sources as shown in Figure 6-3. The network linear responses at the two frequencies f_1 and f_2 and nonlinear response at the frequency $f_1 + f_2$ will be calculated.

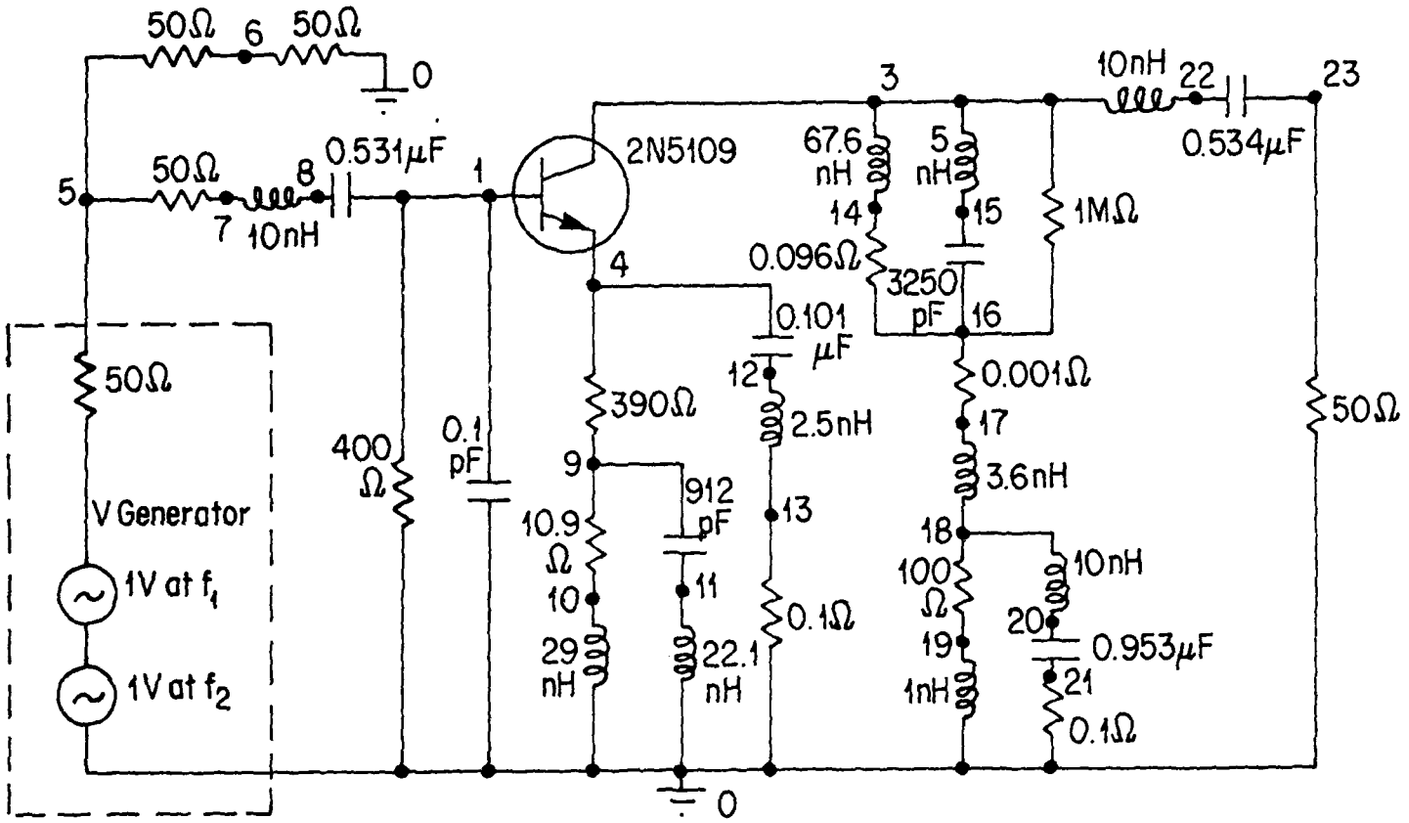

FIGURE 6-2 A 2N5109 RF Amplifier NCAP Coding Circuit Diagram

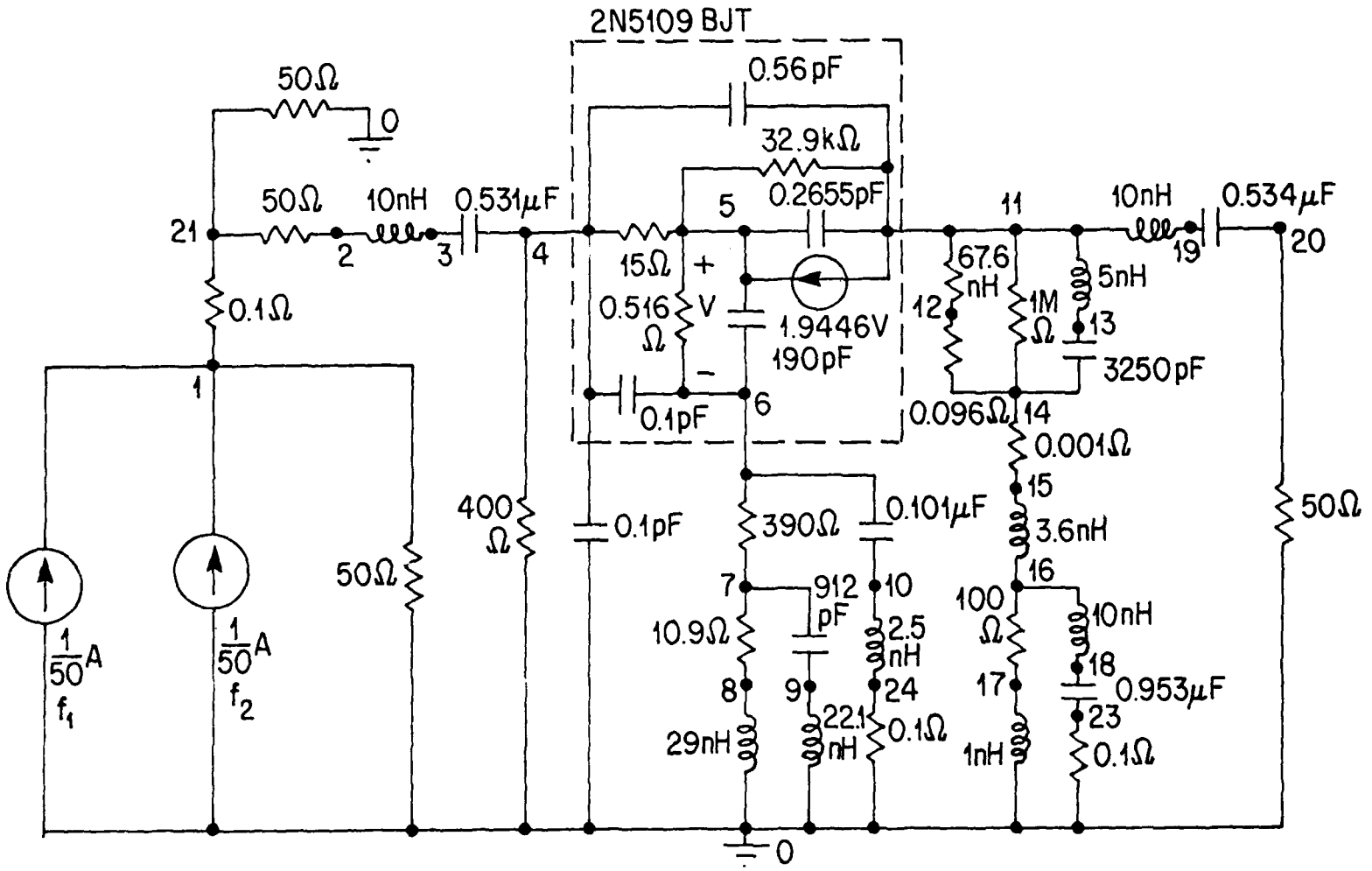

FIGURE 6-3 A 2N5109 RF Amplifier Fortran NCAP Simulation Circuit Diagram, where Only the Linear Portion of the Amplifier is Shown.

6.2.1 Construction of the Linear Nodal Admittance Matrix Y and the Linear Current Excitation Source Vector J_ℓ

We used a direct construction method to build the nodal admittance matrix Y and the linear current source vector J_ℓ. The method is summarized briefly.

(1) Illustrated in Figure 6-4 is a composite branch connected from node i to node j. This branch includes an admittance y_ℓ in series with an independent voltage source e_ℓ, both of which are shunted by a linear current source j_ℓ. The contributions of this branch to the ith and jth rows and columns of the admittance matrix Y and to the ith and jth row of the linear current source vector J_ℓ are shown next:

$$Y = \begin{array}{c} \\ \\ i \\ \\ \\ j \\ \\ \end{array} \begin{array}{c} \begin{array}{cccccc} & & i & & j & \end{array} \\ \left[\begin{array}{cccccc} & & \cdot & & \cdot & \\ & & \cdot & & \cdot & \\ \cdot & \cdot & y_\ell & \cdots & -y_\ell & \cdot\ \cdot \\ & & \cdot & & \cdot & \\ & & \cdot & & \cdot & \\ \cdot & \cdot & -y_\ell & \cdots & y_\ell & \cdot\ \cdot \\ & & \cdot & & \cdot & \\ & & \cdot & & \cdot & \end{array}\right] \end{array} \qquad (6\text{-}23)$$

$$J_\ell = \begin{array}{c} \\ \\ i \\ \\ \\ j \\ \\ \end{array} \left[\begin{array}{c} \cdot \\ \cdot \\ j_\ell \quad - y_\ell e_\ell \\ \cdot \\ \cdot \\ \cdot \\ -(j_\ell \quad - y_\ell e_\ell) \\ \cdot \\ \cdot \end{array}\right] \qquad (6\text{-}24)$$

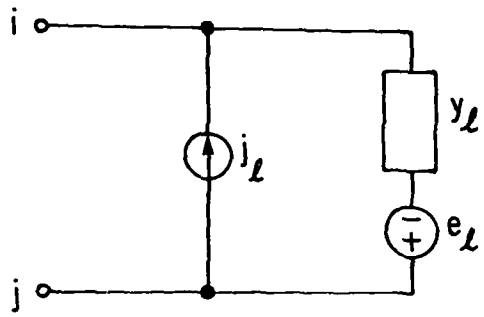

FIGURE 6-4 Composite Branch Containing an Admittance Connected from Node i to Node j

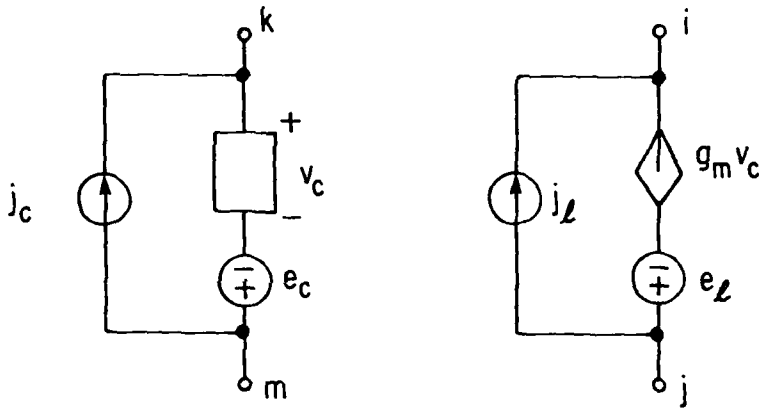

FIGURE 6-5 Composite Branch Containing a Voltage-Controlled Current Source Along with the Controlling Branch

Note that the product $Y^{-1}J_\ell$ generates the linear node-to-datum voltage vector V_ℓ.

(2) Illustrated in Figure 6-5 is a composite branch connected from node i to node j containing a dependent voltage-controlled current source $g_m v_c$ in series with an independent voltage source e_ℓ both of which are shunted by a linear current source j_ℓ. The control voltage v_c is defined by a voltage developed in a composite branch connected from node k to node m. The contribution of these components to the ith and jth rows and kth and mth columns of the admittance matrix Y and to the ith and jth rows of the linear current vector J_ℓ are as follows:

$$Y = \begin{array}{c} \\ \\ \\ i \\ \\ \\ \\ j \\ \\ \\ \end{array} \begin{array}{c} \begin{array}{ccccccc} & & k & & & m & \end{array} \\ \left[\begin{array}{ccccccc} & & \cdot & & & \cdot & \\ & & \cdot & & & \cdot & \\ \cdot & \cdot & g_m & \cdot & \cdot & -g_m & \cdot \; \cdot \\ & & \cdot & & & \cdot & \\ & & \cdot & & & \cdot & \\ & & \cdot & & & \cdot & \\ \cdot & \cdot & -g_m & \cdot & \cdot & g_m & \cdot \; \cdot \\ & & \cdot & & & \cdot & \\ & & \cdot & & & \cdot & \end{array}\right] \end{array} \qquad (6\text{-}25)$$

$$J_\ell = \begin{array}{c} \\ \\ \\ i \\ \\ \\ \\ j \\ \\ \\ \end{array} \left[\begin{array}{c} \cdot \\ \cdot \\ j_\ell \quad -g_m\, e_c \\ \cdot \\ \cdot \\ \cdot \\ -(j_\ell \quad - g_m\, e_c) \\ \cdot \\ \cdot \end{array}\right] \qquad (6\text{-}26)$$

The procedure for constructing Y and J_ℓ is initiated by setting $Y = 0$ and $J_\ell = 0$. Composite branches are added to the network one by one. First the admittance branches of the kind shown in Figure 6-4 are added, and then the controlled source branches of the kind shown in Figure 6-5 are added. When all the composite branches are added, the final results are the desired Y and J_ℓ.

After Y and J_ℓ are constructed, the linear response of the network (i.e. the first-order transfer function) are calculated from the matrix equation

$$YV_1 = J_\ell \tag{6-27}$$

at each excitation frequency of interst. (For example two source excitation frequencies f_i and f_j are used when second-order transfer functions are to be calculated.) Based upon the values of the first-order transfer functions, the second-order current source vector J_{d2} can be evaluated.

6.2.2 Calculation of the Second-Order Current Source Vector J_{d2}.

The magnitude of the second-order nonlinear current source vector J_{d2} is dependent upon the second-order nonlinearities of the nonlinear components in the circuit and the first-order node voltage vector V_1 at each excitation frequency of interest. For the BJT used in the circuit shown in Figure 6-2 several nonlinearities will be considered. One of these is the base-emitter nonlinear resistance. Another is the collector-base nonlinear capacitor. The third is the collector-base nonlinear dependent current generator. The nonlinear base-emitter capacitance was modelled as a linear capacitor for simplicity. The

contribution to the second-order nonlinear current vector J_{d2} by each of these three BJT nonlinear components will now be presented.

(1) Base-emitter nonlinear resistance

The base-emitter nonlinear resistance is connected from node 5 to node 6 in the circuit shown in Figure 6-3. In this circuit the linear term (0.516 Ω) is shown. Now we shall show how the second-order current source associated with the nonlinear base-emitter resistor is determined. The results presented in Section 2.3.5 for a nonlinear resistor are used. For a nonlinear resistor, the second-order current source can be written in the time domain as

$$j_{R2} = K_2 v_r^{\,2} \tag{6-28}$$

where v_r is the voltage across the nonlinear resistor. If the nonlinear resistor is connected from node 5 to node 6, the second-order current source vector J_{R2} in the time domain for the nonlinear resistor contains non-zero elements only in the rows 5 and 6 as shown below.

$$J_{R2} = \begin{array}{c} \\ \\ 5 \\ 6 \\ \\ \\ \end{array} \begin{pmatrix} \cdot \\ \cdot \\ -K_2(v_5 - v_6)^2 \\ K_2(v_5 - v_6)^2 \\ \cdot \\ \cdot \end{pmatrix} \tag{6-29}$$

In the frequency domain at frequency $f_1 + f_2$, Equation (6-29) has the following form:

$$J_{R2} = \begin{array}{c} \\ 5 \\ 6 \\ \\ \end{array} \begin{bmatrix} \vdots \\ -K_2(V_5^1(f_1)-V_6^1(f_1))(V_5^1(f_2)-V_6^1(f_2)) \\ K_2(V_5^1(f_1)-V_6^1(f_1))(V_5^1(f_2)-V_6^1(f_2)) \\ \vdots \end{bmatrix} \tag{6-30}$$

where V_5^1 and V_6^1 denote the first-order transfer functions of voltages $v_5(t)$ and $v_6(t)$ respectively.

(2) Collector-base nonlinear capacitance

The collector base nonlinear capacitance is connected from node 11 to node 5 in the circuit shown in Figure 6-3. In this circuit diagram the linear term (0.2655 pF) is shown. Now we shall show how the second-order current source associated with the nonlinear capacitor is determined. The results presented in Section 2.3.2 for a nonlinear capacitor are used. For a nonlinear capacitor the second-order current source j_{C2} can be written in time domain as

$$j_{C2} = C_2 \frac{d}{dt} v_c^{\,2} \tag{6-31}$$

where v_c is the voltage across the nonlinear capacitor. If the nonlinear capacitor is connected from node 11 to node 5, the second-order current source vector J_{C2} in the time domain for the nonlinear capacitor contains non-zero elements only in the rows 11 and 5 as shown below:

$$J_{C2} = \begin{array}{c} \\ 5 \\ \\ 11 \\ \\ \end{array} \begin{bmatrix} \vdots \\ C_2 \frac{d}{dt}(v_{11} - v_5)^2 \\ \vdots \\ -C_2 \frac{d}{dt}(v_{11} - v_5)^2 \\ \vdots \end{bmatrix} \tag{6-32}$$

In the frequency domain at frequency $f_1 + f_2$, Equation (6-32) has the following form:

$$J_{C2} = \begin{array}{c} \\ 5 \\ \\ 11 \\ \\ \end{array} \begin{bmatrix} \vdots \\ j(\omega_1+\omega_2)C_2[V_5^1(f_1)-V_{11}^1(f_1)][V_5^1(f_2)-V_{11}^1(f_2)] \\ \vdots \\ -j(\omega_1+\omega_2)C_2[V_5^1(f_1)-V_{11}^1(f_1)][V_5^1(f_2)-V_{11}^1(f_2)] \\ \vdots \end{bmatrix} \tag{6-33}$$

where V_{11}^1 denotes the first-order transfer function of the voltage $v_{11}(t)$.

(3) Nonlinear dependent current source

The nonlinear dependent current source is connected from node 11 to node 5 in the circuit shown in Figure 6-3. In this circuit diagram the linear term (1.99446V) is shown. Now we shall show how the second-order current source associated with the nonlinear dependent current source is determined. The results presented in Section 2.3.4 for a nonlinear dependent current source j_y can be

written in time domain as

$$j_y = g_{20}v_x^{\ 2} + g_{02}v_y^{\ 2} + g_{11}v_xv_y \tag{6-34}$$

where v_x is the voltage across the controlling branch x, and v_y is the voltage across the controlled branch y. If the nonlinear dependent current generator is connected from node 11 to node 5, with the controlling branch connected from node 5 to node 6, the second-order current source vector J_{G2} in the time domain for the nonlinear dependent current source contains non-zero elements only in rows 11 and 5 as shown below:

$$J_{G2} = \begin{array}{c} \\ 5 \\ \\ 11 \\ \\ \end{array} \begin{bmatrix} \vdots \\ g_{20}(v_5-v_6)^2 + g_{02}(v_{11}-v_5)^2 + g_{11}(v_5-v_6)(v_{11}-v_5) \\ \vdots \\ -g_{20}(v_5-v_6)^2 - g_{02}(v_{11}-v_5)^2 - g_{11}(v_5-v_6)(v_{11}-v_5) \\ \vdots \end{bmatrix} \tag{6-35}$$

In the frequency domain at frequency $f_1 + f_2$, Equation (6-35) has the following form:

$$
J_{G2} = \begin{array}{r} \\ \\ 5 \\ \\ \\ \\ \\ \\ 11 \\ \\ \\ \\ \\ \end{array}
\begin{pmatrix}
\cdot \\
\cdot \\
g_{20}[V_5^1(f_1)-V_6^1(f_1)][V_5^1(f_2)-V_6^1(f_2)] \\
+ g_{02}[V_{11}^1(f_1)-V_5^1(f_1)][V_{11}^1(f_2)-V_5^1(f_2)] \\
+ g_{11}[V_5^1(f_1)-V_6^1(f_1)][V_{11}^1(f_2)-V_5^1(f_2)] \\
\cdot \\
\cdot \\
-g_{20}[V_5^1(f_1)-V_6^1(f_1)][V_5^1(f_2)-V_6^1(f_2)] \\
- g_{02}[V_{11}^1(f_1)-V_5^1(f_1)][V_{11}^1(f_2)-V_5^1(f_2)] \\
- g_{11}[V_5^1(f_1)-V_6^1(f_1)][V_{11}^1(f_2)-V_5^1(f_2)] \\
\cdot \\
\cdot
\end{pmatrix} \tag{6-36}
$$

By adding together all the components for the second-order nonlinear current vector given in Eqs. (6-30), (6-33), 6-36), we obtain the desired second-order nonlinear current source vector J_{d2} in the frequency domain at the frequency $f = f_1 + f_2$.

6.2.3 Calculation of the Second-Order Nonlinear Transfer Functions

The second-order transfer function vector H_2 for the tuned RF amplifier stage shown in Figure 6-2 is calculated at frequency $f = f_1 + f_2$ by solving the matrix equation

$$Y(f_1 + f_2)\ H_2(f_1,f_2) = \frac{1}{2}\ J_{d2} \tag{6-37}$$

where the current source vector J_{d2} is the sum of the matrix Eqs. (6-30), (6-33), and (6-36). The admittance matrix $Y(f_1 + f_2)$ is the linear nodal matrix evaluated at frequency $f_1 + f_2$. The computer program given in Appendix IV was used. This computer program will now be described briefly.

First the circuit information shown in Figure 6-3 is entered so that the nodal admittance matrix Y can be calculated at each frequency of interest. Next the NCAP input data for the 2N5109 BJT given in Table 2-1 are entered. The computer program given in Appendix IV calculates the nonlinear coefficients for the BJT. The results were given previously in Table 2-2. Next the two excitation frequencies are selected. The values f_1 = 10 MHz and f_2 = -9 MHz were used. At this point all the data necessary for the computation are entered. Now the computation can begin.

First the computer program given in Appendix IV solves for the network first-order transfer functions at f_1 = 10 MHz and f_2 = -9 MHz. A subroutine for solving matrix equations in the library IMSL available at SUNYAB is used. Next the second-order current vector J_{d2} at frequency $f_1 + f_2$ is computed. Also the admittance matrix $Y(f_1 + f_2)$ at the frequency $f_1 + f_2$ is computed. The matrix Eq. (6-37) is solved using the IMSL subroutine. The results for the tuned RF amplifier output transfer function (at node 20 in Figure 6-3) are given in Table 6-3.

Also given in Table 6-3 are the computer program NCAP results for the tuned RF amplifier output transfer function. The NCAP results and the results calculated using the computer program given in Appendix IV are in excellent agreement. The very small numerical differences between these two sets of results may be related to the fact that the computer program NCAP accounts completely for the base-emitter nonlinear diffusion capacitance.

TABLE 6-3

CALCULATED RESULTS FOR THE FIRST AND SECOND ORDER TRANSFER FUNCTIONS FOR THE 2N5109 TUNED RF AMPLIFIER AT THE OUTPUT NODE[a]

ORDER	TRANSFER FUNCTION	SUNYAB PROGRAM (Appendix IV)		NACP(RADC)	
		DB	ANGLE	DB	ANGLE
n = 1	H_1(10 MHz)	19.412	-167.313	19.409	-167.29
n = 1	H_1(-9 MHz)	12.622	128.528	12.620	128.52
n = 2	H_2(10 MHZ_1, -9 MHz)	-29.215	-71.317	-29.408	-83.08

a The output node is node 20 of the FORTRAN coded circuit diagram Figure 6-3, or node 23 of the NCAP coded circuit diagram Figure 6-2.

CHAPTER SEVEN

THE MEASUREMENT AND PREDICTION OF THE SECOND-ORDER TRANSFER FUNCTIONS IN INTEGRATED CIRCUITS

In Chapter Four two amplifier circuits using integrated circuits were presented. The broadband amplifier circuit shown in Figure 4-2 uses a CA3026 dual differential pair as the active device. The unity gain voltage follower circuit shown in Figure 4-11 uses a μA741 operational amplifier (op amp) as the active device. The NCAP model parameters for these two integrated circuits were given in Tables 4-1 and 4-3. Using the circuit information given in Figures 4-2 and 4-11 and NCAP parameters given in Tables 4-1 and 4-3 the second-order transfer functions of the two amplifiers can be calculated by the computer program NCAP. However, as discussed in Chapters Five and Six, the simulation program NCAP first calculates the first-order (linear) voltages at all the nodes in the network at all frequencies of interest. The second-order responses depend upon the values of these first-order node voltages. Thus, accurate values for the first-order node voltages are needed, if accurate results for the second-order calculations are desired. Thus, it is necessary to have accurate linear models for the electronic circuits. Therefore, in this chapter the linear models determined for the complete CA3026 cascode amplifier and the μA741 unity gain buffer amplifier are presented. Accurate linear models are developed by comparing calculated and measured linear transfer functions and by making adjustments to the linear models as appropriate. Then second-order transfer functions of the amplifiers are calculated and compared to values measured in our laboratory.

This chapter is organized in the following manner. First the linear models determined for the CA3026 cascode amplifier and the μA741 op amp unity gain buffer are presented. The measured and predicted values for the output first-order (linear) transfer function of the amplifiers are given. Also included is a description of the experimental system used to measure the second-order transfer functions of the amplifiers and the calculation method used to compute the transfer functions from the measured voltages. The NCAP computer program input data listing for the two amplifiers are tabulated. The NCAP predicted and the experimental measured results are presented and compared at the end of the chapter.

7.1 Linear Model of the CA3026 Cascode Amplifier

The linear model for the CA3026 cascode amplifier is determined by comparing experimental and calculated results of the amplifier linear transfer function VOUT/VIN over the frequency range 100 Hz to 30 MHz. Experiemental values of VOUT/VIN for the cascode amplifier were measured using the measurement system shown in Figure 7-1. The experimental results for the magnitude and phase of VOUT/VIN are shown in Figures 7-2 and 7-3.

Also shown in Figures 7-2 and 7-3 are calculated values of VOUT/VIN obtained using the computer program SPICE2. The calculated values were obtained using the linear equivalent circuit for the cascode amplifier shown in Figure 7-4. The linear equivalent circuit contains linear models for the three CA3026 BJT's (Q1, Q2, and Q3) and linear models for the passive components. The passive component

AD-A082 527 SYRACUSE UNIV NY F/G 9/5

NONLINEAR SYSTEM ANALYSIS IN BIPOLAR INTEGRATED CIRCUITS.(U)

JAN 80 T FANG, J J WHALEN F30602-79-C-0011

UNCLASSIFIED RADC -TR-79-324 NL

3 OF 3

END

DATE FILMED

5-80

DTIC

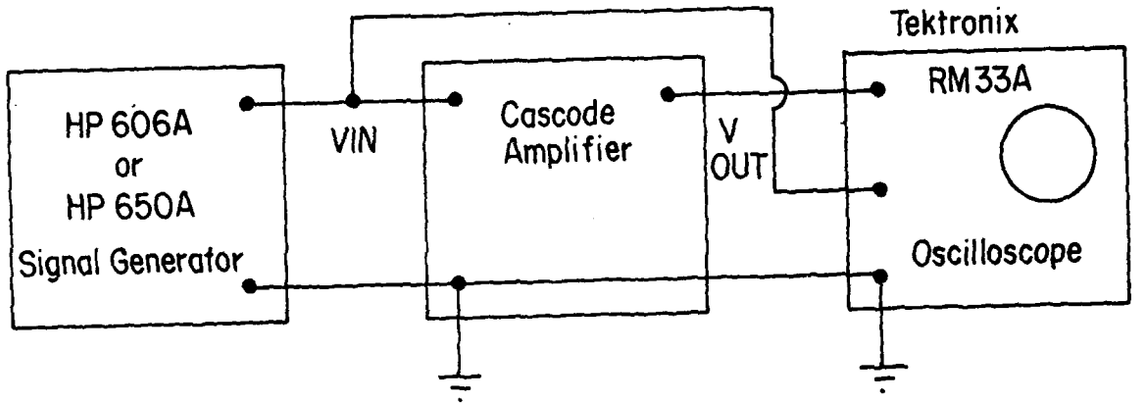

FIGURE 7-1 Experimental Systems for Measuring the First-Order Transfer Function $H_1(f)$ of the CA3026 Cascode Amplifier. Note that $H_1(f)$ = VOUT/VIN

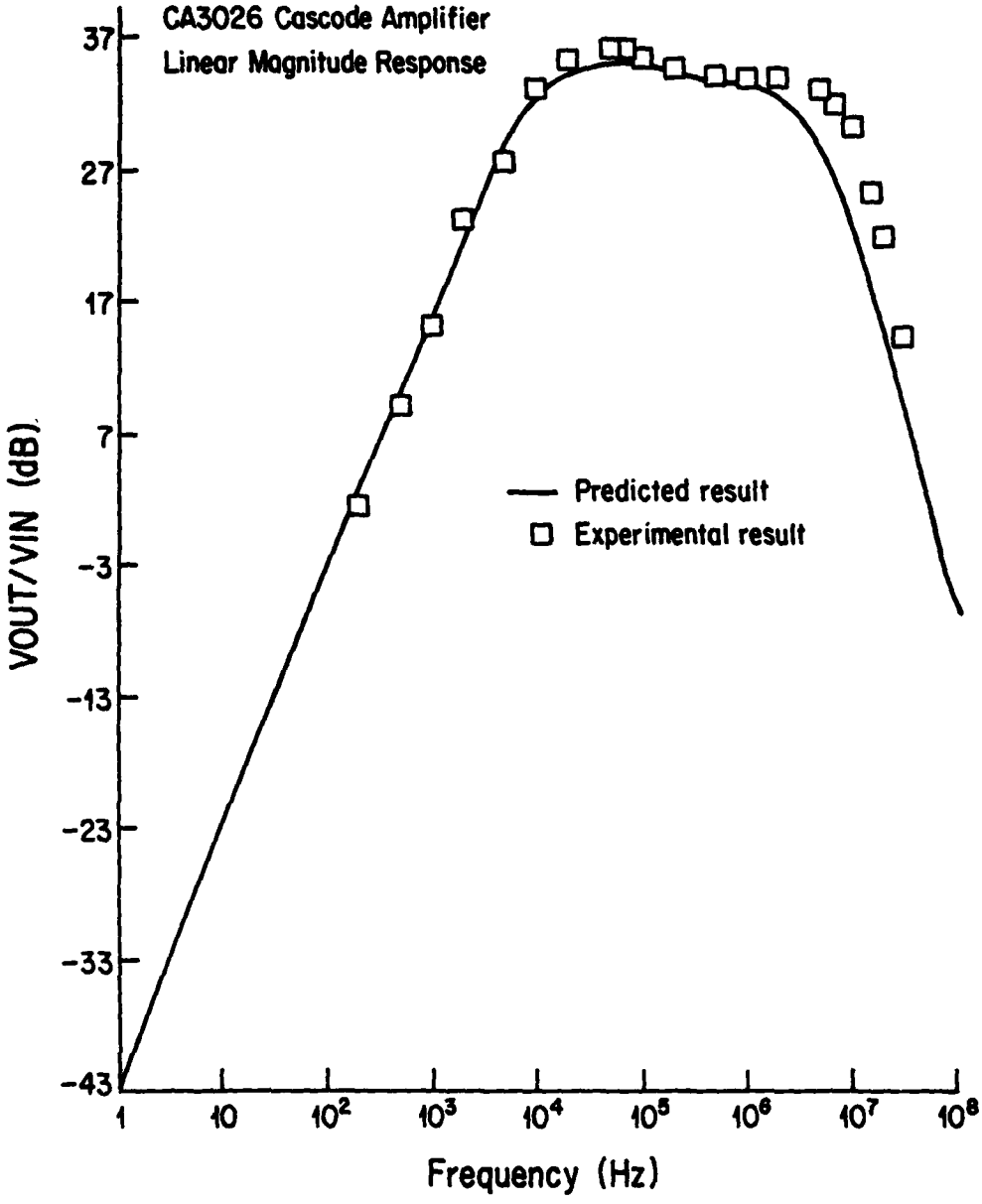

FIGURE 7-2 Measured and Predicted Values for the First-Order Transfer Function VOUT/VIN of the Cascode Amplifier

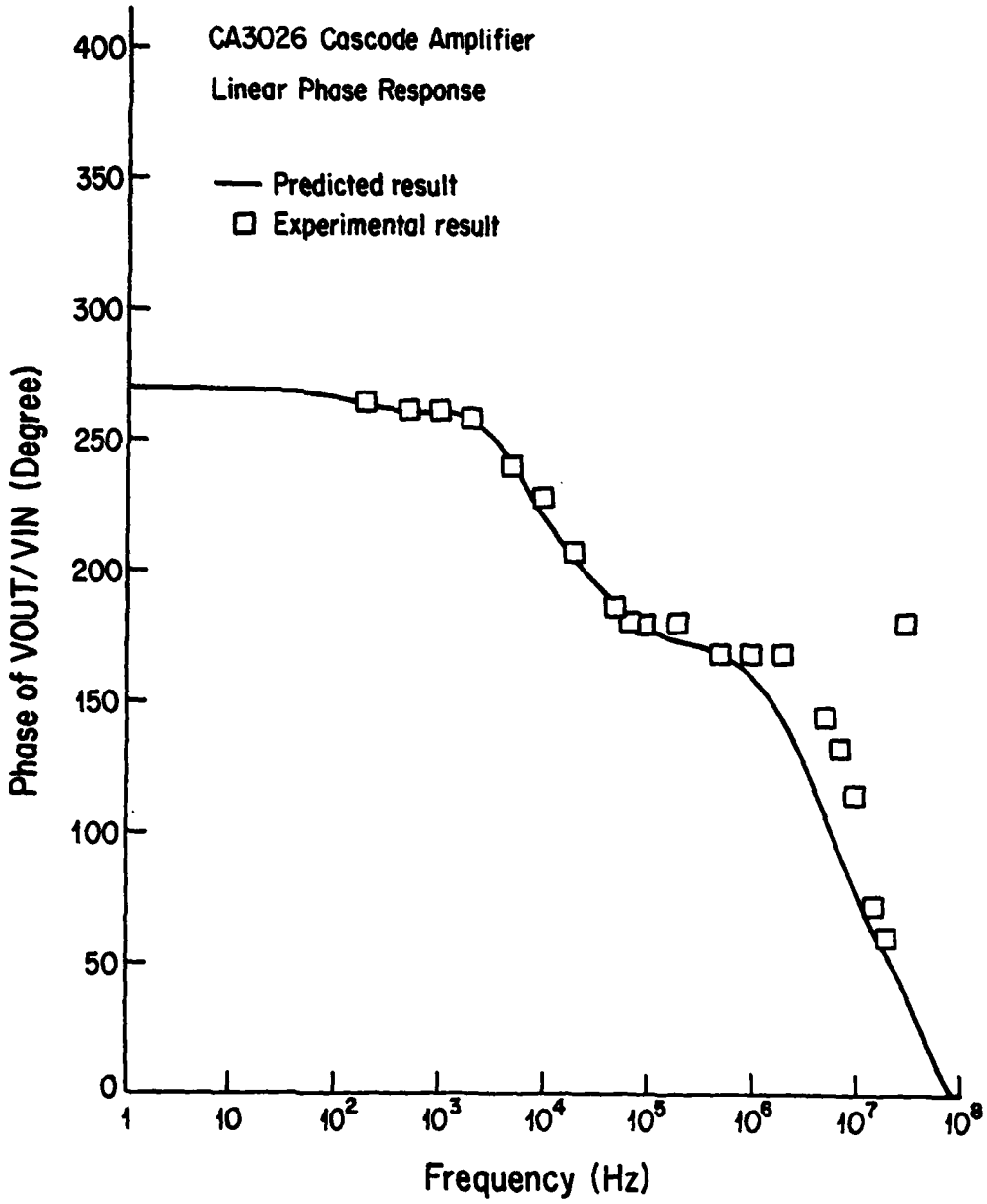

FIGURE 7-3 Measured and Predicted Values for the First-Order Transfer Function VOUT/VIN of the Cascode Amplifier

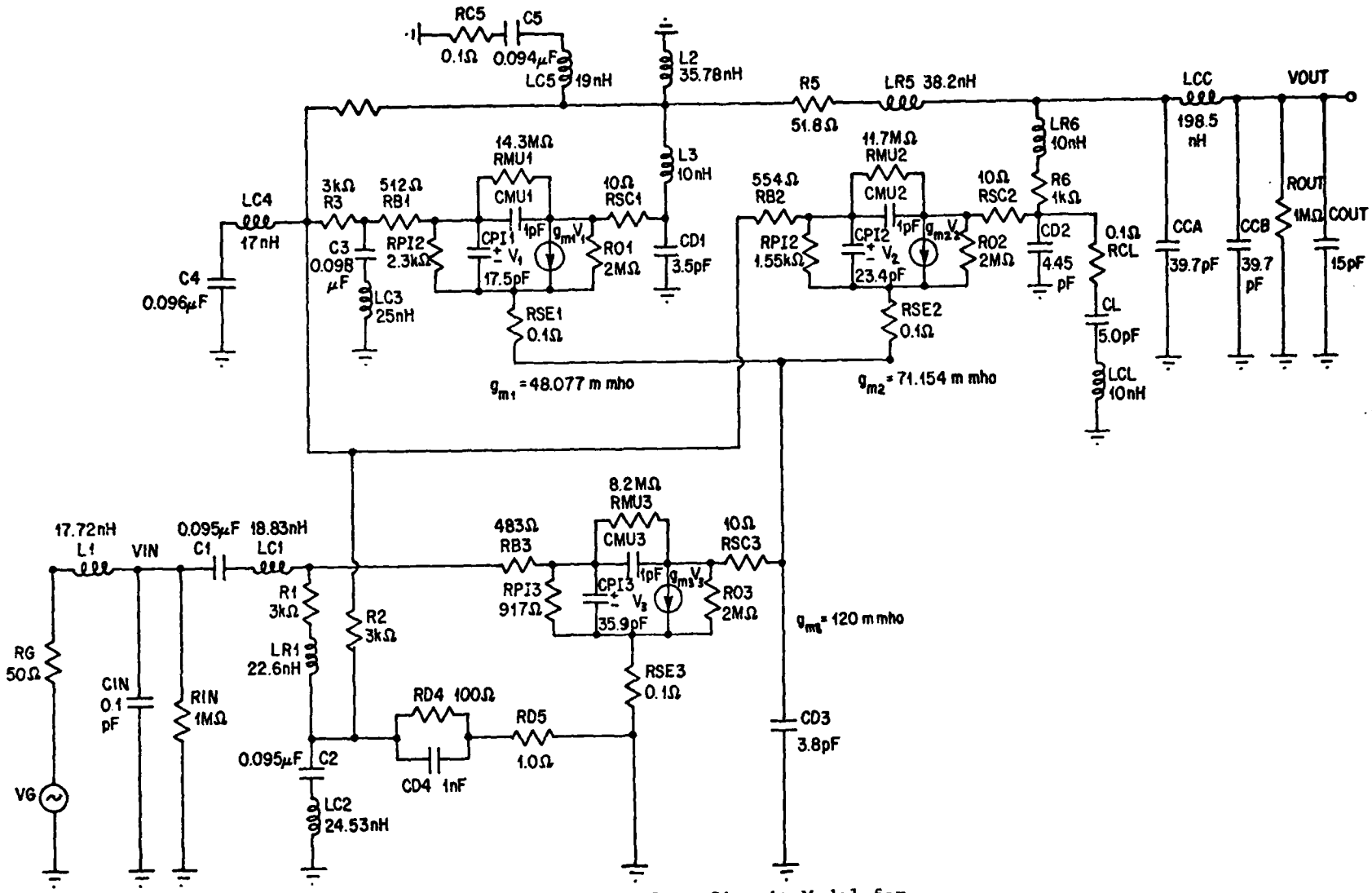

FIGURE 7-4 A Linear Incremental Equivalent Circuit Model for the CA3026 Cascode Amplifier. Note That the Hybrid-Pi Model is Used for the BJT's

models accounted for parasitic effects. Values for the hybrid-pi model parameters used in the linear models for the BJT's are listed in Table 7-1. Methods used to determine the BJT hybrid-pi model parameter values are discussed in Chapter Two and in Ref. (18). Procedures for determining component parasitic elements are described in Ref. (44).

The calculated and experimental values for the magnitude response shown in Figure 7-2 agree within 5 dB over the frequency range 100 Hz to 30 MHz. The calculated and experimental values for the phase response shown in Figure 7-3 agree within 25 degrees over the frequency range 100 Hz to 20 MHz. Above 20 MHz the experimental values for the phase response appear to be beginning to deviate from the measured values. Thus, the linear model for the cascode amplifier circuit shown in Figure 7-4 should be quite suitable for NCAP calculation involving RF frequencies up to 30 MHz which is the upper limit for the HF frequency range. The NCAP calculated results will be given in Section 7.4.

7.2 Linear Model of the μA741 Unity Gain Buffer Amplifier

The linear model for the μA741 unity gain buffer amplifier is determined by comparing experimental and calculated results of the amplifier linear transfer function VOUT/VIN over the frequency range 100 Hz to 3 MHz. Experimental values of VOUT/VIN for the unity gain buffer amplifier were measured using the measurement system shown in Figure 7-5. The experimental results for the magnitude and phase of VOUT/VIN are shown in Figures 7-6 and 7-7.

Also shown in Figures 7-6 and 7-7 are two sets of calculated values of VOUT/VIN obtained using the computer program SPICE2. The calculated values were obtained for the circuit diagram shown in

TABLE 7-1

LINEAR INCREMENTAL HYBRID-PI MODEL PARAMETERS FOR BJT'S IN THE RCA CA3026 INTEGRATED CIRCUIT[a]

Parameter	Q1	Q2	Q3
r_b (ohm)	512	554	483
C_μ ($=C_{jc}+Cb$) (pF)	1.0	1.0	1.0
C_π ($=C_{je}+C_d$) (pF)	17.46	23.37	35.89
r_c (ohm)	2M	2M	2M
g_m (m mho)	48.077	71.154	120.0
r_e (ohm)	20.61	13.93	8.26
r_π (k ohm)	2.288	1.546	0.917

[a] The dc operating point bias emitter currents for transistors Q1, Q2, and Q3 are: I_{EQ_1} = 1.25 mA, I_{EQ_2} = 1.85 mA, I_{EQ_3} = 3.12 mA.

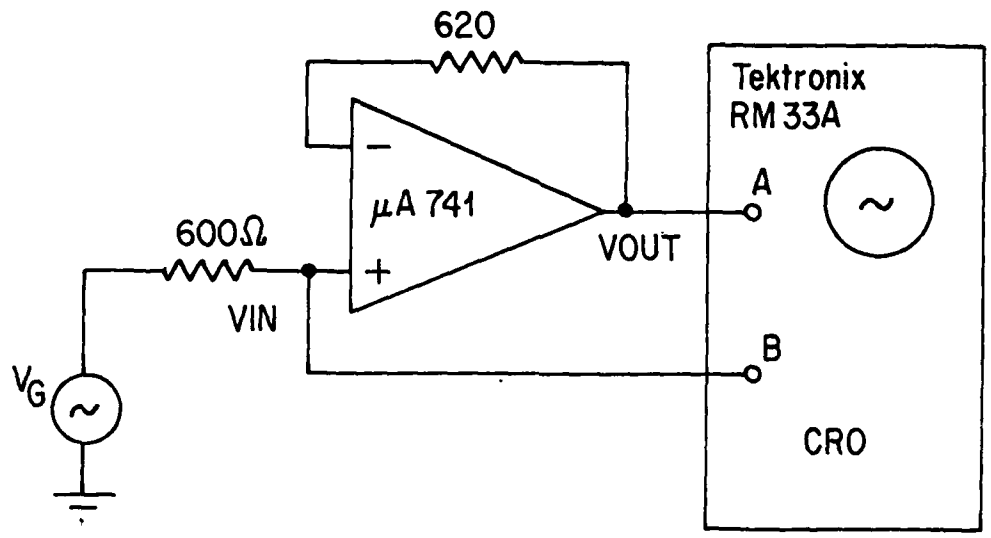

FIGURE 7-5 Experimental System for Measuring the First-Order Transfer Function $H_1(f)$ of the μA741 Unity Gain Buffer. Note that $H_1(f)$ = VOUT/VIN

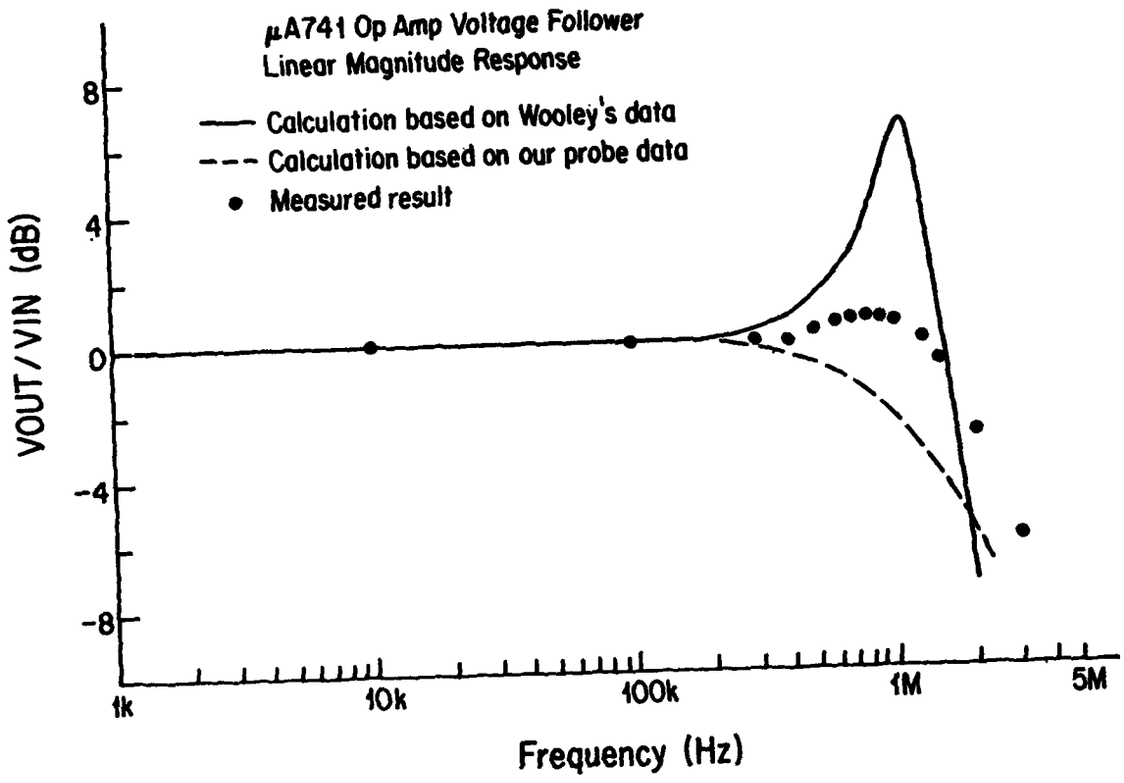

FIGURE 7-6 (a) Measured and Predicted Values for the First-Order Transfer Function VOUT/VIN of the Unity Gain Buffer

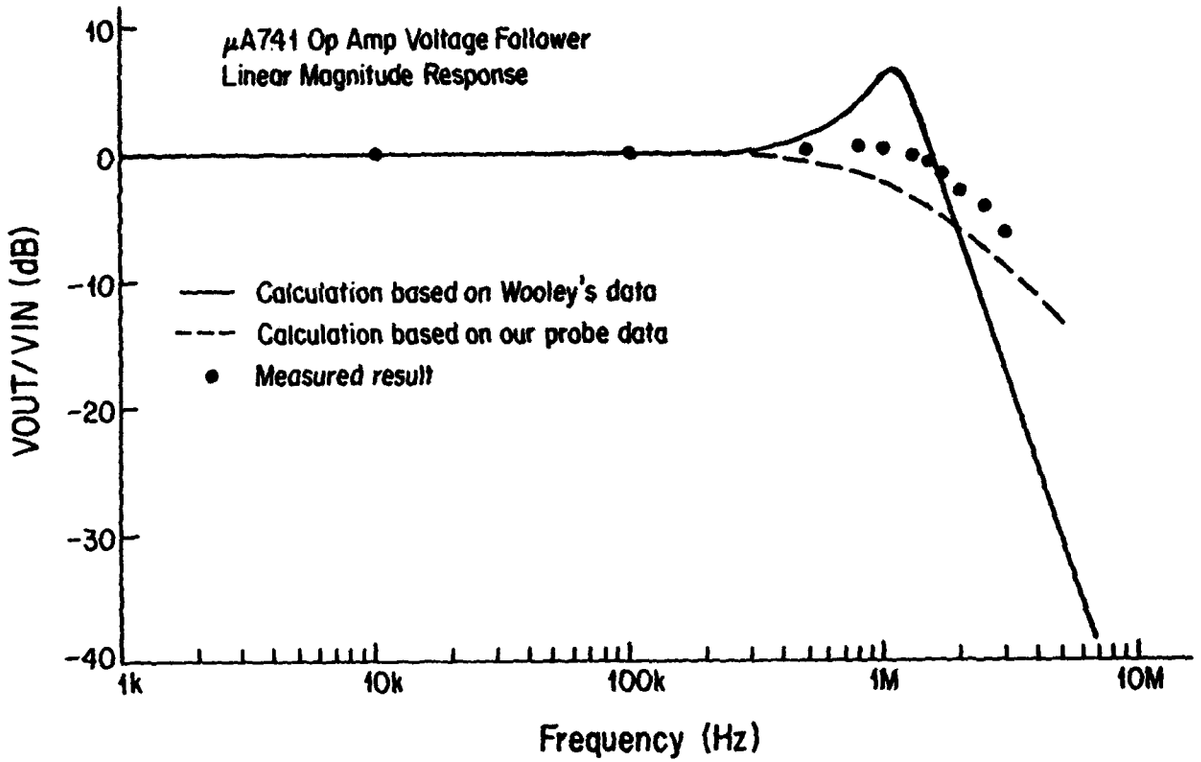

FIGURE 7-6 (b) Measured and Predicted Values for the First-Order Transfer Function VOUT/VIN of the Unity Gain Buffer. (Note Change of the Scale.)

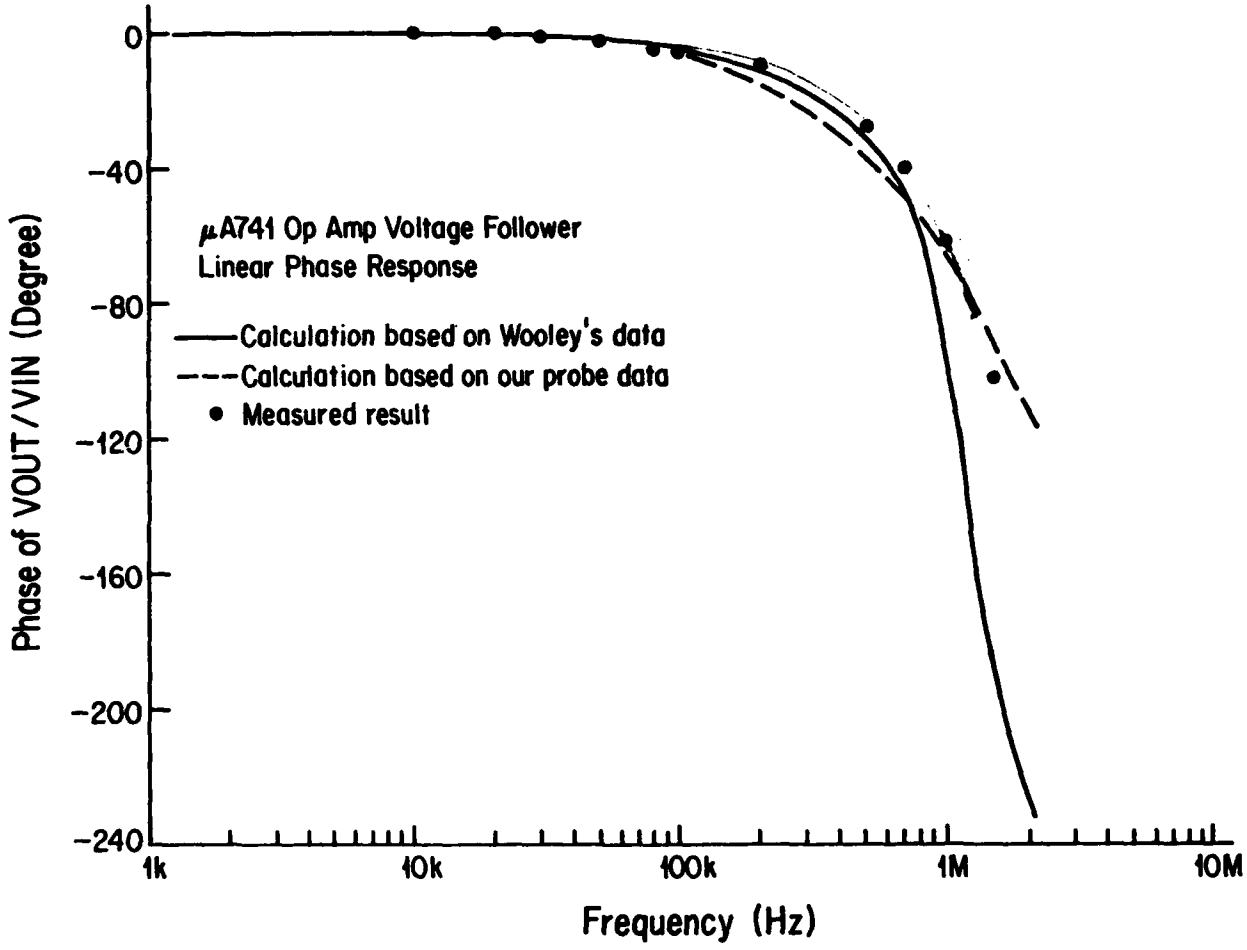

FIGURE 7-7 Measured and Predicted Values for the First-Order Transfer Function VOUT/VIN of the Unity Gain Buffer

Figure 4-11; the SPICE2 coding list is given in Table 4-4. The SPICE2 BJT parameter values are given in Table 4-2. One set of calculated values for VOUT/VIN were obtained using Wooley's BJT parameter values. The other set of calculated values for VOUT/VIN were obtained using the BJT's parameter values determined from probe measurement.

Now let us compare the experimental and calculated values for the op amp magnitude response shown in Figures 7-6(a) and 7-6(b). Expanded scale is used in Figure 7-6(b). Below 100 kHz the measured and calculated values agree exactly. In the frequency range 100 kHz to 3 MHz the measured values and values calculated using our probe data agree within 3 dB. The values calculated using Wooley's data show a peaking effect at 1 MHz and differ from the measured value by 6 dB at 1 MHz. Above 3 MHz the measured and calculated values for the magnitude response decrease rapidly as shown in Figure 7-6(b). Now let us compare the experimental and calculated values for the op amp phase response shown in Figure 7-7. Below 100 kHz the measured and calculated values agree exactly. In the frequency range 100 kHz to 1 MHz the measured values and values calculated using our probe data agree within 10 degrees. The values calculated using Wooley's data differ from the measured value by 40 degrees. Above 1 MHz the measured and calculated values for the phase response are changed rapidly as shown in Figure 7-7. The linear model for the 741 op amp circuit shown in Figure 4-11 has been developed for frequencies up to 3 MHz. However, as will be shown later, RFI predictions at frequencies greater than 3 MHz can be made quite satisfactorily for this circuit. The NCAP calculated results will be given in Section 7.4.

7.3 The Measurement of Second-Order Transfer Functions

There are several second-order transfer functions that could be measured for the IC amplifiers investigated in this dissertation. Both IC amplifiers are basically broadband amplifiers for the frequency range 100 Hz to 1 MHz (or higher). Of particular interest to us is determining how well NCAP can predict how RF signals are demodulated in IC's to produce low frequency response within the frequency region where the IC amplifier is designed to operate. Therefore, the IC amplifiers shown in Figure 4-2 and 4-11 were excited by amplitude modulated RF signals. The RF frequency was varied over the range 50 kHz to 60 MHz; the amplitude modulation index was 0.5, and the AM modulation frequency was either 400 Hz or 1 kHz. At the integrated circuit amplifier output the voltage at the AM modulation frequency was measured using a tuned audio frequency (AF) voltmeter. As will be shown, the voltage measured on the tuned AF voltmeter is directly related to the IC amplifier second-order transfer function $H_2(f_1,-f_2)$.

The measurement system for determining the second-order transfer function $H_2(f_1,-f_2)$ is shown in Figure 7-8. The frequency f_1 is the RF carrier frequency f_{RF}; the frequency f_2 is the lower sideband frequency $f_2 = f_{RF} - f_{AF}$ where the frequency f_{AF} is the modulation frequency. The measurement circuit is simple. The low pass filter is included between the amplifier output and the tuned AF voltmeter in order to reduce RF signals at the AF voltmeter input. This is done because an amplitude modulated RF signal at the tuned AF voltmeter could generate audio frequency responses in the tuned AF voltmeter.

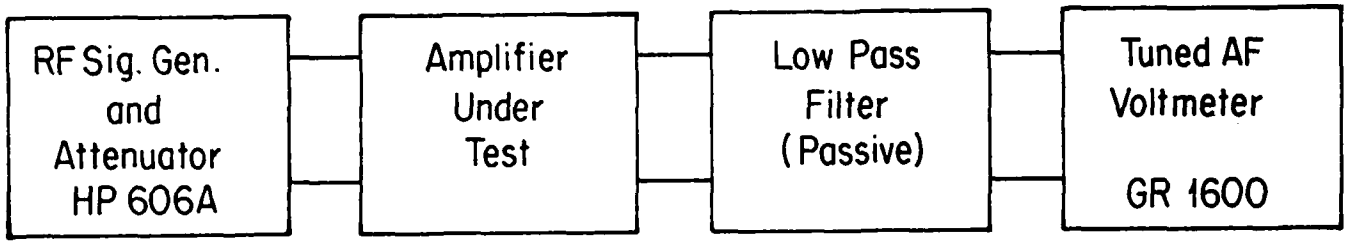

$f_1 = f_{RF}$ $\qquad$ f_{RF} = RF frequency

$f_2 = f_{RF} - f_{AF}$ $\qquad$ f_{AF} = AF frequency

Modulation: 50% AM at f_{AF}

FIGURE 7-8 Experimental System for Measuring Second-Order Transfer Functions $H_2(f_1, -f_2)$

Shown in Figure 7-9 for the CA3026 cascode amplifier and in Figure 7-10 for the 741 op amp voltage follower are the tuned AF voltmeter readings V_M plotted versus the generator available RF power Pgen. (The RF power Pgen is that which will be delivered by the generator to a 50 ohms load resistor.) At low enough values for Pgen a 5 dB increase in the Pgen value causes a 10 dB increase in the V_M value. The analysis to be presented in this section shows that this is to be expected when nonlinear terms of the order greater than two are not important. Thus, the RF generator power must be less than -35 dBm for the CA3026 cascode amplifier and less than -10 dBm for the μA741 op amp voltage follower to avoid higher-order (n > 2) nonlinear effects.

Using data such as those presented in Figures 7-9 and 7-10, the second-order transfer function $H_2(f_1,-f_2)$ can be determined. We begin by expressing the RF generator input signal as

$$V_G = A\ (1 + m\cos 2\pi f_{AF}t)\cos 2\pi f_{RF}t$$

$$= A\cos 2\pi f_{RF}t + \frac{mA}{2}\cos 2\pi(f_{RF}-f_{AF})t + \frac{mA}{2}\cos 2\pi(f_{RF}+f_{AF})t \qquad (7\text{-}1)$$

where A is the amplitude of the modulating signal, m the modulation index, f_{AF} the frequency of the modulation signal, and f_{RF} the RF carrier frequency. Next the frequencies f_1, f_2, and f_3 are defined by the following equations:

$$f_1 = \omega_{RF}/2\pi \qquad (7\text{-}2)$$

$$f_2 = (\omega_{RF}-\omega_{AF})/2\pi \qquad (7\text{-}3)$$

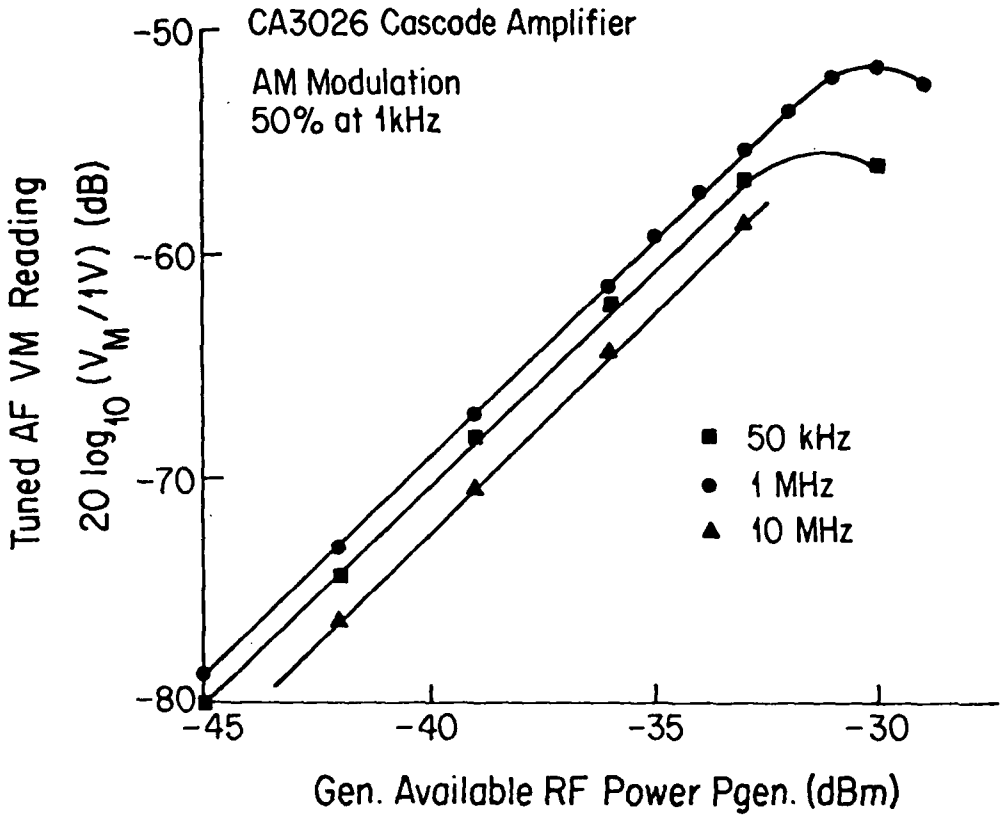

FIGURE 7-9 CA3026 Cascode Amplifier Measured AF Voltage V_M at Wave Analyzer Input Versus Input Power Level

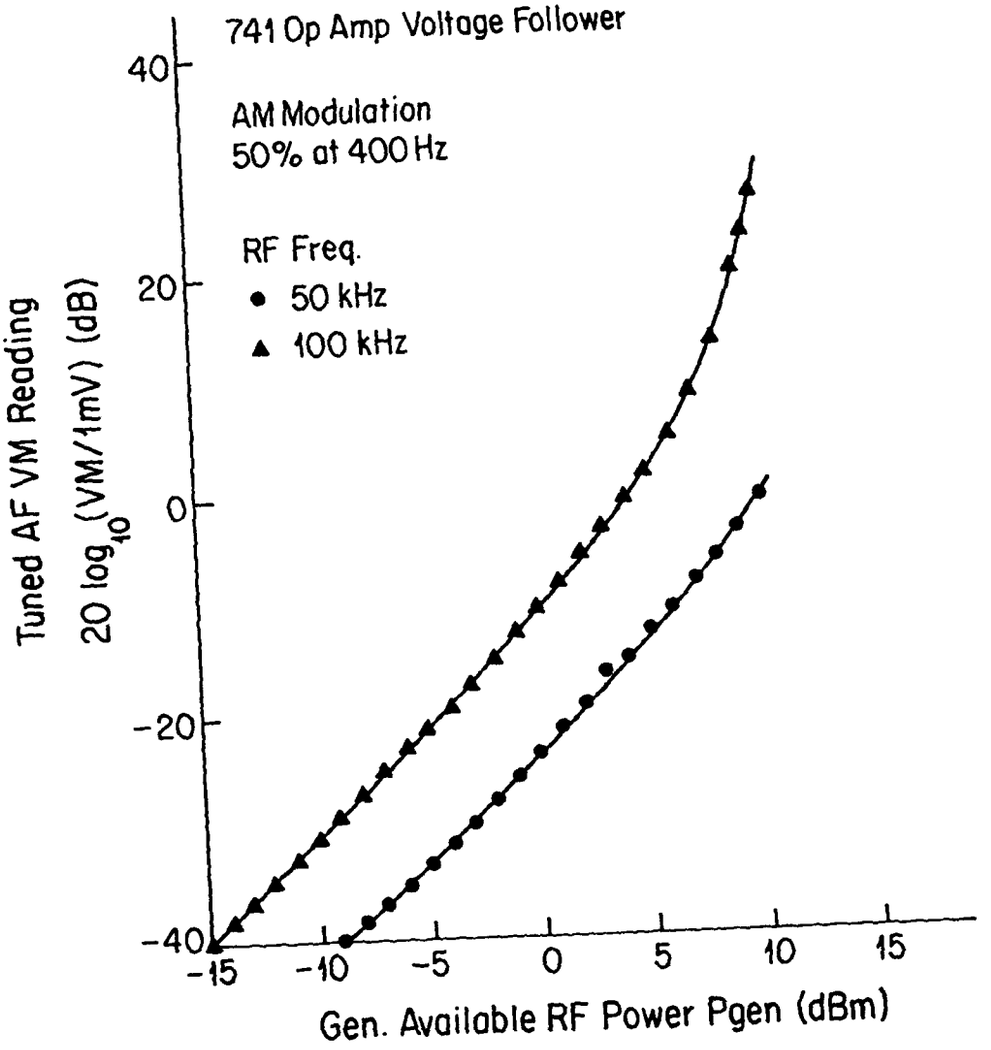

FIGURE 7-10 μA741 Op Amp Voltage Follower Measured AF Voltage V_M at the Wave Analyzer Input Vs Input Power Level Pgen

$$f_3 = (\omega_{RF} + \omega_{AF})/2\pi \tag{7-4}$$

Note that

$$f_{AF} = f_1 - f_2 = f_3 - f_1 \tag{7-5}$$

Then the input signal V_G can be written in the form

$$V_G = x(t) = \frac{1}{2}[A_1 e^{j2\pi f_1 t} + A_2 e^{j2\pi f_2 t} + A_3 e^{j2\pi f_3 t} + A_4 e^{j2\pi f_4 t} + A_5 e^{j2\pi f_5 t} + A_6 e^{j2\pi f_6 t}] \tag{7-6}$$

where $A_4 = A_1^* = A$, $A_5 = A_2^* = mA/2$, $A_6 = A_3^* = mA/2$, $f_4 = -f_1$, $f_5 = -f_2$, and $f_6 = -f_3$. (The symbol * denotes the complex conjugate of an expression.)

The output response y(t) of the amplifier can be written as a combination of transfer functions of different orders:

$$y(t) = \frac{1}{2} \sum_{m=1}^{6} A_m H_1(f_m) \exp(j2\pi f_m t) + \frac{1}{2} \sum_{\substack{i=1 \\ k=1 \\ i \leq k}}^{6} A_i A_k H_2(f_i, f_k) \tag{7-7}$$

+ higher order terms

Of interest to us are the components in the above equation to which the tuned AF voltmeter responds. The AF voltmeter responds only to terms at the modulation frequency f_{AF}. Thus only four components in the above expression contribute to the signal $v_m(t)$ to which the AF voltmeter responds.

The expression for $v_m(t)$ is

$$v_m(t) = \frac{1}{4} A_1 A_5 \; H_2(f_1,f_5) \; \exp[j2\pi(f_1+f_5)t]$$

$$+ \frac{1}{4} A_1 A_6 \; H_2(f_1,f_6) \; \exp[j2\pi(f_1+f_6)t] \qquad (7\text{-}8)$$

$$+ \frac{1}{4} A_2 A_4 \; H_2(f_2,f_4) \; \exp[j2\pi(f_2+f_4)t]$$

$$+ \frac{1}{4} A_3 A_4 \; H_2(f_3,f_4) \; \exp[j2\pi(f_3+f_4)t]$$

Now using the relationships $A_4 = A_1^* = A$, $A_5 = A_2^* = mA/2$, $A_6 = A_3^* = mA/2$, $f_1 + f_5 = f_{AF}$, $f_1 + f_6 = -f_{AF}$, $f_2 + f_4 = -f_{AF}$, and $f_3 + f_4 = f_{AF}$, and assuming the transfer functions $H_2(f_1,f_5)$, $H_2(f_1,f_6)$, $H_2(f_2,f_4)$, and $H_2(f_3,f_4)$ are all equal, Equation (7-8) can be written as

$$v_m(t) = mA^2 \; H_2(f_1,-f_2) \; \cos[2\pi(f_1,-f_2)t] \qquad (7\text{-}9)$$

The AF voltmeter indicates a value for the rms voltage which is denoted as V_M. The AF voltmeter V_M reading can be expressed as

$$V_M = \frac{1}{\sqrt{2}} \; mA^2 \left| H_2(f_1,-f_2) \right| \qquad (7\text{-}10)$$

because the amplitude of the audio frequency signal to which the voltmeter response is $(mA^2)H_2(f_1,-f_2)$ as can be seen by examining Eq. (7-9). The measured rms voltage on the tuned AF voltmeter can also be expressed in dB with respect to a 1 mV reference level as

$$20 \log \left| \frac{V_M}{1mV} \right| = 20 \log \left[\frac{1}{\sqrt{2}} mA^2 \; | H_2(f_1,-f_2)| \right] - 20 \log (10^{-3})$$

$$= 57 + 20 \log m + 40 \log A + 20 \log | H_2(f_1,-f_2)| \qquad (7\text{-}11)$$

Referring to the Thevenin equivalent circuit shown in Figure 7-11 for the H_2 measurement, we can express the average power delivered from the signal generator into a 50 ohms load impedance R_i as

$$Pgen = V_i^2 / R_i = \left(\frac{A}{\sqrt{2}} \frac{R_i}{R_G + R_i} \right)^2 / R_i \qquad (7\text{-}12)$$

where A is amplitude of the unmodulated RF carrier voltage, and V_i is an rms value. Since $R_G = R_i = 50$ ohms, Equation (7-12) becomes

$$Pgen = A^2/400 \qquad (7\text{-}13)$$

Expressing Eq. (7-13) in dBm, the following result is obtained

$$Pgen\ (dBm) = 10 \log \left(\frac{A^2}{400} / 10^{-3} \right) = 4 + 20 \log A \qquad (7\text{-}14)$$

Substituting Eq. (7-14) into Eq. (7-11) with m = 0.5, we obtain

$$20 \log |V_M/1mV| = 2\ Pgen\ (dBm) + 43 + 20 \log |H_2(f_1, -f_2)| \qquad (7\text{-}15)$$

Upon examining Eq. (7-15) we note that a 5 dB change in the Pgen value should cause a 10 dB change in the measured V_M value. As discussed previously only those regions in Figures 7-9 and 7-10 where this rule is obeyed can be used to determine values for the second-order transfer function $H_2(f_1, -f_2)$. Rearranging Eq. (7-15), we obtain the following result for the second-order transfer function

$$20 \log |H_2(f_1, -f_2)| = 20 \log |V_M/1mV| - 43 - 2\ Pgen\ (dBm) \qquad (7\text{-}16)$$

Using Eq. (7-16), values for the second-order transfer function were extracted from the AF voltmeter readings at different RF frequencies. Typical results are given in Table 7-2 for CA3026 cascode amplifier and in Table 7-3 for μA741 op amp voltage follower.

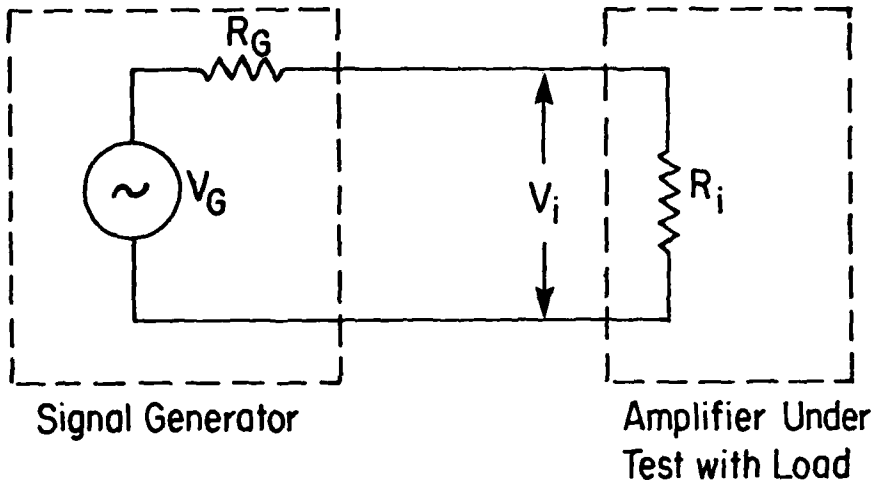

FIGURE 7-11 Schematic of the Thevenin Equivalent Circuit Measuring H_2

TABLE 7-2

SECOND-ORDER TRANSFER FUNCTION MEASUREMENT
OF CA3026 CASCODE AMPLIFIER WITH
Pgen = -35 dBm AND f_{AF} = 1 kHz

RF Freq. f_{RF} (Hz)	AF VM Read. VM (rms mV)	$H_2(f_1,-f_2)$[a] (dB)
50 k	1	27.
100 k	1.1	27.83
200 k	1.15	28.21
500 k	1.17	28.36
1 M	1.15	28.21
2 M	1.05	27.42
5 M	1	27.
7 M	0.92	26.96
10 M	0.82	25.28
15 M	0.66	23.39
20 M	0.51	21.15
30 M	0.32	17.10
50 M	0.16	11.08

[a] The frequency $f_1 = f_{RF}$, and the frequency $f_2 = f_{RF} - f_{AF}$ where f_{AF} = 1 kHz

TABLE 7-3

SECOND-ORDER TRANSFER FUNCTION MEASUREMENT OF
μA741 UNIT GAIN BUFFER WITH Pgen = -10 dBm and f_{AF} = 400 Hz

RF Freq. f_{RF} (Hz)	AF VM Read. VM (rms mV)	$H_2(f_1,-f_2)$[a] (dB)
50 k	0.008	-64.94
60 k	0.011	-62.17
70 k	0.015	-59.48
80 k	0.019	-57.42
90 k	0.0235	-55.58
100 k	0.029	-53.75
150 k	0.064	-46.08
200 k	0.112	-42
250 k	0.18	-37.9
300 k	0.27	-34.37
400 k	0.525	-28.6
500 k	0.92	-23.724
600 k	1.5	-19.48
700 k	2.2	-16.15
800 k	3.0	-13.46
900 k	3.85	-11.29
1 M	4.7	- 9.56
1.5 M	7.1	- 5.97
2 M	6.4	- 6.88
3 M	6.4	- 6.88
4 M	7.0	- 6.2
5 M	7.9	- 6.2
6 M	7.4	- 5.6
7 M	8.2	- 4.72
8 M	9.0	- 3.92
9 M	9.8	- 3.18
10 M	10.5	- 2.58
15 M	13.5	- 0.393
20 M	13.5	- 0.393
30 M	14.5	- 0.23
40 M	13.5	- 0.393
50 M	12.0	- 1.42
60 M	11.0	- 2.17

[a] The frequency $f_1 = f_{RF}$, and the frequency $f_2 = f_{RF} - f_{AF}$ where f_{AF} = 400 Hz.

The experimental values for $H_2(f_1,-f_2)$ given in Table 7-2 for the CA3026 cascode amplifier are plotted versus frequency as shown in Figure 7-12. The experimental values for $H_2(f_1,-f_2)$ given in Table 7-3 for the μA741 unity gain buffer amplifier are plotted versus frequency as shown in Figure 7-13.

7.4 Comparison of Experimental and Calculated Values for the Second-Order Transfer Functions

In this section the experimental values for the second-order transfer function $H_2(f_1,-f_2)$ presented in the previous section will be compared to the values calculated using NCAP. First a comparison of experimental and calculated results for the CA3026 cascode amplifier will be made. Then a similar comparison of experimental and calculated results for the μA741 unity gain voltage follower will be made.

Shown in Figure 7-12 for the CA3026 cascode amplifier are experimental values for $H_2(f_1,-f_2)$ and values calculated using the computer program NCAP. The calculated values were obtained using the NCAP coding circuit diagram for the CA3026 cascode amplifier shown in Figure 7-14. This coding circuit diagram gives the node numbers used in the NCAP program. The associated NCAP input coding list is given in Table 7-4. Upon comparing the calculated and experimental results given in Figure 7-12 it is observed that the calculated values show a little more variation with frequency then do the experimental values. In the frequency range 50 kHz to 10 MHz the experimental values for $H_2(f_1,-f_2)$ are in the range 27 to 29 dB,

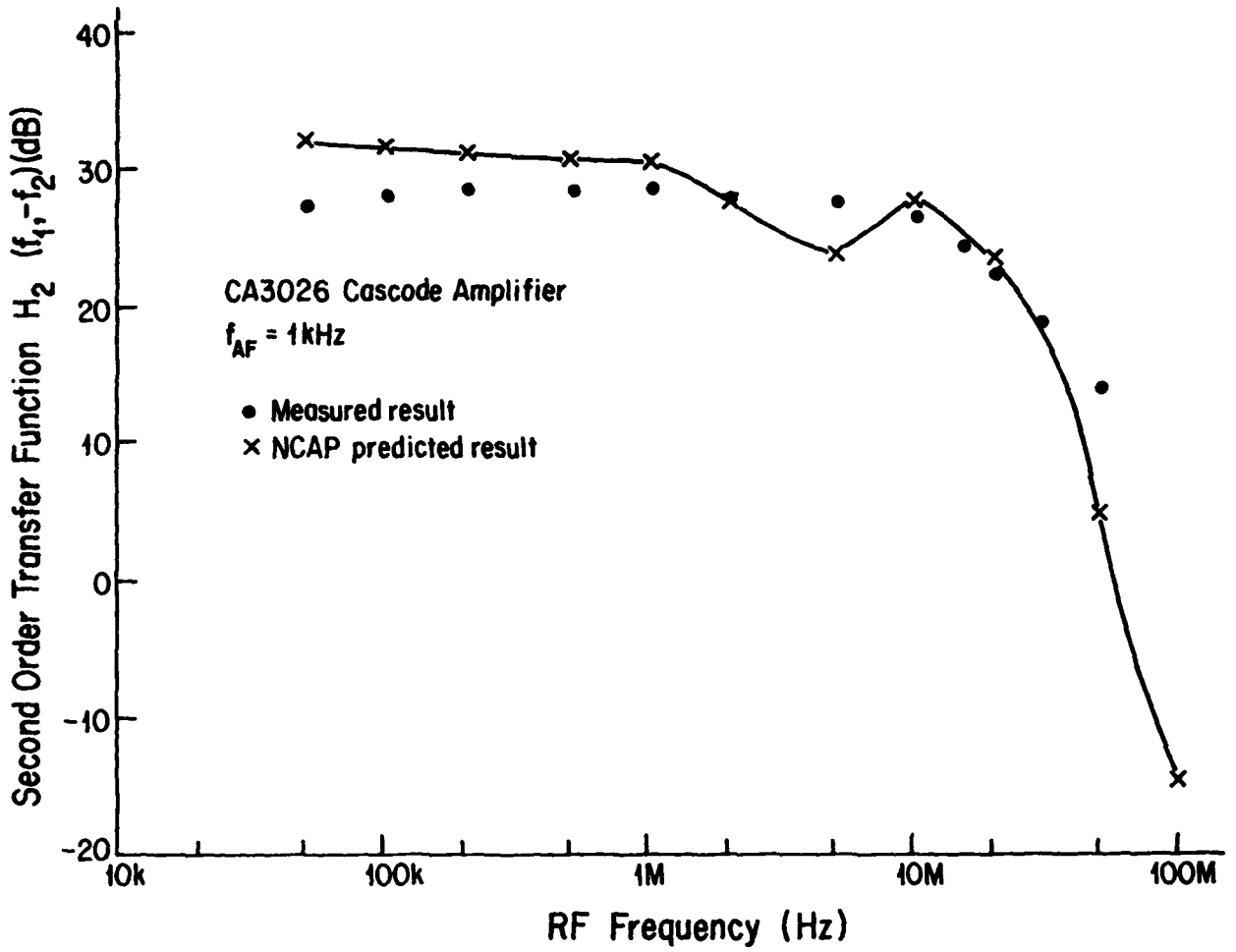

FIGURE 7-12 Calculated and Measured Responses for the Second-Order Transfer Function of the CA3026 Cascode Amplifier

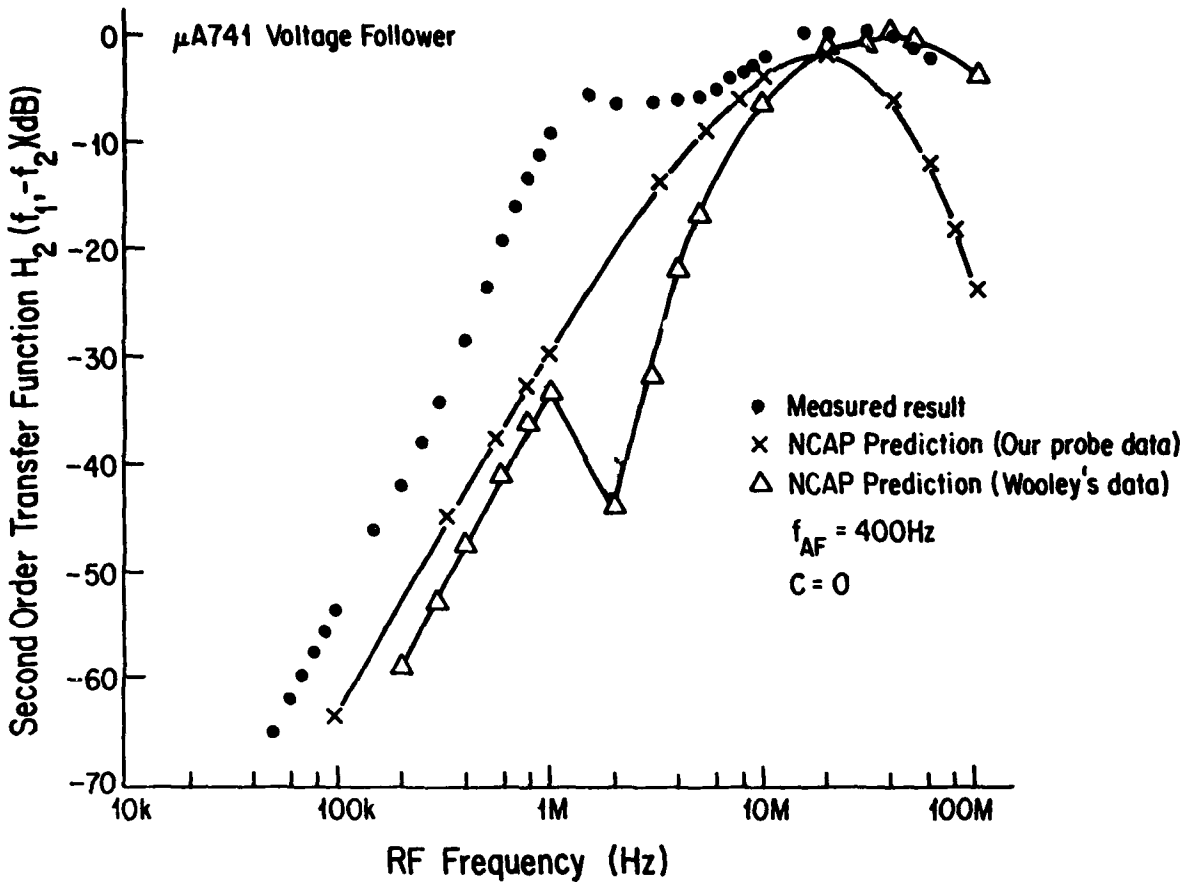

FIGURE 7-13 Calculated and Measured Second-Order Transfer Functions for the μA741 Unity Gain Buffer. Inverting Input is Not Shunted with Capacitances. (C = 0.)

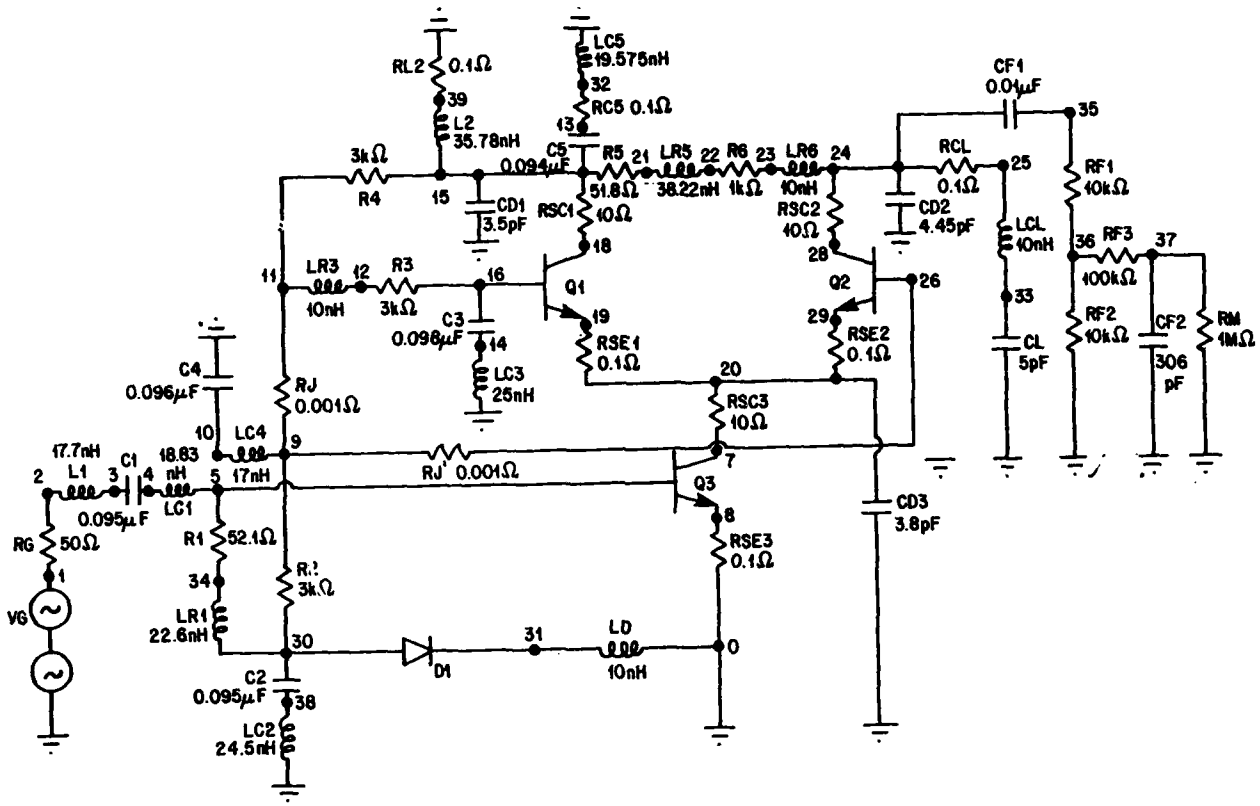

FIGURE 7-14 Cascode Amplifier Circuit Diagram Used to Determine NCAP Input Data

and the calculated values for $H_2(f_1,-f_2)$ are in the range 25 to 32 dB. In this frequency range the difference between the experimental and calculated values for $H_2(f_1,-f_2)$ is 4 to 1 dB. Above 10 MHz the experimental and calculated values for H_2 decrease rapidly with increasing frequency with the calculated values being less than the experimental values. The agreement between the calculated and experimental values for $H_2(f_1,-f_2)$ shown in Figure 7-12 for the CA3026 cascode amplifier may be characterized as being very good qualitatively and quantitatively.

Shown in Figure 7-13 for the unity gain voltage follower are experimental values for $H_2(f_1,-f_2)$ and values calculated using the computer program NCAP. The calculated values were obtained using the NCAP coding circuit diagram for the μA741 unity gain voltage follower shown in Figure 7-15. This coding circuit diagram gives the node numbers used in the NCAP program. The associated NCAP input coding list is given in Table 7-5. The parameter values for the BJT's used in Table 7-5 are those determined using probe measurements. (See Table 4-3). NCAP calculated results were also obtained using Wooley's values for the BJT model parameters which were given previously in Table 4-3. Both sets of calculated results are presented in Figure 7-13. At the RF frequency of 50 kHz both the measured and calculated values for H_2 are less than -50 dB, an extremely small value. As the RF frequency increases from 50 kHz to 1 MHz, both the experimental and calculated values for H_2 increase rapidly. At frequencies near 1 MHz the experimental

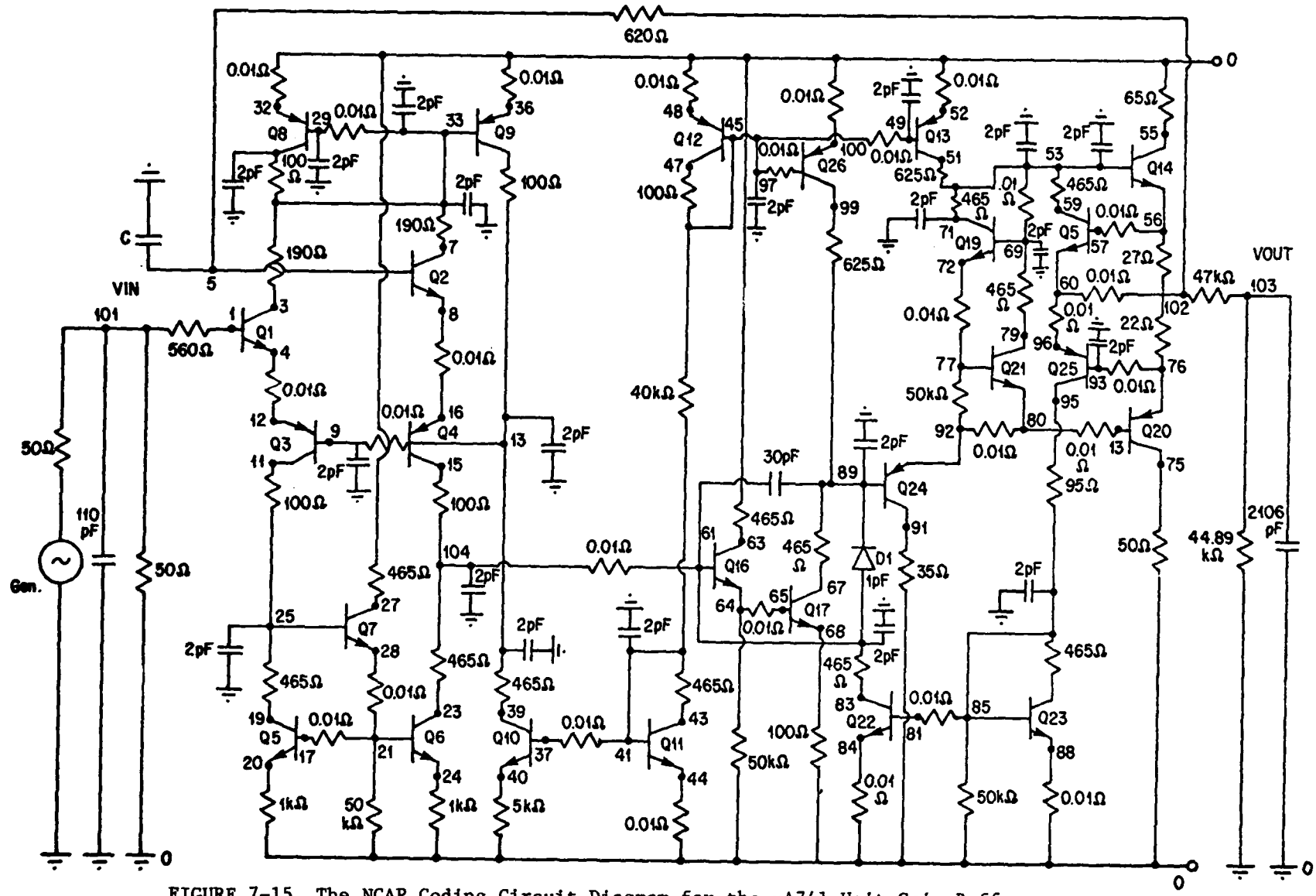

FIGURE 7-15 The NCAP Coding Circuit Diagram for the μA741 Unit Gain Buffer.

values for H_2 begin to reach a plateau in the -10 to 0 dB range. The calculated values for H_2 reaches a plateau region at frequencies in the 5 to 10 MHz range. In the frequency range 10 to 50 MHz the experimental values for H_2 are fairly constant with values near 0 dB. The values calculated for H_2 using Wooley's data are in very good agreement with the experimental values for frequencies in the range 10 to 50 MHz. The values for H_2 calculated using the probe data decrease more rapidly than do the experimental values in this frequency range. Why the values for H_2 calculated using the probe data are lower than those calculated using Wooley's data at frequencies above 10 MHz is not completely understood at this time. One importance difference between the two sets of data is that the collector-substrate capacitance values reported by Wooley (See Table 4-3.) are higher than the 2 pF typical value (not measured) used with the probe data. It appears that a more careful evaluation of the effects of the collector-substrate depletion layer capacitance associated with the collector-substrate junctions used to provide isolation is needed for RF frequencies greater than 10 MHz. Until that evaluation is completed, it is recommended that Wooley's data be used for calculations of nonlinear transfer functions for 741 op amps involving RF frequencies above 10 MHz and that the probe data be used for such calculations involving RF frequencies less than 10 MHz.

The values for H_2 shown in Figure 7-13 for the μA741 unity gain voltage follower are 30 to 40 dB lower than the values for H_2 shown in Figure 7-12 for the CA3026 cascode amplifiers. This result is a circuit effect caused by the large amount of feedback used in the μA741 unity gain voltage follower circuit. (See Figure 4-11.) It is recognized that both AF signals and RF signals were being fed back from the op amp output to the inverting input. It was thought worthwhile to determine the effect of reducing the RF signals feedback by placing a bypass capacitor C from the inverting input to ground. At high enough frequencies the capacitor will tend to behave as an ac short circuit. Two capacitance values selected were 0.2 μF and 200 μF. The new sets of experimental and calculated values for the second-order transfer function H_2 of the μA741 voltage follower are shown in Figure 7-16 (C = 0.2 μF), and in Figure 7-17 (C = 200 μF).

Upon comparing Figures 7-13 and 7-16 it is observed that the 0.2 μF capacitor causes a large increase in the meas .red and calculated values of H_2 at RF frequencies below 100 kHz, and a small increase in the measured and calculated values for H_2 at RF frequencies above 1 MHz. Upon comparing Figures 7-13 and 7-17 it is observed that the 200 μF capacitor causes a large increase (approximately 50 dB) in the measured and calculated values for H_2 over the frequency range 50 kHz to 50 MHz. Clearly the use of a large capacitor such as a 200 μF connected to the op amp inverting input as an RFI supression element would be very counter productive in that it will cause a very large increase in RFI effects in the 741 op amp circuit. This is just one more example of the often unexpected effects that occur in feedback

amplifiers when a circuit change is made.

On comparing the experimental and calculated values for $H_2(f_1,-f_2)$ for the μA741 unity gain voltage follower shown in Figures 7-13, 7-16, and 7-17, it can be said that the computer program NCAP predictions are quite good. Qualitatively the curves of the experimental and calculated values for H_2 versus frequency have essentially the same shape. (Except that there are some unimportant resonance effects which may be related to parasitic elements which are not fully accounted for.) Quantitatively the experimental and calculated values for H_2 versus frequency are in good agreement especially at frequencies above 3 MHz. At frequencies less than 3 MHz the experimental and calculated results decrease rapidly as the frequency decreases and the curves are shifted in frequency from one another by a small amount (of the order of an octive). It is recommended that NCAP nonlinear transfer function calculations be made using our probe results at RF frequencies less than 3 MHz and Wooley's data at RF frequencies above 10 MHz.

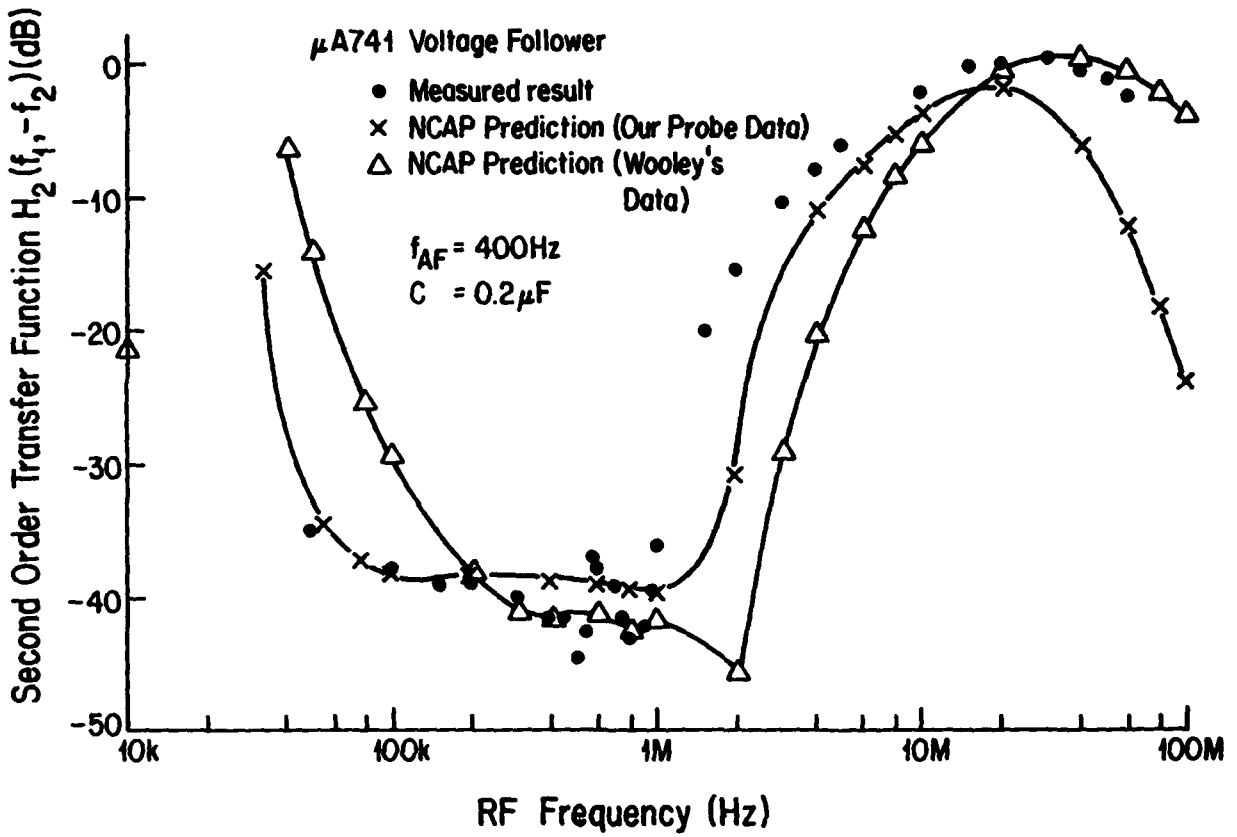

FIGURE 7-16 Calculated and Measured Second-Order Transfer Functions of the μA741 Unity Gain Buffer. Inverting Input is Shunted with a 0.2 μF Capacitor

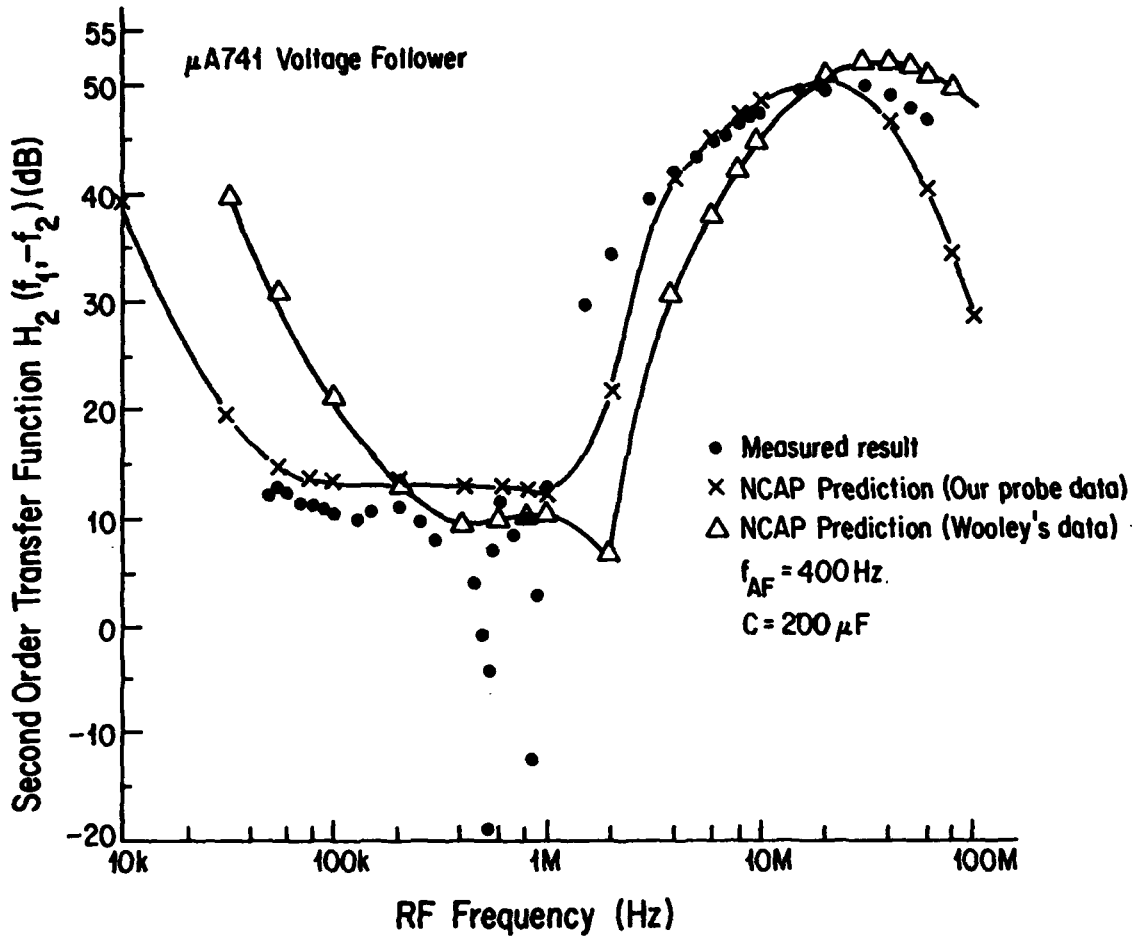

FIGURE 7-17 Calculated and Measured Second-Order Transfer Functions of the μA741 Unity Gain Buffer. Inverting Input is Shunted with a 200 μF Capacitor

TABLE 7-4

CASCODE AMPLIFIER NCAP PROGRAM CODING

```
**PROGRAM AND CASCODE AMPLIFIER USING CA3026 IC
**SUBMITTED OVER SUNY AT BUFFALO
**
*START CIRCUIT
*GENERATOR
NODE 1 0
FR 1 1.0E4 100E6 10 LIN
AMP 1.0 0.0
FR 2 -0.9E3 -9.9999E7 10 LIN
AMP 1.0 0.0
IMP 50.0 0.0
*LINEAR COMPONENTS
R 1 2 0.01
R 5 34 52.1
R 9 30 3.0E3
R 12 16 3.0E3
R 11 15 3.0E3
R 13 32 0.1
R 15 18 10.0
R 21 15 51.8
R 22 23 1.0E3
R 24 25 0.1
R 24 28 10.0
R 19 20 0.1
R 29 20 0.1
R 20 7 10.0
R 8 0 0.1
R 9 26 0.001
R 39 0 0.1
R 9 11 0.001
C 30 38 0.095E-6
C 3 4 0.095E-6
C 10 0 0.096E-6
C 16 14 0.098E-6
C 15 13 0.094E-6
C 15 0 3.5E-12
C 24 0 4.45E-12
C 20 0 3.8E-12
C 33 0 5.0E-12
L 38 0 24.53E-9
L 2 3 17.7E-9
L 4 5 18.83E-9
L 34 30 22.6E-9
L 10 9 17.0E-9
L 31 0 10.0E-9
L 11 12 10.0E-9
L 15 39 35.78E-9
L 32 0 19.575E-9
```

TABLE 7-4 (Continued)

```
L 14 0 25.0E-9
L 21 22 38.22E-9
L 23 24 10.0E-9
L 25 33 10.0E-9
*LINEAR COMPONENTS
R 35 36 1.0E4
R 36 37 1.0E5
R 37 0 1.0E6
C 24 35 0.01E-6
C 37 0 306.0E-12
**DIODE D1
C 30 31 1.0E-9
R 30 31 100
*TRANSISTOR
NODE 16
4.67 0.25 60.0 0.34 1.83E-3 2.0E-3 0.5 110.0 1.99E-12
1.044 5.13E-12 9.86E-9 512.0 14.31E6 0.1E-12 0.1E-12
*TRANSISTOR
NODE 26
4.67 0.25 60.0 0.34 1.83E-3 2.0E-3 0.5 110.0 1.99E-12
1.044 5.13E-12 9.86E-9 554.0 11.7E6 0.1E-12 0.1E-12
*TRANSISTOR
NODE 5
4.67 0.32 60.0 0.34 3.12E-3 2.0E-3 0.5 110.0 1.99E-12
1.044 5.13E-12 9.86E-9 483.0 8.18E6 0.1E-12 0.1E-12
*PRINT SELECT
NODE 37
*END CIRCUIT
*END
```

TABLE 7-5

UNITY GAIN VOLTAGE FOLLOWER NCAP PROGRAM CODING

```
**PROGRAM FOR 741 UNITY GAIN BUFFER
**SUBMITTED OVER SUNY AT BUFFALO
**
*START CIRCUIT
*GENERATOR
NODE 101 0
FR 1 0.1E6 1.0E6 5 LIN
AMP 1.0 0.0
FR 2 -0.996E5 -9.996E5 5 LIN
AMP 1.0 0.0
IMP 0.0 0.0
*LINEAR COMPONENTS
R 101 0 50
R 101 1 560
R 33 3 190
R 12 4 0.01
R 25 11 100
R 25 19 465
R 20 0 1000
R 32 0 0.01
R 33 31 100
R 21 17 0.01
R 27 0 465
R 28 21 0.01
R 21 0 50000
R 33 29 0.01
R 13 9 0.01
R 33 7 190
R 16 8 0.01
R 104 15 100
R 104 23 465
R 24 0 1000
R 36 0 0.01
R 35 13 100
R 39 13 465
R 40 0 5000
R 41 37 0.01
R. 104 61 0.01
R 102 5 620
R 48 0 0.01
R 47 45 100
R 45 41 40000
R 43 41 465
R 44 0 0.01
R 63 0 465
R 64 0 50000
```

TABLE 7-5 (Continued)

```
R 97 45 0.01
R 65 64 0.01
R 89 67 465
R 68 0 100
R 100 0 0.01
R 99 89 625
R 83 61 465
R 84 0 0.01
R 49 45 0.01
R 91 0 35
*LINEAR COMPONENTS
R 52 0 0.01
R 53 51 625
R 71 53 465
R 77 72 0.01
R 92 77 50000
R 85 81 0.01
R 85 0 50000
R 69 53 0.01
R 69 79 465
R 92 80 0.01
R 59 53 465
R 96 60 0.01
R 95 85 95
R 87 85 465
R 88 0 0.01
R 57 56 0.01
R 102 60 0.01
R 93 76 0.01
R 80 73 0.01
R 55 0 65
R 102 56 27
R 102 76 22
R 75 0 50
R 103 102 47000
R 103 0 44890
*LINEAR COMPONENTS
C 33 0 2.0E-12
C 33 0 2.0E-12
C 9 0 2.0E-12
C 13 0 2.0E-12
C 25 0 2.0E-12
C 104 0 2.0E-12
C 29 0 2.0E-12
C 33 0 2.0E-12
C 13 0 2.0E-12
C 41 0 2.0E-12
C 45 0 2.0E-12
C 49 0 2.0E-12
```

TABLE 7-5 (Continued)

```
C 53 0 2.0E-12
C 89 0 2.0E-12
C 53 0 2.0E-12
C 69 0 2.0E-12
C 51 0 2.0E-12
C 85 0 2.0E-12
C 93 0 2.0E-12
C 97 0 2.0E-12
*LINEAR COMPONENTS
C 101 0 110.0E-12
C 89 61 31.0E-12
C 103 0 2106.0E-12
**Q1
*TRANSISTOR
NODE 1
4.34 14.566 20 0.165 7.85E-6 0.5E-3 12.0 400 1.23E-12
1.091 1.23E-12 9.09E-9 830 5.33E6 0.1E-12 0.1E-12
**Q2
*TRANSISTOR
NODE 5
4.34 14.566 20 0.165 7.85E-16 0.5E-3 12.0 400 1.23E-12
1.091 1.23E-12 9.09E-9 830 5.33E6 0.1E-12 0.1E-12
**Q3
*TRANSISTOR
NODE 9
1.48 13.046 100 0.394 7.69E-6 0.1E-3 1.07 35 0.77E-12
1.34 0.23E-12 914E-9 520 0.575E6 0.1E-12 0.1E-12
**Q4
*TRANSISTOR
NODE 13
1.48 12.992 100 0.394 7.69E-6 0.1E-3 1.07 35 0.77E-12
1.34 0.23E-12 914E-9 520 0.575E6 0.1E-12 0.1E-12
**Q5
*TRANSISTOR
NODE 17
3.79 0.53 100 0.247 7.66E-6 0.5E-3 1.21 300 0.61E-12
1.04 0.88E-12 15.07E-9 1040 15.3E6 0.1E-12 0.1E-12
**Q6
*TRANSISTOR
NODE 21
3.79 0.585 100 0.247 7.66E-6 0.5E-3 1.21 300 0.61E-12
1.04 0.88E-12 15.07E-9 1040 15.3E6 0.1E-12 0.1E-12
**Q7
*TRANSISTOR
NODE 25
3.79 28.933 100 0.254 108E-6 0.5E-3 0.84 300 0.61E-12
1.04 0.88E-12 15.07E-9 1040 15.3E6 0.1E-12 0.1E-12
```

TABLE 7-5 (Continued)

```
**Q8
*TRANSISTOR
NODE 29
1.48 0.1 100 0.376 14.9E-6 0.1E-3 1.23 35 0.77E-12
1.34 0.23E-12 914E-9 681 0.575E6 0.1E-12 0.1E-12
**Q9
*TRANSISTOR
NODE 33
1.48 15.453 100 0.376 19.5E-6 0.1E-3 1.17 35 0.77E-12
1.34 0.23E-12 914E-9 681 0.575E6 0.1E-12 0.1E-12
**Q10
*TRANSISTOR
NODE 37
3.79 13.464 100 0.247 19.8E-6 0.5E-3 0.62 300 0.61E-12
1.04 0.88E-12 15.07E-9 1040 15.3E6 0.1E-12 0.1E-12
**Q11
*TRANSISTOR
NODE 41
3.79 0.1 100 0.247 718E-6 0.5E-3 0 300 0.61E-12
1.04 0.88E-12 15.07E-9 1040 15.3E6 0.1E-12 0.1E-12
**Q12
*TRANSISTOR
NODE 45
1.48 0.1 100 0.394 549E-6 0.1E-3 1.37 35 0.77E-12
1.34 0.23E-12 914E-9 681 0.575E6 0.1E-12 0.1E-12
**Q13
*TRANSISTOR
NODE 49
1.72 13.886 130 0.32 45.3E-6 0.2E-3 0.48 0.6 0.38E-12
1.22 0.36E-12 1000E-9 681 1.14E6 0.1E-12 0.1E-12
**Q14
*TRANSISTOR
NODE 53
1.42 14.424 100 0.327 110E-6 2.0E-3 1.26 300 1.0E-12
1.05 3.0E-12 19.1E-9 500 3.96E6 0.1E-12 0.1E-12
**Q15
*TRANSISTOR
NODE 57
3.79 0.573 100 0.247 2.43E-12 0.5E-3 4.33 300 0.61E-12
1.04 0.88E-12 15.07E-9 1040 15.3E6 0.1E-12 0.1E-12
**Q16
*TRANSISTOR
NODE 61
3.79 28.879 100 0.247 11.9E-6 0.5E-3 0.89 300 0.61E-12
1.04 0.88E-12 15.07E-9 1040 15.3E6 0.1E-12 0.1E-12
```

TABLE 7-5 (Continued)

```
**Q17
*TRANSISTOR
NODE 65
3.79 13.504 100 0.247 65.6E-6 0.5E-3 0.65 300 0.61E-12
1.04 0.88E-12 15.07E-9 1040 15.3E6 0.1E-12 0.1E-12
**Q19
*TRANSISTOR
NODE 69
3.79 0.1 100 0.247 11.4E-6 0.5E-3 0.87 300 0.61E-12
1.04 0.88E-12 15.07E-9 1040 15.3E6 0.1E-12 0.1E-12
**Q20
*TRANSISTOR
NODE 73
2.67 14.469 90 0.565 109.0E-6 0.3E-3 1.03 60 1.5E-12
1.13 1.25E-12 360E-9 190 0.147E6 0.1E-12 0.1E-12
**Q21
*TRANSISTOR
NODE 77
3.79 0.54 100 0.247 33.6E-6 0.5E-3 0.73 300 0.1E-12
1.04 0.88E-12 15.07E-9 1040 15.3E6 0.1E-12 0.1E-12
**Q22
*TRANSISTOR
NODE 81
3.79 1.121 100 0.247 4.76E-12 0.5E-3 4.65 300 0.1E-12
1.04 0.88E-12 15.07E-9 1040 15.3E6 0.1E-12 0.1E-12
**Q23
*TRANSISTOR
NODE 85
3.79 0.1 100 0.247 9.7E-17 0.5E-3 1.85 300 0.61E-12
1.04 0.88E-12 15.07E-9 1040 15.3E6 0.1E-12 0.1E-12
**Q24
*TRANSISTOR
NODE 89
3.69 14.092 50 0.252 46.2E-6 0.2E-3 7.4 80 5.08E-12
1.45 1.75E-12 280E-9 195 13.1E6 0.1E-12 0.1E-12
**Q25
*TRANSISTOR
NODE 93
1.48 14.997 100 0.368 5.04E-9 0.17E-3 1.66 35 0.77E-12
1.34 0.23E-12 1307E-9 681 0.575E6 0.1E-12 0.1E-12
**Q26
*TRANSISTOR
NODE 97
1.72 15.37 130 0.32 66.3E-6 0.2E-3 0.87 0.6 1.14E-12
1.22 0.36E-12 1000E-9 681 1.14E6 0.1E-12 0.1E-12
*PRINT SELECT
NODE 103 101
*END CIRCUIT
*END
```

CHAPTER EIGHT

DISCUSSION AND CONCLUSION

The main objective of this dissertation has been to determine how well the nonlinear circuit analysis program NCAP can predict RFI effects in bipolar integrated circuits. Specifically the computer program NCAP has been used to calculate how RF signals are demodulated in broadband IC amplifiers to produce undesired low frequency responses. The NCAP calculated results and experimental results have been compared for two broadband integrated circuit amplifiers. One circuit is a broadband cascode circuit which uses a CA3026 dual differential pair IC. This IC was selected because the differential pair is the basic building block in linear bipolar integrated circuits. The other circuit selected is a unity gain voltage follower circuit which uses a 741 operational amplifier. This IC was selected because the 741 op amp is the most widely used IC.

An important part of this investigation was the determination of the NCAP parameter values for the bipolar transistors in the CA3026 differential pair and the 741 operational amplifier. The NCAP parameter values for the BJT's in the CA3026 are given in Table 4-1 and for the BJT's in the μA741 op amp are given in Table 4-3. Many months of effort were required to determine these parameter values. Probe techniques were used to make measurements from which the NCAP parameter values were determined. Also a combination of analysis techniques were used to convert manufacturer's data (when available) and other investigator's data (especially Wooley[29]) into the format re-

quired by NCAP. It is anticipated that almost all EMC engineers wanting to use NCAP to predict RFI effect in bipolar linear IC's can not take the time required to determine their own NCAP parameter values. Therefore, it is suggested that the NCAP BJT parameter values given in Tables 4-1 and 4-3 be used. It is recommended that the IC schematic provided by the manufacturer be examined to determine which transistors are NPN's and which are PNP's. Also by studying the IC circuit diagram the substrate PNP transistors can be identified. The remaining PNP transistors are usually lateral PNP's. The input stage and intermediate stage transistors are usually small transistors. The output stage transistors are usually large transistors. Dual emitter transistors and dual collector transistors are treated as two transistors. It will usually be necessary to determine the values for the dc collector currents and dc collector-base voltages for each BJT in the integrated circuit. To determine appropriate values for the BJT dc currents and voltages it is recommended that an electronic circuit analysis program such as SPICE2 be used to perform a dc operating point calculation. The Ebers-Moll model parameter values given in Table 4-2 can be used for the dc operating points analysis.

When the NCAP parameter values for the BJT's in an integrated circuit are known, the computer program NCAP can be used to calculate nonlinear transfer functions which are directly related to RFI effects. The program NCAP uses a quasi-linear distortion analysis algorithm based upon a perturbation method. This algorithm is summarized below:

(1) Calculate the dc operating point and expand each nonlinear function by a Taylor series about the quiesent point.

(2) Calculate the linear voltages of the circuit elements by neglecting all nonlinearities of degree $n \geq 2$.

(3) Determine the voltages associated with each second-order distortion current source.

(4) Calculate the second-order distortion products by analyzing the linear circuit with the appropriate distortion current sources at the prescribed frequency.

(5) Determine the voltages associated with each third-order distortion current source.

(6) Calculate the third-order distortion products by analyzing the linear circuit with the appropriate distortion current sources at the prescribed frequency.

(7) Repeat steps 5 and 6 for calculating higher-order distortion products.

Values for the second-order transfer function $H_2(f_1,-f_2)$ were calculated for the CA3026 cascode amplifier and 741 op amp voltage follower circuits. The second-order transfer function $H_2(f_1,-f_2)$ is directly related to the low frequency voltage produced at the IC amplifier output by an amplitude modulated RF signal at the IC amplifier input. (See Eq. 7-15.) A comparison of calculated and experimental values for $H_2(f_1,-f_2)$ was presented in Chapter Seven. This comparison demonstrated that the computer program NCAP can be used quite successfully to predict how amplitude modulated RF signals are demodulated in broadband IC amplifiers.

There are areas where additional efforts are needed. One area involves the determination of accurate linear models for all the components (including resistors, capacitors, inductors, and leads) in the IC amplifier circuit. The accuracy of the linear analysis results determine the accuracy of the second-order analysis results, which in turn determines the accuracy of the third-order analysis results, etc. It is known that parasitic elements play a very important role at frequencies above 1 MHz. New techniques for determining values for parasitic elements are needed. One method that appears promising is the adjoint network gradient optimization technique.[45,52] This method has been applied to the CA3026 cascode amplifier and the results obtained to date look encouraging. It appears possible that this linear optimization scheme could be incorporated directly into NCAP, but first it should be investigated more completely. This is a task worthy of additional effort (by someone else).

There is another area where additional research activity is needed. If the bipolar integrated circuits are analysed at very high frequencies, the NCAP nonlinear T-model may not be appropriate. At frequencies greater than f_T (the frequency at which the common emitter short circuit current gain is 1) the four lumped parasitic elements R_b, R_c, C_1 and C_2 used in the NCAP BJT model may be insufficient to characterize the BJT. For integrated circuit BJT's additional parasitic elements may have to be included. A model illustrating some additional parasitic elements is shown in Figure 8-1. The additional parasitic elements shown in this model account for some of the distributed

R-C transmission line effects associated with the region between the base contact and the active region of the base-emitter junction and with the region between the collector and substrate.[36] It is suggested that models similar to the one shown in Figure 8-1 be developed for RFI analyses for IC amplifiers at RF frequencies greater than 10 MHz. At RF frequencies greater than f_T there is another factor that also should be considered. The nonlinear T-model is an extension of the linear T-model which in turn can be developed from the Ebers-Moll model. The Ebers-Moll model is one form of the charge-control model. The charge-control model is based upon the quasi-static approximation. The quasi-static approximation assumes that the distribution of minority carrier stored in the neutral base region is identical to the dc distribution. At frequencies greater than f_T this basic assumption is probably violated. Therefore, it is reasonable to question the validity of the nonlinear T-model at frequencies greater than f_T. An investigation to determine how well the nonlinear T-model predicts RFI effects in BJT circuits (discrete or integrated) appears to be very much needed. This is a task other researchers might pursue. When improved techniques for determining parasitic elements in passive components and in bipolar junction transistors are developed and questions concerning the validity of the nonlinear T-model at frequencies greater than f_T have been resolved, additional efforts to determine how well the computer program NCAP can predict RFI effects in bipolar linear circuits for RF frequencies in the range 50 to 1000 MHz should be pursued.

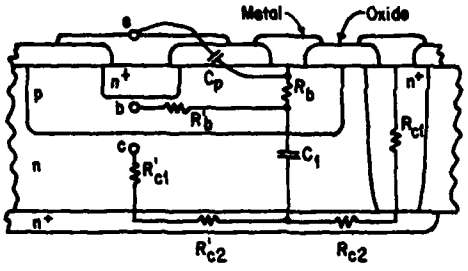

(a)

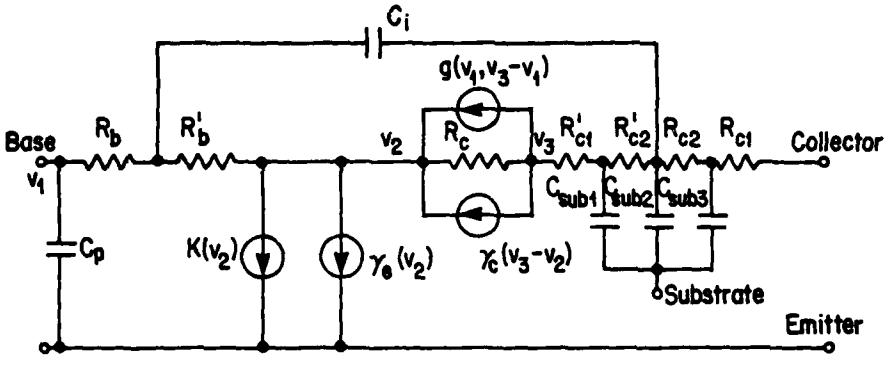

(b)

FIGURE 8-1 Schematic Cross Section of a Transistor with an Equivalent Circuit of Parasitic Elements (a), and the Suggested Nonlinear T-Model (b)

APPENDIX I

STANDARD IEEE NOTATION

The h, y, and z two-port parameters are identified with a double-subscript notation. The first subscript denotes the function of the parameter:

i	Input driving-point parameter
o	Output driving-point parameter
f	Forward transfer parameter
r	Reverse transfer parameter

When these parameters are used to describe BJT properties the second subscript denotes the configuration:

e	Common-emitter
b	Common-base
c	Common-collector

Currents and voltages at the terminals of transistors are designated in the following manner: Subscripts are used to indicate the terminal at which a current flows (reference direction is in the terminal) or the terminal pair at which a voltage appears (reference direction is defined by the order of the subscripts; the plus sign is associated with the terminal identified by the first subscript). Variables of four types are defined:

DC or operating-point variables--upper-case symbols with upper-case subscripts

Total instantaneous variables--lower-case symbols with upper-case subscripts

Incremental instantaneous variables--lower-case symbols with lower-case subscripts

Complex amplitudes of incremental components--upper-case symbols with lower-case subscripts

A voltage v or V next to a node is assumed to be measured with respect to datum, i.e. it is a node-to-datum voltage. Unless otherwise marked, the reference direction is such that the node is positive with respect to ground when v or V is positive.

APPENDIX II

PROBE PREPARATION

Sharp tungsten probe tips are prepared by an etching process. To retain a uniform cross-section for a tungsten tip, a tungsten wire is etched as rapidly as possible. The usual etching reagents such as alkaline potassium ferricyanide or ammonium persulphate act rather slowly and tend to develop a crystalline surface on the wire. Therefore, an electrolytic etching process is used to obtain a sharp tungsten tip.

The electrolytic etching process is illustrated in Figure II-1. As shown in this figure, a tungsten wire with the diameter of 10 mil is made the anode and a tungsten bar the cathode. A saturated solution of potassium hydroxide is used as the electrolyte between the anode and the cathode. This solution is contained in a beaker. Suitable dc current levels range between 100 mA to 400 mA with a corresponding dc voltages range from 10 V to 20 V are employed for the electrolytic etching process. A clock motor providing a mechanical dipping action is used to generate a sharp tip for the tungsten wire. The above electrolytic etching process will take about one minute to provide a satisfactory sharp tip, e.g. tip dimension of 0.1 mil^2 can be readily prepared in 1 to 2 minutes. The actual process time varies with the current level and the probe dipping frequency.

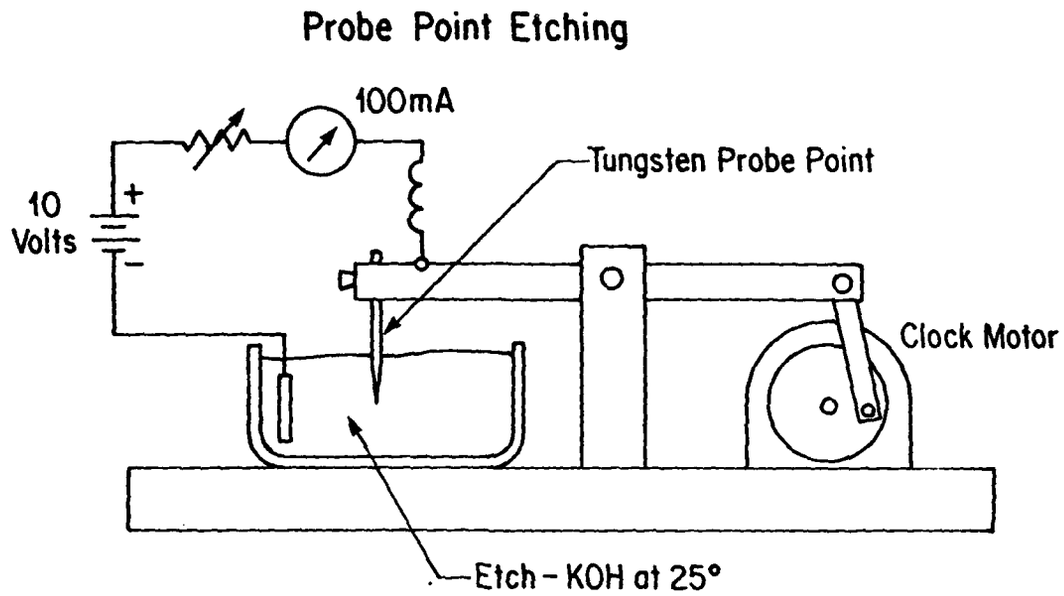

FIGURE II-1 Sharp Tungsten Tip Preparation Diagram

APPENDIX III

μA741 BJT's DC and Junction Capacitance Characteristics

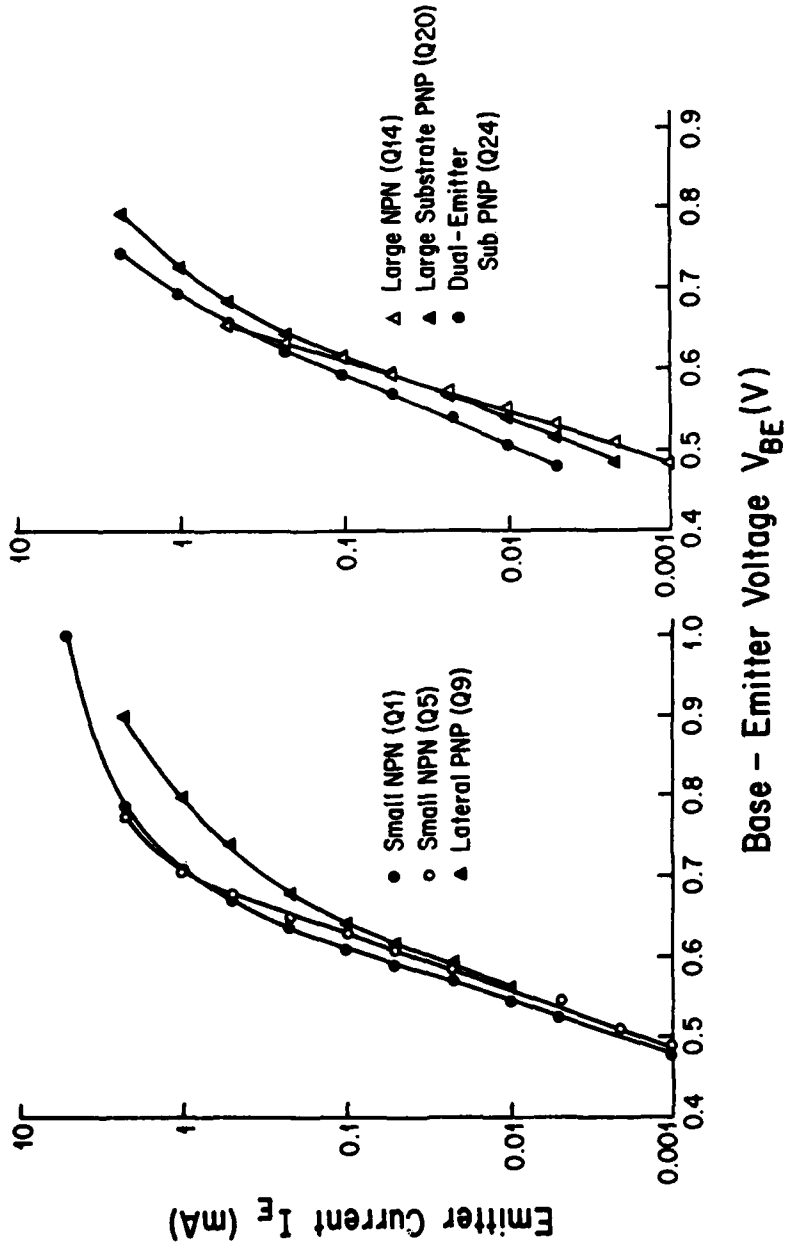

FIGURE III-1 Typical I_E Vs V_{BE} Characteristics of BJT's in the μA741 Operational Amplifier

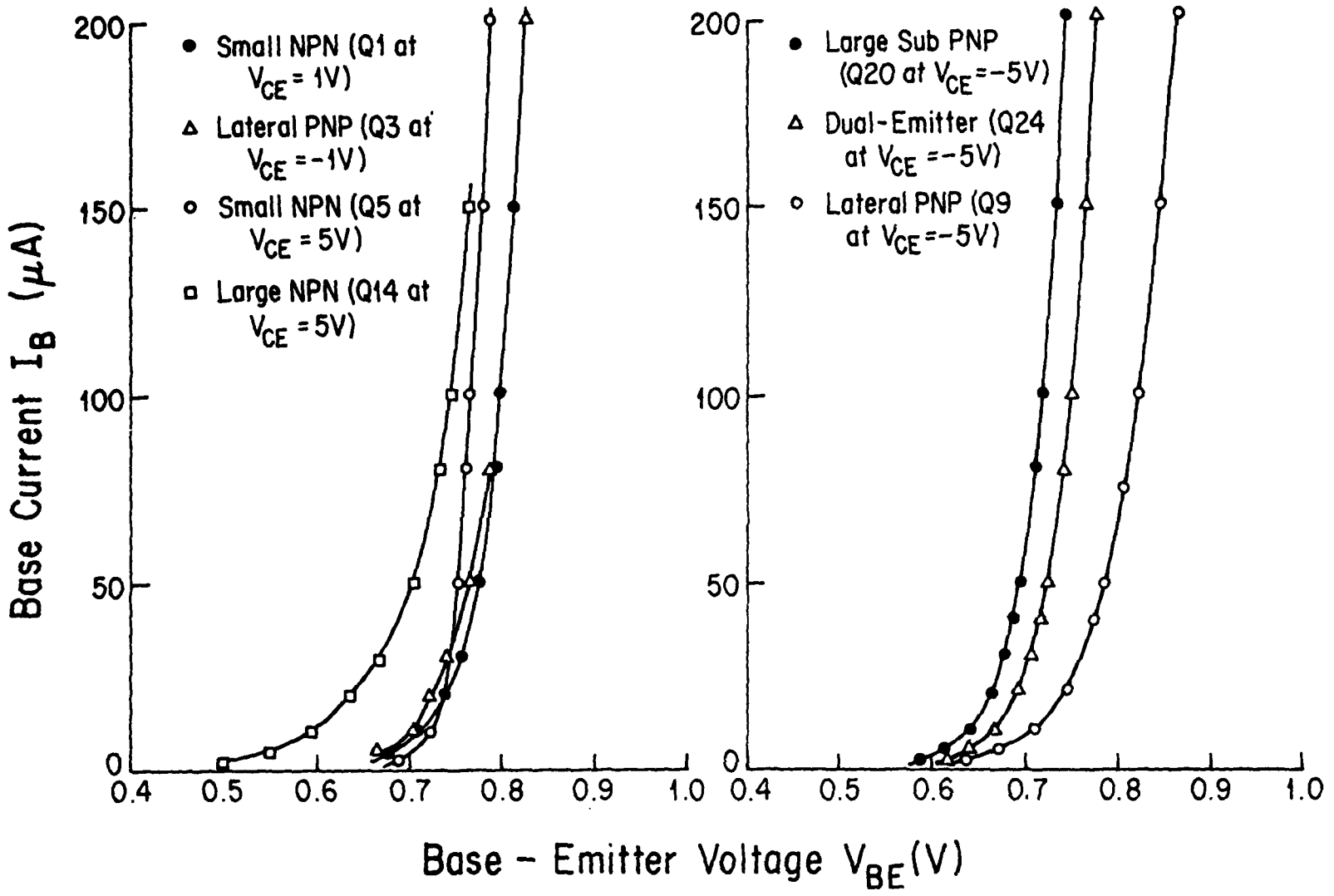

FIGURE III-2 Typical Input Characteristics of BJT's in the μA741 Operational Amplifier

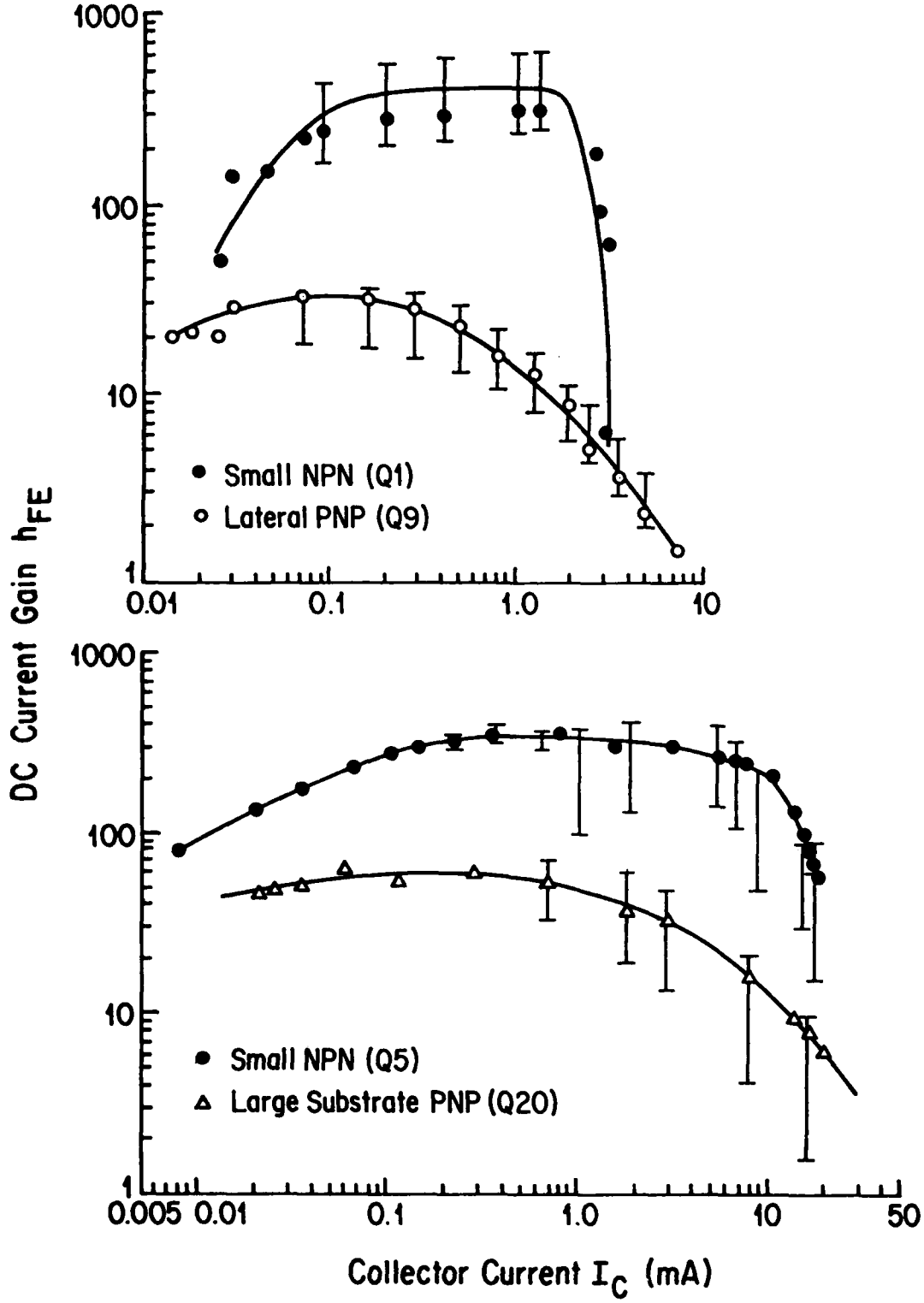

FIGURE III-3 Typical DC Current Gain h_{FE} vs Collector Current I_C for BJT's in μA741 Operational Amplifier

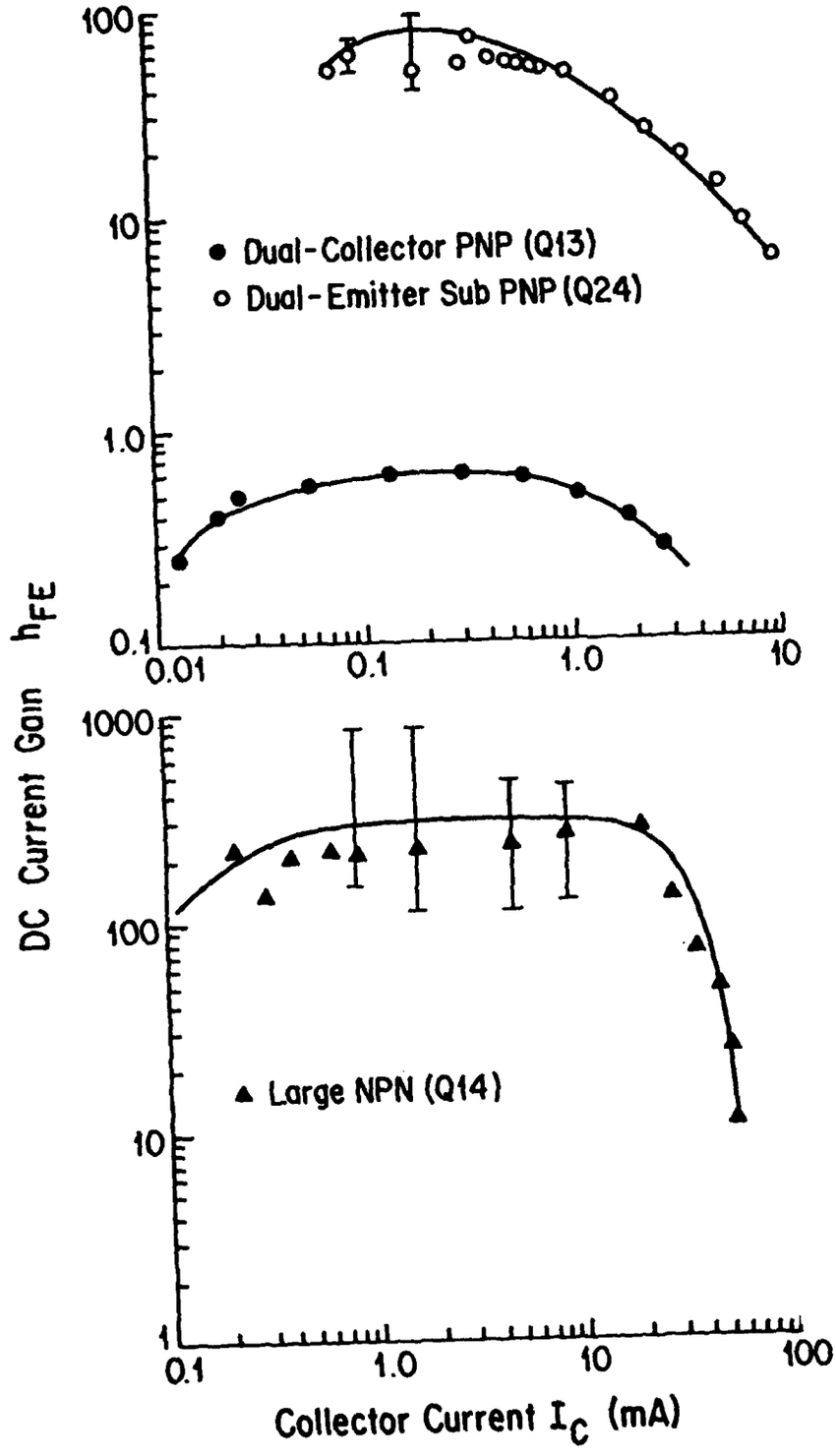

FIGURE III-3. Typical DC Current Gain h_{FE} vs Collector Current I_C Plot for BJT's in μA741 Op Amp. (Continued)

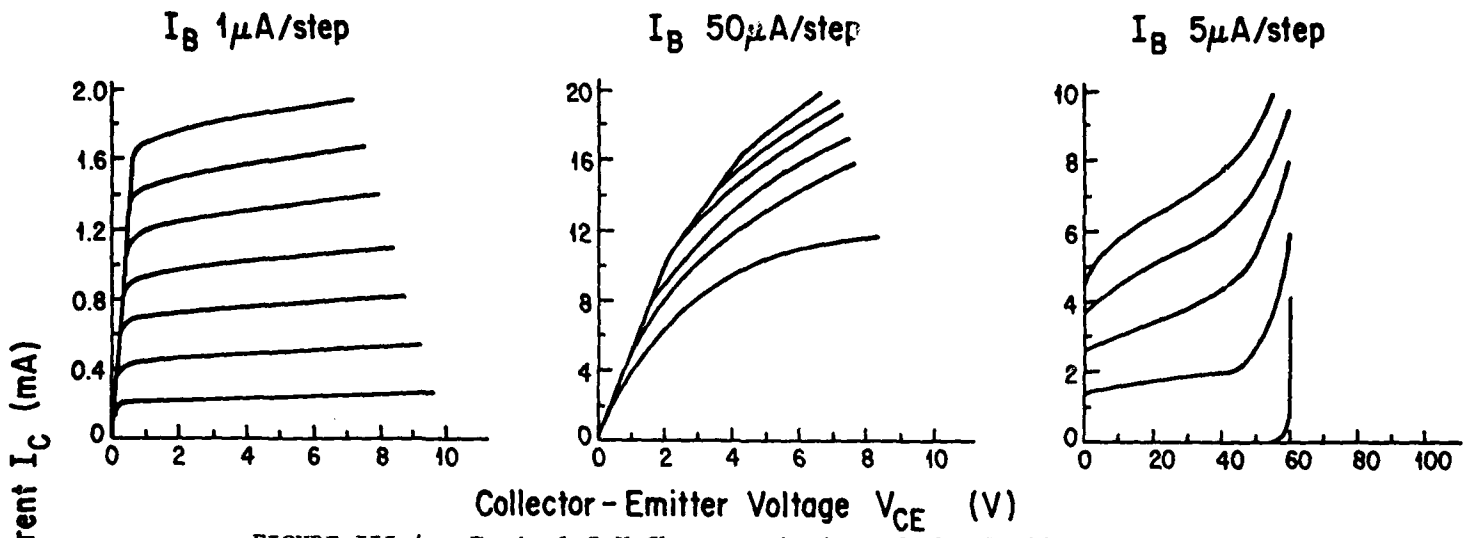

FIGURE III-4. Typical I-V Characteristics of the Small NPN Transistor (Data Obtained from Q5 Measurements).

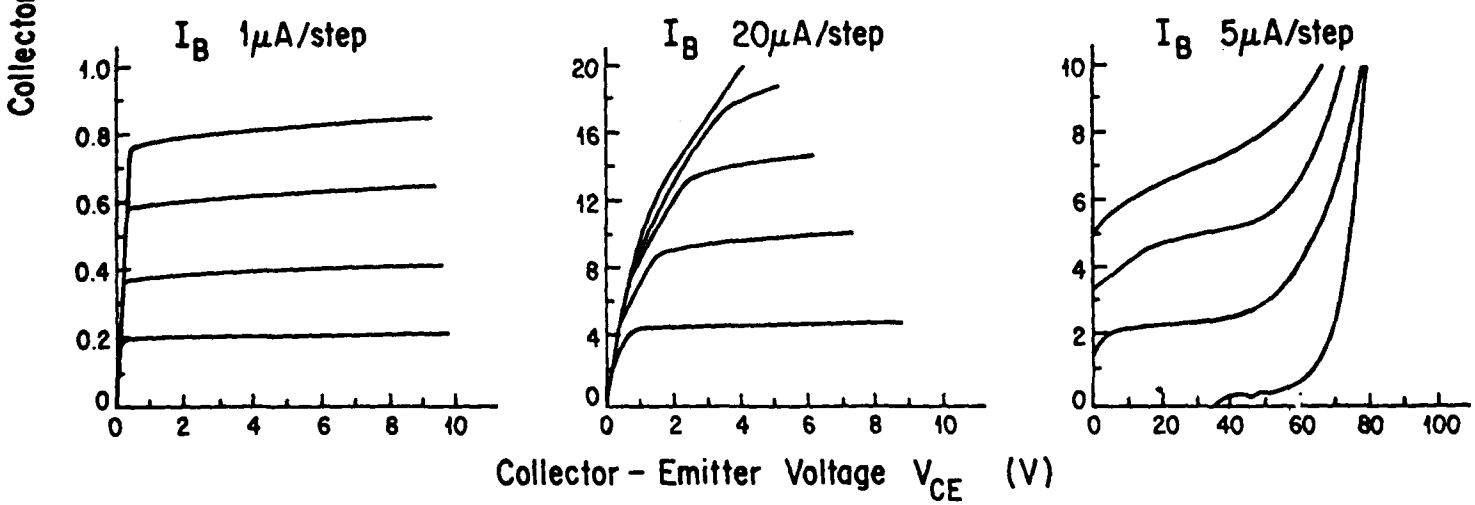

FIGURE III-5. Typical I-V Characteristics of the Large NPN Transistor (Data Obtained from Q14 Measurements).

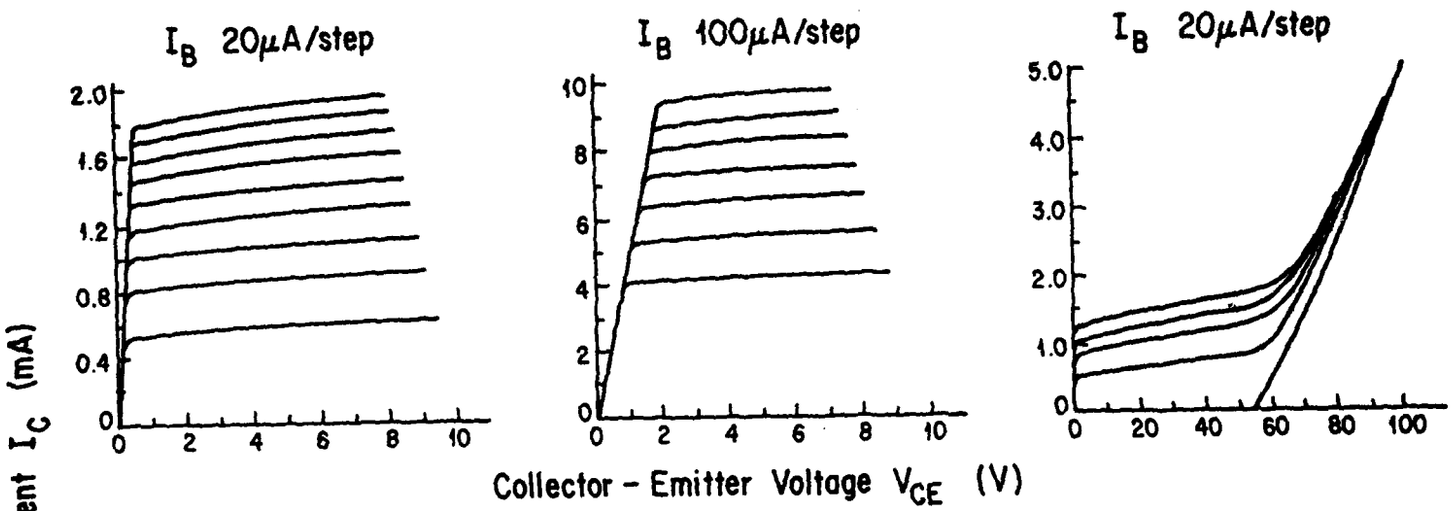

FIGURE III-6. Typical I-V Characteristics of the Lateral PNP Transistor (Data Obtained from Q3 Measurements).

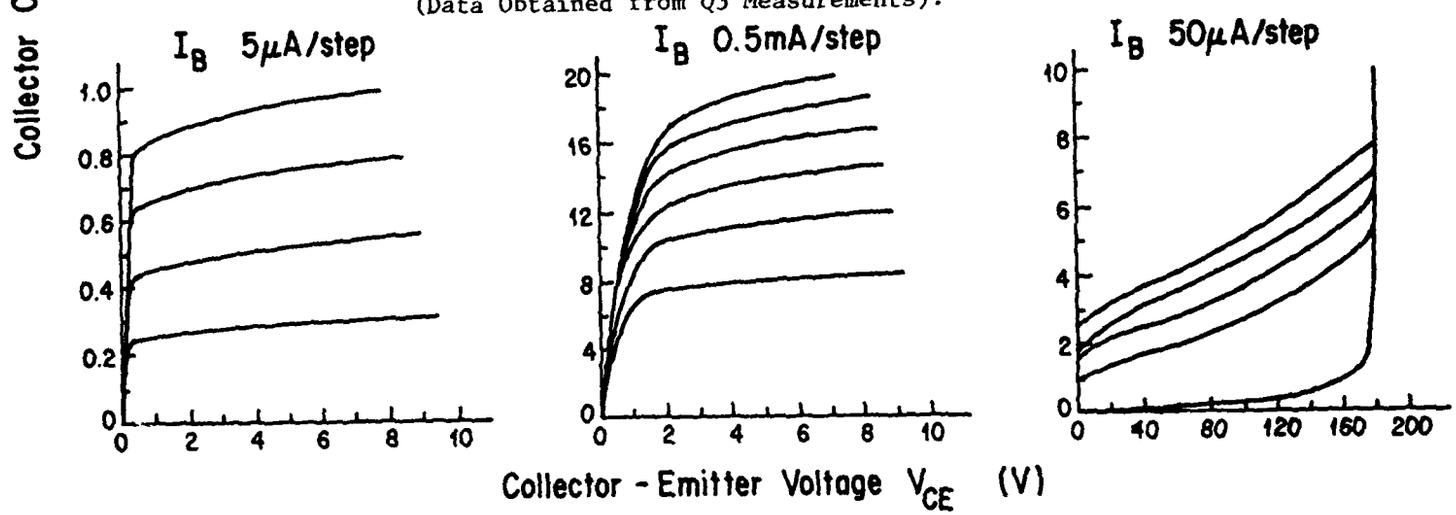

FIGURE III-7. Typical I-V Characteristics of the Large Substrate PNP Transistor (Data Obtained from Q20 Measurements).

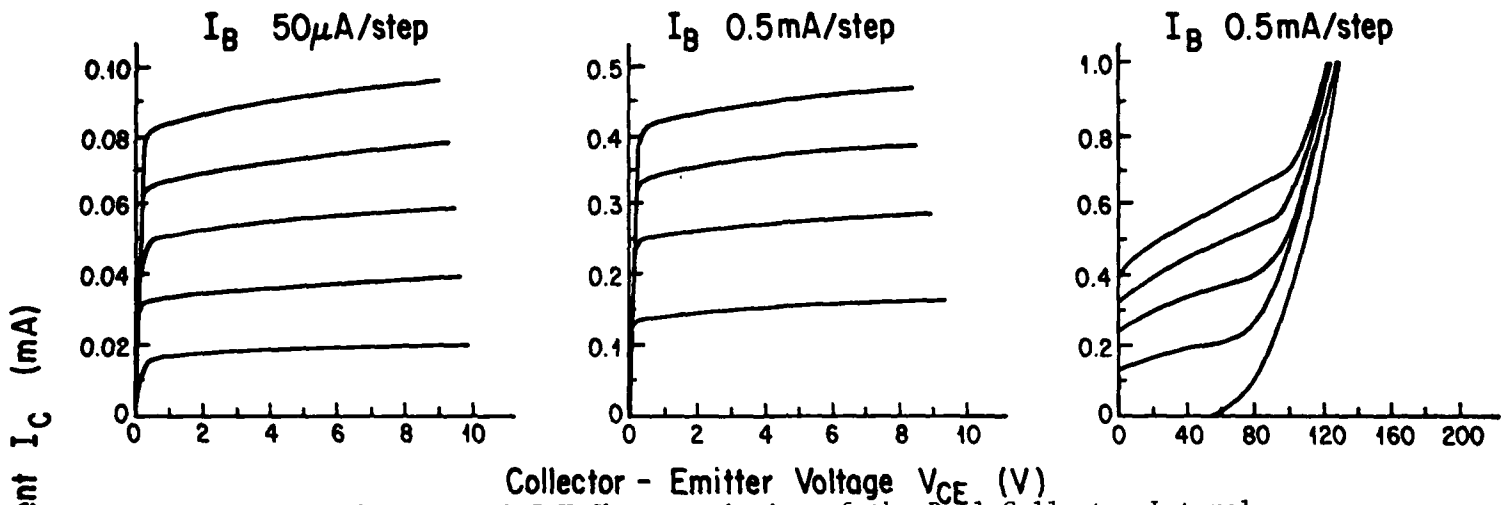

FIGURE III-8. Typical I-V Characteristics of the Dual-Collector Lateral PNP Transistor (Data Obtained from Q13 Measurements).

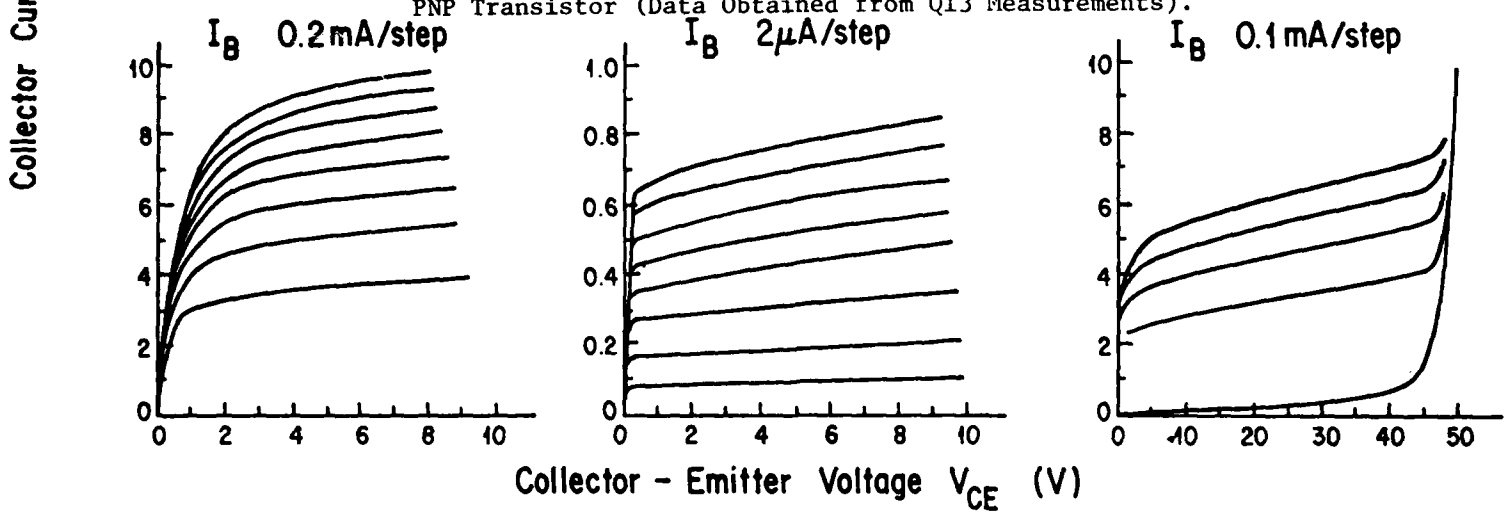

FIGURE III-9. Typical I-V Characteristics of the Dual-Emitter Substrate PNP Transistor (Data Obtained from Q24 Measurements).

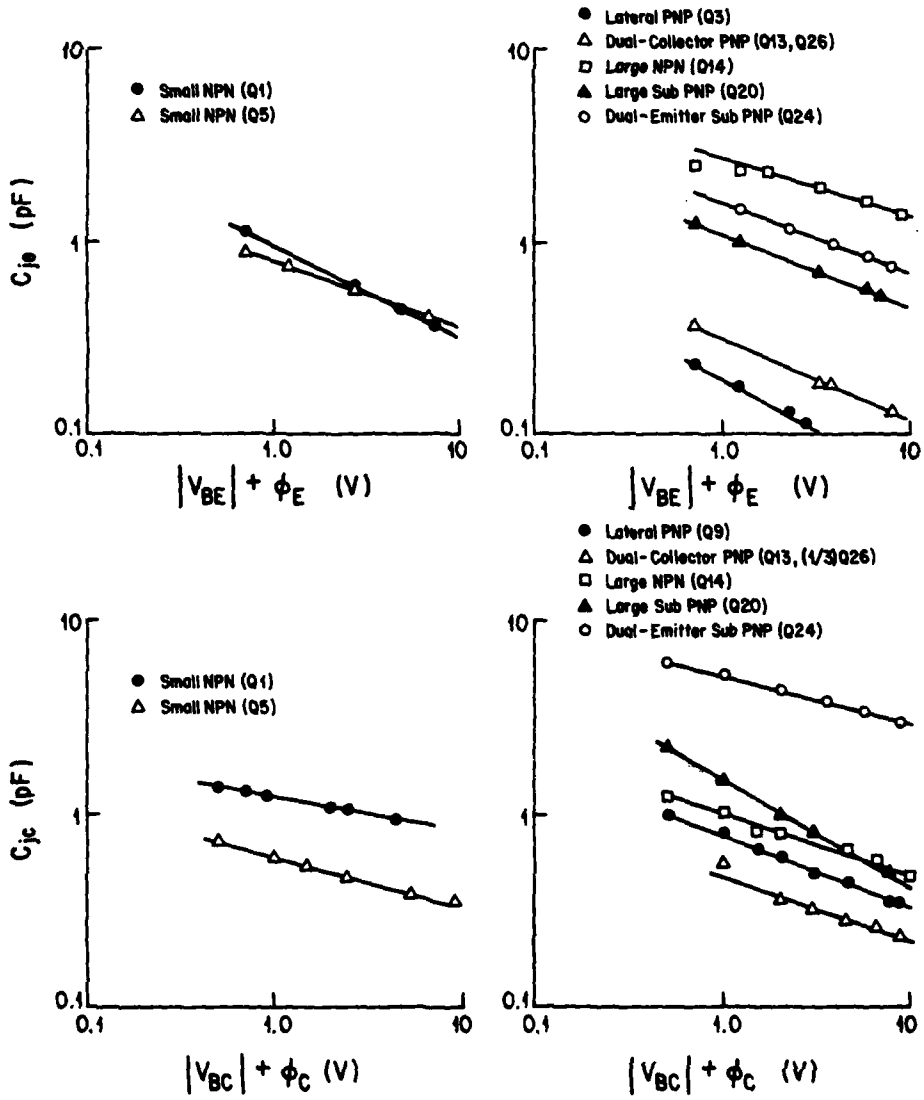

FIGURE III-10 Typical Junction Capacitance vs Junction Voltage Plot of the BJT's in the μA741 Op Amp

APPENDIX IV

FORTRAN PROGRAM FOR CALCULATING FIRST AND SECOND-ORDER TRANSFER FUNCTIONS FOR THE TUNED RF AMPLIFIER SHOWN IN FIGURE 6-2

```
      PROGRAM NCAP(INPUT,OUTPUT,TAPE7,TAPE5=INPUT,TAPE6=OUTPUT)
C     ------------------------------------------------------------------
C     THIS PROGRAM SIMULATES RADC NONLINEAR CIRCUIT ANALYSIS PROGRAM NCAP
C     SAMPLE CALCULATION OF A 2N5109 RF AMPLIFIER IS GIVEN
C     ------------------------------------------------------------------
      EXTERNAL FIE,FM
      REAL K1,K2,K3,IC,ICMAX,MU,K,M,N
      REAL L
      DIMENSION WB(648)
      DIMENSION Y2(24,24),YF1(24,24),YF2(24,24),WA(24),J1(24,1),J2(24,1)
     1,V1(24),V2(24)
      COMPLEX U,ADMTS,ADMTF1,ADMTF2,ADMT,J,Y2,J1,J2,V1,V2,VS,YF1,YF2,T1,
     1T2,T3
      COMMON /P/ N,VCB,VCBO,MU,IC,ICMAX,A,HFEMAX,K,REF,CJE,C2P,RB,RC,C1,
     1C3
      DATA G/1HG/,R/1HR/,C/1HC/,L/1HL/
 1500 FORMAT(2E13.5)
 500  FORMAT(E13.5)
 1000 FORMAT(4E13.5)
 1100 FORMAT(1X,/,1X,*N       = *,E13.5,1X,*VCB     = *,E13.5,1X,*VCBO    =
     1 *,E13.5,1X,*MU      = *,E13.5,/,1X,*IC      = *,E13.5,1X,*ICMAX   =
     2*,E13.5,1X,*A       = *,E13.5,1X,*HFEMAX = *,E13.5,/,1X,*K       = *
     3,E13.5,1X,*REF     = *,E13.5,1X,*CJE     = *,E13.5,1X,*C2P     = *,E1
     43.5,/,1X,*RB      = *,E13.5,1X,*RC      = *,E13.5,1X,*C1      = *,E13
     5.5,1X,*C3      = *,E13.5)
 1050 FORMAT(1H1,1X,*2N5109 NCAP INPUT PARAMETERS:*)
 3500 FORMAT(1X,/,1X,*RESISTIVE NONLINEAR COEFFICIENTS:*,/,/,1X,*K1   = *
     1,E13.5,1X,*K2   = *,E13.5,1X,*K3   = *,E13.5)
 4000 FORMAT(1X,/,1X,*CAPACITIVE NONLINEAR COEFFICIENTS:*,/,/,1X,*C1   =
     1*,E13.5,1X,*C2   = *,E13.5,1X,*C3   = *,E13.5)
 4500 FORMAT(1X,/,1X,*TRANSCONDUCTIVE NONLINEAR COEFFICIENTS:*,/,/,1X,*G
     101 = *,E13.5,1X,*G10 = *,E13.5,/,1X,*G02 = *,E13.5,1X,*G20 = *,E13
     2.5,1X,*G11 = *,E13.5,/,1X,*G03 = *,E13.5,1X,*G30 = *,E13.5,1X,*G12
     3 = *,E13.5,1X,*G21 = *,E13.5)
 5000 FORMAT(4E13.5)
 5100 FORMAT(1X,/,1X,*2N5109 RF AMPLIFIER AC CIRCUIT INFORMATION:*,/)
 2000 FORMAT(A1,3X,I3,I3,E13.5,I3,I3)
 2100 FORMAT(1X,A1,I3,I3,E13.5,I3,I3)
 5500 FORMAT(1X,/,1X,*SAMPLE CALCULATED RESULTS OF TRANSFER FUNCTIONS AR
     1E LIST BELOW:*,/)
 2500 FORMAT(1X,*H1(20) = *,2E13.5,1X,*H1(22) = *,2E13.5,1X,*FREQUENCY =
     1 *,E13.5)
 3000 FORMAT(1X,*H2(20) = *,2E13.5,1X,*H2(22) = *,2E13.5,1X,*FREQUENCY =
     1 *,*(*,E13.5,1X,E13.5,*)*)
 6000 FORMAT(1X,/)
C     ------------------------------------------------------------------
C     READ IN INPUT EXCITATION
C     ------------------------------------------------------------------
      READ(5,1500)VX1,VX2
C     ------------------------------------------------------------------
C     READ IN INPUT SOURCE IMPEDANCE
C     ------------------------------------------------------------------
      READ(5,500)RX
C     ------------------------------------------------------------------
C     READ IN 2N5109 NCAP INPUT PARAMETER
C     ------------------------------------------------------------------
      READ(5,1000)N,VCB,VCBO,MU
```

```
      READ(5,1000)IC,ICMAX,A,HFEMAX
      READ(5,1000)K,REF,CJE,C2P
      READ(5,1000)RB,RC,C1,C3
C     ------------------------------------------------------------------
C     PRINT 2N5109 NCAP INPUT PARAMETER
C     ------------------------------------------------------------------
      WRITE(6,1050)
      WRITE(6,1100) N,VCB,VCBO,MU,IC,ICMAX,A,HFEMAX,K,REF,CJE,C2P,RB,RC,
     1C1,C3
C     ------------------------------------------------------------------
C     CALCULATE NONLINEAR COEFFICIENTS OF THE 2N5109
C     ------------------------------------------------------------------
      CALL COEF(K1,K2,K3,GA1,GA2,GA3,G01,G10,G02,G20,G11,G03,G30,G12,G21
     1)
      WRITE(6,3500)K1,K2,K3
      WRITE(6,4000)GA1,GA2,GA3
      WRITE(6,4500)G01,G10,G02,G20,G11,G03,G30,G12,G21
      U=(0.,1.)
C     ------------------------------------------------------------------
C     READ IN SWEEP FREQUENCY INFORMATION
C     ------------------------------------------------------------------
      READ(5,5000) FSTART,FSTOP,FINC,DF
C     ------------------------------------------------------------------
C     READ IN 2N5109 RF AMPLIFIER AC CIRCUIT INFORMATION
C     ------------------------------------------------------------------
      WRITE(6,5100)
      DO 55 I=1,40
      READ(5,2000)TYPE,NFROM,NTO,VALUE,NFC,NTC
      WRITE(6,2100)TYPE,NFROM,NTO,VALUE,NFC,NTC
      WRITE(7,2100) TYPE,NFROM,NTO,VALUE,NFC,NTC
55    CONTINUE
      REWIND 7
      WRITE(6,5500)
      DO 60 II=1,100
      F1=FSTART+(II-1)*FINC
      F2=DF-F1
      IF(F1.GT.FSTOP)GO TO 65
      W1=6.2832*F1
      W2=6.2832*F2
      DO 5 I1=1,24
      DO 5 I2=1,24
      YF1(I1,I2)=0.
      YF2(I1,I2)=0.
      Y2(I1,I2)=0.
5     CONTINUE
      YF1(1,1)=1./RX
      YF2(1,1)=1./RX
      Y2(1,1)=1./RX
      DO 10 I=1,40
      READ(7,2100) TYPE,NFROM,NTO,VALUE,NFC,NTC
      IF(TYPE.EQ.G)GO TO 15
      IF(TYPE.NE.R)GO TO 20
      ADMTF1=1./VALUE
      ADMTF2=1./VALUE
      ADMTS=1./VALUE
      GO TO 25
20    IF(TYPE.NE.C)GO TO 30
```

```
      ADMTF1=U*W1*VALUE
      ADMTF2=U*W2*VALUE
      ADMTS=U*(W1+W2)*VALUE
      GO TO 25
30    IF(TYPE.NE.L)GO TO 10
      ADMTF1=1./(U*W1*VALUE)
      ADMTF2=1./(U*W2*VALUE)
      ADMTS=1./(U*(W1+W2)*VALUE)
25    YF1(NFROM,NFROM)=YF1(NFROM,NFROM)+ADMTF1
      YF2(NFROM,NFROM)=YF2(NFROM,NFROM)+ADMTF2
      Y2(NFROM,NFROM)=Y2(NFROM,NFROM)+ADMTS
      IF(NTO.EQ.0)GO TO 10
      YF1(NTO,NTO)=YF1(NTO,NTO)+ADMTF1
      YF2(NTO,NTO)=YF2(NTO,NTO)+ADMTF2
      Y2(NTO,NTO)=Y2(NTO,NTO)+ADMTS
      YF1(NFROM,NTO)=YF1(NFROM,NTO)-ADMTF1
      YF2(NFROM,NTO)=YF2(NFROM,NTO)-ADMTF2
      Y2(NFROM,NTO)=Y2(NFROM,NTO)-ADMTS
      YF1(NTO,NFROM)=YF1(NTO,NFROM)-ADMTF1
      YF2(NTO,NFROM)=YF2(NTO,NFROM)-ADMTF2
      Y2(NTO,NFROM)=Y2(NTO,NFROM)-ADMTS
      GO TO 10
15    ADMT=VALUE
      YF1(NFROM,NFC)=YF1(NFROM,NFC)+ADMT
      YF2(NFROM,NFC)=YF2(NFROM,NFC)+ADMT
      Y2(NFROM,NFC)=Y2(NFROM,NFC)+ADMT
      YF1(NFROM,NTC)=YF1(NFROM,NTC)-ADMT
      YF2(NFROM,NTC)=YF2(NFROM,NTC)-ADMT
      Y2(NFROM,NTC)=Y2(NFROM,NTC)-ADMT
      YF1(NTO,NFC)=YF1(NTO,NFC)-ADMT
      YF2(NTO,NFC)=YF2(NTO,NFC)-ADMT
      Y2(NTO,NFC)=Y2(NTO,NFC)-ADMT
      YF1(NTO,NTC)=YF1(NTO,NTC)+ADMT
      YF2(NTO,NTC)=YF2(NTO,NTC)+ADMT
      Y2(NTO,NTC)=Y2(NTO,NTC)+ADMT
10    CONTINUE
C     ------------------------------------------------------------------
C     CALCULATE FIRST ORDER (LINEAR) CURRENT SOURCE
C     ------------------------------------------------------------------
      DO 35 I=1,24
      J1(I,1)=0.
      J2(I,1)=0.
35    CONTINUE
      J1(1,1)=VX1/RX
      J2(1,1)=VX2/RX
C     ------------------------------------------------------------------
C     CALCULATE FIRST ORDER (LINEAR) TRANSFER FUNCTION
C     ------------------------------------------------------------------
      CALL GAUSS(YF1,J1)
      CALL GAUSS(YF2,J2)
      DO 40 I=1,24
      V1(I)=J1(I,1)
      V2(I)=J2(I,1)
40    CONTINUE
      WRITE(6,2500)V1(20),V1(22),F1
      WRITE(6,2506)V2(20),V2(22),F2
C     ------------------------------------------------------------------
```

```
C     CALCULATE SECOND ORDER CURRENT SOURCE
C     ------------------------------------------------------------------
      DO 45 I=1,24
      J1(I,1)=0.
45    CONTINUE
      T1=-K2*(V1(5)-V1(6))*(V2(5)-V2(6))
      J1(5,1)=T1+J1(5,1)
      J1(6,1)=J1(6,1)-T1
      T2=-(F1+F2)*6.283*U*GA2*(V1(11)-V1(5))*(V2(11)-V2(5))
      J1(11,1)=J1(11,1)+T2
      J1(5,1)=J1(5,1)-T2
      T3=-GO2*(V1(11)-V1(5))*(V2(11)-V2(5))-0.5*G11*(V1(11)-V1(5))*(V2(5
     1)-V2(6))-0.5*G11*(V2(11)-V2(5))*(V1(5)-V1(6))-G20*(V1(5)-V1(6))*(V
     22(5)-V2(6))
      J1(11,1)=J1(11,1)+T3
      J1(5,1)=J1(5,1)-T3
C     ------------------------------------------------------------------
C     CALCULATE THE SECOND ORDER TRANSFER FUNCTION
C     ------------------------------------------------------------------
      CALL GAUSS(Y2,J1)
      DO 50 I=1,24
      V1(I)=J1(I,1)
50    CONTINUE
      WRITE(6,3000) V1(20),V1(22),F1,F2
      REWIND 7
      WRITE(6,6000)
60    CONTINUE
65    STOP
      END


      FUNCTION FM(X)
C     ------------------------------------------------------------------
C     FUNCTION OF AVALANCHE MULTIPLICATION
C     ------------------------------------------------------------------
      REAL IC,ICMAX,M,N,MU,K
      COMMON /P/ N,VCB,VCBO,MU,IC,ICMAX,A,HFEMAX,K,REF,CJE,C2P,RB,RC,C1,
     1C3
      S1=(X/VCBO)**N
      FM=1./(1.-S1)
      RETURN
      END

      FUNCTION FIE(X)
C     ------------------------------------------------------------------
C     FUNCTION OF EMITTER CURRENT
C     ------------------------------------------------------------------
      REAL ICMAX,IC,N,MU,K
      COMMON /P/ N,VCB,VCBO,MU,IC,ICMAX,A,HFEMAX,K,REF,CJE,C2P,RB,RC,C1,
     1C3
      S1=(ALOG(X/ICMAX))/2.3
      S2=HFEMAX/(1.+A*S1*S1)
      FIE=X*(1.+S2)/S2
      RETURN
      END
```

```
      SUBROUTINE GAUSS(Y,J)
C     ------------------------------------------------------------------
C     SIMULTANEOUS EQUATIONS SOLVER BY USING GAUSSIAN ELIMINATION
C     ------------------------------------------------------------------
      COMPLEX Y(24,24),A(24,25),PIVOT,B,J(24,1)
      N=24
      DO 20 I1=1,24
      DO 20 I2=1,25
      IF(I2.EQ.25) A(I1,I2)=J(I1,1)
      IF(I2.EQ.25) GO TO 20
      A(I1,I2)=Y(I1,I2)
   20 CONTINUE
      NP1=N+1
      EPS=1.0E-30
      IC=1
      IR=1
    1 PIVOT=A(IR,IC)
      IPIVOT=IR
      DO 2 I=IR,N
      IF(CABS(A(I,IC)).LE.CABS(PIVOT)) GO TO 2
      PIVOT=A(I,IC)
      IPIVOT=I
    2 CONTINUE
      IF(CABS(PIVOT).LE.EPS) GO TO 8
      IF(IPIVOT.EQ.IR) GO TO 4
      DO 3 K=IC,NP1
      B=A(IPIVOT,K)
      A(IPIVOT,K)=A(IR,K)
      A(IR,K)=B
    3 CONTINUE
    4 CONTINUE
      DO 5 K=IC,NP1
    5 A(IR,K)=A(IR,K)/PIVOT
      IF(IR.EQ.N) GO TO 10
      IRP1=IR+1
      DO 7 IP=IRP1,N
      B=A(IP,IC)
      IF(CABS(B).LE.EPS) GO TO 7
      DO 6 K=IC,NP1
      A(IP,K)=A(IP,K)-A(IR,K)*B
    6 CONTINUE
    7 CONTINUE
      IR=IR+1
      IC=IC+1
      GO TO 1
    8 WRITE(6,9)
    9 FORMAT(1X,*DETERMINANT EQUAL TO ZERO. NO UNIQUE SOLUTION.*)
      STOP
   10 NM1=N-1
      DO 12 K=1,NM1
      NMK=N-K
      DO 11 JJ=1,K
      NP1MJ=N+1-JJ
   11 A(NMK,NP1)=A(NMK,NP1)-A(NMK,NP1MJ)*A(NP1MJ,NP1)
   12 CONTINUE
      DO 13 I=1,N
      J(I,1)=A(I,25)
   13 CONTINUE
      RETURN
      END
```

```
      SUBROUTINE CDEF(K1,K2,K3,GA1,GA2,GA3,G01,G10,G02,G20,G11,G03,G30,G
     112,G21)
C     ------------------------------------------------------------------
C     THIS SUBROUTINE CALCULATES NONLINEAR COEFFICIENTS OF A BJT
C
C     K1, K2, K3 ----EMITTER-BASE RESISTIVE COEFFICIENTS
C     GA1, GA2, GA3 -BASE-COLLECTOR JUNCTION CAPACITANCE COEFFICIENTS
C     GMN ----------BASE-COLLECTOR DEPENDENT CURRENT SOURCE COEFFICIENTS
C     ------------------------------------------------------------------
      DIMENSION B(3),AA(3),DER(3),DM(3)
      EXTERNAL FIE,FM
      REAL K1,K2,K3,IC,ICMAX,MU,K,M,N,IE
      COMMON /P/ N,VCB,VCBO,MU,IC,ICMAX,A,HFEMAX,K,REF,CJE,C2P,RB,RC,C1,
     1C3
      XKTO=0.02567041
      XIC=IC
      IE=FIE(XIC)
      K1=IE/XKTO
      K2=IE/((XKTO*REF)**2.)/2.0
      K3=IE/((XKTO*REF)**3.)/6.0
      RE=1./K1
      GA1=K*(VCB)**(-MU)
      GA2=-0.5*K*MU*(VCB)**(-MU-1.)
      GA3=(1./6.)*K*MU*(MU+1.)*(VCB)**(-MU-2.)
      M=1./(1.-(VCB/VCBO)**N)
      CALL DERIV(FIE,XIC,DER)
      AA(1)=DER(1)
      AA(2)=DER(2)/2.0
      AA(3)=DER(3)/6.0
      B(1)=1./AA(1)
      B(2)=-AA(2)/(AA(1)**3.0)
      B(3)=(2.0*AA(2)*AA(2)-AA(1)*AA(3))/(AA(1)**5.)
      XVCB=VCB
      CALL DERIV(FM,XVCB,DER)
      DM(1)=DER(1)
      DM(2)=DER(2)/2.0
      DM(3)=DER(3)/6.0
      G10=B(1)*M*K1
      G01=B(1)*DM(1)*IE
      G20=B(1)*M*K2+B(2)*M*M*K1*K1
      G02=B(1)*IE*DM(2)+B(2)*DM(1)*DM(1)*IE*IE
      G11=2.*B(2)*K1*M*DM(1)*IE
      G30=B(1)*M*K3+2.*B(2)*K1*K2*M*M+B(3)*M*M*M*K1*K1*K1
      G21=2.*B(2)*K2*M*DM(1)*IE+3.*B(3)*M*M*K1*K1*DM(1)*IE
      G12=2.*B(2)*K1*M*DM(2)*IE+3.*B(3)*M*K1*DM(1)*DM(1)*IE*IE
      G03=B(1)*DM(3)*IE+2.*B(2)*DM(1)*DM(2)*IE*IE+B(3)*DM(1)*DM(1)*DM(1)
     1*IE*IE*IE
      RETURN
      END
```

```
      SUBROUTINE DERIV(FCT,T,DER)
C     ------------------------------------------------------------------
C     SUBROUTINE OF NUMERICAL DIFFERENTIATION
C     ------------------------------------------------------------------
      EXTERNAL FCT
      DIMENSION DER(3),XX(15),Z1(15),Z2(11),Z3(7)
      X=T
      H=X/500.
      X=X-8.*H
      DO 1 I=1,15
      X=X+H
      XX(I)=FCT(X)
1     CONTINUE
      N=15
      CALL DET5(H,XX,Z1,N,IER)
      DER(1)=Z1(8)
      DO 2 I=3,13
      J=I-2
      XX(J)=Z1(I)
2     CONTINUE
      N=11
      CALL DET5(H,XX,Z2,N,IER)
      DER(2)=Z2(6)
      DO 3 I=3,9
      J=I-2
      XX(J)=Z2(I)
3     CONTINUE
      N=7
      CALL DET5(H,XX,Z3,N,IER)
      DER(3)=Z3(4)
      RETURN
      END
```

2N5109 NCAP INPUT PARAMETERS:

N	=	.60000E+01	VCB	=	.50000E+01	VCBO	=	.40000E+02	MU	=	.28500E+00
IC	=	.50000E-01	ICMAX	=	.18000E-01	A	=	.36300E+00	HFEMAX	=	.8460CE+02
K	=	.42000E-12	REF	=	.10000E+01	CJE	=	.10000E-10	C2P	=	.36000E-08
RB	=	.15000E+02	RC	=	.32900E+05	C1	=	.10000E-12	C3	=	.56000E-12

RESISTIVE NONLINEAR COEFFICIENTS:

K1 = .19724E+01 K2 = .38419E+02 K3 = .49867E+03

CAPACITIVE NONLINEAR COEFFICIENTS:

C1 = .26549E-12 C2 = -.75664E-14 C3 = .64819E-15

TRANSCONDUCTIVE NONLINEAR COEFFICIENTS:

G01	=	.22851E-06	G10	=	.19446E+01						
G02	=	.11426E-06	G20	=	.37754E+02	G11	=	-.28734E-07			
G03	=	.30475E-07	G30	=	.48788E+03	G12	=	-.14367E-07	G21	=	-.27180E-06

2N5109 RF AMPLIFIER AC CIRCUIT INFORMATION:

J	1	0	-.20000E-01	0	0
R	1	21	.10000E+00	0	0
R	2	21	.50000E+02	0	0
R	21	22	.50000E+02	0	0
R	22	0	.50000E+02	0	0
L	2	3	.10000E-07	0	0
C	3	4	.53100E-06	0	0
R	4	0	.40000E+03	0	0
C	4	0	.10000E-12	0	0
R	4	5	.15000E+02	0	0
R	5	6	.50700E+00	0	0
C	5	6	.19228E-09	0	0
R	6	7	.39000E+03	0	0
R	7	8	.10900E+02	0	0
L	8	0	.29000E-07	0	0
C	7	9	.91200E-09	0	0
L	9	0	.22100E-07	0	0
C	4	11	.56000E-12	0	0
C	5	11	.26550E-12	0	0
R	5	11	.32900E+05	0	0
C	6	10	.10100E-06	0	0
L	10	24	.25000E-08	0	0
R	24	0	.10000E+00	0	0
G	11	5	.19446E+01	5	6
L	11	12	.67600E-07	0	0
R	12	14	.96000E-01	0	0
L	11	13	.50000E-08	0	0
C	13	14	.32500E-08	0	0
R	11	14	.10000E+07	0	0
R	14	15	.10000E-02	0	0
L	15	16	.36000E-08	0	0
R	16	17	.10000E+03	0	0
L	17	0	.10000E-08	0	0
L	16	18	.10000E-07	0	0
C	18	23	.95300E-06	0	0
R	23	0	.10000E+00	0	0
L	11	19	.10000E-07	0	0
C	19	20	.53400E-06	0	0
R	20	0	.50000E+02	0	0
C	4	6	.10000E-12	0	0

SAMPLE CALCULATED RESULTS OF TRANSFER FUNCTIONS ARE LIST BELOW:

```
H1(20) =   -.26640E+01  -.33457E+01 H1(22) =    .24827E+00  -.94799E-02 FREQUENCY =    .90000E+07
H1(20) =   -.11379E+01   .22801E+01 H1(22) =    .24859E+00   .94909E-02 FREQUENCY =   -.80000E+07
H2(20) =    .12614E-01  -.34256E-01 H2(22) =   -.51152E-01  -.41716E-02 FREQUENCY =    .90000E+07   -.80000E+07)

H1(20) =   -.29608E+01  -.34751E+01 H1(22) =    .24822E+00  -.95279E-02 FREQUENCY =    .91000E+07
H1(20) =   -.12240E+01   .23633E+01 H1(22) =    .24856E+00   .94613E-02 FREQUENCY =   -.81000E+07
H2(20) =    .12542E-01  -.34208E-01 H2(22) =   -.51057E-01  -.40963E-02 FREQUENCY = (   .91000E+07   -.81000E+07)

H1(20) =   -.33078E+01  -.36011E+01 H1(22) =    .24816E+00  -.95894E-02 FREQUENCY =    .92000E+07
H1(20) =   -.13192E+01   .24513E+01 H1(22) =    .24853E+00   .94366E-02 FREQUENCY =   -.82000E+07
H2(20) =    .12458E-01  -.34155E-01 H2(22) =   -.50951E-01  -.40063E-02 FREQUENCY = (   .92000E+07   -.82000E+07)

H1(20) =   -.37156E+01  -.37168E+01 H1(22) =    .24809E+00  -.96661E-02 FREQUENCY =    .93000E+07
H1(20) =   -.14250E+01   .25443E+01 H1(22) =    .24850E+00   .94173E-02 FREQUENCY =   -.83000E+07
H2(20) =    .12358E-01  -.34096E-01 H2(22) =   -.50830E-01  -.38993E-02 FREQUENCY = (   .93000E+07   -.83000E+07)

H1(20) =   -.41969E+01  -.38114E+01 H1(22) =    .24800E+00  -.97593E-02 FREQUENCY =    .94000E+07
H1(20) =   -.15431E+01   .26426E+01 H1(22) =    .24847E+00   .94037E-02 FREQUENCY =   -.84000E+07
H2(20) =    .12240E-01  -.34026E-01 H2(22) =   -.50687E-01  -.37729E-02 FREQUENCY = (   .94000E+07   -.84000E+07)

H1(20) =   -.47663E+01  -.38672E+01 H1(22) =    .24789E+00  -.98696E-02 FREQUENCY =    .95000E+07
H1(20) =   -.16755E+01   .27464E+01 H1(22) =    .24844E+00   .93964E-02 FREQUENCY =   -.85000E+07
H2(20) =    .12100E-01  -.33939E-01 H2(22) =   -.50513E-01  -.36253E-02 FREQUENCY = (   .95000E+07   -.85000E+07)

H1(20) =   -.54356E+01  -.38572E+01 H1(22) =    .24774E+00  -.99963E-02 FREQUENCY =    .96000E+07
H1(20) =   -.18248E+01   .28560E+01 H1(22) =    .24841E+00   .93960E-02 FREQUENCY =   -.86000E+07
H2(20) =    .11936E-01  -.33827E-01 H2(22) =   -.50296E-01  -.34561E-02 FREQUENCY = (   .96000E+07   -.86000E+07)

H1(20) =   -.62252E+01  -.37400E+01 H1(22) =    .24755E+00  -.10135E-01 FREQUENCY =    .97000E+07
H1(20) =   -.19940E+01   .29712E+01 H1(22) =    .24838E+00   .94032E-02 FREQUENCY =   -.87000E+07
H2(20) =    .11746E-01  -.33677E-01 H2(22) =   -.50018E-01  -.32685E-02 FREQUENCY = (   .97000E+07   -.87000E+07)

H1(20) =   -.71263E+01  -.34556E+01 H1(22) =    .24729E+00  -.10276E-01 FREQUENCY =    .98000E+07
H1(20) =   -.21870E+01   .30918E+01 H1(22) =    .24835E+00   .94189E-02 FREQUENCY =   -.88000E+07
H2(20) =    .11531E-01  -.33470E-01 H2(22) =   -.49655E-01  -.30730E-02 FREQUENCY = (   .98000E+07   -.88000E+07)

H1(20) =   -.81157E+01  -.29236E+01 H1(22) =    .24696E+00  -.10398E-01 FREQUENCY =    .99000E+07
H1(20) =   -.24084E+01   .32171E+01 H1(22) =    .24831E+00   .94440E-02 FREQUENCY =   -.89000E+07
H2(20) =    .11304E-01  -.33183E-01 H2(22) =   -.49182E-01  -.28933E-02 FREQUENCY = (   .99000E+07   -.89000E+07)
```

```
H1(20) =   -.91171E+01  -.20525E+01 H1(22) =    .24654E+00  -.10466E-01 FREQUENCY =    .10000E+08
H1(20) =   -.26649E+01   .33457E+01 H1(22) =    .24827E+00   .94799E-02 FREQUENCY =   -.90000E+07
H2(20) =    .11088E-01  -.32790E-01 H2(22) =   -.48573E-01  -.27733E-02 FREQUENCY = (   .10000E+08   -.90000E+07)

H1(20) =   -.99806E+01  -.77358E+00 H1(22) =    .24603E+00  -.10430E-01 FREQUENCY =    .10100E+08
H1(20) =   -.29608E+01   .34751E+01 H1(22) =    .24822E+00   .95279E-02 FREQUENCY =   -.91000E+07
H2(20) =    .10931E-01  -.32273E-01 H2(22) =   -.47826E-01  -.27808E-02 FREQUENCY = (   .10100E+08   -.91000E+07)

H1(20) =   -.10487E+02   .89324E+00 H1(22) =    .24549E+00  -.10236E-01 FREQUENCY =    .10200E+08
H1(20) =   -.33078E+01   .36011E+01 H1(22) =    .24816E+00   .95894E-02 FREQUENCY =   -.92000E+07
H2(20) =    .10896E-01  -.31643E-01 H2(22) =   -.46979E-01  -.29953E-02 FREQUENCY = (   .10200E+08   -.92000E+07)

H1(20) =   -.10420E+02   .27739E+01 H1(22) =    .24499E+00  -.98591E-02 FREQUENCY =    .10300E+08
H1(20) =   -.37156E+01   .37168E+01 H1(22) =    .24809E+00   .96661E-02 FREQUENCY =   -.93000E+07
H2(20) =    .11040E-01  -.30952E-01 H2(22) =   -.46124E-01  -.34711E-02 FREQUENCY = (   .10300E+08   -.93000E+07)

H1(20) =   -.97025E+01   .45582E+01 H1(22) =    .24462E+00  -.93315E-02 FREQUENCY =    .10400E+08
H1(20) =   -.41969E+01   .38114E+01 H1(22) =    .24800E+00   .97593E-02 FREQUENCY =   -.94000E+07
H2(20) =    .11377E-01  -.30288E-01 H2(22) =   -.45383E-01  -.41897E-02 FREQUENCY = (   .10400E+08   -.94000E+07)

H1(20) =   -.84713E+01   .59428E+01 H1(22) =    .24445E+00  -.87409E-02 FREQUENCY =    .10500E+08
H1(20) =   -.47663E+01   .38672E+01 H1(22) =    .24789E+00   .98696E-02 FREQUENCY =   -.95000E+07
H2(20) =    .11857E-01  -.29730E-01 H2(22) =   -.44838E-01  -.50537E-02 FREQUENCY = (   .10500E+08   -.95000E+07)

H1(20) =   -.70028E+01   .67848E+01 H1(22) =    .24446E+00  -.81827E-02 FREQUENCY =    .10600E+08
H1(20) =   -.54386E+01   .38572E+01 H1(22) =    .24774E+00   .99963E-02 FREQUENCY =   -.96000E+07
H2(20) =    .12392E-01  -.29303E-01 H2(22) =   -.44484E-01  -.59371E-02 FREQUENCY = (   .10600E+08   -.96000E+07)

H1(20) =   -.55570E+01   .71248E+01 H1(22) =    .24459E+00  -.77169E-02 FREQUENCY =    .10700E+08
H1(20) =   -.62252E+01   .37400E+01 H1(22) =    .24755E+00   .10135E-01 FREQUENCY =   -.97000E+07
H2(20) =    .12901E-01  -.28979E-01 H2(22) =   -.44253E-01  -.67449E-02 FREQUENCY = (   .10700E+08   -.97000E+07)

H1(20) =   -.42872E+01   .70993E+01 H1(22) =    .24479E+00  -.73597E-02 FREQUENCY =    .10800E+08
H1(20) =   -.71263E+01   .34556E+01 H1(22) =    .24729E+00   .10276E-01 FREQUENCY =   -.98000E+07
H2(20) =    .13331E-01  -.28703E-01 H2(22) =   -.44049E-01  -.74285E-02 FREQUENCY = (   .10800E+08   -.98000E+07)

H1(20) =   -.32444E+01   .66514E+01 H1(22) =    .24500E+00  -.70998E-02 FREQUENCY =    .10900E+08
H1(20) =   -.81197E+01   .29236E+01 H1(22) =    .24696E+00   .10396E-01 FREQUENCY =   -.99000E+07
H2(20) =    .13650E-01  -.28427E-01 H2(22) =   -.43793E-01  -.79649E-02 FREQUENCY = (   .10900E+08   -.99000E+07)

H1(20) =   -.24194E+01   .64697E+01 H1(22) =    .24521E+00  -.69182E-02 FREQUENCY =    .11000E+08
H1(20) =   -.91171E+01   .20525E+01 H1(22) =    .24654E+00   .10466E-01 FREQUENCY =   -.10000E+08
H2(20) =    .13832E-01  -.28114E-01 H2(22) =   -.43436E-01  -.83302E-02 FREQUENCY = (   .11000E+08   -.10000E+08)
```

REFERENCES

1. HAMILTON, D. J., and W. G. HOWARD: "Basic Integrated Circuit Engineering", McGraw-Hill Book Company, New York, 1975.

2. GRAY, P. R., and R. G. MEYER: "Analysis and Design of Analog Integrated Circuits", John Wiley & Sons, Inc., New York, 1977.

3. NAGEL, L. W.: "SPICE2: A Computer Program to Simulate Semiconductor Circuits", Memo. No. ERL-M520, Electronic Research Lab., College of Eng., U. C. Berkeley, CA 94720, May 1975.

4. COHEN, E.: "Program Reference for SPICE2", Memo. No. ERL-M592, Electronic Research Lab., College of Eng., U. C. Berkeley, CA 94720, June 1976.

5. BOWERS, J. C. and R. S. STEPHEN: "SCEPTRE: A Computer Program for Circuit and System Analysis", Prentice-Hall, Inc., Englewood Cliffs, New Jersey, 1971.

6. EBERS, J. J., and J. L. MOLL: Large-Signal Behavior of Junction Transistors, Proc. IRE, Vol. 42, pp. 1761-1772, December 1954.

7. EARLY, J. M.: Effects of Space-Charge Layer Widening in Junction Transistor, Proc. IRE, Vol. 46, pp. 1401-1406, November 1952.

8. GRAY, P. E., D. DEWITT, A. R. BOOTHROYD, and J. F. GIBBONS: "Physical Electronics and Circuit Models of Transistors", SEEC, Vol. 2, John Wiley & Sons, Inc., New York, 1964.

9. GIBBONS, J. F.: "Semiconductor Electronics", McGraw-Hill Book Company, New York, 1960.

10. BURGER, R. M., and R. P. DONOVAN: "Fundamentals of Silicon Integrated Device Technology", Vol. 2, Prentice-Hall, Inc., Englewood Cliffs, New Jersey, 1968.

11. POON, H. C., and J. C. MECKWOOD: Modelling of Avalanche Effect in Integral Charge Control Model, IEEE Trans. Electron Devices, Vol. ED-19, pp. 90-97, January 1972.

12. SZE, S. M.: "Physics of Semiconductor Devices", John Wiley & Sons, Inc., New York, 1969.

13. KIRK, C. T. Jr.: A Theory of Transistor Cutoff Frequency (fT) Falloff at High Current Densities, IRE Trans. Electron Devices, Vol. ED-9, pp. 164-174, March 1962.

14. WEBSTER, W. M.: On the Variation of Junction Transistor Current Gain Amplification Factor with Emitter Current, Proc. IRE, Vol. 42, pp. 914-920, June 1954.

15. GUMMEL, H. K.: A Charge Control Relation for Bipolar Transistors, Bell System Tech. J., Vol. 49, pp. 115-120, January 1970.

16. GUMMEL, H. K., and H. C. POON: An Integral Charge-Control Model of Bipolar Transistors, Bell System Tech. J., Vol. 49, pp 827-852, May 1970.

17. ABRAHAM, R. P.: Transistor Behavior at High Frequencies, IRE Trans. Electron Devices, Vol. ED-7, pp. 59-69, January 1960.

18. GRAY, P. E., and C. L. SEARLE: "Electronic Principles-Physics, Models, and Circuits", John Wiley & Sons, Inc., New York, 1969.

19. GETREU, IAN: Modelling the Bipolar Junction Transistors, Electronics, pp. 114-120, September 1974.

20. GETREU, IAN: Modelling the Bipolar Junction Transistors, Electronics, pp. 71-75, October 1974.

21. GETREU, IAN: Modelling the Bipolar Junction Transistors, Electronics, pp. 137-143, November 1974.

22. KULKE, B., and S. L. MILLER: Accurate Measurement of Emitter and Collector Series Resistances in Transistors, Proc. IRE (Lett.), Vol. 45, p. 90, January 1957.

23. HUANG, J. S. T.: Rapid Determination of Emitter- and Collector-Bulk Resistances, IEEE J. of Solid-State Circuits, Vol. SC-11, pp. 343-344, April 1976.

24. SEARLE, C. L. et al: "Elementary Circuit Properties of Transistors", SEEC, Vol. 3, John Wiley & Sons, Inc., New York, 1964.

25. MILLMAN, J., and C. C. HALKIAS: "Electronic Devices and Circuits", McGraw-Hill Book Company, New York, 1967.

26. SANSEN, W. M. C., and R. G. MEYERS: Characterization and Measurement of the Base and Emitter Resistances of Bipolar Transistors, IEEE J. of Solid-State Circuits, Vol. SC-7, pp. 492-498, December 1972.

27. THORNTON, R. D. et al: "Handbook of Basic Transistor Circuits and Measurements", SEEC, Vol. 7, John Wiley & Sons, Inc., New York, 1966.

28. "Linear Integrated Circuits and MOS Devices", RCA Solid State Databook Series, Vol. SSD-201, pp. 336-343, RCA Corporation, 1972.

29. WOOLEY, B. A., S. Y. J. WONG, and D. O. PEDERSON: A Computer-Aided Evaluation of the 741 Amplifier, IEEE J. Solid-State Circuits, Vol. SC-6, pp. 357-365, December 1971.

30. "XR-Chip Custom IC Design Kit, Design Guidelines and Electrical Specifications", Exar Integrated Systems, Inc., 750 Palomar Ave., Sunnyvale, California, 94086.

31. VOLTERRA, V.: "Theory of Functionals and of Integral and Integro-Differential Equations", Dover Publications, New York, 1959.

32. WIENER, N.: "Response of a Nonlinear Device to Noise", M. I. T. Radiation Laboratory Report V-16S, April 1942.

33. NARAYANAN, S.: Transistor Distortion Analysis Using Volterra Series Representations, Bell System Tech. J., Vol. 46, pp. 991-1024, May-June 1967.

34. NARAYANAN, S.: Application of Volterra Series to Intermodulation Distortion Analysis of Transistor Feedback Amplifier, IEEE Trans. Circuit Theory, Vol. CT-17, pp. 518-527, November 1970.

35. NARAYANAN, S.: Intermodulation Distortion of Cascaded Transistors, IEEE J. of Solid-State Circuits, Vol. SC-4, pp. 97-106, June 1969.

36. POON, H. C.: Modelling of Bipolar Transistor Using Integral Charge-Control Model with Applications to Third-Order Distortion Studies, IEEE Trans. on Electronic Devices, Vol. ED-19, pp. 719-731, June 1972.

37. KUO, Y. L., and J. D. WITKOWSKI: Computer-Aided Distortion Analysis of Bipolar Transistor Circuits, Proc. 1972 IEEE Int. Symp. on Circuit Theory, April 1972.

38. MEYER, R. G., M. J. SHENSA, and R. ESCHENBACH: Cross Modulation and Intermodulation in Amplifiers at High Frequencies, IEEE J. of Solid-State Circuits, Vol. SC-7, pp. 16-23, February 1972.

39. GRAHAM. J. W., and L. EHRMAN: "Nonlinear System Modelling and Analysis with Applications to Communications Receivers", Tech. Report RADC-TR-73-178, Rome Air Development Center, Griffiss Air Force Base, New York, June 1973, 766278/6.

40. WEINER, D. D., and J. SPINA: "The Modelling and Analysis of Weakly Nonlinear Systems", 1979, Van Nostrand-Reinhold (in press).

41. EHRMAM, L.: "Electronic Device Modelling", Tech. Report RADC-TR-73-407, Rome Air Development Center, Griffiss Air Force Base, New York, January 1974, 776091/1GI.

42. FAIR, R. B.: Harmonic Distortion in the Junction Field-Effect Transistor with Field-Dependent Mobility, IEEE Trans. on Electronic Devices, Vol. ED-19, pp. 9-13, January 1972.

43. "IMSL Library Reference Manual", International Mathematical and Statistical Libraries, Inc., Sixth Floor, GNB Building, 7500 Bellaire Boulevard, Houston, Texas 77036.

44. WHALEN, J., and C. PALUDI: Computer-Aided Analysis of Electronic Circuits - the Need to Include Parasitic Elements, Int. J. of Electronics, Vol. 43, pp. 501-511, November 1977.

45. DIRECTOR, S. W.: Survey of Circuit Oriented Optimization Techniques, IEEE Trans. Circuit Theory, Vol. CT-18, pp. 3-10, January 1971.

46. DIRECTOR, S. W., and R. A. ROHRER: The Generalized Adjoint Network and Network Sensitivity, IEEE Trans. Circuit Theory, Vol. CT-16, pp. 318-323, August 1969.

47. DIRECTOR, S. W., and R. A. ROHRER: Automatic Network Design - The Frequency Domain Case, IEEE Trans. Circuit Theory, Vol. CT-16, pp. 330-337, August 1969.

48. BANDLER, J. W.: Optimization Methods for Computer-Aided Design, IEEE Trans. Microwave Theory and Techniques, Vol. MIT-17, pp. 533-552, August 1969.

49. COOPER, L., and D. STEINBERG: "Introduction to Methods of Optimization", W. B. Saunders Company, Philadelphia, Pennsylvania, 1970.

50. FLETCHER, R., and C. M. REEVES: Function Minimization by Conjugate Gradients, Computer J., Vol. 7, pp. 149-154, July 1964.

51. FLETCHER, R., and M. J. D. POWELL: A Rapidly Convergent Descent Method for Minimization, Computer J., Vol. 6, pp. 163-168, June 1963.

52. WILDE, D. J.: "Optimum Seeking Methods", Prentice-Hall, Inc., Englewood Cliffs, New Jersey, 1964.

53. "Transmission Systems for Communications", Bell Telephone Laboratories, Inc., 3rd ed., New York, 1964.

54. RICHARDSON, R. E., V. G. PUGLIELLI, and R. A. AMADORI: Microwave Interference Effect in Bipolar Transistors, IEEE Trans. EMC, Vol. EMC-17, pp. 216-219, November 1975.

55. KAPLAN, G.: Computer Aided Design, IEEE Spectrum, Vol. 12, pp. 40-46, October 1975.

56. LOTSCH, H. K. V.: Theory of Nonlinear Distortion Produced in a Semiconductor Diode, IEEE Trans. Electron Devices, Vol. ED-15, pp. 294-307, May 1968.

57. NEIL, T. B. M.: Improved Method of Analyzing Nonlinear Electrical Networks, Electron Letters, Vol. 5, pp. 13-15, January 1969.

58. VALENTE, J.: The Nonlinear Circuit Analysis Program NCAP, 1977 IEEE Int. Electromagnetic Compatibility Symposium Record, Seattle, Washington, August 2-4, 1977.

59. BUSSGANG, J. J., L. EHRMAN, and J. W. GRAHAM: Analysis of Nonlinear Systems with Multiple Inputs, Proc. IEEE, Vol. 62, pp. 1088-1119, August 1974.

60. KUO, Y. L.: Distortion Analysis of Bipolar Transistor Circuits, IEEE Trans Circuit Theory, Vol. CT-20, pp. 709-716, November 1973.